**The Dissertation Committee for John Timothy Cullinane
certifies that this is the approved version of the following dissertation:**

Thermodynamics and Kinetics of Aqueous Piperazine with Potassium

Carbonate for Carbon Dioxide Absorption

Committee:

_____
Gary Rochelle, Supervisor

_____
John G. Ekerdt

_____
Benny D. Freeman

_____
Craig Schubert

_____
Frank Seibert

Thermodynamics and Kinetics of Aqueous Piperazine with Potassium Carbonate for Carbon Dioxide Absorption

by

John Timothy Cullinane, B.S.; M.S.

Dissertation

Presented to the Faculty of the Graduate School of

the University of Texas at Austin

in Partial Fulfillment

of the Requirements

for the Degree of

Doctor of Philosophy

The University of Texas at Austin

May, 2005

To My Family

Acknowledgments

also worked with several undergraduate students during my work here. Thanks to Dan Ellenberger for his help on the density, viscosity, and solid solubility work.

I would like to extend special thanks to George Goff. I have thoroughly enjoyed the past four years of sharing a lab and many of the same experiences, hardships, and character-building experiences. George has been extremely helpful in my development as a researcher; I always learned from our discussions of research ideas. We've also shared plenty of memorable times outside of work. George has been a good co-worker and a good friend and I thank him for that.

During my graduate career, I have had many opportunities. In particular, the chance to interact with industrial sponsors has greatly enhanced my learning. I would like to thank Dr. Craig Schubert of The Dow Chemical Company and Dr. Jim Critchfield of Huntsman Chemical for their time and interest in my research and professional development.

I have also had the pleasure of take classes and learning from some excellent faculty members including Professors Bill Koros, Venkat Ganesan, and Buddy Mullins. Professor Bruce Eldridge was also a valuable part of my learning, not only from a teaching standpoint, but as part of the SRP program. I thank Professor Del Ottmers for the opportunity to TA under his tutelage. Professor Ben Shoulders from the UT Department of Chemistry was a tremendous help with the NMR measurements.

Thanks to my family. My mother and father have been tremendous influences on me and have been wonderful role models. My father, being an engineer himself, has always been available for my questions and taken an interest in my career. My

mother's constant encouragement has helped support me throughout my academic career. I will always be grateful to them for the opportunities they have provided to me.

Finally, I would like to thank my wife, Christa. She has been very understanding with the time I have devoted to this work and has been a constant source of encouragement. Her contributions to our home have made my time at work easier and her companionship has made me a better person.

Thermodynamics and Kinetics of Aqueous Piperazine with Potassium Carbonate for Carbon Dioxide Absorption

Publication No. _____

John Timothy Cullinane, Ph.D.

The University of Texas at Austin, 2005

Supervisor: Gary T. Rochelle

This work proposes an innovative blend of potassium carbonate (K_2CO_3) and piperazine (PZ) as a solvent for CO_2 removal from combustion flue gas in an absorber/stripper. The equilibrium partial pressure and the rate of absorption of CO_2 were measured in a wetted-wall column in 0.0 to 6.2 m K^+ and 0.6 to 3.6 m PZ at 25 to 110°C. The equilibrium speciation of the solution was determined by ^{1}H NMR under similar conditions. A rigorous thermodynamic model, based on electrolyte non-random two-liquid (ENRTL) theory, was developed to represent equilibrium behavior. A rate model was developed to describe the absorption rate by integration of eddy diffusivity theory with complex kinetics. Both models were used to explain behavior in terms of equilibrium constants, activity coefficients, and rate constants.

The addition of potassium to the amine increases the concentration of CO_3^{2-}/HCO_3^- in solution. The buffer reduces protonation of the amine, but increases the

amount of carbamate species, yielding a maximum reactive species concentration at a K^+:PZ ratio of 2:1. The carbamate stability of piperazine carbamate and dicarbamate resembles that of primary amines and has approximately equal values for the heats of reaction, ΔH_{rxn} (18.3 and 16.5 kJ/mol). The heat of CO_2 absorption is lowered by K^+ from -75 to -40 kJ/mol. The capacity increases as total solute concentration increases, comparing favorably with 5 M monoethanolamine (MEA).

The rate approaches second-order behavior with PZ and is highly dependent on other strong bases. In 1 M PZ, the overall rate constant is 102,000 s^{-1}, 20 times higher than in MEA. The activation energy is 35 kJ/kmol. In K^+/PZ, the most significant reactions are PZ and piperazine carbamate with CO_2 catalyzed by carbonate. Neutral salts in aqueous PZ increase the apparent rate constant, by a factor of 8 at 3 M ionic strength. The absorption rate in 5 m K^+/2.5 m PZ is 3 times faster than 30 wt% MEA. A pseudo-first order approximation represents the absorption rate under limited conditions. At high loadings, the reaction approaches instantaneous behavior. Under industrial conditions, gas film resistance may account for >80% of the total mass transfer resistance at low loadings.

Contents

List of Tables

List of Figures

Chapter 1: Introduction

This chapter introduces the general problem of CO_2 emission into the atmosphere, including a review of common sources. Capturing CO_2 with the traditional absorption/stripping process is discussed in terms of problems in implementing the technology, specifically the large energy requirement of the system. A new solvent, a concentrated mixture of aqueous potassium carbonate and piperazine, is introduced as an improvement to current technology and the scope of this work is presented.

1.1. Emission and Remediation of Carbon Dioxide

Recent emphasis on the release of greenhouse gases, and the resulting potential for global warming, has raised concerns over the emission of gases such as CO_2. As the political and environmental demand increases, efficient methods for the capture and sequestration of CO_2 from the atmosphere will become increasingly important. Many types of processes generate CO_2. A vast majority of these involve the combustion of

fossil fuels, resulting in the release of acidic contaminants (e.g. H_2S, SO_x, NO_x, CO_2). Given the breadth of processes involving the release of CO_2 into the atmosphere, it is important to identify appropriate targets for remediation.

1.1.1. Sources of Carbon Dioxide

Both natural and anthropogenic sources contribute to the ongoing emission of greenhouse gases, particularly carbon dioxide. While natural emissions from volcanoes, forest fires, and biomass decomposition are significant, they are relatively constant from year to year. Man-made CO_2 emissions from power plants, manufacturing, and automobiles have increased steadily since the industrial revolution and have become a major concern and a contributing factor to global warming.

The major sources of man-made CO_2 emissions are listed in Table 1.1 (EPA, 2004). Fossil fuel combustion accounts for >95% of the CO_2 emitted annually. The balance originates from processes such as iron and steel production, cement manufacturing, and ammonia production.

Table 1.1. Annual CO_2 Emissions in the United States in Tg CO_2 Eq.

Source	1999	2000	2001	2002
Fossil Fuel Combustion	5,488.8	5,673.6	5,558.8	5,611.0
Iron and Steel Production	64.4	65.7	59.1	54.4
Cement Manufacturing	40.0	41.2	41.4	42.9
Waste Combustion	17.6	18.0	18.8	18.8
Ammonia/Urea Production	20.6	19.6	16.2	17.7
Lime Production	13.5	13.3	12.8	12.3
Limestone/Dolomite Use	8.1	6.0	5.7	5.8
Gas Flaring	6.9	5.8	5.4	5.3
Aluminum Production	5.9	5.7	4.1	4.2
Soda Ash	4.2	4.2	4.1	4.1
Others	6.3	6.0	5.3	5.8
Total	**5,676.3**	**5,859.0**	**5,731.8**	**5,782.4**

Given the overwhelming percentage of emissions from fossil fuel combustion, it becomes useful to analyze this source as individual sectors for simplified classification. CO_2 emissions are shown in Figure 1.1 for four point-source sectors, including electricity generation and the residential, commercial, and industrial sectors (EPA, 2004). The transportation sector is also included.

Electricity generation accounts for 40.3% of the CO_2 emissions from fossil fuel combustion in the U.S. annually (EPA, 2004). Coal-fired power plants are the most prominent point-source of CO_2, constituting 83% of the power plant emissions, or one-third of the total CO_2 emitted annually from combustion sources. The industrial sector, made up of ammonia production and other manufacturing processes, produces approximately 17% of the total. Residential and commercial sectors, incorporating mainly combustion for heating, combine to emit 11% of the total emissions. Transportation makes up the remaining 32%.

Historically, coal has been the most significant source of electricity (EIA, 2002). As shown in Figure 1.2, the use of coal as a power source has steadily risen since 1950. Compared to other fossil fuels, the percentage of electricity produced from coal has also steadily climbed from 66% in 1950 to 71% in 2002. Natural gas use has also risen and petroleum combustion has remained fairly stable. Power from renewable sources and nuclear power (not shown) have increased, but fossil fuel combustion still comprises 70% of the power production in the United States. It is apparent that coal has been and continues to be the preferred fuel source.
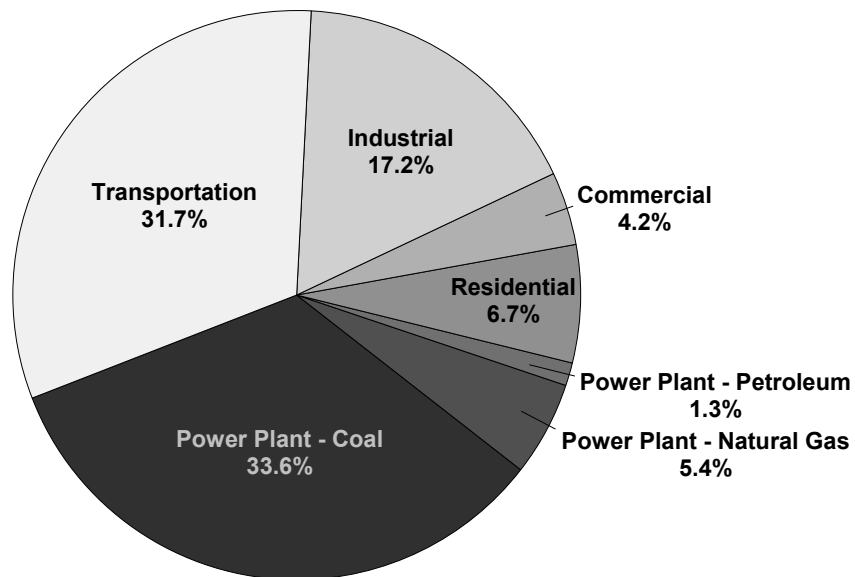
Figure 1.1. CO$_2$ Emissions from Fossil Fuel Combustion in the U.S. (2002), Total Emissions: 5564.2 Tg CO$_2$ Eq.
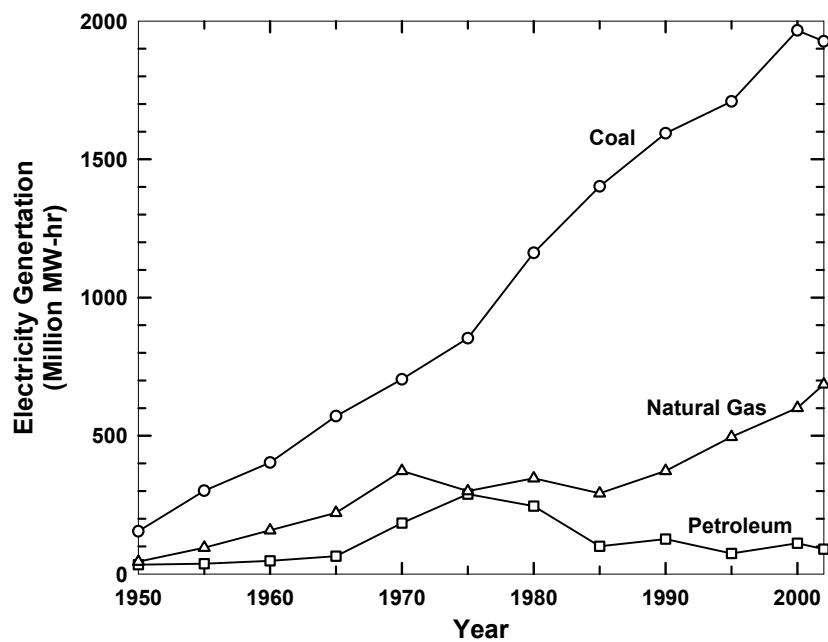
Figure 1.2. History of Electricity Production from Fossil Fuels

Another important factor to consider is the efficiency of fuels for power production. The efficiency is directly related to the amount of fuel, and thus the amount of CO_2 produced, necessary to produce given quantities of electricity. Of the three main plant types, natural gas-fired plants are the most efficient (55 to 60%) and the cleanest burning in terms of carbon, producing 0.45 kg CO_2/kW-hr (IEA, 2001). Power production from petroleum fuels gives 0.80 kg CO_2/kW-hr. Coal-fired plants produce the most carbon, approximately 0.96 kg CO_2/kW-hr, and are only 40 to 50% efficient.

It is clear that the largest potential application for CO_2 capture is coal-fired power plants. Coal combustion is a well-established technology accounting for 50% of the power in the U.S. The abundance of coal as a natural resource makes it a cheap, readily available fuel. In short, it is the largest contributor to overall CO_2 emissions and trends suggest an expanding share of the power production market. Improvements in capture technology for coal-fired power plants will be essential for making a significant impact on U.S. CO_2 emissions; therefore, most of the research presented in this work is targeted to conditions of coal-fired power plants.

1.1.2. Carbon Dioxide Capture

A wide variety of processes have been developed for the removal of acidic impurities from gas streams including membranes, cryogenics, adsorption, and, most commonly, absorption into a chemical solvent (IEA, 2001). With membranes, high purity streams are difficult to achieve, particularly on the scale of CO_2 capture from power plants. Cryogenic separation of CO_2 would produce a high pressure, liquid CO_2 stream, but the cost of refrigeration is often prohibitive and the removal of water would

be required, increasing the cost of the process. This technology is usually only considered for highly concentrated CO_2 streams. Adsorption has been tested, but a low capacity and poor CO_2 selectivity limit the potential for application to CO_2 capture.

To date, capture by absorption methods provides the most economical response to separating CO_2 from bulk gas streams (IEA, 2001). Other methods may be applied in niche applications and may be developed as long term solutions, but significant advancements are required in these technologies before implementation in power plants can be considered. For this reason, this work focuses on the development of a more efficient absorption technology.

The absorption of CO_2 into chemical or physical solvents is a well-developed technology that has been applied to numerous commercial processes, including gas treating and ammonia production (Kirk-Othmer, 2004). Much research has been performed on this technology over the past 50 years, particularly on developing an understanding of specific solvent characteristics. While a considerable body of work has been published on specific amines, little work has been done on understanding or representing complex mixtures which are often the most effective technologies.

1.1.3. Sinks and Sequestration of Carbon Dioxide

Following the successful capture of a concentrated carbon dioxide stream, the gas must be stored or utilized with minimal loss to the atmosphere. The transportation and storage of CO_2 will be a significant cost associated with the remediation of emissions; therefore, the development of efficient methods is critical to the application of capture technology to industrial processes. The following discussion briefly

introduces a few of the currently recognized options for storage, though sequestration technologies are outside the scope of this work.

Natural storage of CO_2 is an ideal storage solution, but it will be difficult to achieve efficiently. Naturally occurring sinks for CO_2 include grasslands, forests, and other biological processes. Natural sinks consume approximately 700 Tg CO_2 Eq. per year, far below that emitted into the atmosphere (EPA, 2004). Reforestation efforts are being pursued to increase natural carbon sequestration; however, processes such as this often require long time frames and large land areas to be effective.

Terrestrial locations are also a viable option for sequestering CO_2. Various geological formations have been proposed as suitable for storage, including depleted oil reservoirs and saline reservoirs, each with various advantages (IEA, 2001). Depleted oil reservoirs are well-defined storage options given the extensive exploration from oil recovery. Saline reservoirs are naturally occurring aquifers containing salt water. The CO_2 would dissolve into the water and react with the salts to from other minerals.

Other sequestration technologies may serve as a useful process fluid as well as viable storage options. Enhanced oil recovery (EOR) is one proven method of sequestering CO_2 while utilizing the gas to enhance the recovery of oil (IEA, 1995). In this process, CO_2 is injected into an oil reserve, improving the recovery of heavy oils and geologically storing the CO_2. In a similar process, CO_2 may be injected into unminable coal seams (IEA, 2001). The CO_2 would adsorb onto the coal and displace natural methane deposits, making the recovery of a fuel possible. The CO_2 would remain sequestered as long as the coal bed remained undisturbed. In both cases, the

requirements of a convenient source of high pressure CO_2 and verification of long-term CO_2 fixation limit the potential of EOR as a wide-spread sequestration technology.

The ocean, the largest natural sink for CO_2, has been proposed as a potential storage location given its prominent place in the natural CO_2 cycle (IEA, 2002). The capacity for CO_2 is large, but the physical rate of absorption limits the annual uptake of CO_2. In oceanic sequestration, the transport of CO_2 is accelerated by direct dispersion of the gas below the ocean surface, either by a fixed pipeline or ship. Concerns over the use of this technology stem from the cost of transporting CO_2 to the dispersion point and the impact of pH changes on the biological life existing near the dispersion point.

1.2. Carbon Dioxide Capture by Absorption/Stripping

1.2.1. Technology Description

One of the most mature, and most researched, technologies for acid gas capture from waste gas streams is an absorber/stripper process that uses a circulated chemical solvent (Kohl and Reisenfeld, 1985). Processes such as this are currently used in ammonia production and natural gas treating. There are several variations of this flowsheet, including a temperature swing and an isothermal process.

In the most common absorption process, the temperature swing variation (Figure 1.3), a waste gas stream containing CO_2 enters the bottom of an absorber (Kohl and Reisenfeld, 1985). The CO_2 is removed and the treated gas exits the top of the column. A CO_2-lean solvent enters the top of the absorber and counter-currently contacts the gas phase in packing or on trays. The CO_2 is absorbed, and the rich solvent exits the absorber. The rich solvent is pre-heated in a cross exchanger and pumped to the top of

a stripper. Heat, from intermediate or low pressure steam, is applied, regenerating the solvent. A concentrated CO_2 stream is recovered. Some heat is recovered from the lean solvent, though the solvent requires further cooling before its re-use in the absorber.
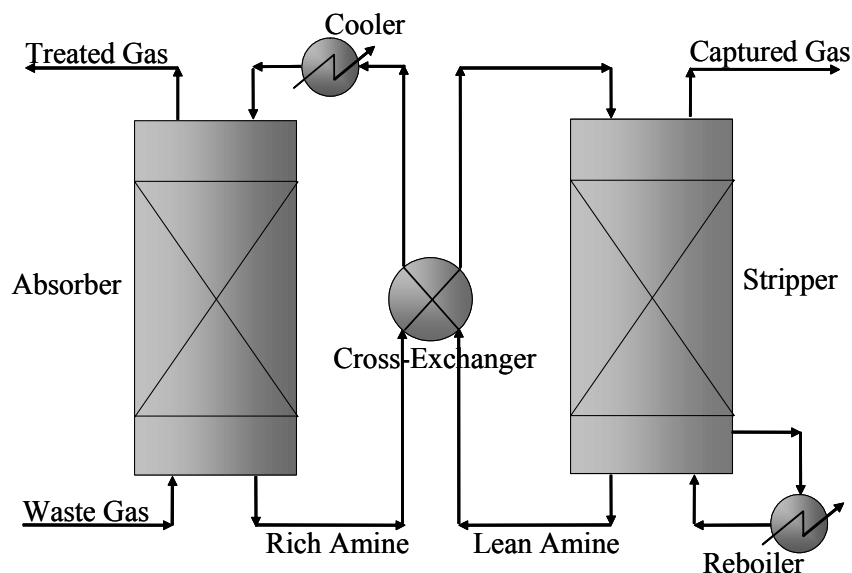
Figure 1.3. Absorber/Stripper Process Flowsheet

A variety of conditions is encountered depending on the specific application of the process. Table 1.2 shows some of the constraints specific to the most common CO_2 removal applications and the potential conditions for removal in a power plant setting (Kirk-Othmer, 2004). In general, natural gas treating and ammonia processing involve concentrated CO_2 streams and high total pressures. Also, outlet concentration limits are set according to process requirements. Treating power plant flue gas will be similar in that CO_2 concentrations range from 2 to 3 vol% for natural gas and 10 to 15 vol% for coal-fired plants, but the total pressure will be near atmospheric. The treating would target approximately 90% removal.

9

Table 1.2. Process Conditions in Absorber/Stripper Applications to CO_2 Capture

Process	Inlet CO_2 (vol %)	Outlet CO_2 (vol %)	P_{TOT} (atm)
Natural Gas	0 – 50	1 – 2	10 – 70
Ammonia	17 – 19	0.01 – 0.2	30
Coal Power Plant	10 – 15	1 – 1.5	1 – 1.3
Natural Gas Power Plant	2 – 3	0.2 – 0.3	1 – 1.3

1.2.2. Factors in Cost

While CO_2 capture has been proposed for power plant applications, the cost of implementing this technology is currently prohibitive. Estimates suggest an 80% increase in the cost of electricity from coal fired power plants with CO_2 capture (Rubin *et al.*, 2004). The components of this cost must be understood to effectively improve upon the process and move towards commercialization.

In a study of a standardized, coal-fired power plant (including flue gas desulfurization), Rao and Rubin (2002) categorize and quantify contributions to the overall cost of CO_2 capture by 30 wt% monoethanolamine (MEA), considered state-of-the-art technology, and subsequent sequestration. The capture and compression of CO_2 accounts for 80% of the total cost. The balance of the cost (20%) is due to transportation and sequestration. The obvious obstacle for implementation is the capture of CO_2; therefore, a significant opportunity for reducing costs lies with improving the capture process.

Within the capture process, compression accounts for 34% of the cost (Rao and Rubin, 2002). The efficiency of this component will be dictated by pressure and temperature of the concentrated gas stream. Approximately 17% of the total operating

cost is from the circulation of the solvent and gas through the columns by pumps and blowers. Minimizing pressure drop, and consequently packing height, may be an important consideration in reducing cost.

The most significant cost of CO_2 capture is the energy requirement for solvent regeneration, making up 49% of the total capture cost. The regeneration energy required can be estimated from three solvent properties, as discussed below. Though others may be important, the following are the most significant factors in determining the cost regeneration (Rochelle *et al.*, 2001).

The capacity of a solvent is a measure of the amount of CO_2 absorbed per unit of solvent. The capacity defines the total CO_2 concentration change over a set range of equilibrium partial pressures, reflecting the vapor-liquid equilibrium characteristics of the solvent. A high solvent capacity indicates that more CO_2 can be absorbed/stripped with a set amount of energy. Thus, given a constant circulation rate, the process becomes more efficient.

The heat of CO_2 absorption is another important solvent property. As CO_2 reacts with the solvent in the absorber, heat is liberated. Excluding latent and sensible heat, an amount of heat equivalent to this must be applied to reverse the reaction and remove CO_2 from the solution in the stripper. The application of this property to energy assessments is straightforward in that a reduction ordinarily lowers the required energy per mol of CO_2.

Improving the rate of CO_2 absorption into a solvent impacts several facets of the process and provides additional process flexibility. A faster rate of absorption, for a

11

given separation, allows the reduction of the liquid flowrate or a reduction in packing height, saving costs associated with liquid holdup, pressure drop, and latent heat. Alternatively, the absorber can be run closer to equilibrium, which may be the more favorable option depending on the solvent capacity.

An improved solvent for CO_2 capture can result in significant energy savings. The performance of potential solvents should be screened and compared according to improvements made in the aforementioned properties.

1.2.3. Solvents

Many solvents have been applied to gas treating, but the most effective are generally considered to be aqueous amines or hot potassium carbonate (hotpot) solvents. The variety of amines is endless, but some of the more common are shown in Table 1.3. Amines have an advantage over the hotpot process in that the absorption rate of CO_2 by amines is fast; however, the heat of absorption is also high. In contrast, absorption into potassium carbonate has a heat of absorption similar to physical solvents, but is limited by slow absorption rates.

In high pressure applications, physical solvents are utilized. Some of the more common solvents are Selexol, Rectisol, and Purisol (Kirk-Othmer, 2004). Because physical solvents do not react with CO_2, the solvent is not consumed at high partial pressures. Additionally, the heat of absorption is limited to the enthalpy of physical absorption, much less than the reactive solvents. The processes are limited by selectivity and slow rates of absorption.

In research of CO_2 removal from flue gas, the current state-of-the-art technology is generally considered to be a 30 wt% (7 m) aqueous solution of MEA. MEA has a high capacity for CO_2 and high rate of absorption, but its performance is limited by several factors, including a high heat of absorption and corrosion issues. One approach to improving solvent performance is blending amines or promoting potassium carbonate with amines. The idea is to add a fast reacting amine, such as MEA, with a system with a low heat of absorption, such as MDEA or K_2CO_3, to take advantage of both properties. Much of this technology is implemented in ammonia production where DEA-promoted K_2CO_3 is common.

Table 1.3. Common Amines in Gas Treating (Kohl and Riesenfeld, 1985)

Class	Name (Abbr.)	Structure
Primary Amine	Monoethanolamine (MEA)	
	Diglycolamine® (DGA)[a]	
Secondary Amine	Diethanolamine (DEA)	
	Diisopropanolamine (DIPA)	
Tertiary Amine	Triethanolamine (TEA)	
	Methyldiethanolamine (MDEA)	
Hindered Amine	Isobutanolamine (AMP)	

a. Diglycolamine (DGA) is a registered trademark of Huntsman Chemical.

1.3. Potassium Carbonate/Piperazine for Carbon Dioxide Capture

1.3.1. Solvent Description

This work proposes a new solvent, containing concentrated aqueous potassium carbonate and piperazine, for CO_2 capture from waste gas streams. The structure of piperazine (PZ) and its derivatives in aqueous solution with CO_2 are shown in Figure 1.4. Piperazine carbamate (PZCOO⁻) and piperazine dicarbamate (PZ(COO⁻)$_2$) are products of the reaction with PZ. Protonated piperazine (PZH⁺) and protonated piperazine carbamate (H⁺PZCOO⁻) are known stable molecules at moderate pH. A di-protonated PZ exists below a pH of approximately 5.5, but conditions in this work never approach low pH, so this species is excluded from consideration.
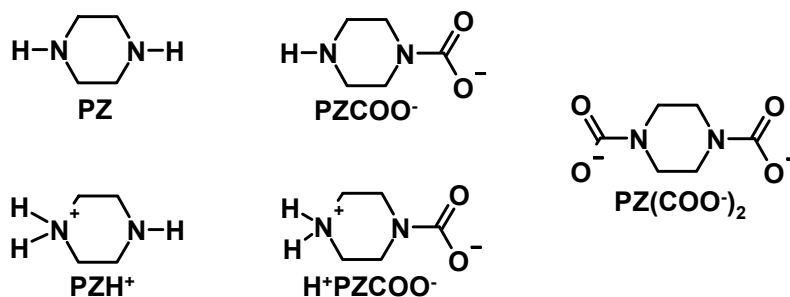
Figure 1.4. Structures of Piperazine in the Presence of CO_2

The solvent holds several advantages over traditional amines. First, because PZ is a diamine, the solvent can react with two moles of CO_2 per mole of amine. Coupled with the potassium carbonate in solution, which provides an additional sink for "storage" of the absorbed CO_2, the solvent has the potential for a higher CO_2 capacity than other amines. Also, the two amine functional groups will favorably affect the rate of absorption. Second, the amine has a high pK_a, similar to that of MEA. A high pK_a

generally translates into a fast rate of absorption. Third, the large quantity of carbonate/bicarbonate in solution serves as a buffer, reducing the protonation of the amine and leaving more amine available for reaction with CO_2.

1.3.2. Research Needs

Several critical questions should be addressed to develop a better understanding of K^+/PZ mixtures and amines as applied to CO_2 capture. As discussed in Section 1.2.2., there is a need to quantify several critical performance characteristics. While quantifying specific performance characteristics, it becomes beneficial to further develop the underlying fundamental science.

Thus far, little research has been published on the thermodynamics or kinetics of polyamines or salt-amine mixtures. Research on vapor-liquid equilibrium (VLE) of CO_2 in the solvent will define capacity and heats of absorption. Of fundamental interest in the understanding of the thermodynamics is a description of amine speciation with CO_2 and, for PZ, an identification of differences resulting from the unique, heterocyclic ring structure. It is also important to identify VLE benefits by using similar molecules. In promoted K_2CO_3 systems, the impact of high ionic strength on equilibria is largely unknown. An effective thermodynamic representation of K^+/PZ will improve the fundamental understanding of other amine solutions and mixtures.

Addressing the rate of absorption will complete the understanding of overall solvent performance. Investigations of the rate behavior will also support previous theories of amine reactions with CO_2. Verifying a reaction mechanism and supporting the Brønsted theory of base catalysis will improve the kinetic representation of amine

15

systems. Also, research on kinetics in K^+/PZ will improve the modeling of neutral salt effects important in high ionic strength environments. Additionally, validating an effective absorption rate model will aid the general understanding and methods for describing reactive transport in a complex system.

1.3.3. Previous Work

Some prior work on PZ as a CO_2 absorbent has been published and is summarized in Table 1.4, but most of the data are at conditions outside the range of interest for this work. Most of the VLE data are at CO_2 loadings above 0.75 mol CO_2/mol amine, compared to the 0.1 to 0.5 range encountered in flue gas treating. Bishnoi (2000) presents some data on PZ, but the majority of his work focuses on PZ/MDEA blends. The most comprehensive study of aqueous PZ is given by Ermatchkov *et al.* (2003) who reports speciation data for a wide range of conditions.

Table 1.4. Summary of Previous Work on Piperazine

Solvent	[PZ] (M)	T (^{o}C)	CO_2 Loading	Source	Data Type
Aq. PZ	0.2 – 0.6	25 - 70	0.0 – 1.0	Bishnoi (2000)	NMR, VLE, Rate
	0.1 – 1.45	10 – 60	0.0 – 1.0	Ermatchkov *et al.* (2003)	NMR
	2 – 4	40 – 120	> 0.75	Kamps *et al.* (2003)	VLE
	0.1 – 1.0	20 – 50	> 0.8	Aroua and Salleh (2004)	VLE
PZ + Amine	0.6	25 – 70	0.0 – 0.7	Bishnoi (2002,2002)	NMR, VLE, Rate
	0.0 – 1.2	40 - 60	0.0 – 0.5	Dang (2001)	VLE, Rate
Amine + K_2CO_3	N/A	Various	Various	Various, See Section 2.2.6.	VLE, Rate

Though general studies of the solvent performance of amine/K_2CO_3 solvents are common, detailed data on thermodynamics and kinetics are not available in the open literature. Properties of PZ/K_2CO_3 have not been previously explored. This work

builds on the data set for aqueous PZ and expands the solvent to include concentrated K_2CO_3.

Other work, though not addressing PZ specifically, is closely related to this investigation through methods and modeling techniques and should be mentioned. Austgen (1989) developed the rigorous thermodynamic model used in this work and applied it to modeling MEA- and DEA-promoted MDEA. Glasscock (1990) initiated a study on the modeling of CO_2 absorption into DEA and DEA/MDEA. These works demonstrate the ability of various modeling techniques to effectively represent amine mixtures over a broad range of conditions, though none specifically address high ionic strength solvents. Also, the prior work in this area focuses on simpler solvent systems; this work will attempt to extend these methods to a more complex application.

1.3.4. Objectives and Scope

Following the above rational for needed research on this solvent and in the general field of gas treating with amines, this work strives to satisfy several critical objectives, encompassing both scientific explorations and practical considerations:

1. Quantify and model fundamental thermodynamic properties that determine solvent behavior over conditions relevant to gas treating.

2. Determine the rate of CO_2 absorption into K^+/PZ mixtures and relate the performance to kinetic theory in other amine solvents.

3. Investigate the feasibility of applying the K^+/PZ mixture in an industrial gas treating process and identify controlling variables.

4. Anticipate practical limitations of applying the solvent to CO_2 capture in the proposed process.

The scope of the proposed work encompasses, to a large extent, conditions that would be encountered by applying the solvent to large-scale CO_2 removal from flue gas. That is, the temperature range of interest is from 40 to $120^{\circ}C$ and the gas phase CO_2 concentration is 0.1 to 10%.

Objective 1 is satisfied by experimental and modeling investigations of important thermodynamic properties. Data on the vapor-liquid equilibrium of CO_2 over 0.0 to 6.2 m K^+ and 0.0 to 3.6 m PZ have been measured in a wetted-wall column at 40 to $110^{\circ}C$. The equilibrium speciation of PZ in 2.5 to 6.2 m K^+ and 0.6 to 3.6 m PZ was measured using proton nuclear magnetic resonance spectroscopy. The physical solubility of CO_2 in K^+/PZ mixtures (up to 5.0 m K^+ and 2.5 m PZ) was determined by the N_2O analogy.

A rigorous thermodynamic model, based on the electrolyte non-random two-liquid (ENRTL) theory, was developed using the model originally coded by Austgen (1989). The model was extended to include K^+ and PZ and used, in conjunction with the experimental measurements, to develop a broad picture of thermodynamic behavior and to infer practical consequences of that behavior. Scientific conclusions concerning the stability of PZ carbamates and the pK_a of species were formed. Enthalpies predicted by the model are comparable to literature values and used to generalize the behavior of aqueous PZ and K^+/PZ. The influence of ionic strength on thermodynamic behavior was successfully correlated and interpreted with the activity coefficient model.

18

The second objective was met with measurements of the rate of CO_2 absorption in the wetted-wall column in a variety of solvents (0.0 to 6.2 m K^+ and 0.6 to 3.6 m PZ) between 25 and 110°C. A kinetic model, based on the model of Bishnoi (2000), was developed from the observed behavior to model the boundary layer for the absorption of CO_2 into K^+/PZ.

Using the data and the model, rate constants describing the reaction of PZ with CO_2 were regressed as part of a termolecular reaction mechanism. Furthermore, the rate constants were structured to satisfy the Brønsted theory of acid-base catalysis. Given the high ionic strength of the solvent, studies into neutral salt effects were deemed appropriate. The influence of salt on the reaction rate was interpreted and generalized. The model was used to correlate the flux of CO_2 into the solvent under various conditions and to arrive at conclusions concerning generalized rate behavior and important parameters for mass transfer.

Objective 3 is satisfied from interpretations of the thermodynamic and kinetic behavior as understood from experimental investigations. From the electrolyte NRTL model, correlations of VLE behavior were used to estimate the CO_2 capacity of the solvent and the heat of absorption. The rigorous rate model was applied to understanding the importance of kinetics and diffusion parameters. In comparing the rate of absorption to the instantaneous rate and gas film resistance contributions, conclusions about the performance of the solvent in an industrial process are achieved.

The fourth objective of this work includes practical considerations of solvent development. A basic study of the solid solubility of K^+/PZ mixtures was initiated to

19

determine viable solvent compositions. Solubility limits were quantified in concentrated mixtures of K_2CO_3/PZ and $KHCO_3$/PZ at 25 and 40^oC. The solubility limits also serve as an important addition to the thermodynamic investigations. Physical properties, such as density and viscosity, have been measured and reported to improve modeling and interpretation of fluid dependent parameters.

Chapter 2: Literature Review

This chapter introduces basic theory and literature pertaining to a study of CO_2 absorption by aqueous amines. A brief discussion on mass transfer with chemical reactions is presented, highlighting basic terminology. Approximations and limiting conditions are also discussed. Generalized equilibrium and rate behavior of amine solvents is presented with a particular emphasis on promoted-K_2CO_3 and prior work in the area. Research on acid-base catalysis theory and the effect of neutral salts are reviewed in the context of application to CO_2 reactions with amines.

2.1. Mass Transfer with Fast Chemical Reaction

2.1.1. Mass Transfer Theory

Detailed information on the transport of molecular species is commonly modeled with a microscopic material balance. In the simplest form, one species

diffuses into another as in the physical absorption of a gas into a liquid. The flux, N_{CO_2}, can be calculated at the gas-liquid interface ($x = 0$) as

$$N_{CO_2} = -D_{CO_2} \left. \frac{\partial [CO_2]}{\partial x} \right|_{x=0}. \qquad (2.1)$$

Thus, the flux is proportional to a concentration driving force across films, or boundary layers, and a group representing the diffusion and spatial direction of mass transfer. In the case of gas absorbing into a liquid (Figure 2.1), a gas film and a liquid film exist. Flux is the same at any point within the boundary layer, giving

$$N_{CO_2} = \begin{cases} K_G \left(P_{CO_2} - P_{CO_2}^* \right) \\ k_g \left(P_{CO_2} - P_{CO_2,i} \right) \\ k_l^o \left([CO_2]_i - [CO_2]_b \right) \text{ or } \dfrac{k_l^o}{H_{CO_2}} \left(P_{CO_2,i} - P_{CO_2}^* \right) \end{cases}, \qquad (2.2)$$

where K_G is the overall gas phase mass transfer coefficient, k_g is the gas film mass transfer coefficient, and k_l^o is the liquid film mass transfer coefficient. P_{CO_2} represents the bulk gas partial pressure of CO_2, $P_{CO_2,i}$ represents the partial pressure of CO_2 at gas-liquid interface, and $P_{CO_2}^*$ denotes the equilibrium partial pressure of CO_2 in the bulk liquid. H_{CO_2} is the Henry's constant of CO_2 in the solvent.

Mass transfer coefficients are a proportionality of flux to the driving force and are functions of the effective diffusivities. That is, k_g is a function of gas properties and reflective of the diffusion of CO_2 from the bulk gas to the gas liquid interface. Likewise, k_l^o is a representation of CO_2 transport from the interface to the bulk liquid.

22
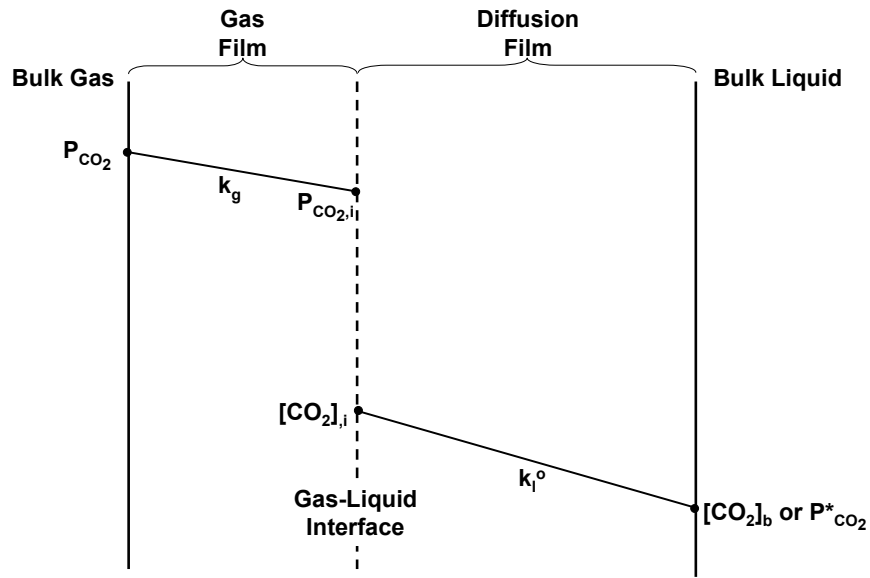
Figure 2.1. Physical Mass Transfer of CO₂ into a Bulk Liquid

Given Equation (2.2), mass transfer can be represented by series addition of resistances to mass transfer. In physical absorption, the overall resistance is equal to the gas film resistance plus the liquid film resistance, or

$$\frac{1}{K_G} = \frac{1}{k_g} + \frac{H}{k_l^o} \tag{2.3}$$

The consequence of chemical reaction in the liquid boundary layer is an accelerated absorption rate and a reduction in equilibrium partial pressure. In the case of fast chemical reaction, most of the reaction occurs in a thin layer near the gas-liquid interface, which is shown in Figure 2.2 as a reaction film. The equilibrium concentration at the interface is now controlled by the chemical reaction. For reversible reactions, the driving force for reaction is given by equilibrium considerations and the

diffusion of CO_2 to the reaction film. See Section 2.1.3. A representation can again be written as a series resistance

$$\frac{1}{K_G} = \frac{1}{k_g} + \frac{H_{CO_2}}{Ek_l^o} + \frac{1}{k_{l,PROD}^o} \frac{\partial P_{CO_2}^*}{\partial [CO_2]_T}$$

(2.4)

where $\partial P_{CO_2}^* / \partial [CO_2]_T$ gives the slope of the equilibrium curve. This term is essentially the instantaneous, or diffusion controlled, transport of CO_2. E is an enhancement factor accounting for the reaction of CO_2 and is defined as the flux of CO_2 with reaction normalized by the flux of CO_2 by physical absorption. In this work, the enhancement factor is referred to as a gas phase mass transfer coefficient across the liquid film, called a normalized flux or k_g'.

$$k_g^{'} = \frac{Ek_l^o}{H_{CO_2}}$$

(2.5)
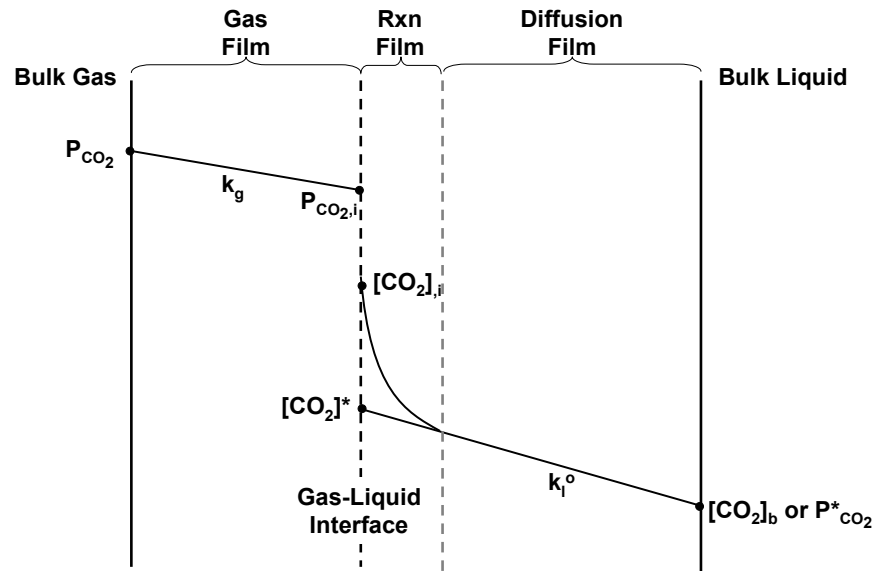
Figure 2.2. Mass Transfer of CO_2 into a Bulk Liquid with Fast Chemical Reaction

2.1.2. Mass Transfer Models

One of the earliest, and simplest, mass transfer models is called film theory and was first proposed by Lewis and Whitman (1924). Film theory is a steady-state model, resulting in a simple representation of mass transfer in the boundary layer. The assumption is mass transfer occurs across a stagnant film of given thickness δ.

A physical mass transfer coefficient, k_l^o, gives a proportional dependence of flux on the diffusion coefficient, which disagrees with most experimental data. Additionally, the film model predicts discontinuities at the gas-liquid interface and at δ, implying a more complicated model of mass transfer is required to accurately describe diffusion of species in a boundary layer.

Two other theories have garnered widespread use due their applicability to a range of problems. The Higbie penetration theory (Higbie, 1935) and the surface renewal theory (Danckwerts, 1951) are unsteady-state theories that assume molecules contact the gas-liquid interface for various amounts of time, yielding a contact time distribution. Both theories produce a flux that is dependent on the square root of the diffusivities, giving a better representation of observed behavior, but they are more complicated to solve.

The eddy diffusivity theory (Equation (2.6)), proposed by King (1966), is a steady-state theory that assumes a significant convective contribution to the diffusion of species in the boundary layer. Near the interface, diffusion processes are dominant. Approaching the bulk solution results in greater contributions from convective fluid movement, or eddies.

$$\frac{\partial}{\partial x}\left[\left(D_{CO_2}+\varepsilon x^2\right)\frac{\partial[CO_2]}{\partial x}\right]=0 \qquad (2.6)$$

Glasscock (1990) showed that the eddy diffusivity theory gives a solution within 5% of the surface renewal or penetration theory without the complications of time dependence. For this reason, Bishnoi (2000) chose this theory as the basis for his mass transfer model, which is incorporated into this work.

2.1.3. Reversible Reactions

The reactions considered in this work are reversible, and require special consideration of the appropriate driving force. Given a simple, reversible reaction of a reactant, R, with the dissolved gas, CO_2,

$$R+CO_2 \underset{k_r}{\overset{k_f}{\rightleftharpoons}} P , \qquad (2.7)$$

the overall expression for rate is

$$r=k_f[R][CO_2]-k_r[P]. \qquad (2.8)$$

An equilibrium constant, assuming [R] >> [CO$_2$], can also be defined as

$$K=\frac{k_f}{k_r}=\frac{[P]}{[R][CO_2]^*} , \qquad (2.9)$$

where * indicates the concentration in equilibrium as defined by the above expression. The rate is now given in terms of the driving force imposed by the actual concentration and the equilibrium concentration of the dissolved gas.

$$r=k_2[R]\left([CO_2]-[CO_2]^*\right) \qquad (2.10)$$

The reversible rate expression can, therefore, be calculated using the equilibrium constant.

$$r = k_2 [R] \left([CO_2] - \frac{[P]}{K[R]} \right)$$
(2.11)

2.1.4. Pseudo-First Order Reaction

The complexity of representing mass transfer with fast chemical reactions as an analytical expression has led to the development of useful simplifications. One such simplification is the pseudo-first order approximation. This approximation assumes that the liquid reactant concentration is constant throughout the boundary layer, eliminating the need for rigorous accounting of speciation in the reactive boundary layer. In other words, the reaction rate can be represented by the bulk solution composition.

The pseudo-first order assumption is applied as follows. The concentration profile of CO_2 reacting with an amine in a second order reaction is given by

$$D_{CO_2} \frac{\partial^2 [CO_2]}{\partial x^2} - k_2 [Am][CO_2] = 0 .$$
(2.12)

Assuming the amine concentration across the reactive boundary layer is constant and equal to the bulk liquid concentration,

$$D_{CO_2} \frac{\partial^2 [CO_2]}{\partial x^2} - k_1 [CO_2] = 0 ,$$
(2.13)

where k_1 is a pseudo-first order rate constant representing $k_2[Am]_b$.

The solution to this equation, for reversible reactions, is

$$N_{CO_2} = \frac{\sqrt{D_{CO_2} k_2 [Am]_b}}{H_{CO_2}} \left(P_{CO_2,i} - P^*_{CO_2} \right) .$$
(2.14)

27

The subscript b indicates bulk solution composition. The resulting expression for the normalized flux is

$$k'_{g,PFO} = \frac{\sqrt{D_{CO_2} k_2 [Am]_b}}{H_{CO_2}}.$$ (2.15)

This approximation requires that the concentration of the amine and $P_{CO_2}{}^*$ at the gas-liquid interface be approximately equal to those in the bulk solution. Thus, the flux must be low relative to the reactant and product concentrations. An increase in reaction kinetics relative to diffusion processes may result in the depletion of the reactant, or an accumulation of the products, at the gas-liquid interface. Likewise, a high driving force may deplete the reactant and introduce large errors into this approximation.

2.1.5. Instantaneous Reactions

A special case of mass transfer with chemical reaction is one where the reaction occurs fast enough to be considered instantaneous with respect to the diffusion process. Some reactions between gases and liquids are commonly represented as instantaneous, such as the absorption of NH_3 by aqueous HCl and H_2S by an alkaline solution. Under some circumstances, describing the absorption process of CO_2 by an amine as instantaneous may be appropriate. Generally, this occurs at high temperatures where kinetics have increased or at high loadings where the accumulation of CO_2 products places diffusion limitations on the reaction.

Consider a simplified situation in which

$$CO_2 + R \xrightarrow{k_1} P$$ (2.16)

28

and $k_1 \rightarrow \infty$ (the reaction is instantaneous). The reaction of CO_2 with R occurs at some distance, δ, from the gas-liquid interface. Conditions require that R diffuse to and P diffuse away from the reaction plane at least as fast as CO_2 reaches it, resulting in

$$N_{CO_2} = \frac{D_{CO_2}[CO_2]^*}{\delta}\left(1 + \frac{D_R[R]_b}{D_{CO_2}[CO_2]^*}\right). \tag{2.17}$$

Or, if film theory applies,

$$N_{CO_2} = k_l^o[CO_2]^*\left(1 + \frac{D_R[R]_b}{D_{CO_2}[CO_2]^*}\right). \tag{2.18}$$

For the circumstance of sparingly soluble gas in a liquid, the expression is simplified to

$$N_{CO_2} = k_l^o\frac{D_R[R]_b}{D_{CO_2}}. \tag{2.19}$$

This approximation is of practical importance for several reasons. First, if the reaction is instantaneous, the rate can be modeled with a simple model with no consideration of kinetics. Second, the influence of the gas film resistance can be quantified relative to the reaction rate for modeling absorber/stripper processes. Third, the prediction of instantaneous behavior relative to various reactions allows the determination of rate limiting behavior.

Similar solutions can be found for more complex reactions. For amines reacting with CO_2, several representations for instantaneous reaction can be derived. The condition where all reactions are considered instantaneous will be referred to as the global instantaneous case, designated by GBL,INST. With a small driving force, an approximate solution to this condition can be calculated from equilibrium behavior as

$$N_{CO_2,GBL,INST} = k_l^o \sqrt{\frac{D_P}{D_{CO_2}}} \frac{\partial [CO_2]_T}{\partial P_{CO_2}^*} \left(P_{CO_2,i} - P_{CO_2}^* \right), \qquad (2.20)$$

where D_P represents the diffusion coefficients of the reaction products and $[CO_2]_T$ is the molar liquid CO_2 concentration.

Other instantaneous reactions can be considered to determine the contribution of a particular class of reactions to the overall reaction rate. An instantaneous flux for the formation of amine carbamates can be defined as

$$N_{CO_2,PZ,INST} = \lim_{\substack{(k_{Am-b} \to \infty) \\ \sum_{Am} \sum_b}} N_{CO_2}. \qquad (2.21)$$

A comparison to the global instantaneous case reveals the potential limiting reactions under given conditions.

2.2. Solvents for CO_2 Absorption

The following discussion covers the major thermodynamic and kinetic conclusions for various types of amines and presents key findings that are applied in interpreting results of this work. The review is not intended to be a comprehensive listing of all work done in the area. Several authors have compiled detailed literature reviews on amines. See Mahajani and Joshi (1988), Versteeg *et al*. (1996), and Rochelle *et al*. (2001) for more detail.

2.2.1. Potassium Carbonate

The value of potassium carbonate as a CO_2 absorbent has been recognized since the early 1900's. The process evolved over the years into a viable commercial process, often used in treating synthesis gas (Benson and Field, 1959). The preferred

embodiment is a 40 wt% K_2CO_3 solution in an isothermal absorber/stripper at 100^oC and 15 to 20 atm.

Much of the commercial validation was done by Benson *et al.* (1954) and Benson *et al.* (1956). These two studies show important pilot plant characterization of hot potassium carbonate (hotpot) versus aqueous MEA and conclude that, under specific configurations, hotpot is an efficient CO_2 absorbent.

The absorption of CO_2 into aqueous K_2CO_3 is commonly represented by the overall reaction

$$CO_3^{2-} + H_2O + CO_2(aq) \rightleftharpoons 2HCO_3^- , \tag{2.22}$$
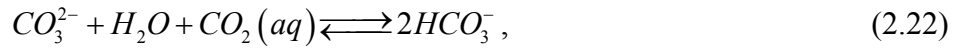
though the reaction is usually described in terms of two parallel, reversible reactions.

$$CO_2(aq) + OH^- \rightleftharpoons HCO_3^- \tag{2.23}$$

$$HCO_3^- + OH^- \rightleftharpoons CO_3^{2-} + H_2O \tag{2.24}$$

Since the reaction with hydroxide is the rate-limiting step, the reaction rate is represented as a second order rate expression.

$$r_{CO_2} = k_{OH^-}\left[OH^-\right]\left[CO_2\right] \tag{2.25}$$

This reaction, though important to the solution equilibrium, is generally much slower than aqueous amines, limiting its application in processes requiring a high percentage of removal. It is often advantageous to add a promoter to increase the absorption rate. The energy required to reverse the reaction is typically less than that required for amine solvents.

31

The rate constant has been measured by Pinsent *et al*. (1956), Nijsing *et al*. (1959), Hikita and Asai (1963), and Pohorecki and Moniuk (1988) and is reported in Chapter 4.

2.2.2. Primary and Secondary Amines

The reversible reaction of CO_2 with primary and secondary amines produces an amine carbamate. Caplow (1968) proposed a reaction mechanism for carbamate formation through a "zwitterion" intermediate, an ionic, but net-neutral molecule. The "zwitterion" mechanism illustrated below is a two-step process: the CO_2 reacts with the amine to form an intermediate followed by the extraction of the proton by bases present in solution.

$$O{=}C{=}O \; + \; \overset{R'}{\underset{R}{\diagdown}}NH \; \underset{k_r}{\overset{k_f}{\rightleftharpoons}} \; \overset{R'}{\underset{R}{\diagdown}}\overset{+}{N}\overset{H}{\diagdown}C{=}O,\;O^- \tag{2.26}$$

$$\overset{R'}{\underset{R}{\diagdown}}\overset{+}{N}\overset{H}{\diagdown}C{=}O,\;O^- \; + \; H_2O \; \overset{k_b}{\longrightarrow} \; \overset{R'}{\underset{R}{\diagdown}}N{-}C\overset{O^-}{\diagdown}O \; + \; H{-}\overset{+}{O}H_2 \tag{2.27}$$
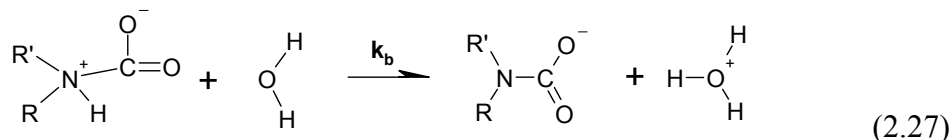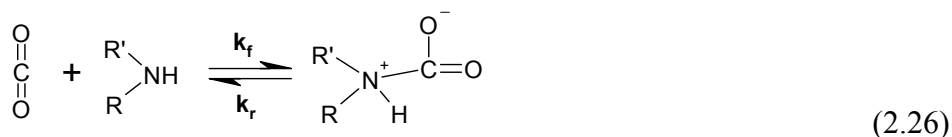
Given the two-step, "zwitterion" mechanism, the rate of reaction can be written in the following form.

$$r_{CO_2} = \frac{[Am][CO_2]}{\dfrac{1}{k_f} + \dfrac{k_r}{k_f \sum k_b[b]}} \tag{2.28}$$

Most researchers find that the reaction of CO_2 with aqueous primary amines is first order with respect to the amine. This suggests that the reaction rate is limited by

the formation of the zwitterion, $k_b \to \infty$. In this case, the rate expression can be simplified to

$$r_{CO_2} = k_f [Am][CO_2].$$
(2.29)

Researchers also find that the CO_2 reaction with secondary amines frequently approaches a second-order reaction with respect to the amine. Assuming the extraction of the proton by a base is rate-limiting, or $\Sigma k_b[b] \ll k_r$, Equation (2.28) can be simplified to

$$r = \sum_b k_{Am-b} [Am][b][CO_2],$$
(2.30)

where k_{Am-b} represents the combination of k_f, k_r, and k_b. For example, if PZ is the reacting amine and water is the base, the nomenclature is

$$k_{PZ-H_2O} = \frac{k_f k_{H_2O}}{k_r}.$$
(2.31)

Recent work by Crooks and Donnellan (1989) suggests the use of a single-step, termolecular mechanism to describe the reaction. The rate expression resulting from the termolecular mechanism is identical to Equation (2.30). The authors argue that while the "zwitterion" mechanism explains observed reaction rates, the mechanism is not thermodynamically consistent and the physical significance of the "zwitterion" is questionable. This view is supported by the recent ab initio study of carbamate formation by da Silva and Svendsen (2004). Because there is no direct evidence that an intermediate exists, the reaction can be represented as termolecular with no adverse effects (Benson, 1960).

Several investigations of amine systems utilize the "zwitterion" mechanism in its entirety to describe amine kinetics, but the values of k_f often have questionable significance or little impact on the reaction rate (Blauwhoff *et al.*, 1984; Bosch *et al.*, 1990; Littel *et al.*, 1992a; Kumar *et al.*, 2003). With a termolecular interpretation, varying orders of reaction can be obtained if the amine is also considered an acting base; therefore, regardless of the chosen mechanism, an equally effective representation of the reaction rate can be obtained. While it is difficult to make conclusions concerning the actual mechanism, the termolecular mechanism is comparably attractive in its simplicity and has been chosen to represent the data in this work.

Equilibrium representations of primary and secondary amines in water can be relatively complex. In addition to the equilibria of components in water, the carbamate and protonation of the amine must be considered.

$$Am + CO_2 + H_2O \rightleftharpoons AmCOO^- + H_3O^+ \tag{2.32}$$

$$AmH^+ + H_2O \rightleftharpoons Am + H_3O^+ \tag{2.33}$$
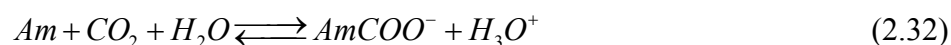
From carbamate formation and subsequent protonation, primary and secondary amines can theoretically absorb 0.5 mol CO_2/mol amine and are somewhat limited in their capacity to absorb CO_2. The carbamate reaction also has a high heat of absorption, making the solution difficult to regenerate.

There is an extensive collection of literature available on the kinetics of CO_2 with primary amines, particularly MEA. Jensen *et al.* (1954), Clarke (1964), Danckwerts and Sharma (1966), Sada *et al.* (1976b), Hikita *et al.* (1977), and Penny and

34

Ritter (1983) report second-order rate constants for MEA of approximately 7000 m^3/kmol-s. DGA is reported to have a rate constant of 5000 m^3/kmol-s (Alper, 1990a; Littel *et al.*, 1992b).

Secondary amines give similar rates as primary amines, but rates are usually reported in terms of the "zwitterion" mechanism. Kinetics of DEA and DIPA are reported by Sada *et al.* (1976a), Hikita *et al.* (1977), Laddha and Danckwerts (1981), Versteeg and van Swaaij (1988a), and Littel *et al.* (1992a).

2.2.3. Tertiary Amines

The reaction of tertiary amines with CO_2 differs significantly from primary or secondary amines in that an amine carbamate is not formed. Instead, the reaction produces a protonated amine and bicarbonate ion, resulting in a high capacity and a low heat of absorption. The reaction is consistent with a single-step mechanism, as with primary or secondary amines, but the products resemble a homogeneous catalysis of CO_2 hydrolysis. The absorption rate for tertiary amines is considerably slower and water must be present for this reaction to proceed.

$$\begin{array}{c} R'' \\ | \\ R'-N \\ | \\ R \end{array} + \begin{array}{c} H \\ \diagdown \\ O \\ \diagup \\ H \end{array} + \begin{array}{c} O \\ || \\ C \\ || \\ O \end{array} \rightleftharpoons \begin{array}{c} R'' \\ | + \\ R'-N-H \\ | \\ R \end{array} + \begin{array}{c} O^- \\ | \\ HO-C \\ \diagdown\!\!| \\ O \end{array} \tag{2.34}$$
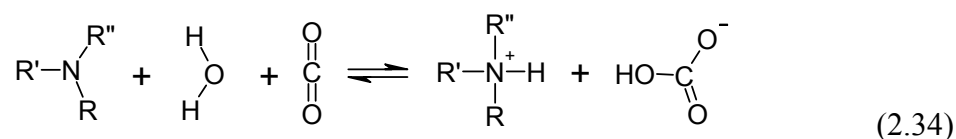
The rate of this reaction is typically represented with a second-order reaction.

$$r_{CO_2} = k_2 [Am][CO_2] \tag{2.35}$$

Several tertiary amines have been investigated for CO_2 absorption and selective removal of H_2S, including TEA and DMMEA (dimethylmonoethanolamine), though

MDEA is the most common used in gas treating. Investigations of MDEA kinetics include work by Blauwhoff *et al*. (1984), Versteeg and van Swaaij (1988a), Toman and Rochelle (1989), and Rinker *et al*. (1995). An average second-order rate constant is 4 m^3/kmol-s. Results for TEA are similar, giving a rate constant of approximately 2 m^3/kmol-s (Sada *et al*., 1976a; Donaldson and Nguyen, 1980; Crooks and Donnellan, 1990; Littel *et al*., 1990b).

2.2.4. Hindered Amines

Hindered amines have been developed for use in a number of processes including CO_2 removal. Hindered amines are primary or secondary amines whose structure inhibits the formation of carbamate species. A formal definition has been adopted as "a primary amine in which the amino group is attached to a tertiary carbon, or a secondary amine in which the amino group is attached to a secondary or a tertiary carbon atom" (Sartori and Savage, 1983). Some solvents contain severely hindered amines for the selective removal of H_2S.

In representing the interaction of CO_2 with hindered amines, several reactions must be considered. The reaction of CO_2 with moderately hindered amines includes the formation of a carbamate species as in the case of non-hindered amines.

$$Am + H_2O + CO_2 \rightleftharpoons AmCOO^- + H_3O^+ \tag{2.36}$$
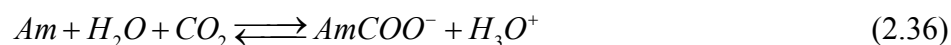
This reaction is often significantly slower and contributes less to the overall reaction rate than for primary or secondary amines due to the low carbamate stability. It is theorized that the subsequent decomposition of the carbamate to bicarbonate may contribute to the reaction equilibrium.

36

$$AmCOO^- + H_2O \rightleftharpoons AmH^+ + HCO_3^- \qquad\qquad (2.37)$$

While the formation and decomposition of carbamate may be important under some conditions, the reaction is mainly characterized by the direct formation of bicarbonate, as in the case of tertiary amines.

$$Am + H_2O + CO_2 \rightleftharpoons AmH^+ + HCO_3^- \qquad\qquad (2.38)$$

To the extent that this reaction, and not carbamate formation, drives the reaction, the capacity will approach 1 mol of CO_2 per mol of amine.

In general, the formation of bicarbonate allows a high solution capacity, but because little carbamate species form, the kinetics are slow. A higher free amine concentration partially counteracts the slow kinetics, but the overall rate of absorption may be slower than non-hindered primary or secondary amines.

Most studies of hindered amines focus on quantifying the kinetics of CO_2 absorption into AMP. Studies by Sharma (1965), Yih and Shen (1988), and Alper (1990b) suggest an overall second-order rate constant of 500 to 1,000 m^3/kmol-s. Bosch *et al.* (1990) and Seo and Hong (2000) indicate more complicated "zwitterion" type rates of varying reaction orders. This is also suggested by Xu *et al.* (1993) in an investigation of 2-piperidineethanol (PE). Little work on quantifying carbamate stability has been published. Sartori and Savage (1983) report $K_c < 0.1$ for AMP based on work with ^{13}C NMR.

2.2.5. Piperazine

Some work has been done previously on aqueous PZ and its behavior with CO_2. Ermatchkov *et al*. (2003) present speciation data from ^{1}H NMR experiments for 0.1 to 1.45 m PZ and CO_2 loadings of 0.1 to 1.0 mol CO_2/mol PZ. The temperature ranges from 10 to 60°C. This data set is essential for establishing a basis for a model of PZ thermodynamics, defining equilibrium constants and temperature dependences. Kamps *et al*. (2003) report total pressure data of CO_2/PZ mixtures from 40 to 120°C. Unfortunately, most of this data are above loadings of 1.0 mol CO_2/mol PZ limiting its use in this work. Aroua and Salleh (2004) give equilibrium CO_2 partial pressure data for aqueous PZ under similar conditions (20 to 50°C and loadings > 0.8). Again, the high loading data are of limited use in modeling PZ at absorber/stripper conditions.

There is some research on PZ as a promoter in amines. Dang (2001) gives data for the absorption rate of CO_2 into PZ/MEA. The thermodynamics are represented by a simple equilibrium model based on previously determined equilibrium constants, but the work does show that PZ is an effective rate promoter for MEA. Bishnoi (2000) presents data on PZ/MDEA and rigorously models the thermodynamics and reaction rate. While information applicable to K^+/PZ is limited, the work of Bishnoi provides a foundation for the modeling and interpretation presented in this work.

2.2.6. Amine-Promoted Potassium Carbonate

The process of CO_2 removal by absorption into K_2CO_3 has been used in natural gas treating and ammonia production for many years. The process has a low heat of absorption, making solvent regeneration more energy efficient. The rate of absorption

38

is slow and absorber performance suffers. To counteract the slow absorption rates, amines can be added in small quantities to promote the hotpot process. The following discussion summarizes important work in the development of these solvents. A list of the investigations of the more common amine-promoters is presented in Table 2.1.

Work by Shrier and Danckwerts (1969) measured the effects of various amines on absorption rate and quantified the effects as an enhancement over the absorption rate into K_2CO_3. The amine concentration was 0.1 M and the K_2CO_3 concentration was approximately 2 M. The study shows that the most effective promoters among the secondary amines are 2-ethylaminoethanol (EAE), 2-methylaminoethanol (MAE), and DEA. The primary amines, monoisopropanolamine (MIPA) and MEA, also promote the absorption rate. The difference in enhancements is interpreted in terms of equilibrium. The authors recognized that primary amines form a more stable carbamate than secondary amines, and thus, less free primary amine will be available for reaction.

Laddha and Danckwerts (1982) examined the effects of K_2CO_3 and K_2SO_4 on the rate of absorption into 1.0 M MEA and DEA. The authors found that, for DEA, the overall rate constant is increased by a factor of 2 with the addition of 0.4 M K_2SO_4. The same concentration of K_2CO_3 yields an increase of a factor of 7. While ionic strength has some effect on rates, carbonate has an additional base-catalysis effect. The authors also found that K_2CO_3 affects MEA in the same way that K_2SO_4 effects DEA; therefore, the specific effect of carbonate ion is not as significant in MEA.

Table 2.1. Selected Studies of Amine-Promoted K_2CO_3

Amine	[Amine] (kmol/m³)	[K_2CO_3] (kmol/m³)	T (°C)	Source	Method	Thermo	Rates
MEA	0.1	2	25	Shrier and Danckwerts (1969)	Stirred Cell	Yes	Yes
	1.0	0.4 – 1.0	11 – 25	Laddha and Danckwerts (1982)	Stirred Cell	No	Yes
	0.1	2.75	100	Mahajani and Danckwerts (1982)	BaCl	Yes	No
	0.1	2.75	100	Mahajani and Danckwerts (1983)	Stirred Cell	No	Yes
DEA	0.1	2	25	Shrier and Danckwerts (1969)	Stirred Cell	Yes	Yes
	1.0	0.4 – 1.0	11 – 25	Laddha and Danckwerts (1982; 1982)	Stirred Cell	No	Yes
	0.1	2.75	100	Mahajani and Danckwerts (1982)	BaCl	Yes	No
	0.0 – 0.314	2.75	100	Mahajani and Danckwerts (1983)	Stirred Cell	No	Yes
	0.6	2.0	40 – 120	Sartori and Savage (1983)	Autoclave/ Wetted-Sphere	Yes	Yes
	0.3 – 0.7	5.0	50 – 100	Tseng *et al.* (1988)	Wetted-sphere	No	Yes
	0.6	2.0	90	Bosch *et al.* (1989)	Modeling	-	-
DIPA	0.1	2.75	100	Mahajani and Danckwerts (1982)	BaCl	Yes	No
	0.101	2.75	100	Mahajani and Danckwerts (1983)	Stirred Cell	No	Yes
TEA	0.097	2.75	100	Mahajani and Danckwerts (1983)	Stirred Cell	No	Yes

An investigation of carbamate equilibrium in hot potassium carbonate was initiated by Mahajani and Danckwerts (1982). The study reports equilibrium constants at 100^oC for four amines, MEA; DEA; DIPA; and AMPD, as determined by rapid mixing with barium chloride. The stability of carbamate decreased as MEA > AMPD > DEA > DIPA, leading the authors to conclude that steric effects are responsible for determining equilibrium.

Mahajani and Danckwerts (1983) also measured the effect of amines on the desorption rates of CO_2 from potash at stripper conditions (100^oC). Amines chosen for comparison in this study include DEA, MEA, DIPA, and AMP. The authors find that DEA is a better promoter for the CO_2 desorption than the others. This is due to the equilibrium of DEA in comparison to the carbonate buffer. They also conclude that absorption should also be enhanced, if the driving force is reversed.

A study of amine promoters of K_2CO_3 was published by Sartori and Savage (1983) with an emphasis on hindered amines. Equilibrium and absorption rates are reported for DEA and an unspecified hindered amine. The major conclusions from this work are that the capacity and the absorption rate are increased by hindered amines due to steric hindrance. The low carbamate stability increases the formation of the bicarbonate and maintains a high concentration of free amine in solution.

Savage *et al*. (1984) investigated the VLE and rate behavior in DEA- and hindered amine-promoted K_2CO_3. Results indicate that the promoters increase the rate by a factor of 5 to 10 in K_2CO_3. The authors attribute the large promotion effect to the amine serving as a homogeneous catalyst for CO_2 hydrolysis.

41

Tseng *et al*. (1988) modeled the absorption rate of CO_2 by 2 and 5 wt% DEA in 30 wt% K_2CO_3. Equilibrium behavior was represented by data from previous work. Rate constants for the amine, hydroxide, and carbonate were regressed and activation energies were determined. The authors observe a changing reaction order that is accounted for in the interpretation of the "zwitterion" mechanism; however, a discontinuity of rate constants suggests the behavior is not accurately represented.

Pohorecki *et al*. (1988) report findings on 0.05 to 0.20 M EAE in 1.5 M K_2CO_3 and present several important findings, including the support of earlier findings that the rate is dependent on CO_3^{2-} content. Some experiments were run in the presence of neutral salts to buffer the ionic strength. In contrast to the previous work by Laddha and Danckwerts (1982), it is proposed that ionic strength, not concentration of the carbonate ion, is largely responsible for the increased absorption rates. The work does not rigorously account for speciation of the amine, so it is difficult to distinguish between equilibrium and kinetic effects. Still, the authors recognize the potential importance of both ionic strength and carbonate concentration on the rate.

Kumar *et al*. (2003) measured the rate of absorption in amino acid-promoted K_2CO_3 in a stirred cell. The reaction order of taurine and glycine is reported to increase from 1 at concentrations greater than 1.0 M K^+. The work concludes that either the "zwitterion" or termolecular mechanism adequately represents the observed behavior.

2.3. Contributions to Reaction Kinetics

2.3.1. Acid and Base Catalysis

A major contribution to kinetic theory and physical chemistry was the development of the theory of homogeneous catalysis by acids and bases. Much of the original work in this area was done by Brønsted (1928). This work laid the foundation for interpreting reaction mechanisms in terms of acid/base concentrations and provided an important link between equilibrium strength and reaction rates. This section briefly reviews some of the critical work in this area and relates them to the reaction of CO_2 with amines.

The Brønsted theory defines a base as a molecule tending to unite with a hydrogen nucleus and an acid as a molecule tending to split from a hydrogen nucleus. Thus, in general, an equilibrium can be defined so that

$$A \underset{\longleftarrow}{\overset{K}{\longrightarrow}} A^- + H^+, \tag{2.39}$$

where A is the acid and A^- is the corresponding base. Because in any solution the concentration of hydrogen ion is small, it is more physically meaningful to describe the above reaction relative to the hydronium equilibrium.

$$H_3O^+ \underset{\longleftarrow}{\overset{K_w}{\longrightarrow}} H_2O + H^+ \tag{2.40}$$

So, most reactions are represented as

$$A + H_2O \underset{\longleftarrow}{\overset{K_a}{\longrightarrow}} A^- + H_3O^+, \tag{2.41}$$

where $K_a = K/K_w$. K_a is representative of the strength of the acid (or base) and is usually written as

43

$$pK_a = -\log_{10} K_a .$$
(2.42)

Early work in physical chemistry indicated that many reactions depend proportionally on the concentration of hydronium or hydroxyl ions in solution. Brønsted held that the properties of these ions as acids and bases are not unique and the catalytic effect on reactions should extend to other molecules. To date, a large body of work has been performed corroborating and expounding on this theory.

One of the first efforts to distinguish the acid/base catalysis theory was a study of the mutarotation of glucose (Brønsted and Guggenheim, 1927). This paper includes a study of pyridine, a cyclic amine, and correlates the reaction rate of glucose with the base strength. Conclusions of the theory were summarized by Livingston (1930):

1) Any acid or base may act as a catalyst.

2) The concentration of protons in any solution is small enough that the catalytic effect is negligible.

3) The rate constant associated with the catalyst is different for each acid or base and is different for each reaction.

Brønsted (1928) also found that the catalytic effect of bases on reaction rates can be given as function of the base strength (i.e. dissociation constant). So, for a simple reaction of the form

$$A + b_1 \xrightarrow{\ k_{b_1}\ } Prod ,$$
(2.43)

where b_1 is the catalyzing base, the following expression applies.

$$\log_{10} k_{b_1} = x + \chi\, pK_{a,b_1}$$
(2.44)

where χ and x are reaction-specific constants and pK_{a,b_1} represents the base strength.

A study of the decomposition of nitramide demonstrated that amines are effective as base catalysts and can be represented in this general form (Bell and Trotman-Dickenson, 1949; Trotman-Dickenson, 1949). In addition, it was determined that the rate constant for the reaction could be correlated by four distinguishable classes of amines: primary, secondary, tertiary, and heterocyclic. Sharma (1965) summarized the rate constants of numerous amines reacting with CO_2 and demonstrated that a correlation with base strength applies. Other researchers in the area have shown similar correlating behavior (Littel *et al.*, 1992a; Rochelle *et al.*, 2001).

Though base catalysis has been widely recognized as a contributing factor in the kinetics of amines reacting with CO_2, this reaction involves two bases: the amine, Am, reacts with the CO_2 and the base, b_1, catalyzes the reaction.

$$CO_2 + Am + b_1 \xrightarrow{\ k_{Am-b_1}\ } AmCOO^- + H^+b_1 \qquad (2.45)$$
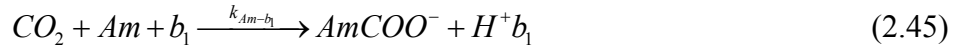
Following the sequence of reaction according to the proposed mechanism (Equations (2.26) and (2.27)), there are two correlations with base strength. The termolecular reaction rate can be expressed as a product of the two correlations (Equation (2.30)).

$$k_{Am-b_1} = \frac{k_f}{k_r} k_{Am-b_1} = \left(10^{a_{Am} + b_{Am} pK_{a,Am}} \right)\left(10^{a_1 + b_1 pK_{a,b_1}} \right) \qquad (2.46)$$

Thus,

$$\log_{10} k_{Am-b_1} = \left(a_{Am} + b_{Am} pK_{a,Am} \right) + \left(a_{b_1} + b_{b_1} pK_{a,b_1} \right). \qquad (2.47)$$

Since the amine-CO_2 interaction can be assumed constant, the contribution of unknown bases in this complex reaction may still be correlated by the difference in base strength.

$$\log_{10} k_{Am-b_2} = \log_{10} k_{Am-b_1} + \chi \left(pK_{a,b_2} - pK_{a,b_1} \right) \tag{2.48}$$

From the previous efforts in this field and the proven validity of Brønsted theory as applied to the capture of CO_2, the kinetic mechanism proposed in this work can justifiably rely in a large part on the correlation of kinetics to base strength.

2.3.2. Neutral Salt Effects

During a reaction between two or more molecules, the molecules come together in a configuration of high potential energy relative to that of the reactants and products. The molecules pass through this transition state as the reaction proceeds to the products. The resulting theory can be written generically so that a bi-molecular reaction occurs as

$$A^{z_A} + B^{z_B} \underset{\longleftarrow}{\overset{K}{\longrightarrow}} \left((AB)^* \right)^{z_A + z_B} \xrightarrow{k^*} \text{Products}, \tag{2.49}$$
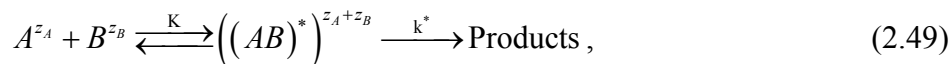
where (AB)* represents the transition state, or a reaction intermediate, and z is the charge of the species. An important corollary of this theory is that the reactants and transition state are considered to be in equilibrium. For this reaction, an equilibrium constant is written in the form

$$K = \frac{\left[(AB)^* \right]}{[A][B]} \frac{\gamma_{(AB)^*}}{\gamma_A \gamma_B}. \tag{2.50}$$

The rate of consumption of the intermediate is considered to be

$$r = k^* \left[(AB)^* \right]. \tag{2.51}$$

Then,

$$r = k^* K [A][B] \frac{\gamma_A \gamma_B}{\gamma_{(AB)^*}} \qquad (2.52)$$

or as it is more commonly written,

$$r = k_2 [A][B]. \qquad (2.53)$$

The rate constant can then be represented as

$$\log_{10} k_2 = \log_{10} k_2^o + \log_{10} \left(\frac{\gamma_A \gamma_B}{\gamma_{(AB)^*}} \right). \qquad (2.54)$$

The representation of the above rate expression leads to two distinct explanations of the effects of neutral salts on reactive systems. Primary and secondary salt effects have been independently observed in a variety of reactive systems.

2.3.2.1. Primary Salt Effect

The primary salt effect is a consequence of the change in activity coefficients with changing electrolyte concentration and ordinarily occurs with the reaction of two ions. In this case, the concentrations of species A and B are unchanged, but the ratio $\gamma_A \gamma_B / \gamma_{(AB)^*}$ may undergo significant deviations from ideality depending on the ionic character of the intermediate.

Various forms can be used to represent the activity coefficient behavior in solution. With the expanded Debye-Hückel relationship, the rate constant (with activity coefficients) can be expressed in terms of ionic strength, I.

$$\log_{10} k = \log k_{10}^o - \frac{-z_a z_b A \sqrt{I}}{1 + Ba\sqrt{I}} + CI \qquad (2.55)$$

47

A, B, and C are ion specific constants and a is the ion size parameter. In concentrated salt solutions, the expression is often dominated by the linear term CI. Thus, a simplification can be made in which log k is proportional to the ionic strength.

$$\log k_{10} = \log k_{10}^{\infty} + CI \tag{2.56}$$

This phenomenon has been observed in numerous systems. Much of the early work in this area was performed by Brønsted in his development of theory. Brønsted and Teeter (1924) quantified a primary salt effect in the reaction of mercuric nitrate with chloropentammine cobaltic nitrate. The two positively-charged reactants show a distinct increase in reaction rate with additional ionic strength. Other ionic reactions demonstrate similar behavior (Olson and Simonson, 1949).

2.3.2.2. Secondary Salt Effect

A secondary salt effect may alter the reaction rate by changing the concentrations of A and B while the activity coefficient ratio remains constant (Brønsted and Teeter, 1924). This is usually associated with enhancing the dissociation of the reactive ions through the addition of neutral salts, though the effect has been observed in reactions of neutral species. Thus, the important distinction here is that the effect is not a kinetic effect per se, but rather a change in "inter-ionic forces" (Brønsted and King, 1925).

One study, particularly useful for demonstrating the secondary salt effect, quantifies the effect of neutral salts on the decomposition of nitroso-triacetone-amine where hydroxyl ion is an active catalyst (Brønsted and King, 1925). In the presence of a piperidine buffer, whose equilibrium can be written

48

$$C_5H_{11}N + H_2O \rightleftharpoons C_5H_{12}N^+ + OH^-, \qquad\qquad (2.57)$$
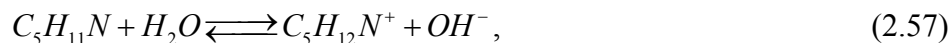
the effect of neutral salts is verified to increase the reaction velocity by increasing the hydroxyl concentration. The salts increase the stability of the ions in solution and move the above equilibrium to the right. An 18% increase in the apparent rate constant is observed with the addition of 0.2 N NaCl. In the presence of a phosphate buffer, where

$$PO_4^{3-} + H_2O \rightleftharpoons HPO_4^{2-} + OH^-, \qquad\qquad (2.58)$$

the stability of the lesser charge distribution pushes the equilibrium to the left in the presence of neutral salts. A negative salt effect (a reduction of the catalytic species, OH^-) is expected and observed. The apparent rate constant is 42% lower in 0.2 N NaCl.

2.3.2.3. Combinatorial Effects

Many of the initial investigations into the neutral salt effect rely on carefully designed experiments to isolate the primary or secondary mechanism for study. In this regard, the investigations represent highly idealized work. In more complicated, and non-ideal, systems, both primary and secondary salt effects may play a significant role in determining the reaction rate. Some studies have been performed on systems with no attempt to isolate either the primary or secondary salt effect, and represent the overall impact of neutral salt addition on reactions.

French (1928) studied the iodine-catalyzed decomposition of hydrogen peroxide. The influence of up to 2 M of several neutral salts increased reaction rates by as much as a factor of two. Grube and Schmid (1926) measured the effect of

concentrated neutral salts on the hydrolysis of cyanamide. The authors again find the reaction rates in 2 M ionic strength increase by a factor of two.

Neutral salts have also been shown to positively influence the absorption rate of CO_2 into amines. Data from Danckwerts and Sharma (1966) and Laddha and Danckwerts (1982) suggest a significant promotion effect due to ionic strength.

Given the high ionic strengths encountered in this work, salt effects are expected to play a significant role in determining the rate of CO_2 absorption. Pohorecki *et al*. (1988) and Kloosterman *et al*. (1987) documented this effect in potassium carbonate systems and applied a correction for ionic strength to the rate constant. It is no doubt a factor in all work with promoted K_2CO_3, though it is rarely recognized and never quantified.

Chapter 3: Experimental Methods

This chapter outlines the experimental methods and apparatuses used in this work for quantifying the behavior of K^+/PZ mixtures, including discussions on data analysis and limitations. A wetted-wall column was used to measure the equilibrium partial pressure of CO_2 and the rate of CO_2 absorption. Nuclear magnetic resonance spectroscopy was used to measure PZ speciation in the presence of CO_2. Measurements of density, viscosity, physical CO_2 solubility, and solid solubility were also performed. The methods for determining these properties are presented.

3.1. Wetted-Wall Column

A wetted-wall column was used for all vapor-liquid equilibrium and CO_2 absorption rate experiments in this work. The apparatus was originally built by Mshewa (1995) and has been used in several recent investigations including Pacheco (1998), Bishnoi (2000), Dang (2001), and Cullinane (2002).

3.1.1. Equipment Description

The wetted-wall column, shown in Figure 3.1, consists of a stainless steel tube 9.1 cm long with a 1.26 cm outer diameter. The total contact area, 38.52 cm^2, is calculated as the longitudinal area of the tube, 36.03 cm^2, and the area of the top of the column (considered a hemisphere due to the shape of liquid film), 2.49 cm^2. The column is enclosed by a thick-walled glass cylinder with an outside diameter of 2.54 cm to provide the gas-liquid contact chamber. The hydraulic diameter (outer diameter minus inner diameter) of the enclosure is 0.44 cm, giving a cross-sectional area for gas flow of 1.30 cm^2. The chamber is housed inside a second thick-walled glass cylinder (10.16 cm OD) that serves as an insulating bath with circulating heat transfer fluid.
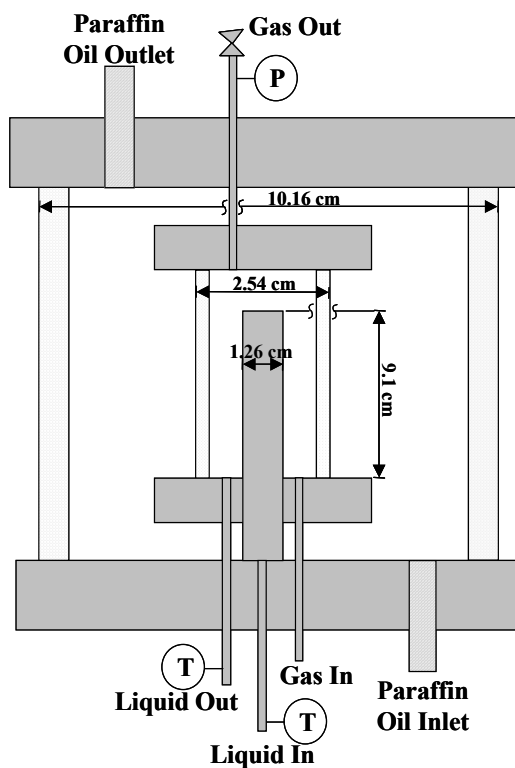
Figure 3.1. Diagram of the Wetted-Wall Column Construction

A representation of the full experimental setup is shown in Figure 3.2. The liquid solution was contained in a reservoir (a series of modified calorimetric bombs) with a total volume of 1,400 cm^3. The fluid was pushed from the reservoir to the gas-liquid contact chamber. The fluid flowed up through the middle of the column, overflowed at the top, and evenly distributed on the outer surface of the column. The liquid was collected at the bottom of the column and pumped back to the solution reservoir. A liquid rotameter indicated the volumetric flowrate of the liquid. It was calibrated with water, giving the following equations:

$$Q_{w,T_{ref}} \left(cm^3/s \right) = 0.4512x - 0.2901, \tag{3.1}$$

$$Q_{sol,T_{ref}} \left(cm^3/s \right) = Q_{w,T_{ref}} \sqrt{\frac{(7.83 - \rho_{T_{ref}})}{(7.83 - 0.997)\rho_{T_{ref}}}}, \tag{3.2}$$

and

$$Q_{sol} \left(cm^3/s \right) = Q_{sol,T_{ref}} \sqrt{\frac{7.83 - \rho^2}{7.83 - \rho_{T_{ref}}^2}}, \tag{3.3}$$

where Q_w is the volumetric flowrate of water, Q_{sol} is the volumetric flowrate of the solution, ρ is the density of the solution in g/cm^3, and x is the rotameter reading. The value of 7.83 represents the density of the rotameter float. The subscript T_{ref} refers to the value at a standard temperature of 25°C. The liquid temperature was measured at the inlet and outlet of the contactor by Type-J thermocouples ($\pm$ 2.2^{o}C).
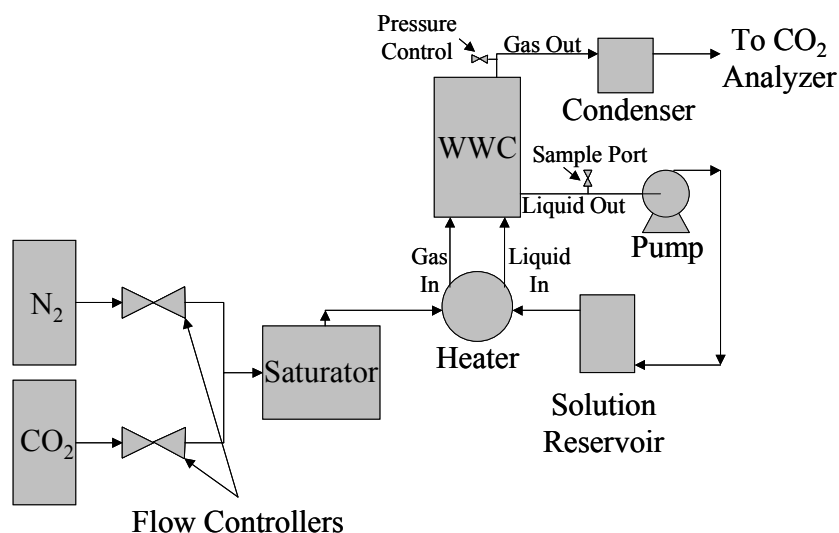
Figure 3.2. Flowsheet of the Wetted-Wall Column Experiment

Nitrogen and CO_2 were contained in cylinders and the flowrate was governed by Brooks mass flow controllers. For N_2, a 20 SLPM controller (S/N 8708HCO33980) was used. For CO_2, three controllers were available: 250 SCCM (S/N 9310HCO38404/2), 1 SLPM (S/N 8707HCO33415), and 2 SLPM (S/N 9310HCO38406/2). Two cylinders of CO_2 (one > 99% pure and the other 5000 ppm$_v$) were also used, providing additional flexibility in selecting gas rates and concentrations. The metered gases were mixed and saturated with water at the operating temperature of the column in a sealed vessel immersed in a heat bath. The water depth in the saturation vessel was generally greater than 5 in. For experiments at high temperatures (> 100°C), two vessels were used in series, each containing approximately 5 in. of water.

After saturation, the gas was introduced to the bottom of the column through a 1/8 in. tube. It subsequently flowed counter-currently past the liquid film. The gas exited the top of the column through 1/8 in. tubing and was routed to a condenser. The

condenser was constructed from a 1 L Erlenmeyer flask submerged in an ice bath. The gas entered and exited at the top of the condenser while the condensing water was allowed to settle at the bottom of the flask. Much of the gas was vented from a valve on the condenser to reduce load on downstream components. Approximately 1 L/min of the gas was sent to a drying column containing magnesium perchlorate to remove excess moisture. The dry gas was then sent to a gas analyzer for composition determination. Pressure in the column was controlled by a needle valve on the gas outlet tubing. An analog pressure gauge (Matheson, P/N 63-3122) was used to monitor pressures between 35 and 55 psig ($\pm$ 2 psig).

3.1.2. Gas Analysis

The concentration of CO_2 in the outlet gas was measured by Horiba PIR-2000 gas analyzers. The available range of the analyzers was adjustable, varying from 0.05 to 25 vol%, with an expected accuracy of 0.1% of full scale. The equipment uses IR spectroscopy to measure the amount of CO_2 in the gas phase. The analyzers were calibrated prior to each experiment by bypassing the wetted-wall column and adjusting the CO_2 flowrate in the feed gas to give known concentrations. A chart recorder was used during the calibrations and experiments to record the response of the analyzers. Readings from the recorder are expected to be accurate to 0.2% of full scale.

3.1.3. Liquid Analysis

During each experiment, liquid samples were taken from the wetted-wall column so that a liquid CO_2 concentration could be determined. The samples were withdrawn from a septum on the liquid outlet tubing by a 150 μL syringe. The samples

were diluted; generally, 100 µL of sample was placed in 5 mL DI H_2O. For analysis, the diluted samples were injected into 30 wt% H_3PO_4 sparged with nitrogen. The acid liberated all inorganic carbon from the solution and the nitrogen sweep gas (~ 0.5 L/min) carried the gas phase to the Horiba PIR-2000 gas analyzer (range 0.05 vol%). The gas stream was passed through a drying column of magnesium perchlorate prior to entering the analyzers.

This method was calibrated prior to each use by injecting several known volumes of 7 mM Na_2CO_3. Generally, volumes of 50, 100, 150, and 200 µL were used to obtain a calibration curve for the analyzer response. During the calibration and the experiments, the response was recorded on a chart recorder. Because sharp peaks are obtained, the peak height, and not peak area, was assumed to be representative of the CO_2 concentration.

3.1.4. Physical Mass Transfer Coefficients

3.1.4.1. Gas Film Mass Transfer Coefficient

The gas film mass transfer coefficient, k_g, in the wetted-wall column was determined by Bishnoi (2000) using SO_2 absorption into 0.1 M NaOH. The results of these experiments are correlated with a form for k_g proposed by Hobler (1966).

$$Sh = 1.075 \left(ReSc \frac{d}{h} \right)^{0.85} \qquad (3.4)$$

The Reynolds number is defined as

$$Re = \frac{u\rho d}{\mu}, \qquad (3.5)$$

where u is the linear velocity of the gas, ρ is the density, and μ is the viscosity. Also, d is the hydraulic diameter of the annulus (0.44 cm) and h is the height of the wetted-wall column (9.1 cm). The Schmidt number is

$$Sc = \frac{\mu}{\rho D_{CO_2}}.$$

(3.6)

D_{CO_2} is the diffusion coefficient of CO_2. The gas film transfer coefficient can be found from the following definition of the Sherwood number.

$$Sh = \frac{RT k_g h}{D_{CO_2}}$$

(3.7)

where T is the temperature and R is the gas constant.

Experiments in the wetted-wall column were run with high gas rates (5 to 7 L/min) to minimize the gas film resistance to mass transfer. Most data points had 20 to 50% gas film resistance. Figure 3.3 shows k_g as a function of gas flowrates.

3.1.4.2. Liquid Film Mass Transfer Coefficient

Mshewa (1995) and Pacheco (1998) determined the liquid film mass transfer coefficient, k_l^o, of the wetted-wall column by CO_2 desorption from water and ethylene glycol. Mshewa originally used a theoretical prediction of k_l^o based on work from Vivian and Peaceman (1956). Pacheco determined that additional data and an expanded correlation were needed to accommodate varying experimental conditions. This correlation was developed from falling-film theory developed by Pigford (1941) using a momentum balance as presented by Bird *et al.* (1960).

57
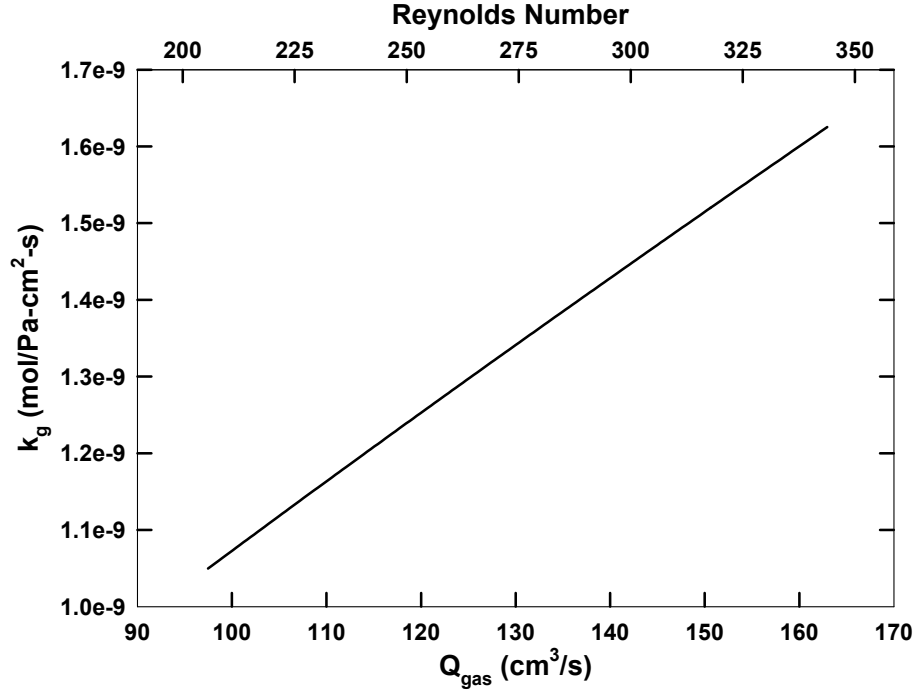
Figure 3.3. Gas Film Resistance as a Function of Gas Flowrate at 60°C with N₂ Saturated to Water

From the parabolic velocity profile resulting from the momentum balance, a representation of k_l^o can be obtained. Pacheco (1998) chose a form of the expression given by Hobler (1966),

$$k_l^o = \frac{Q_{sol}}{A}\left(1 - \Theta\right),$$
(3.8)

where A is the contact area of mass transfer and Θ represents a dimensionless driving force of the diffusing gas in the liquid film, calculated as follows:

$$\Theta = \frac{[CO_2]_i - [CO_2]_o^{out}}{[CO_2]_i - [CO_2]_o^{in}} = 0.7857\exp(-5.121\eta) + 0.1001\exp(-39.21\eta) +$$
$$0.036\exp(-105.6\eta) + 0.0181\exp(-204.7\eta), \quad \text{for } \eta > 0.01$$

$$(3.9)$$

or

$$\Theta = 1 - 3\sqrt{\frac{\eta}{\pi}}, \quad \text{for } \eta < 0.01, \qquad (3.10)$$

where $[CO_2]_o^{in}$ and $[CO_2]_o^{out}$ represent the concentration of CO_2 in the bulk liquid at the inlet and outlet of the wetted-wall column, respectively, and $[CO_2]_i$ is the concentration of CO_2 at the gas-liquid interface. η is a dimensionless penetration distance defined as

$$\eta = \frac{D_{CO_2}\tau}{\delta^2}, \qquad (3.11)$$

and τ is the surface contact time, defined as

$$\tau = \frac{h}{u_s}. \qquad (3.12)$$

The height of the wetted-wall column is represented by h.

The film thickness, δ, is given by

$$\delta = \sqrt[3]{\frac{3\mu Q_{sol}}{\rho g W}}, \qquad (3.13)$$

where μ is the liquid viscosity, Q is the volumetric flowrate of the liquid, ρ is the liquid density, g is the gravity constant, and W is the circumference of the column. A liquid surface velocity, u_s, is given by

59

$$u_s = \frac{\rho g \delta^2}{2\mu} .$$
(3.14)

Most experiments in the wetted-wall column were run so that k_l^o was between 0.007 and 0.014 cm/s.

3.1.5. Interpretation of Experimental Measurements

Several data points were collected during each experiment at various bulk gas partial pressures. The flux of CO_2 into or out of the solution can be characterized by the overall gas phase mass transfer coefficient.

$$N_{CO_2} = K_G \left(P_{CO_2,b} - P_{CO_2}^* \right)$$
(3.15)

The mass transfer coefficient, K_G, is calculated as the slope of the flux versus the log mean pressure, P_{lm}. The P_{lm} is defined as a log mean average of bulk gas partial pressures of CO_2 across the wetted-wall column and is assumed representative of $P_{CO_2,b}$.

$$P_{lm} = \frac{P_{CO_2,in} - P_{CO_2,out}}{\ln \left(P_{CO_2,in} / P_{CO_2,out} \right)}$$
(3.16)

The equilibrium partial pressure, $P_{CO_2}^*$, can be found by considering points close to equilibrium and interpolating to a flux of 0.0, a technique initiated by Critchfield (1988). A demonstration of this procedure is shown in Figure 3.4.

An expression of the liquid film resistance, which includes the kinetics of CO_2 absorption, can be written as

$$N_{CO_2} = k_g' \left(P_{CO_2,i} - P_{CO_2}^* \right),$$
(3.17)

60

where k_g' is a normalized flux, a mass transfer coefficient for the partial pressure driving force across the liquid film. The normalized flux was calculated from the following expression.

$$k_g' = \left(\frac{1}{K_G} - \frac{1}{k_g} \right)^{-1}$$

(3.18)

For CO_2 absorption by amines, chemical reaction effects typically dominate the physical mass transfer inside the liquid film; therefore, k_g' can be related to the rate of CO_2 absorption as well as the kinetics of the absorption process.
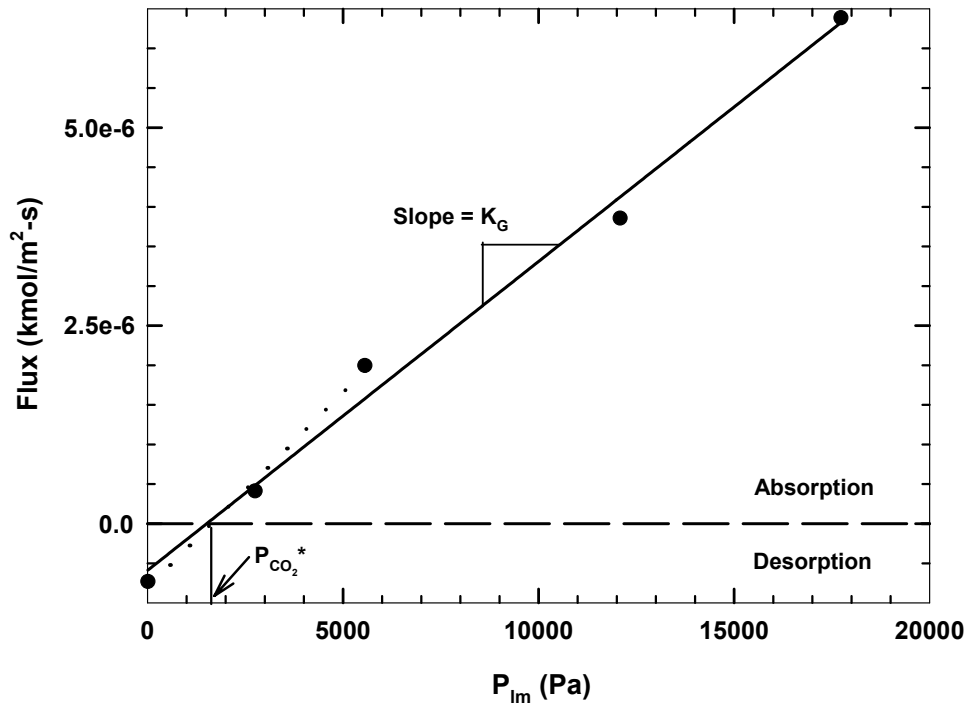
Figure 3.4. Graphical Representation of Determining $P_{CO_2}^*$ and K_G for 3.6 m K^+/0.6 m PZ at 40°C and Loading = 0.693 mol CO_2/(mol K^+ + mol PZ)

61

3.2. Nuclear Magnetic Resonance Spectroscopy

Proton nuclear magnetic resonance (^{1}H NMR) spectroscopy was used to determine the equilibrium distribution of piperazine species in the liquid phase. A Varion INOVA 500 NMR was used for the measurements. The machine has a field strength of 500 MHz and is capable of variable temperature work.

Samples were made with K_2CO_3, $KHCO_3$, PZ and water. Approximately 20% of the water was replaced with D_2O (heavy water). One drop of 2,2-dimethyl-2-silapentane-5-sulfonic acid (DSS) in D_2O was added to each sample to maintain a constant chemical shift reference. After all components were dissolved with mild heating, the samples were placed in Wilmad 507-PP NMR tubes. A slight vacuum was applied and the tube was permanently sealed by a simple glass blowing technique.

Bishnoi (2000) assigned the proton peaks for PZ based on their correlation to the carbon-13 spectrum. The chemical shifts vary somewhat with loading and solvent conditions, but the distinctiveness of the peaks allows easy identification based solely on the ^{1}H spectrum. A typical spectrum is shown in Figure 3.5. The PZ/PZH$^+$ and PZ(COO$^-$)$_2$ peaks show up as single peaks near 2.9 and 3.2 ppm respectively. PZCOO$^-$ and H$^+$PZCOO$^-$ are represented by two triplet peaks centered near 2.8 and 3.3; the sum of the two triplets gives the total carbamate concentration.
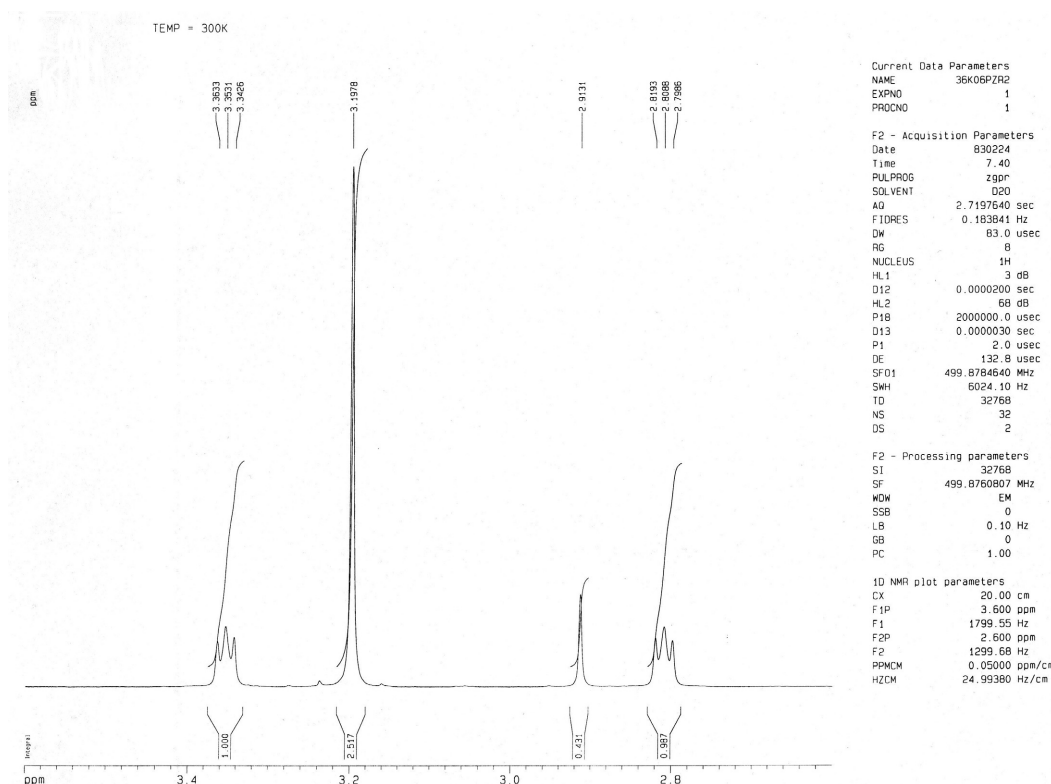
Figure 3.5. Proton NMR Spectrum of 3.6 m K$^+$/0.6 m PZ, Loading = 0.630 mol CO$_2$/(mol K$^+$ + mol PZ), 27°C

One major limitation of ^{1}H NMR as applied in this work is its inability to distinguish between some chemical species that are in equilibrium. This is related to the field strength of the machine and the velocity of the equilibrium exchange. For example, the 500 MHz machine used in this work has an inherent time scale of 2×10^9 s (1/500 MHz). Any two species whose equilibrium occurs at a faster rate will be indistinguishable. Therefore, in this work, protonated and un-protonated forms of PZ can not be measured independently; all peaks, in this case, represent the sum of the two species. This condition also imposes a temperature limit. At temperatures near 60°C, the velocities of the carbamate equilibria become sufficiently fast as to blur previously

63

well-defined peaks. Compare Figure 3.5 and Figure 3.6, the same solution measured at 27 and 60°C, for a demonstration of peak broadening. In some cases, the severity of the peak broadening renders the measurement useless for quantitative interpretations. Nearly all data points collected in this work are at or below 60°C.
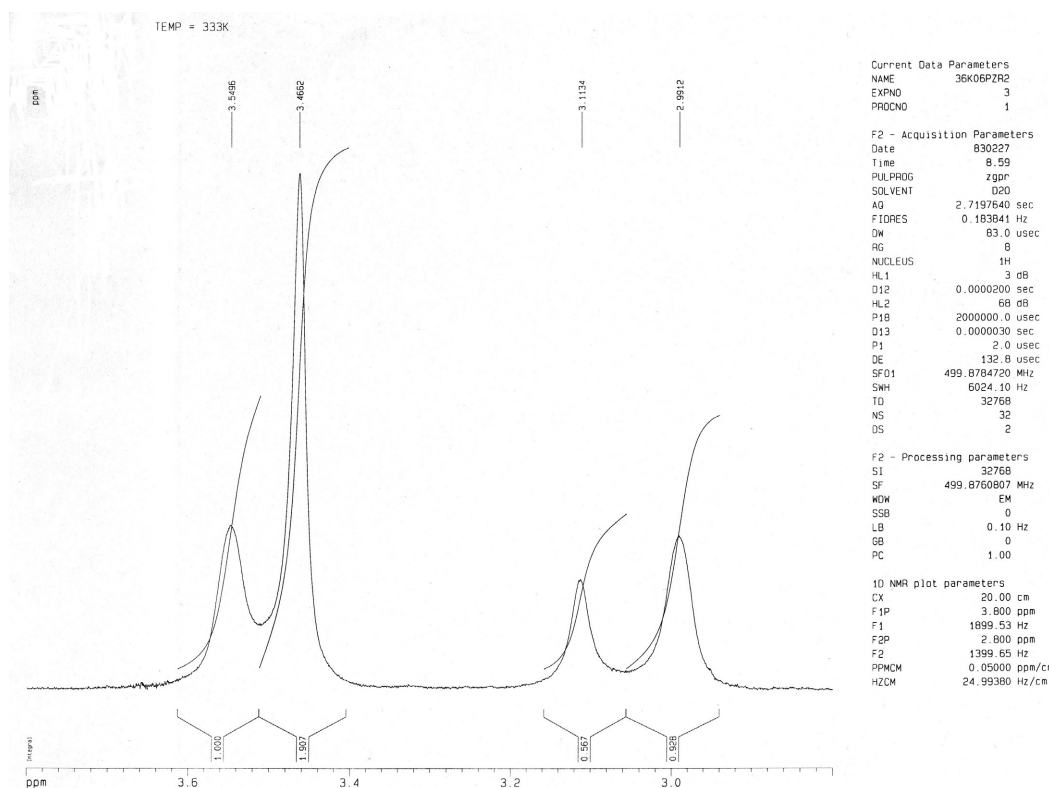
Figure 3.6. Proton NMR Spectrum of 3.6 m K$^+$/0.6 m PZ, Loading = 0.630 mol CO$_2$/(mol K$^+$ + mol PZ), 60°C

3.3. Solid Solubility

Both piperazine and potassium carbonate are solids at their standard state conditions. Because the imposition of solid solubility restricts the total solvent concentration, quantification of the limits are required to identify viable commercial

64

solvent formulations and provide additional thermodynamic information for concentrated mixtures.

Approximately 100 g of concentrated K^+ and PZ was prepared so that a precipitate would form. The solutions were immersed in a constant temperature bath and stirred with a magnetic stir plate for at least 12 hours to ensure solid-liquid equilibrium. Once equilibrium was achieved, a 10 mL sample of the saturated liquid was removed by pipette and placed in a beaker. The sample was titrated with 2 N HCl to an endpoint indicated by methyl orange pH indicator (range 3.0 to 4.4). The solution was then briefly boiled, driving off dissolved CO_2. A base titration was done, using 2 N NaOH, to an endpoint of -265 mV as indicated by a pH meter. This voltage reading was found to correspond roughly to the endpoint of pH 11 in the concentrated solutions.

The acid titration gives the total alkalinity of the sample. The base titration gives the equivalents of PZ in solution. (CO_2 was boiled off so that no bicarbonate or carbonate formed during the base titration.) So, the resulting calculations may be made for a sample of fixed volume.

$$mol\ acid\ =\ mol\ K^+\ +\ 2 \cdot mol\ PZ \qquad (3.19)$$

$$mol\ base\ =\ 2 \cdot mol\ PZ \qquad (3.20)$$

A small liquid sample was collected and analyzed for loading as described previously in Section 3.1.3.

3.4. Physical Properties

3.4.1. Density

The density of K^+/PZ mixtures was measured with a Mettler/Paar #DMA46 Digital Density meter. The measurement is based on the principle that a resonating frequency in an object is inversely proportional to the square root of mass.

$$f \propto \frac{1}{\sqrt{m}} \tag{3.21}$$

A fixed volume of solution is injected into the apparatus and a frequency of vibration is measured. From the estimated mass, the density is calculated.

The instrument was calibrated with air and water, giving constants for the density calculation of the form

$$a = \frac{T^2_{water} - T^2_{air}}{\rho_{water} - \rho_{air}}, \tag{3.22}$$

and

$$b = T^2_{water} - a\rho_{water}, \tag{3.23}$$

where T is the measured period of oscillation. Density of the unknown is calculated as

$$\rho = \frac{T^2 - b}{a}. \tag{3.24}$$

Densities of aqueous K^+/PZ mixtures were measured at 25 and 40°C. Density is reported to ± 0.001 g/cm³. The results of the experiments are recorded in Appendix A. It was determined that the amine had little effect on density over the range of soluble concentrations; this effect has also been observed with other amines (Weiland *et al.*,

1998). A small dependence on temperature and loading was also observed, but the main contribution to density was the salt concentration (K_2CO_3/$KHCO_3$). The measured density compares well with the measurements of K_2CO_3 solutions by Hitchcock and McIlhenny (1935).

An empirical representation of density was derived for use in calculations. The expression was used in all calculations involving density in this work. Model predictions are compared to the experimental data in the previous tables.

$$\rho\left(\frac{g}{cm^3}\right) = 1.130 + 0.0537\left[K^+\right] - 1.204 \times 10^{-3}\left[K^+\right]^2 + 1.882 \times 10^{-3}\left[PZ\right]$$
$$- 0.442 \times 10^{-3}T + 9.010 \times 10^{-3}\alpha$$

(3.25)

where [i] is the concentration of species i in molal, T is temperature in Kelvin, and α is the loading in mol CO_2/(mol K^+ + mol PZ).

3.4.2. Viscosity

An extensive collection of data exists quantifying the viscosity of aqueous electrolyte solutions, including K_2CO_3 (Bates and Baxter, 1929; Hitchcock and McIlhenny, 1935; Bocard and Mayland, 1962; Goncalves and Kestin, 1981; Moniuk and Pohorecki, 1991; Vazquez *et al*., 1994). The data sets include a wide variety of conditions (0 to 7.5 m K_2CO_3 and 0 to 2.0 m $KHCO_3$ at 20 to 60°C).

Though data are available, correlating the viscosity of electrolyte solutions can be considerably difficult as fluid properties vary widely with composition and temperature. Some authors use complex group contribution methods or matrix

calculations to express density. The most convenient method of correlating viscosity, however, is by an empirical expression. The simplest form representing the data is

$$\ln \mu = \ln \mu_w + C_1 [Salt],$$ (3.26)

where μ represents the dynamic viscosity in the mixture, μ_w is the dynamic viscosity of water, and C_1 is a constant for specific salts (Moniuk and Pohorecki, 1991; Vazquez *et al.*, 1994).

The viscosity of aqueous organic mixtures has also been studied in detail. Cook and Lowe (1976) report the viscosity of aqueous PZ in dilute solutions (< 0.2 m PZ) and represent the data in the following empirical form.

$$\mu = \mu_w + C_1 [Am] + C_2 [Am]^2$$ (3.27)

No studies of aqueous electrolyte-organic mixtures could be found in the literature; therefore, the viscosity of K^+/PZ mixtures at conditions encountered in this work was measured in a routine Cannon-Fenske viscometer (Cannon Instrument Co., No. 100, 3–15 cSt). The measurements are based on fluid flow through a capillary tube, which is directly related to fluid viscosity.

A representation of the viscometer is shown in Figure 3.7. The viscometer was placed in a water bath to maintain the desired temperature. A sample of a set volume was placed in section A. The fluid was drawn up to point B in the viscometer by a suction bulb. The time of the meniscus moving from point B to C was measured by a stopwatch.
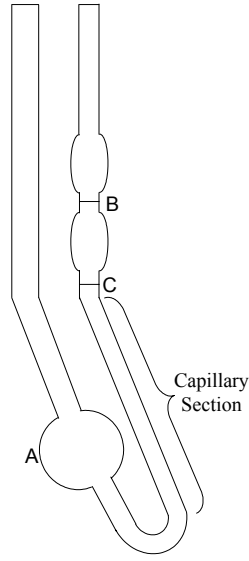
Figure 3.7. Cannon-Fenske Viscometer

Viscosity, in mPa-s (or cP), is related to time by

$$\mu = \beta \rho t,$$ (3.28)

where β is the viscometer constant determined through calibrations in cSt/s (or mm^2/s^2), ρ is the solution density in g/cm^3, and t is the measured time in seconds. The instrument was calibrated with water at 25, 40, 60 and 70°C. A constant solution volume of 7 mL was used during calibration and measurement.

The results of the viscosity experiments are given in Appendix A. An empirical representation, based on a combination of the expressions for aqueous salts and aqueous PZ, was derived from the data. The regressed constants are reported in Table 3.1.

$$\mu = \left(\mu_w^{A_0+1} \exp\left(B\left[K^+\right] + C\alpha^2 \right) + De^{E/T}\left[PZ\right] + Fe^{G/T}\left[PZ\right]^2 \right) \times$$
$$\left(1 + H\left[K^+\right]\left[PZ\right] + I\frac{\left[K^+\right]\left[PZ\right]}{T} \right)$$ (3.29)

69

where

$$A_0 = A_1 \left[K^+ \right] + A_2 \left[K^+ \right]^2 , \qquad (3.30)$$

[i] represents the concentration of species i in molal, T is the temperature in Kelvin, and α is loading as mol CO_2/(mol K^+ + mol PZ). The viscosity is given in cP.

The viscosity of water is well known. The expression here was derived from data found in CRC (2000).

$$\ln \mu_w = -46.288 + \frac{3703.7}{T} + 5.924 \ln T \qquad (3.31)$$

Table 3.1. Coefficients for Empirical Viscosity Model

A_1	-0.021
A_2	2.79E-03
B	0.153
C	-0.020
D	2.00E-05
E	2943.4
F	2.43E-08
G	4076.7
H	-0.082
I	35.24

3.4.3. Physical Solubility

The physical solubility of CO_2 in solution is an important parameter for defining concentrations in the liquid phase. Because CO_2 reacts quickly with amines and carbonate, a true physical solubility can not be determined. Clarke (1964), based on the work of Amdur *et al*. (1952), proposed that N_2O, a molecule with the same molecular weight and a similar electrical configuration, could be used as a representation of CO_2

behavior in reactive systems. The assumption for the N_2O analogy is that the ratio of CO_2 to N_2O solubility is constant for all systems.

$$\frac{H_{CO_2}}{H_{N_2O}} = \text{constant} \tag{3.32}$$

Given this relation, the solubility of N_2O can be measured in amine solutions and a solubility of CO_2 can be approximated by relating the ratio to that in water. That is

$$H_{CO_2,Am} = H_{N_2O,Am} \left(\frac{H_{CO_2,w}}{H_{N_2O,w}} \right). \tag{3.33}$$

The Henry's constants for CO_2 and N_2O in water were correlated by Versteeg and van Swaaij (1988b).

$$H_{CO_2,w} \left(\frac{mol}{L \cdot Pa} \right) = 3.54 \times 10^{-4} \exp\left(\frac{2044}{T(K)} \right) \tag{3.34}$$

$$H_{N_2O,w} \left(\frac{mol}{L \cdot Pa} \right) = 1.17 \times 10^{-4} \exp\left(\frac{2284}{T(K)} \right) \tag{3.35}$$

The physical solubility of N_2O in K^+/PZ mixtures was determined using the apparatus depicted in Figure 3.8. The apparatus was built by Al-Jauied (2004) and is similar to that used in the work of Al-Ghawas (1989) to determine the physical solubility of N_2O in amines. The apparatus consisted of a sample cell (~250 mL), a gas washing bottle, a manometer, and a mercury reservoir of adjustable height. The entire apparatus, except for the mercury reservoir, was immersed in a constant temperature bath.
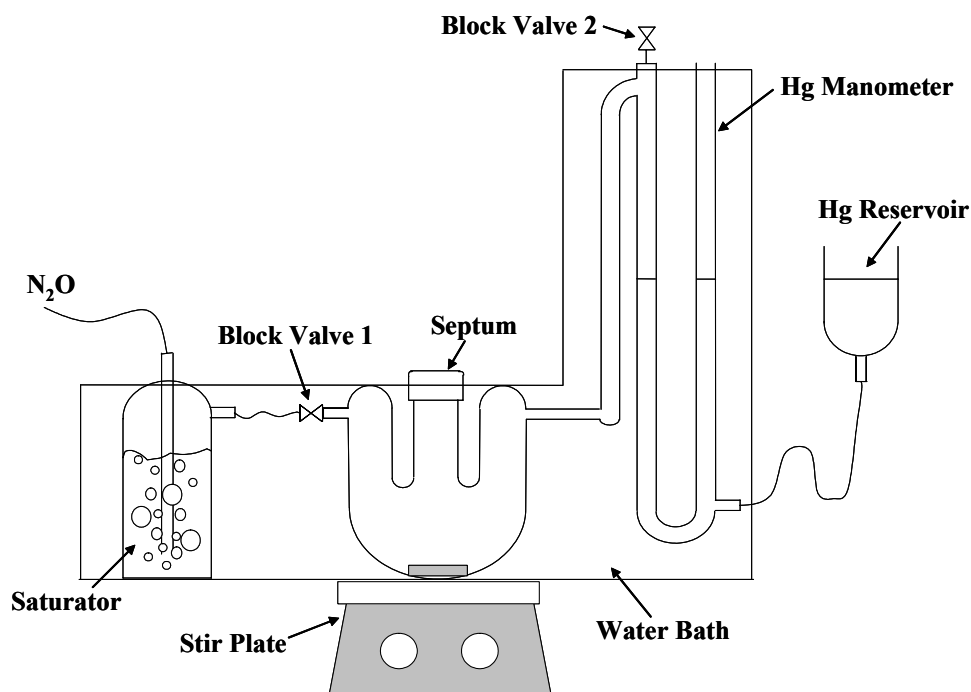
Figure 3.8. Apparatus for Physical Solubility Measurements

To measure the solubility of N_2O in a sample, the empty sample cell was flushed with N_2O for approximately 20 minutes. The N_2O gas was sparged through water in the gas washing bottle, saturating the gas at the desired operating temperature prior to entering the sample cell. The flow of N_2O was stopped; block valves on the inlet and outlet of the apparatus trapped the gas inside the sample cell.

A sample of known volume and mass was injected into the cell and the corresponding volume change was monitored on the manometer. The sample was degassed using a vacuum pump prior to injection. The height of the mercury reservoir was adjusted to maintain atmospheric pressure inside the system. The solution was stirred and allowed to equilibrate for approximately one hour. The volume change, as

indicated by the manometer, minus the volume of liquid injected gave the volume (solubility) of N_2O in the sample at equilibrium. The solubility of CO_2 was calculated using the analogy described previously.

3.4.4. Diffusion Coefficient

3.4.4.1. Diffusion of CO_2

The diffusion coefficient of CO_2 in solution was also estimated by the N_2O analogy. This method has been used previously in several studies on CO_2 absorption by amines and is similar to the analogy presented for physical solubility. The diffusivity of CO_2 and N_2O in water were determined by Versteeg and van Swaaij (1988b) and Tamimi *et al.* (1994a, 1994b). The data were correlated by Pacheco (1998) and are given by the following expressions.

$$D_{CO_2,w}\left(cm^2/s\right) = 0.02397 \exp\left(\frac{-2122.2}{T(K)}\right) \tag{3.36}$$

$$D_{N_2O,w}\left(cm^2/s\right) = 0.04041 \exp\left(\frac{-2288.4}{T(K)}\right) \tag{3.37}$$

D_{N_2O} in amines was correlated to viscosity and temperature by Pacheco (1998).

$$D_{N_2O,Am}\left(cm^2/s\right) = 5.533 \times 10^{-8} \frac{T(K)}{\mu(cP)^{0.545}} \tag{3.38}$$

The ratio of D_{CO_2} to D_{N_2O} is assumed to be constant; therefore, the diffusivity of CO_2 in amine solutions is estimated by

$$D_{CO_2,Am} = D_{N_2O,Am} \frac{D_{CO_2,w}}{D_{N_2O,w}}. \tag{3.39}$$

73

3.4.4.2. Diffusion of Amines and Ions

For fast kinetics, the diffusion of the amine and products to and from the gas-liquid interface may limit the overall reaction rate. Additionally, it defines, under high fluxes, concentration gradients existing in the boundary layer. It is important, therefore, to obtain an accurate prediction of the diffusion coefficient of the organic and ionic components in aqueous solution.

In the simplest form, the diffusion of molecules can be described by the Stokes-Einstein relation. It has been shown that, at infinite dilution, the diffusion coefficient of the amine is related to the molar volume of the solute. A more sophisticated model, the Wilke-Chang correlation (Wilke and Chang, 1955), was used in this work, giving the diffusion coefficient as a function of solvent viscosity, temperature, and solvent specific parameters.

$$D_{Am}^{\infty} = \frac{1.17 \times 10^{-13} \left(\xi_{sol} MW_{sol} \right)^{0.5} T}{V_{Am}^{0.6} \mu_{sol}} \tag{3.40}$$

where ∞ denotes the diffusion coefficient of the amine at infinite dilution in water, V indicates molar volume, MW_{sol} is the molecular weight of the solvent, and ξ_{sol} represents the solvent specific parameter (2.6 for water).

The Wilke-Chang correlation predicts the diffusion coefficient of amines and other organic molecules, such as carboxylic acids, to within 10% (Albery *et al*., 1967; van der Wielen *et al*., 1997; Schramke *et al*., 1999). Predictions also match the experimentally determined diffusion coefficient of piperidine, a six-membered ring structure with only one nitrogen (Barradas *et al*., 1971). It is also reported that little

difference is realized in mobility between neutral, mono-, and di-valent ions; therefore, the diffusivities of protonated species can be assumed to be equal to their un-protonated counterparts (van der Wielen, 1997). Given the numerous sources verifying the ability of Wilke-Chang to estimate the diffusion coefficient of organics, ions, and specifically amines, it is assumed a reasonable estimate will be obtained for species in this work.

The diffusion coefficient of PZ was estimated using a molar volume of 0.1052 m^3/kmol predicted from the group contribution method of Le Bas (1915). Because the absorption rate model (Section 4.2) requires a charge balance, the diffusion coefficients of all ions must be assumed equal. An average value for all ionic species was estimated by setting all diffusion coefficients equal to that of $PZCOO^-$. The molar volume of $PZCOO^-$ is predicted to be 0.1311 m^3/kmol (Le Bas, 1915). For comparison, the molar volume of $PZ(COO^-)_2$ is 0.1570 m^3/kmol. By assuming $PZCOO^-$ is representative of the molar volume for all species, differences in D_{Am}^∞ of approximately 10% are expected from the true value of PZH^+ and $PZ(COO^-)_2$.

The extrapolation of D^∞ to higher concentrations has been determined to be dependent on the specific solute-solvent interaction. In general, the diffusion coefficient of amines can be related to D^∞ and viscosity by

$$D_{Am} = D_{Am}^\infty \left(\frac{\eta_w}{\eta_{Am}} \right)^{0.6} \tag{3.41}$$

(Campbell and Lam, 1973; Snijder *et al.*, 1993; Hikita *et al.*, 1981; Albery *et al.*, 1967; van der Wielen, 1997).

3.5. Chemicals and Materials

The potassium carbonate [584-08-7] and potassium bicarbonate [298-14-6] used in this work were obtained from Fisher and were 100% and 99.9% pure, respectively. Anhydrous piperazine [110-85-0] (>99%,) was purchased from Sigma-Aldrich. Solution loading was varied by adjusting the carbonate and bicarbonate content while maintaining a constant K^+ concentration. The reported K^+ molality is reported referenced to K_2CO_3.

Deuterium oxide (D_2O) [7789-20-0], 99.9%, used in the NMR experiments was obtained from Cambridge Isotope Laboratories, Inc. The HCl [7647-01-0] used in pH titrations was purchased from Fisher as certified 2.005-1.995 N. The NaOH [1310-73-2] was also purchased from Fisher and certified as 2.02-1.98 N.

Nitrogen [7727-37-9] used in all experiments was >99% pure and was supplied by the Department of Physics at The University of Texas at Austin. Carbon dioxide (>99% pure) [124-38-9] was purchased from Matheson Tri-gas. The 5000 ppm_v CO_2 was purchased from Praxair. N_2O [10024-97-2] used in solubility experiments was purchased from Air Liquide and was >99% pure.

Chapter 4: Thermodynamic and Rate Models

This chapter presents a basic description of models used in this work. A rigorous thermodynamic model was created to predict equilibrium in mixed K^+/PZ solutions. It is an excess Gibbs energy model based on electrolyte non-random two-liquid (ENRTL) theory. A rigorous kinetic code is applied to modeling the absorption rate of CO_2 into the mixed solvent. The model accounts for both diffusion and reaction in a gas-liquid interface using the eddy diffusivity theory with the appropriate reversible reactions. Both models are stand-alone programs written in FORTRAN. A non-linear regression program, GREG, enables the finding of unknown parameters within the models. Its incorporation into the work is also discussed.

4.1. Thermodynamics Model

4.1.1. Introduction

One major focus in this work is the development of an equilibrium representation of a complex chemical solution in a closed system. For K^+/PZ mixtures, several reactions can be written to define the equilibrium of the liquid and vapor phases (Equations (4.1) to (4.9)). Because the species in solution react, the equilibrium concentrations of each depend on the nominal solution composition of parent species (e.g. PZ, CO_2) and temperature.

$$CO_2(g) \rightleftharpoons CO_2(aq) \tag{4.1}$$

$$H_2O(g) \rightleftharpoons H_2O(aq) \tag{4.2}$$

$$CO_2(aq) + 2 \cdot H_2O \rightleftharpoons HCO_3^- + H_3O^+ \tag{4.3}$$

$$HCO_3^- + H_2O \rightleftharpoons CO_3^{2-} + H_3O^+ \tag{4.4}$$

$$2 \cdot H_2O \rightleftharpoons H_3O^+ + OH^- \tag{4.5}$$

$$PZH^+ + H_2O \rightleftharpoons PZ(l) + H_3O^+ \tag{4.6}$$

$$PZ(l) + CO_2(aq) + H_2O \rightleftharpoons PZCOO^- + H_3O^+ \tag{4.7}$$

$$H^+PZCOO^- + H_2O \rightleftharpoons PZCOO^- + H_3O^+ \tag{4.8}$$

$$PZCOO^- + CO_2 + H_2O \rightleftharpoons PZ(COO^-)_2 + H_3O^+ \tag{4.9}$$
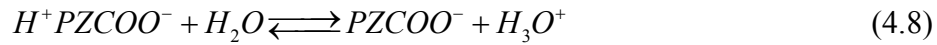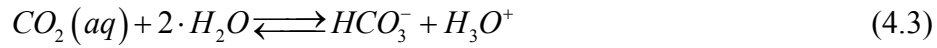
The problem becomes calculating the equilibrium compositions as defined by these reactions when the macroscopic properties of the mixture are known. The known

properties include total K^+ concentration, total PZ concentration, total CO_2 concentration, and temperature. In addition to the equilibrium set by the above reactions, non-idealities present in concentrated electrolyte solutions must be represented to arrive at a rigorous solution.

In this work, the problem is solved with a basic bubble point calculation. A complete picture of the liquid phase is obtained using an activity coefficient model with a minimization of Gibbs energy. The vapor phase is calculated from the liquid speciation and temperature using an equation of state. The equilibrium condition, activity coefficient model, and equation of state are described in the following sections.

4.1.2. Chemical Equilibrium and Excess Gibbs Energy

The problem of calculating the equilibrium composition of a reactive system requires a condition of equilibrium and specific information relating the components of the closed system. The general condition of phase equilibrium is given by an equality of fugacity, a representation of chemical behavior.

$$\hat{f}_i^\alpha = \hat{f}_i^\beta \qquad (4.10)$$

The Lewis/Randall rule defines the dependence of fugacity on concentration in an ideal solution as

$$\hat{f}_i^{ideal} = x_i f_i, \qquad (4.11)$$

where x_i is the mole fraction of species i. To the extent that a solution does not behave ideally, a correction can be introduced in the form of an activity coefficient, γ.

$$\gamma_i = \frac{\hat{f}_i}{\hat{f}_i^{ideal}} = \frac{\hat{f}_i}{x_i f_i} \qquad (4.12)$$

The condition of equilibrium stems from the definition of Gibbs energy, a measure of the chemical potential of the solution. By definition, the change in Gibbs energy for any irreversible process must proceed so that

$$dG^{Tot} \leq 0.$$
(4.13)

This inequality provides that, in a closed system at constant temperature and pressure, changes occur so that total Gibbs energy decreases. In other words, total Gibbs energy is minimized at the equilibrium condition. This constraint results in an equilibrium constant for each reaction in the closed system (Smith *et al.*, 1996).

$$K = \prod_i (\gamma_i x_i)^{\nu_i} = \exp\left(\frac{-\Delta G}{RT}\right)$$
(4.14)

While total Gibbs energy provides a general condition for equilibrium, it is more convenient to express liquid behavior in terms of excess Gibbs energy. Excess Gibbs energy represents a deviation from ideal behavior in liquid solution. Mathematically, this is a difference in the real and ideal chemical potential.

$$g_i^{ex} = g_i - g_i^{ideal}$$
(4.15)

where g_i is a partial molar Gibbs energy of species i related to the solution fugacity by

$$g_i = \chi_i + RT \ln \hat{f}_i,$$
(4.16)

where χ_i is an integration constant. Substituting this general expression for Gibbs energy into Equation (4.15) and applying the Lewis/Randall rule, the excess Gibbs energy is directly related to the activity coefficient by

$$g_i^{ex} = RT \ln \frac{\hat{f}_i}{x_i f_i} = RT \ln \gamma_i.$$
(4.17)

Most activity coefficient models, such as the ENRTL, rely on minimizing the excess Gibbs free energy of the system. So, the model must find the minimum of the Gibbs energy while satisfying defined equilibrium constants for each reaction. This provides that fluid behavior can be described at an ideal condition, normally infinite dilution in water, as defined by the equilibrium constants. Deviations from ideal behavior can be accounted for by an activity coefficient model.

4.1.3. Electrolyte NRTL Model

The rigorous thermodynamic model used in this work is based on the electrolyte non-random two-liquid (ENRTL) theory and was initially programmed by Austgen (1989) in his work on the thermodynamics of MEA and DEA in solution with MDEA. The model has been used since by Posey (1996) for MEA and DEA solutions and Bishnoi and Rochelle (2002b) for PZ/MDEA blends. This work extends the model to include potassium and piperazine.

An abbreviated description of the theory behind the ENRTL model and gas phase calculations is presented in the following sections. A more thorough discussion of the model theory, construction, and solution method can be found in Chen *et al*. (1982), Chen *et al*. (1986), Mock *et al*. (1986), Austgen (1989), and Glasscock (1990).

The ENRTL model was initially developed by Chen *et al*. (1982) as an extension to the existing theory for dilute electrolyte solutions. The ENRTL model predicts solution behavior of concentrated electrolytes beyond the applicable range of the Pitzer-Debye-Huckel model or other theoretical activity coefficient models. Since

its inception, the model has found widespread industrial use in simulations of gas treating processes (Chen and Mathias, 2002).

The ENRTL model spans both dilute and concentrated electrolyte solutions. It assumes that, in dilute solutions, molecules are far apart and the contribution to the excess Gibbs energy is dominated by long-range (LR) forces. The two contributions to long-range forces (PDH and Born) are discussed in Section 4.1.3.1. In concentrated solutions, molecules will be closely interacting with one another and the ENRTL model assumes a dominant contribution from short-range (SR) interactions as presented in Section 4.1.3.2. The total contribution to excess Gibbs free energy can be calculated as

$$\frac{g_i^{ex*}}{RT} = \frac{g_{LR,i}^{ex*}}{RT} + \frac{g_{SR,i}^{ex*}}{RT} = \left(\frac{g_{PDH,i}^{ex*}}{RT} + \frac{g_{Born,i}^{ex}}{RT} \right) + \frac{g_{NRTL,i}^{ex*}}{RT}, \tag{4.18}$$

or, from Equation (4.17),

$$\ln \gamma_i = \left(\ln \gamma_{PDH,i} + \ln \gamma_{Born,i} \right) + \ln \gamma_{NRTL,i}. \tag{4.19}$$

4.1.3.1. Long-Range Forces

Pitzer-Debye-Huckel Model

In dilute solutions (<1 M), excess Gibbs free energy is represented by the following theoretical relationship describing ionic interactions.

$$g_{PDH}^{ex*} = -RT \left(\sum_k x_k \right) \left(\frac{1000}{MW} \right)^{0.5} \left(\frac{4 A_\phi I_x}{\rho} \right) \ln\left(1 + \rho I_x^{0.5}\right) \tag{4.20}$$

where x is the mole fraction, MW is the molecular weight of the solvent, ρ is the parameter of closest approach, and I_x is the ionic strength defined in terms of mole fraction and charge, z.

$$I_x = \frac{1}{2}\sum_i x_i z_i^2 \tag{4.21}$$

The asterisk refers to the unsymmetric excess Gibbs free energy. The Debye-Huckel parameter, A_ϕ, can be found using N_o, Avogadro's number; ρ_s, solvent density; e, electron charge; D_s, dielectric constant of the solvent; and k, Boltzmann constant.

$$A_\phi = \frac{1}{3}\left(\frac{2\pi N_o \rho_s}{1000}\right)^{0.5}\left(\frac{e^2}{D_s kT}\right)^{1.5} \tag{4.22}$$

The solvent dielectric constant was calculated as

$$D_s = \sum_i x_i D_i \,, \tag{4.23}$$

where x_i is the mass fraction and D_i is the dielectric constant of species i. The dielectric constants of water and piperazine as used in this work are shown in Table 4.1.

Table 4.1. Dielectric Constants of Molecular Species in the ENRTL Model

Species	$D_i = A + B\left(\dfrac{1}{T(K)} - \dfrac{1}{273.15}\right)$		Source
	A	**B**	
Water	88.365	33030	Helgeson (1974) per Bishnoi (2000)
Piperazine[a]	4.719	1530	CRC (2000)

a. Assumed to be that of piperidine.

Born Equation

  In mixed solvents, the reference state for ions becomes confounded due to the changing dielectric constant. The Born equation was introduced to the long-range

contributions to Gibbs energy to maintain a reference state of infinite dilution in water for the ions. The correction is of the form

$$g_{Born}^{ex} = RT \left(\frac{e^2}{2kT} \right) \left(\sum_i \frac{x_i z_i^2}{r_i} \right) \left(\frac{1}{D_m} - \frac{1}{D_w} \right),$$

(4.24)

where D_m and D_w is the dielectric constant of the mixed solvent and water, respectively (Harned and Owen, 1958). This correction accounts for the difference in Gibbs energies between ions in a mixed solvent and in water.

4.1.3.2. Short-Range Forces (Non-Random Two-Liquid Model)

As the solutions become more concentrated, a term describing interactions between neutral and ionic species and neutral and neutral species becomes necessary. These interactions are described as local, or short-range forces.

Wilson (1964) derived an equation for excess free energy of mixed non-electrolytes. The basis for the derivation is a distribution of molecules, i and j, around a central molecule, i, given by

$$\frac{x_{ji}}{x_{ii}} = \frac{x_j \exp\left(-\frac{g_{ji}}{RT} \right)}{x_k \exp\left(-\frac{g_{ii}}{RT} \right)}.$$

(4.25)

Renon and Prausnitz (1968) reformulated the assumptions of Wilson into the non-random two-liquid (NRTL) model, arriving at a modification of the molecular distribution to account for "non-randomness" of mixing.

$$\frac{x_{ji}}{x_{ii}} = \frac{x_j \exp\left(-\alpha_{ij} \dfrac{g_{ji}}{RT}\right)}{x_i \exp\left(-\alpha_{ij} \dfrac{g_{ii}}{RT}\right)} \tag{4.26}$$

where α is an adjustable parameter. The authors continue by suggesting values for α ranging between 0.1 and 0.4, which depend on the molecules and solvent in the system. The addition of the non-randomness parameter, α, extends the applicability of the model to a wide variety of solutions.

Both the Wilson and NRTL model use an expression for the Gibbs free energy of mixing of the form

$$\frac{g^M}{RT} = \sum_i x_i \ln \xi_i \,, \tag{4.27}$$

where ξ is the volume fraction of i around a central molecule. The volume fraction is derived from the molecular distributions given above and can be written as

$$\xi_i = \frac{x_i V_i \exp\left(-\dfrac{g_{ij}}{RT}\right)}{\sum_j x_j V_j \exp\left(-\dfrac{g_{ij}}{RT}\right)} \,, \tag{4.28}$$

where V signifies the molar volume. The energy of mixing is related to the excess Gibbs energy by

$$\frac{g^{ex}}{RT} = \frac{g^M}{RT} - \sum_i x_i \ln x_i \,. \tag{4.29}$$

Chen *et al*. (1982, 1986) extended this equation to multi-component solutions of neutral and ionic species. Chen's extension of this model incorporates three distinct

cells, or groups of interacting ions and molecules as depicted in Figure 4.1, and makes two assumptions on the physical description of interacting species:

1. Two cells include a central cation, c, or a central anion, a, and assume like-ion repulsion. This means that the central ion is surrounded by molecules and oppositely charged ions.

2. One cell consists of a centrally located molecule, m, with local electroneutrality, meaning a time-average charge around the central molecule equals zero.
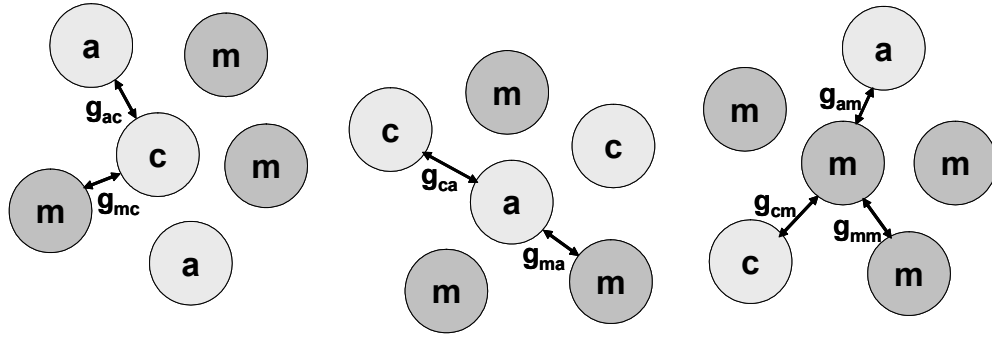
Figure 4.1. Distribution of Molecules as Cells in the Electrolyte NRTL Theory

Multiple interactions within cells can be defined as specific to two interacting species. In other words, the Gibbs energy contribution can be modeled as a function of binary interactions, defined as

$$\tau_{ji,ki} = \frac{g_{ji} - g_{ki}}{RT}.$$ (4.30)

A global model can therefore be constructed to account for the sum of species specific interactions within an average solution composition.

The excess Gibbs energy is predicted from the NRTL theory as

$$
\frac{g_{NRTL}^{ex}}{RT} = \sum_{m}\left(X_m \frac{\sum_{j} X_j G_{jm}\tau_{jm}}{\sum_{k} X_k G_{km}} \right) + \sum_{c} X_c \left(\sum_{a'}\left(\frac{X_{a'}\sum_{j} G_{jc,a'c}\tau_{jc,a'c}}{\sum_{a''} X_{a''}\sum_{k} X_k G_{kc,a'c}} \right) \right) +
$$
$$
\sum_{a} X_a \left(\sum_{c'}\left(\frac{X_{c'}\sum_{j} G_{ja,c'a}\tau_{ja,ca}}{\sum_{c''} X_{c''}\sum_{k} X_k G_{ka,c'a}} \right) \right) \qquad (4.31)
$$

where

$$
G_{cm} = \frac{\sum_{a} X_a G_{ca,m}}{\sum_{a'} X_{a'}}, \quad G_{cm} = \frac{\sum_{c} X_c G_{ca,m}}{\sum_{c'} X_{c'}}, \qquad (4.32)
$$

$$
G_{jc,a'c} = \exp\left(-\alpha_{jc,a'c}\tau_{jc,a'c}\right), \quad G_{ja,c'a} = \exp\left(-\alpha_{ja,c'a}\tau_{ja,c'a}\right), \qquad (4.33)
$$

and

$$
G_{im} = \exp\left(-\alpha_{im}\tau_{im}\right), \quad G_{ca,m} = \exp\left(-\alpha_{ca,m}\tau_{ca,m}\right), \qquad (4.34)
$$

$$
\alpha_{cm} = \frac{\sum_{a} X_a \alpha_{ca,m}}{\sum_{a'} X_{a'}}, \quad \alpha_{am} = \frac{\sum_{c} X_c \alpha_{ca,m}}{\sum_{c'} X_{c'}}. \qquad (4.35)
$$

Also, $\tau_{ma,ca} = \tau_{am} - \tau_{ca,m} + \tau_{m,ca}$, $\tau_{mc,ac} = \tau_{cm} - \tau_{ca,m} + \tau_{m,ca}$, $X_j = x_j C_j$ ($C_j = Z_j$ for ions

and 1 for molecules), α is the nonrandomness parameter, and τ is the binary interaction

parameter.

The reference state of the NRTL contribution can be converted to the

unsymmetric convention with the correction of infinite dilution activity coefficients.

$$
\frac{g_{NRTL}^{ex^*}}{RT} = \frac{g_{NRTL}^{ex}}{RT} - \left(\sum_{m \neq w} x_m \ln \gamma_m^{\infty} + \sum_{c} x_c \ln \gamma_c^{\infty} + \sum_{a} x_a \ln \gamma_a^{\infty} \right) \qquad (4.36)
$$

where

$$\ln \gamma_m^\infty = \tau_{wm} + G_{mw}\tau_{mw} \tag{4.37}$$

$$\ln \gamma_c^\infty = Z_c \left(G_{cw}\tau_{cw} + \frac{\sum_{a'} x_{a'}\tau_{wc,a'c}}{\sum_{a''} x_{a''}} \right) \tag{4.38}$$

$$\ln \gamma_a^\infty = Z_a \left(G_{aw}\tau_{aw} + \frac{\sum_{c'} x_{c'}\tau_{wa,c'a}}{\sum_{c''} x_{c''}} \right) \tag{4.39}$$

The subscript w represents water.

4.1.4. Thermodynamic Model Default Settings

For modeling K^+/PZ mixtures in this work, nonrandomness parameters for molecule-molecule pairs and water-ion pairs were set to 0.2 according to the recommendation of Renon and Prausnitz (1968). For amine-ion pairs, values were set to 0.1. Molecule-molecule interaction parameters (τ) are given by

$$\tau = A + B/T(K). \tag{4.40}$$

The default value of A is 0.0 and the default temperature dependence, B, is 0.0. The interaction parameters for molecule-ion pair and ion pair-molecule are given by

$$\tau = A + B\left(\frac{1}{T(K)} - \frac{1}{353.15(K)} \right) \tag{4.41}$$

with default values for A of 15.0 and -8.0 respectively. If the molecule is water, the values are 8.0 and -4.0. The default temperature dependence, B, is 0.0. Ion pair-ion pair interactions are normally insignificant and not included in this model.

88

4.1.5. Vapor-Liquid Equilibrium

Recall that equilibrium with the vapor phase is represented in terms of fugacity, a function of concentration and pressure.

$$\hat{f}_i^v = y_i \hat{\phi}_i P \tag{4.42}$$

where

$$\hat{\phi}_i = \frac{\hat{f}_i^v}{y_i P} \tag{4.43}$$

More exactly, as an extension of residual properties, ϕ can be written as

$$\ln \hat{\phi}_i = \int_0^P \left(\frac{PV_i}{RT} - 1 \right) \frac{dP}{P}. \tag{4.44}$$

An equation of state (EOS) is needed to describe the molar volume, V_i.

The Redlich-Kwong-Soave (RKS) equation of state was chosen for this work (Soave, 1972). This expression can be written as pressure explicit,

$$P = \frac{RT}{V-b} - \frac{a(T,\omega)}{V(V+b)}, \tag{4.45}$$

or as cubic in terms of volume.

$$V^3 - \frac{RT}{P}V^2 + \frac{\left(a\alpha(T,\omega) - bRT - Pb^2\right)}{P}V - \frac{a\alpha(T,\omega)b}{P} = 0 \tag{4.46}$$

T and P represent the temperature and pressure of the vapor phase and R represents the gas constant. The attraction between molecules and their size are represented in the equation by parameters a and b respectively.

In Equation (4.46), a is a function of temperature and the acentric factor, ω, and can be written

$$a(T,\omega) = a\alpha(T,\omega), \tag{4.47}$$

where

$$\alpha(T,\omega) = \left[1 + f_\omega\left(1 - T_r^{0.5}\right)\right]^2, \tag{4.48}$$

and

$$f_\omega = 0.48508 + 1.55171\omega - 0.15613\omega^2. \tag{4.49}$$

The terms α and f_ω were determined empirically to fit known vapor pressures. The parameter b is calculated as in the original Redlich-Kwong equation

$$b = 0.086640\frac{RT_C}{P_C}, \tag{4.50}$$

where T_C and P_C represent the critical temperature and pressure.

Expressions for a and b for gas mixtures were developed by Redlich and Kwong (1948) and are applied in the model.

$$a_{mix} = \sum_i\sum_j x_i x_j \left(a_i\alpha_i a_j\alpha_j\right)^{0.5} \tag{4.51}$$

$$b_{mix} = \sum_i x_i b_i \tag{4.52}$$

Application of the mixing rules allows the calculation of vapor phase fugacity from Equation (4.42). The equilibrium model solves Equation (4.46) using a Newton-Raphson method where the initial guess for V is obtained from the ideal gas law.

4.1.6. Reference States

In this work, the reference state for water and PZ is described by the symmetric convention. This means the activity coefficient of water (or PZ) is defined so that

$$\gamma_w \to 1 \text{ as } x_w \to 1. \tag{4.53}$$

CO_2, ions, and H^+PZCOO^- are described by the nonsymmetric convention, meaning the activity coefficients are referenced to pure water so that

$$\gamma_i^* \to 1 \text{ as } x_i \to 0. \tag{4.54}$$

The two conventions are related by

$$\frac{\gamma_i}{\gamma_i^*} = \lim_{x_i \to 0} \gamma_i = \gamma_i^\infty, \tag{4.55}$$

where γ_i^∞ represents the symmetrically normalized activity coefficient of solute i, or the value of γ_i as the solution approaches its pure water reference state.

The structure of the model treats PZ as a solvent, resulting in two definitions of equilibrium constants that contain PZ. Constants are normally reported in literature as referenced to infinite dilution in water and can be represented as

$$K_{Am}^* = \frac{x_{Am} x_{H_3O^+}}{x_{AmH^+} x_{H_2O}} \cdot \frac{\gamma_{Am}^* \gamma_{H_3O^+}^*}{\gamma_{AmH^+}^* \gamma_{H_2O}^*}. \tag{4.56}$$

The constants utilized in the model are normalized so that

$$K_{Am} = \frac{x_{Am} x_{H_3O^+}}{x_{AmH^+} x_{H_2O}} \cdot \frac{\gamma_{Am} \gamma_{H_3O^+}^*}{\gamma_{AmH^+}^* \gamma_{H_2O}^*}. \tag{4.57}$$

The constants are therefore related by

$$K_{Am} = K_{Am}^* \frac{\gamma_{Am}}{\gamma_{Am}^*} = K_{Am}^* \gamma_{Am}^\infty .$$
(4.58)

Equilibrium constants reported in this work must be corrected for the infinite dilution activity coefficient of the amine prior to comparison with other work. An estimate of γ_{PZ}^∞ is presented in Chapter 5.

Also of note is that PZ is considered a liquid. While the melting point is 106°C, it was assumed that liquid phase properties more adequately represent PZ behavior in aqueous solution. The requirement of this assumption is that the vapor pressure of PZ is represented by liquid PZ. The consequence of this assumption is that equilibrium constants, enthalpies, and other properties relating to PZ behavior are referenced to the liquid form of the amine (e.g. heat of dissolution is not considered).

4.1.7. Solution Method (Non-Stoichiometric Method)

A non-stoichiometric solution method was used to solve for the equilibrium composition of K^+/PZ mixtures from total system properties (total PZ and K^+, total CO_2, and temperature). By defining the activity coefficients and equilibrium constants through a rigorous model, such as the ENRTL model, the Gibbs energy of the solution can be calculated. For a defined system, the algorithm minimizes the Gibbs free energy within the constraints of material balances. The Gibbs energy is related to the chemical potential, and thus the activity coefficients, as presented in Section 4.1.2.

For K^+/PZ mixtures, there are eleven unknown species to be considered. Potassium ion, though constant, is considered an unknown to increase model flexibility

for future applications. Hydronium ion (H_3O^+) is neglected because its concentration is assumed to be very small. Five elements are identified for the material balances: K^+, PZ, C, H, and O. PZ (minus the hydrogens) can be considered an element because the core of the molecule is constant. The material balances are then

$$
\begin{cases}
n_{K^+} = n_{K^+,Tot} \\
n_{PZ} + n_{PZH^+} + n_{PZCOO^-} + n_{H^+PZCOO^-} + n_{PZ(COO^-)_2} = n_{PZ,Tot} \\
n_{CO_2} + n_{CO_3^{2-}} + n_{HCO_3^-} + n_{PZCOO^-} + n_{H^+PZCOO^-} + 2n_{PZ(COO^-)_2} = n_{C,Tot} \\
2n_{H_2O} + n_{OH^-} + n_{HCO_3^-} + 2n_{PZ} + 3n_{PZH^+} + n_{PZCOO^-} + 2n_{H^+PZCOO^-} = n_{H,Tot} \\
n_{H_2O} + n_{OH^-} + 2n_{CO_2} + 3n_{CO_3^{2-}} + 3n_{HCO_3^-} + 2n_{PZCOO^-} + 2n_{H^+PZCOO^-} + 4n_{PZ(COO^-)_2} = n_{O,Tot}
\end{cases}
\tag{4.59}
$$

Lagrangian multipliers, λ, are used for each element so that the chemical potential of each species can be expressed as

$$
\begin{cases}
\mu_{CO_2} - \lambda_C - 2\lambda_O = 0 \\
\mu_{K^+} - \lambda_{K^+} = 0 \\
\mu_{H_2O} - 2\lambda_H - \lambda_O = 0 \\
\mu_{HCO_3^-} - \lambda_C - \lambda_H - 3\lambda_O = 0 \\
\mu_{CO_3^{2-}} - \lambda_C - 3\lambda_O = 0 \\
\mu_{OH^-} - \lambda_H - \lambda_O = 0 \\
\mu_{PZ} - \lambda_{PZ} - 2\lambda_H = 0 \\
\mu_{PZH^+} - \lambda_{PZ} - 3\lambda_H = 0 \\
\mu_{PZCOO^-} - \lambda_{PZ} - \lambda_C - \lambda_H - 2\lambda_O = 0 \\
\mu_{H^+PZCOO^-} - \lambda_{PZ} - \lambda_C - 2\lambda_H - 2\lambda_O = 0 \\
\mu_{PZ(COO^-)_2} - \lambda_{PZ} - 2\lambda_C - 4\lambda_O = 0
\end{cases}
\tag{4.60}
$$

This gives eleven equations, dependent upon chemical potential, to be solved simultaneously. The chemical potentials are minimized and an equilibrium composition is determined. A more thorough discussion of the non-stoichiometric method and the solution algorithm by Smith and Missen (1988) can be found in Austgen (1989).

4.2. Kinetic/Rate Model

4.2.1. Introduction

A substantial amount of research on CO_2 absorption by amines has been published in the open literature. With each new solvent or solvent blend, new challenges of representing solvent behavior arise, leading to a better understanding of the fundamental processes in gas absorption. A rigorous analysis of the experimental data is imperative to arrive at a complete picture of the solution behavior.

Bishnoi (2000) programmed a rigorous mass transfer model to quantify and interpret experimental results on a fundamental level by simulating the absorption of gas into a reactive liquid. The model corrects for gas film resistance and uses the eddy diffusivity theory to describe mass transfer with chemical reaction in the liquid boundary layer. This work extends the model for a K^+/PZ mixture.

The problem is calculating the flux of CO_2 into or out of the solvent by considering temperature, total solvent composition, the gas and liquid film mass transfer coefficients, and the bulk gas partial pressure. The model iteratively solves for the concentration profiles of all species in solution across the boundary layer. Through material balances and reaction rates, a flux is predicted, which is directly related to the diffusion of reactants and products and the kinetics of reacting species. Values of diffusion coefficients and rate constants are obtained by fitting the model to experimental data.

4.2.2. Modeling Mass Transfer with Chemical Reaction

For describing the concentration profiles within the reactive boundary layer, Bishnoi (2000) used the eddy diffusivity theory (King, 1966).

$$\frac{\partial}{\partial x}\left[\left(D_i + \varepsilon x^m\right)\frac{\partial [i]}{\partial x}\right] - R_i = 0 \tag{4.61}$$

$$\left.\begin{cases} i = i_i, \ x = 0 \\ i = i_b, \ x \to \infty \end{cases}\right\} \tag{4.62}$$

where ε is a proportionality constant. A value of 2 was used for m, giving a square root dependence on the diffusion coefficient, which is consistent with most experimental observations (Prasher and Fricke, 1974). This results in a k_l^o of the form

$$k_l^o = \frac{2}{\pi}\sqrt{\varepsilon D_{CO_2}} \ . \tag{4.63}$$

Glasscock and Rochelle (1989) have shown that this theory adequately describes absorption by amines and gives a solution equivalent to surface renewal theory under most conditions.

A numerical solution to the equation requires a bounded space; therefore, the above equation was transformed using an expression proposed by Versteeg (1987).

$$r = \frac{2}{\pi}\arctan\left(x\sqrt{\frac{\varepsilon}{D_i}}\right) \tag{4.64}$$

A derivation of the resulting equation, shown below, is presented in Bishnoi (2000).

$$\left(C_1 + C_2 D_i\right)\frac{\partial^2 [i]}{\partial r^2} + \left(C_3 + C_4 D_i\right)\frac{\partial [i]}{\partial r} - R_i = 0 \tag{4.65}$$

where

95

$$C_1 = \frac{4\varepsilon}{\pi^2} \sin^2\left(\frac{\pi}{2}r\right)\cos^2\left(\frac{\pi}{2}r\right) \qquad (4.66)$$

$$C_2 = \frac{4\varepsilon}{\pi^2 D_i} \cos^4\left(\frac{\pi}{2}r\right) \qquad (4.67)$$

$$C_3 = -\frac{4\varepsilon}{\pi} \sin^3\left(\frac{\pi}{2}r\right)\cos\left(\frac{\pi}{2}r\right) + \frac{4\varepsilon}{\pi} \tan\left(\frac{\pi}{2}r\right)\cos^2\left(\frac{\pi}{2}r\right) \qquad (4.68)$$

$$C_4 = -\frac{4\varepsilon}{\pi} \sin\left(\frac{\pi}{2}r\right)\cos^3\left(\frac{\pi}{2}r\right) \qquad (4.69)$$

The boundary conditions become

$$\left\{ \begin{matrix} i = i_i, \ r = 0 \\ i = i_b, \ r = 1 \end{matrix} \right\}. \qquad (4.70)$$

Bishnoi numerically solved the differential equation for each species using a finite difference method. The spatial variable r was divided into 38 nodes. The first eleven nodes, including node 1 at the gas-liquid interface, are spaced 1.0E-4. The next nine nodes are spaced 1.0E-3, followed by nine nodes with a spacing of 1.0E-2. The final nine nodes that approach the bulk solution have a spacing of 0.1. A small Δr is required near the interface to maintain accuracy because reaction and mass transfer cause rapid changes in species concentrations. Further into solution, where concentration gradients are smaller, the Δr was increased to reduce computation time.

Three-point forward difference equations were used to describe derivatives at the gas-liquid interface. Within the boundary layer, three-point central difference equations were used for nodes of equal grid size. Nodes involving a change in grid size were represented by the method of Liu *et al.* (1995).

The flux at the interface is calculated by the derivative given by the forward difference approximation, resulting in

$$\left.\frac{\partial [CO_2]}{\partial r}\right|_{r=0} = \frac{1}{2\Delta r}\left(-3[CO_2]_0 + 4[CO_2]_1 - [CO_2]_2\right), \qquad (4.71)$$

where the subscripts 0, 1, and 2 refer to nodes a distance of Δr apart beginning at the interface (node 0, $\Delta r = 1\times10^{-4}$). This results in an implicit, upper limit to the calculated flux for very fast reactions. In the limit, $[CO_2]_2$ represents the equilibrium concentration and $[CO_2]_0$ is the value at the interface. $[CO_2]_1$ will approach $[CO_2]_2$. Thus, the expression reduces to

$$\left.\frac{\partial [CO_2]}{\partial r}\right|_0 = \frac{-3}{2\Delta r}\left([CO_2]_i - [CO_2]^*\right). \qquad (4.72)$$

The flux will no longer be a true flux, but a maximum flux defined by the driving force and the grid spacing, Δr. In these cases, reducing the grid size should be considered. For calculating instantaneous flux in this work, the Δr of 1×10^{-4} was replaced by a Δr of 1×10^{-6}.

The boundary conditions are at $r = 0$, the gas-liquid interface, and $r = 1$, the bulk liquid. At the gas-liquid interface, the concentration of CO_2 is given by the partial pressure at the interface as calculated from the gas film resistance and bulk partial pressure. Species involved in buffering reactions are given by a flux balance (Equation (4.73)). Chemical equilibrium between the proton exchanges and charge balance is also assumed. The boundary condition at $r = 1$ is given by equilibrium speciation provided by the ENRTL model discussed in Section 4.1.

$$
\begin{cases}
[CO_2] = \dfrac{P_{CO_2,i}}{H_{CO_2}\gamma_{CO_2}} \\[2mm]
D_{PZ}\nabla[PZ] + D_{PZH^+}\nabla\left[PZH^+\right] = 0 \\[2mm]
\nabla\left[K^+\right] = 0 \\[2mm]
D_{PZCOO^-}\nabla\left[PZCOO^-\right] + D_{H^+PZCOO^-}\nabla\left[H^+PZCOO^-\right] = 0 \\[2mm]
D_{CO_3^{2-}}\nabla\left[CO_3^{2-}\right] + D_{HCO_3^-}\nabla\left[HCO_3^-\right] = 0 \\[2mm]
\nabla\left[PZ(COO^-)_2\right] = 0 \\[2mm]
\left[K^+\right] + \left[PZH^+\right] - \left[OH^-\right] - 2\left[CO_3^{2-}\right] - \left[HCO_3^-\right] - \left[PZCOO^-\right] - 2\left[PZ(COO^-)_2\right] = 0
\end{cases}
\tag{4.73}
$$

Calculations at each node within the boundary layer ($0 < r < 1$) are made with the balances shown in Equation (4.74). The equilibrium conditions of the proton exchanges and charge balance is included. Species balances are solved for PZ and CO_2 so that each species is conserved at each node. Material balances for CO_2, $PZCOO^-$ and H^+PZCOO^-, and $PZ(COO^-)_2$ are also included to account for the reversible reaction of each species throughout the reactive film.

$$
\begin{cases}
\nabla^2[PZ] + \nabla^2\left[PZH^+\right] + \nabla^2\left[PZCOO^-\right] + \nabla^2\left[H^+PZCOO^-\right] + \nabla^2\left[PZ(COO^-)_2\right] = 0 \\[2mm]
\nabla^2\left[K^+\right] = 0 \\[2mm]
\nabla^2[CO_2] + \nabla^2\left[CO_3^{2-}\right] + \nabla^2\left[HCO_3^-\right] + \nabla^2\left[PZCOO^-\right] + \nabla^2\left[H^+PZCOO^-\right] + 2\nabla^2\left[PZ(COO^-)_2\right] = 0 \\[2mm]
\nabla^2[CO_2] - R_{PZ} - R_{PZCOO^-} - R_{OH^-} - R_{PZ,HCO_3^-} - R_{PZCOO^-,HCO_3^-} = 0 \\[2mm]
\nabla^2\left[PZCOO^-\right] + \nabla^2\left[H^+PZCOO^-\right] - R_{PZCOO^-} - R_{PZCOO^-,HCO_3^-} + R_{PZ} = 0 \\[2mm]
\nabla^2\left[PZ(COO^-)_2\right] - R_{PZCOO^-} = 0 \\[2mm]
\left[K^+\right] + \left[PZH^+\right] - \left[OH^-\right] - 2\left[CO_3^{2-}\right] - \left[HCO_3^-\right] - \left[PZCOO^-\right] - 2\left[PZ(COO^-)_2\right] = 0
\end{cases}
\tag{4.74}
$$

The rigorous model requires specific knowledge of the equilibrium behavior within the boundary layer to calculate the correct driving force. To reduce complexity and computation time, rigorous thermodynamics are not calculated at each node within the boundary layer and serve only as the bulk liquid boundary condition. Activity-based equilibrium constants, from the ENRTL model, are used with activity coefficients to calculate concentration-based equilibrium constants, defined in Equation (4.75), at

bulk solution conditions. These constants are used to describe equilibrium in the boundary layer. The implicit assumption is that activity coefficients and water concentration do not change from the gas-liquid interface to the bulk solution. This approximation will be valid since the ionic strength does not change significantly across the boundary layer.

$$
\begin{cases}
\bar{K}_w = \left[H_3O^+ \right]\left[OH^- \right] \\[6pt]
\bar{K}_{HCO_3^-} = \dfrac{\left[HCO_3^- \right]}{\left[CO_2 \right]\left[OH^- \right]} \\[10pt]
\bar{K}_{CO_3^{2-}} = \dfrac{\left[CO_3^{2-} \right]}{\left[HCO_3^- \right]\left[OH^- \right]} \\[10pt]
\bar{K}_{PZH^+} = \dfrac{\left[OH^- \right]\left[PZH^+ \right]}{\left[PZ \right]} \\[10pt]
\bar{K}_{PZCOO^-} = \dfrac{\left[PZCOO^- \right]\left[H_3O^+ \right]}{\left[PZ \right]\left[CO_2 \right]} \\[10pt]
\bar{K}_{H^+PZCOO^-} = \dfrac{\left[H^+PZCOO^- \right]\left[OH^- \right]}{\left[PZCOO^- \right]} \\[10pt]
\bar{K}_{PZ(COO^-)_2} = \dfrac{\left[PZ(COO^-)_2 \right]\left[H_3O^+ \right]}{\left[PZCOO^- \right]\left[CO_2 \right]}
\end{cases}
\tag{4.75}
$$

4.2.3. Rate Expressions

4.2.3.1. Carbamate Formation

Recall the proposed two-step mechanism of CO_2 reacting with primary and secondary amines suggested by Caplow (1968). Two interpretations include a "zwitterion" mechanism or a termolecular mechanism, resulting in

$$
r_{CO_2} = \sum_b k_{Am-b} \left[Am \right]\left[b \right]\left[CO_2 \right].
\tag{4.76}
$$

The reaction of CO_2 with the amine to form carbamate species accounts for a majority of the absorption rate. The following amine reactions, considered relevant from the chosen mechanistic framework, are included in the model.

$$PZ + CO_2 + \begin{cases} OH^- \xrightleftharpoons{k_{PZ-OH^-}} PZCOO^- + H_2O \\ H_2O \xrightleftharpoons{k_{PZ-H_2O}} PZCOO^- + H_3O^+ \\ PZ \xrightleftharpoons{k_{PZ-PZ}} PZCOO^- + PZH^+ \\ CO_3^{2-} \xrightleftharpoons{k_{PZ-CO_3^{2-}}} PZCOO^- + HCO_3^- \\ PZCOO^- \xrightleftharpoons{k_{PZ-PZCOO^-}} PZCOO^- + H^+PZCOO^- \end{cases} \tag{4.77}$$

$$PZCOO^- + CO_2 + \begin{cases} H_2O \xrightleftharpoons{k_{PZCOO^- - H_2O}} PZ(COO^-)_2 + H_3O^+ \\ PZ \xrightleftharpoons{k_{PZCOO^- - PZ}} PZ(COO^-)_2 + PZH^+ \\ CO_3^{2-} \xrightleftharpoons{k_{PZCOO^- - CO_3^{2-}}} PZ(COO^-)_2 + HCO_3^- \\ PZCOO^- \xrightleftharpoons{k_{PZCOO^- - PZCOO^-}} PZ(COO^-)_2 + H^+PZCOO^- \end{cases} \tag{4.78}$$
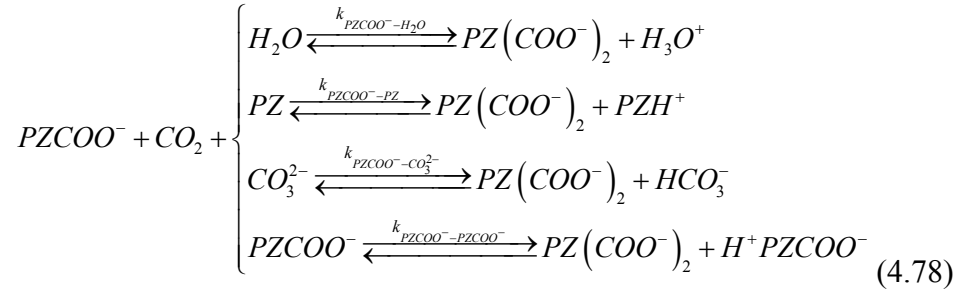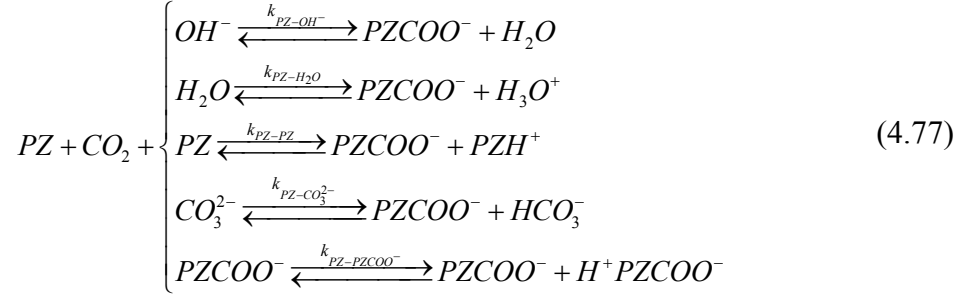
Because hydroxide and PZCOO⁻ do not coexist, the contribution of hydroxide was not considered in Equation (4.78). All proton exchange reactions were considered to be at equilibrium at all times. The resulting expressions for the reversible rate of CO_2 with PZ and PZCOO⁻ are

$$r = \sum_b k_{PZ-b}[b]\left([PZ][CO_2] - \frac{\bar{K}_W}{\bar{K}_{PZCOO^-}}\frac{[PZCOO^-]}{[OH^-]}\right) \tag{4.79}$$

and

$$r = \sum_b k_{PZCOO^- - b}[b]\left([PZCOO^-][CO_2] - \frac{\bar{K}_W}{\bar{K}_{PZ(COO^-)_2}}\frac{[PZ(COO^-)_2]}{[OH^-]}\right). \tag{4.80}$$

The temperature dependence of these rate constants is given by

$$k^{\infty} = k^o \exp\left(\frac{-\Delta H_a}{R}\left(\frac{1}{T(K)} - \frac{1}{298.15}\right)\right),$$ (4.81)

where k^{∞} represents the rate constant in the absence of significant ionic strength, k^o is the specific rate constant, and ΔH_a is the activation energy for the specific reaction.

The values of all regressed model parameters from this work are presented in Chapter 6. Parameters include the above rate constants, an activation energy (assumed constant for all amine-base reactions), and a correction for ion diffusivities.

4.2.3.2. Bicarbonate Formation

Based on work with tertiary amines and experience with base-catalyzed reactions, amines and hydroxide are expected to catalyze the formation of bicarbonate ion (Littel *et al*., 1990b; Bishnoi, 2000). Three parallel reactions are included in the model to account for this effect.

$$CO_2 + OH^- \xrightleftharpoons{k_{OH^-}} HCO_3^-$$ (4.82)

$$PZ + CO_2 + H_2O \xrightleftharpoons{k_{PZ}} PZH^+ + HCO_3^-$$ (4.83)

$$PZCOO^- + CO_2 + H_2O \xrightleftharpoons{k_{PZCOO^-}} H^+PZCOO^- + HCO_3^-$$ (4.84)
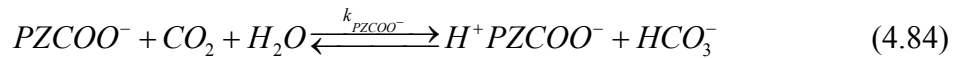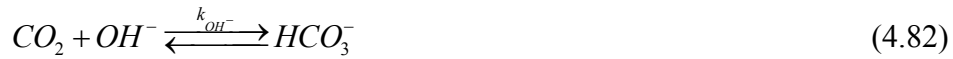
The formation of bicarbonate in this manner is typically much slower than the reaction of CO_2 with amines and has little effect on the absorption rate under most conditions, but must be included to properly model equilibrium in the boundary layer. A generalized, second-order rate expression for these reactions can be written as

$$r = \sum_b k_b [b] \left([CO_2] - \frac{1}{\bar{K}_{HCO_3^-}} \frac{\left[HCO_3^- \right]}{\left[OH^- \right]} \right), \tag{4.85}$$

where b, in this case, represents the active catalyst OH⁻, PZ, or PZCOO⁻.

The rate constants for amine-catalyzed bicarbonate formation were assumed equal to that of the MDEA-catalyzed reaction given by Littel (1991).

$$k_{Am} \left(\frac{m^3}{kmol \cdot s} \right) = 1.34 \times 10^9 \exp \left(\frac{-5771.0}{T(K)} \right) \tag{4.86}$$

The rate constant for CO_2 reacting with OH⁻ is well defined in the literature and is given as a function of ionic strength (1988).

$$\log_{10} k_{OH^-} = \log_{10} k_{OH^-}^\infty + \sum_i \kappa_i I_i \tag{4.87}$$

where

$$\log_{10} k_{OH^-}^\infty = 11.916 - \frac{2382.0}{T(K)} \tag{4.88}$$

and κ is an ion-specific parameter and I_i is ionic strength calculated as

$$I_i = \frac{1}{2} \left(C_i z_i^2 \right). \tag{4.89}$$

C_i is the molar concentration and z_i is the charge or species i.

An ionic strength correction is made to all amine rate constants (Equations (4.79), (4.80), and (4.89)) according to the theory of salt effects, presented in Chapter 2. The correction is

$$k = k^\infty \exp(0.3I). \tag{4.90}$$

I is the summation of molar ionic strength. This correction is addressed in Chapter 6.

4.2.4. Solution Method

The solution of the boundary layer is an iterative process, determined by the application of the aforementioned reactions and boundary conditions. An initial guess of the partial pressure of CO_2 at the interface, $P_{CO_2,i}$, is calculated as 95% of the bulk gas partial pressure.

Newton's method was used to simultaneously solve the differential equations and material balances. A Jacobian matrix is calculated with a step size of 4%. A Gaussian elimination with forward elimination and backward substitution was used to solve the matrix using the appropriate material balances and boundary conditions.

The converged solution of the Jacobian matrix gives a concentration profile of all species for a given $P_{CO_2,i}$. A flux, N_{CO_2}, is calculated based on the concentration change of CO_2 near the gas-liquid interface. The calculated species flux is compared to the flux based on the given gas film coefficient and gas phase driving force. That is, a function, f, is created for a secant method solution.

$$f^n = N_{CO_2}^n - k_g \left(P_{CO_2,b} - P_{CO_2,i}^n \right)$$
(4.91)

where n indicates the current iteration. The procedure is repeated after perturbing the initial guess for $P_{CO_2,i}$ by 5%. Subsequent values of $P_{CO_2,i}$ are calculated by linear interpolation.

$$P_{CO_2,i}^{n+1} = P_{CO_2,i}^n - f^n \frac{\left(P_{CO_2,i}^n - P_{CO_2,i}^{n-1} \right)}{f^n - f^{n-1}}$$
(4.92)

The iterations continue until the difference between $P_{CO_2,i}^{n+1}$ and $P_{CO_2,i}^n$ is less than 0.1%.

4.3. Non-Linear Regression Model

4.3.1. Description of GREG

The regression of parameters in the thermodynamic and rate models was performed using the Generalized REGression package, GREG, developed by Caracotsios (1986). GREG is a multiple parameter, non-linear regression tool that minimizes the difference between a model calculated value, F_i, that is a function of given parameter values, x_j, and a user-provided observed value, OBS_i.

$$Obj = \sum_{i=1}^{n} \left[F_i\left(x_j\right) - OBS_i \right]^2 \tag{4.93}$$

Some data, such as the activity of water and mole fractions (speciation data), were regressed as is. For equilibrium partial pressure data, where the values ($F_i(x_j)$) varied over several decades, a logarithmic transformation of the data (i.e. $\ln(P_{CO_2}{}^*)$) was used to give even weight to all data points. In each case where multiple data sets were simultaneously regressed, the data types were weighted so that each gave a comparable contribution to the sum-of-squares error.

The generic character of the model allows its coupling with any user-defined model. GREG is highly versatile, capable of being applied to the regression of any model parameter. Parameters regressed in this work include equilibrium constants, binary interaction parameters, and rate constants.

4.3.2. Interface with the Thermodynamic and Rate Models

GREG is completely external to all other programs. The model, or main program, is essentially the inner part of a loop that runs once for every observed

parameter supplied. The results are stored in an array and returned to GREG for statistical calculations.

A simple flowsheet is shown in Figure 4.2, showing how GREG interacts with other programs for i = 1 to n, where n is the number of observed parameters. The regression driver provides GREG with information important to the regression, including the initial parameter values (x_j), the upper and lower bounds, the maximum change, and the tolerance for termination of the regression. The observed, or experimental data, is provided to the regression driver through an input file and subsequently transferred to GREG. GREG then supplies the necessary parameter values and executes the main program. The main program reads input from data files and returns a calculated result, F_i, to GREG. GREG changes the values of x_j until the objective function is minimized and a final solution is obtained.
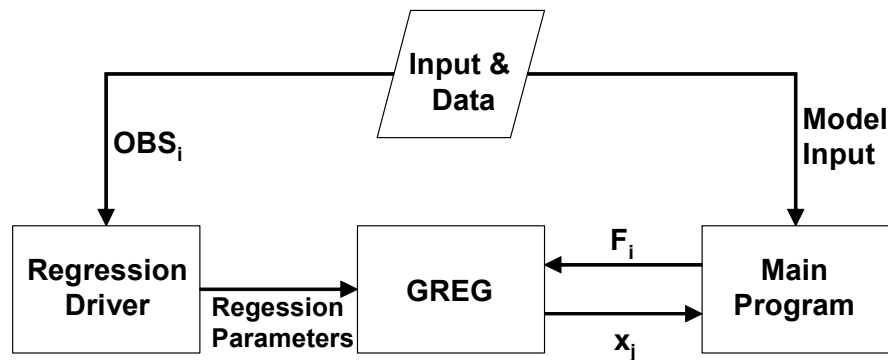
Figure 4.2. Transfer of Data during a Regression with GREG

4.3.3. Results and Statistics from GREG

In addition to the parameter values and sum of squares, a confidence interval and correlation parameters were calculated. An understanding of these values improves the significance and clarity of the regressed parameters for representing a given data set.

A confidence interval was calculated for each given mean parameter value, $\bar{x}$. The confidence interval expresses the certainty of which the true value of a parameter is known. In this work, the confidence interval is reported as a standard deviation, σ. The standard deviation is calculated as

$$\sigma_x = \sqrt{\frac{1}{n-1}\sum_{j=1}^{n}\left(x_j - \bar{x}\right)^2} \; . \tag{4.94}$$

GREG also calculates a correlation matrix, which identifies potential interference from the dependence of regressed parameters on each other. The correlation between two variables, x and y, is given by the correlation coefficient, $\rho(x,y)$.

$$\rho\left(x,y\right) = \frac{Cov\left(x,y\right)}{\sigma_x \sigma_y} \tag{4.95}$$

where Cov(x,y), the covariance, is calculated as

$$Cov\left(x,y\right) = \frac{1}{n-1}\sum_{j=1}^{n}\left(x_j - \bar{x}\right)\left(y_j - \bar{y}\right). \tag{4.96}$$

The covariance quantifies the linear relationship between variables x and y. An important constraint is that the absolute value of covariance is always less than the product of standard deviations.

106

$$\left| Cov(x,y) \right| \le \sigma_x \sigma_y \qquad (4.97)$$

Also, the covariance is symmetric, so that

$$Cov(x,y) = Cov(y,x). \qquad (4.98)$$

Thus, the correlation coefficient is bounded between -1 and 1. Values of $\rho(x,y)$ of -1 and 1 indicate perfectly correlated parameters, meaning x and y are linearly dependent. Small values (i.e. $\left| \rho(x,y) \right| \to 0$) indicate completely independent values of x and y.

Chapter 5: Thermodynamics of Potassium Carbonate, Piperazine, and Carbon Dioxide Mixtures

Absorption processes incorporating various aqueous amine solvents have long been known as effective for the treatment of waste gas streams, particularly for removing acidic components (CO_2, H_2S). For any new or existing solvent, an understanding of the thermodynamics and the ability to model equilibrium behavior is important for process development, design, and optimization. This chapter examines thermodynamic properties attained by blending PZ with K_2CO_3 in a concentrated aqueous mixture.

Measurements of CO_2 solubility in a wetted-wall column in 0.6 to 3.6 m PZ and 2.5 to 6.2 m K^+ at 40 to 110°C are presented. Piperazine speciation was also determined using ^{1}H NMR for 0.6 to 3.6 m PZ and 3.6 to 6.2 m K^+ at 25 to 70°C and the results are reported here. Other thermochemical properties, the physical solubility of CO_2 and the

solid solubility of the potassium salt and the piperazine solid, were also explored and reported.

As discussed in Chapter 4, a rigorous thermodynamic model of aqueous potassium carbonate/piperazine was developed to describe the vapor- and liquid-phase equilibrium of the solvent with CO_2. The model was sequentially fitted to a variety of data, beginning with simple binary systems and extending to complex, multi-component electrolyte mixtures. Representation of the VLE and speciation is achieved and demonstrated over the range of solvents investigated. Predictions of thermodynamically significant properties, such as solvent capacity, heat of absorption, and stoichiometric behavior are presented.

5.1. Model Description

Eight equilibrium reactions, shown below, are included in the model for K^+/PZ. The equilibrium constants for reactions (5.1) through (5.4) are shown in Table 5.1. Constants for reactions (5.5) through (5.7) were regressed from experimental data and are presented in Section 5.4.3.

$$CO_2(aq) + 2 \cdot H_2O \rightleftharpoons HCO_3^- + H_3O^+ \tag{5.1}$$

$$HCO_3^- + H_2O \rightleftharpoons CO_3^{2-} + H_3O^+ \tag{5.2}$$

$$2 \cdot H_2O \rightleftharpoons H_3O^+ + OH^- \tag{5.3}$$

$$PZH^+ + H_2O \rightleftharpoons PZ(l) + H_3O^+ \tag{5.4}$$

$$PZ(l) + CO_2(aq) + H_2O \rightleftharpoons PZCOO^- + H_3O^+ \tag{5.5}$$

$$H^+ PZCOO^- + H_2O \rightleftharpoons PZCOO^- + H_3O^+ \qquad (5.6)$$

$$PZCOO^- + CO_2 + H_2O \rightleftharpoons PZ\left(COO^-\right)_2 + H_3O^+ \qquad (5.7)$$
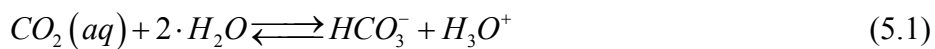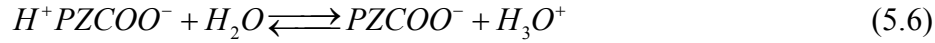
Edwards *et al.* (1978) correlated the work of several researchers to represent reactions (5.1) through (5.3). $K_{HCO_3^-}$ is based on data from Harned and Davis (1943), Ellis (1959), and Ryzhenko (1963). The equation for $K_{CO_3^{2-}}$ is based on the work of Harned and Scholes (1941), Cuta and Strafelda (1954), and Ryzhenko (1963). K_w was correlated from data by Harned and Robinson (1940) and Ackermann (1958). Posey (1996) deemed the correlations by Edwards *et al.* to be appropriate for modeling acid gas systems. The determination of the equilibrium constant for PZ dissociation (5.4) is derived from Hetzer *et al.* (1968) and is addressed in Section 5.4.2.

Table 5.1. Defined Equilibrium Constants (Mole Fraction-Based) in the ENRTL Model

Eq. #	Equilibrium Constant	$\ln K_i = A + B/T + C \ln T$			Source
		A	**B**	**C**	
(5.1)	$K_{HCO_3^-} = \dfrac{a_{HCO_3^-} \cdot a_{H_3O^+}}{a_{CO_2} \cdot a_{H_2O}^2}$	231.4	-12092	-36.78	Edwards *et al.* (1978), Posey (1996)
(5.2)	$K_{CO_3^{2-}} = \dfrac{a_{H_3O^+} \cdot a_{CO_3^{2-}}}{a_{HCO_3^-} \cdot a_{H_2O}}$	216.0	-12432	-35.48	Edwards *et al.* (1978), Posey (1996)
(5.3)	$K_w = \dfrac{a_{H_3O^+} \cdot a_{OH^-}}{a_{H_2O}^2}$	132.9	-13446	-22.48	Edwards *et al.* (1978), Posey (1996)
(5.4)	$K_{PZH^+} = \dfrac{a_{PZ} \cdot a_{H_3O^+}}{a_{PZH^+} \cdot a_{H_2O}}$	241.5	-21918	-34.35	Hetzer *et al.* (1968)

The ENRTL model was fit to experimental data by regressing equilibrium constants and binary interaction parameters from multiple, independent data sets using GREG as presented in Chapter 4. A sequential regression, beginning with simple mixtures and progressing to more complex solutions, was used to maintain thermodynamic consistency. Table 5.2 summarizes the sequence and data types used in the regressions. Table 5.3 reports the regressed parameters and values from each step.

Table 5.2. Summary of Data and Sources for the Regression of Parameters in the ENRTL Model

#	Name	Data Type	Conc. (m)	T (°C)	Source(s)	Data Pts.[a]
1	CO_2	N_2O Solubility	K_2CO_3: 0.0 – 1.25 $KHCO_3$: 0.0 – 1.25	25	Joosten and Danckwerts (1972)	8
			K_2CO_3: 0.0 – 2.4 $KHCO_3$: 0.0 – 3.6 PZ: 0.0 – 1.8	25	This Work	18
2	K_2CO_3/H_2O	P_{H_2O}*	K_2CO_3: 0.4 – 7.5	25 – 90	Puchkov and Kurochkina (1970)	42
			K_2CO_3: 0.15 – 7.2	25 - 140	Aseyev (1999)	614
3	$KHCO_3/H_2O$	P_{CO_2}*	K_2CO_3: 1.8 – 4.8 Conv.: 0 – 87%[b]	70 - 140	Tosh *et al.* (1959)	120
4	PZ/H_2O	UNIFAC	PZ: 0 – 2.4	25 - 80	Gmehling (1982)	21
5	$PZ/CO_2/H_2O$	NMR	PZ: 0.1 – 1.48 α: 0.15 – 1.0[c]	20 - 60	Ermatchkov *et al.* (2003)	218
		P_{TOT}	PZ: 2 – 4 α: 0.5 – 1.0[c]	40 - 120	Kamps *et al.* (2003)	29
		P_{CO_2}*	PZ: 0.64 α: 0.3 – 1.0[c]	40 - 70	Bishnoi (2000)	17
6	$PZ/K^+/CO_2/H_2O$	NMR	K_2CO_3: 3.6 – 6.2 PZ: 0.6 – 3.6 α: 0.35 – 0.7[c]	27 – 70	This Work	112
		P_{CO_2}*	K_2CO_3: 2.5 – 6.2 PZ: 0.6 – 3.6 α: 0.35 – 0.76[c]	40 - 110	This Work	58

a. Total number of data points used in the regression.
b. Conversion to $KHCO_3$ as reported by Tosh *et al.* (1959).
c. α is loading as defined by mol CO_2/(mol K^+ + mol PZ).

Table 5.3. Regressed Binary Interaction Parameters for the ENRTL Model

#	Name	Interaction	A	σ_A	B	σ_B	τ, 298K
1	CO_2	PZ, CO_2	5.03	Indt.[a]	-	-	**5.03**
		K^+, CO_3^{2-}, CO_2	-3.46	0.09	-	-	**-3.46**
		K^+, HCO_3^-, CO_2	-4.88	0.24	-	-	**-4.88**
		K^+, $PZCOO^-$, CO_2	-5.46	6.63	-	-	**-5.46**
		K^+, $PZ(COO^-)_2$, CO_2	-4.07	0.98	-	-	**-4.07**
2	K_2CO_3/ H_2O	H_2O, K^+, CO_3^{2-}	9.48	0.05	1582	172	**10.31**
		K^+, CO_3^{2-}, H_2O	-4.52	0.01	-377	30	**-4.72**
3	$KHCO_3$/ H_2O	H_2O, K^+, HCO_3^-	7.86	0.04	2863	Indt.[a]	**9.36**
		K^+, HCO_3^-, H_2O	-3.44	Indt.[a]	-601	74	**-3.75**
4	PZ/H_2O	H_2O, PZ	3.66	0.31	-310	Indt.[a]	**2.62**
		PZ, H_2O	6.46	0.15	-2648	Indt.[a]	**-2.42**
5[b]	PZ/CO_2/ H_2O	H_2O, PZH^+, HCO_3^-	9.07	0.44	-	-	**9.07**
		PZH^+, $PZCOO^-$, H_2O	-3.79	0.98	-	-	**-3.79**
		H_2O, H^+PZCOO^-	3.91	0.57	-	-	**3.91**
6	PZ/K^+/ CO_2/H_2O	H_2O, K^+, $PZCOO^-$	10.84	0.55	-	-	**10.84**
		H_2O, K^+, $PZ(COO^-)_2$	8.99	0.34	-	-	**8.99**
		K^+, $PZCOO^-$, PZ	-14.74	0.88	-	-	**-14.74**
		K^+, CO_3^{2-}, PZ	-9.55	0.98			**-9.55**
		K^+, HCO_3^-, H^+PZCOO^-	-7.27	2.90	-	-	**-7.27**
		K^+, $PZ(COO^-)_2$, H^+PZCOO^-	-5.91	2.50	-	-	**-5.91**

a. Indeterminate: Represents a high correlation between parameters.
b. Six parameters for equilibrium constants also regressed.

5.2. Physical Solubility

The solubility of N_2O was measured in K^+/PZ mixtures to arrive at an activity coefficient for CO_2 by way of the N_2O analogy outlined in Chapter 2. The physical solubility is an important thermodynamic parameter, defining the equilibrium concentration of the species in the liquid in the absence of chemical equilibria. Representing the data as an activity coefficient enables the incorporation of physical solubility in the rigorous ENRTL framework as interaction parameters, not simply an empirical equation.

The activity coefficient can be calculated from physical solubility with the following reasoning. Recall that Henry's law applies to dilute solutions so that

$$P_{CO_2} = H_{CO_2} \gamma^*_{CO_2} x_{CO_2} . \tag{5.8}$$

In this work, infinite dilution in water is the chosen reference state, so $\gamma_{CO_2}^* \to 1$ and the expression for Henry's constant in pure water can be written

$$H_{CO_2}^w = \frac{P_{CO_2}}{x_{CO_2}}. \tag{5.9}$$

The activity coefficient in the mixed solvent can then be calculated from the ratio of an apparent Henry's constant in the mixed solvent and the Henry's constant in water.

$$\gamma_{CO_2}^* = \frac{H_{CO_2}}{H_{CO_2}^w} \tag{5.10}$$

Thus, the solubility of CO_2 in this work is interpreted as the Henry's constant in water corrected by the activity coefficient of CO_2 in the mixed solvent.

The physical solubility of N_2O was measured in aqueous PZ and interpreted as CO_2 solubility. The results of these experiments are shown in Table 5.4 and Figure 5.1. The addition of PZ to water has little effect on the activity coefficient of CO_2 at 25 or 40°C. Even in concentrated solutions ($\sim$ 1.5 M), γ_{CO_2} increases by less than 10%, which is consistent with previous work on amines (Littel *et al.*, 1992c; Browning and Weiland, 1994; Sada *et al.*, 1978; Versteeg and van Swaiij, 1988). Only a small increase in activity coefficient could be identified at these low amine concentrations.

The physical solubility of CO_2 was also measured in aqueous K_2CO_3 and $K_2CO_3/KHCO_3$ mixtures (30 and 70% of the total molar salt concentration respectively) at 25°C for comparison with previous work. Results of these experiments are reported in Table 5.5. Figure 5.2 compares these results to those of Joosten and Danckwerts (1972), who report the solubility of N_2O in equimolar mixtures of K_2CO_3 and $KHCO_3$,

and Weisenberger and Schumpe (1996), who developed an empirical solubility model based on van Krevelen coefficients.

Table 5.4. Physical Solubility of CO_2 in Aqueous PZ

T (°C)	[PZ] (M)	H_{CO_2} (atm-L/mol)	$\sigma_{H_{CO_2}}$	$\gamma_{CO_2,meas}$	$\gamma_{CO_2,pred}$
25	0.00	29.65	1.68	1.01	1.00
	0.57	30.36	0.72	1.03	1.01
	1.09	29.91	0.91	1.02	1.03
	1.56	31.60	1.02	1.08	1.05
40	0.00	40.02	1.94	0.98	1.00
	1.09	41.98	1.44	1.03	1.01
	1.56	39.87	1.02	0.98	1.02
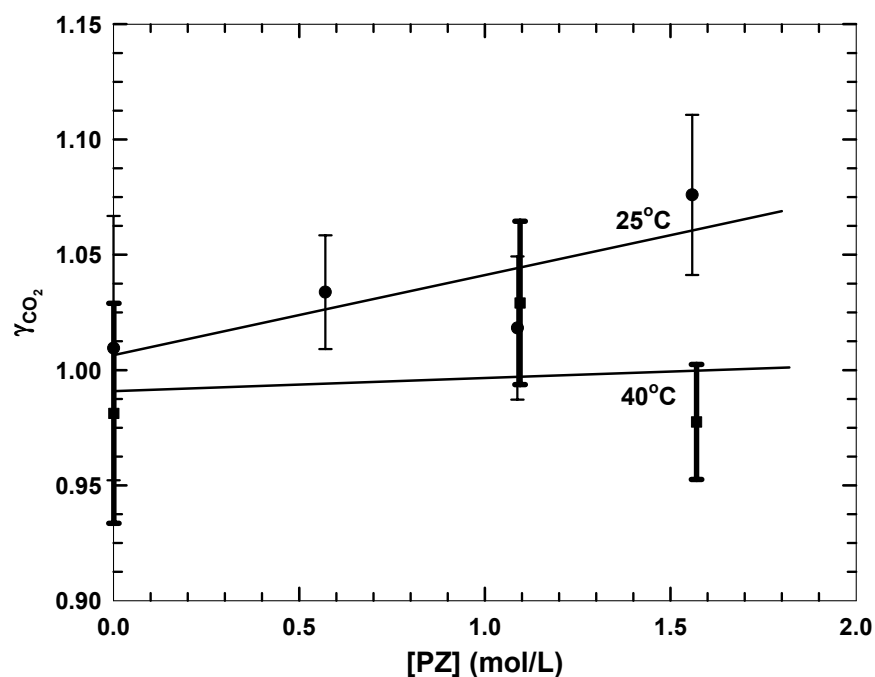
Figure 5.1. Physical Solubility of CO_2 in Aqueous PZ

As shown in the figure, the experimental data and model calculations give similar estimates of activity coefficients. At a given ionic strength, $KHCO_3$ has a more significant impact on γ_{CO_2}. Measurements in K_2CO_3 closely match the model of

114

Weisenberger and Schumpe (1996). At a constant ionic strength, the activity coefficient increases as K_2CO_3 is replaced with $KHCO_3$. Though the solubility in 100% $KHCO_3$ can not be measured experimentally, the model estimation is shown to be consistent with measured data and gives a higher γ_{CO_2}.

Table 5.5. Physical Solubility of CO_2 in Aqueous K_2CO_3/$KHCO_3$

$[K_2CO_3]$ (M)	$[KHCO_3]$ (M)	I (M)	H_{CO_2} (atm-L/mol)	$\sigma_{H_{CO_2}}$	$\gamma_{CO_2,meas}$	$\gamma_{CO_2,pred}$
1.17	0.00	3.51	65.89	3.97	2.24	2.32
1.71	0.00	5.14	96.56	2.54	3.29	3.20
2.23	0.00	6.68	125.77	1.66	4.28	4.20
2.71	0.00	8.12	152.44	20.47	5.19	5.29
0.54	1.27	2.89	71.99	2.32	2.45	2.12
0.76	1.76	4.03	79.54	5.38	2.71	2.70
0.79	1.85	4.22	91.82	14.21	3.13	2.87
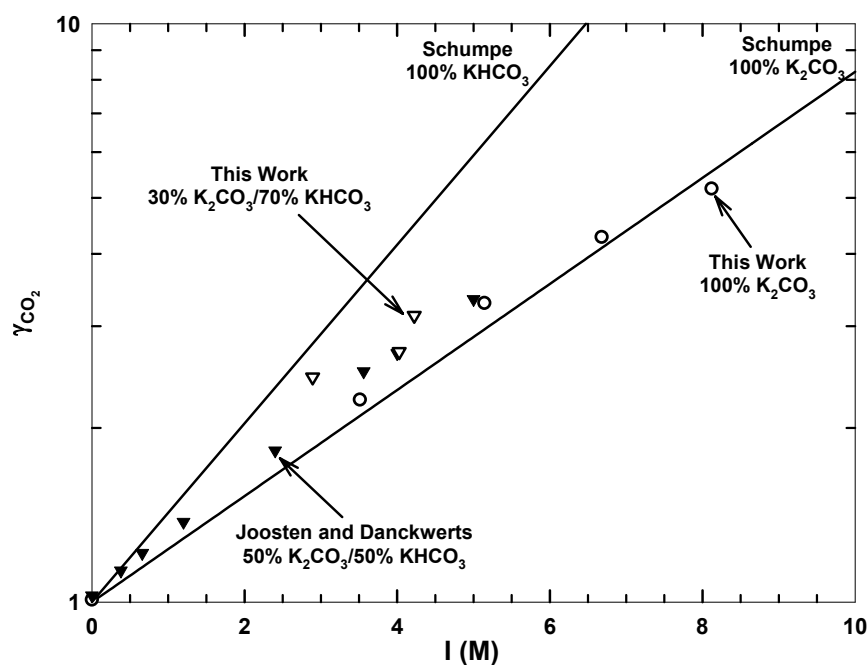
Figure 5.2. Physical Solubility of CO_2 in K_2CO_3/$KHCO_3$ at 25°C

The physical solubility of N_2O was also measured in K^+/PZ mixtures representative of the concentrated solutions investigated in this work. The results are reported in Table 5.6 and represented graphically in Figure 5.3. Empirically, the solubility behaves so that the nominal ionic strength is sufficient for calculating the Henry's constant.

Table 5.6. Physical Solubility of CO_2 in Aqueous K^+/PZ Mixtures

$[K_2CO_3]$ (M)	$[KHCO_3]$ (M)	$[PZ]$ (M)	Nominal I (M)	Calc. I (M)	H_{CO_2} (atm-L/mol)	$\sigma_{H_{CO_2}}$	$\gamma_{CO_2,meas}$	$\gamma_{CO_2,pred}$
0.54	0.00	1.09	1.63	0.77	42.97	0.39	1.46	1.46
1.07	0.00	1.07	3.22	1.53	62.03	5.24	2.11	2.19
0.00	1.06	1.06	1.06	1.65	46.27	1.32	1.58	1.41
0.00	2.03	1.02	2.03	3.00	63.40	2.44	2.16	2.09
0.00	2.83	1.41	2.83	4.18	80.62	9.14	2.74	2.70
0.00	3.62	1.81	3.62	5.40	102.75	0.69	3.50	3.44
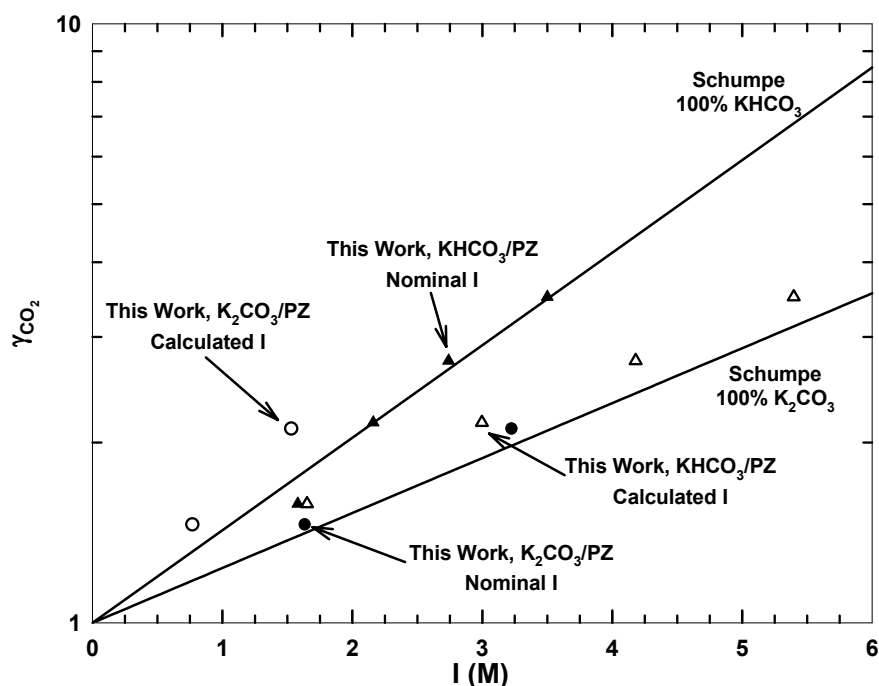
Figure 5.3. Physical Solubility of CO_2 in K^+/PZ at 25°C

116

5.3. Aqueous Potassium Carbonate/Bicarbonate

The osmotic coefficient of water at 25°C as interpreted from several researchers is shown in Figure 5.4. The osmotic coefficient is defined as

$$\phi = \frac{-\ln\gamma_{H_2O}}{3[Salt]MW_{H_2O}},$$
(5.11)

where [Salt] is the molal concentration of potassium salt and MW_{H_2O} is the molecular weight of water in kg/mol. Only data from Puchkov and Kurochkina (1970) and Aseyev (1999) were used in the regression of parameters. The data are from total pressure measurements; the data, and associated limitations, are understood. Also, the data span a comprehensive range of conditions (25 to 140°C and 0 to 60 wt% K_2CO_3).

As a result of distinctive differences and potential inaccuracies in the reported activities (shown in Figure 5.4 as osmotic coefficient), some data were eliminated from the parameter regression. Sarbar *et al*. (1982) and Roy *et al*. (1984) present data as obtained through isopiestic and electrochemical methods. The resulting activity of water is based on theoretical calculations. Apelblat (1992) presents a limited amount of data for saturated salt solutions. The reported activities rely on measurements of solvent concentration as well as vapor pressure and may be subject to additional error.
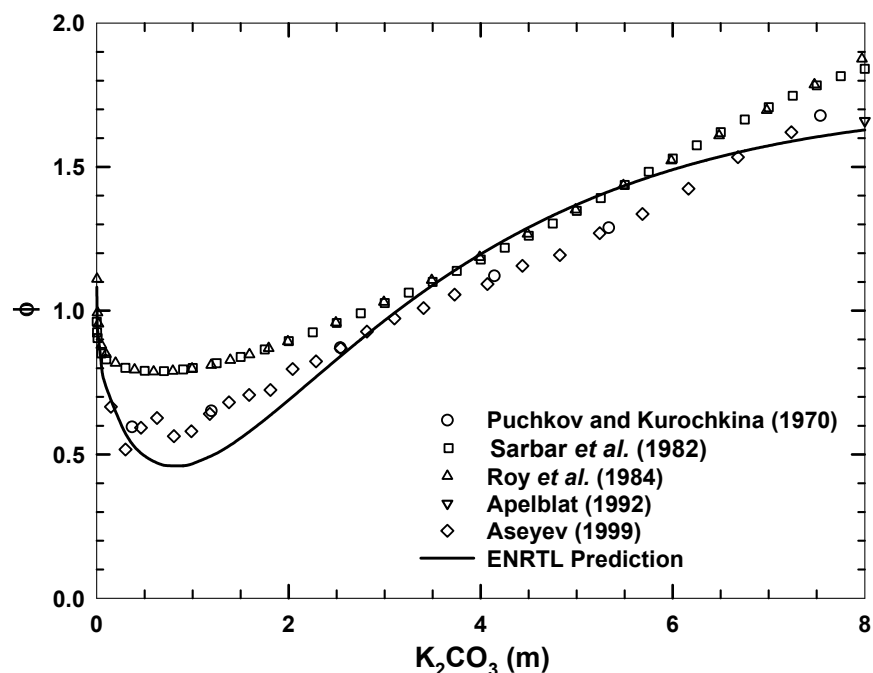
Figure 5.4. Osmotic Coefficient of Water in Aqueous K$_2$CO$_3$ at 25°C

Binary interaction parameters found in the regression for K$_2$CO$_3$/H$_2$O are shown in Table 5.3. The values compare well to those found for other salt pairs by Chen *et al*. (1982). The ENRTL model describes the data well throughout the range of concentrations. It is interesting to note that the form of the model correlation is different from measured trends, leading to systematic errors. Still, the maximum deviation from osmotic coefficients is approximately ±15%, or ±5% from activities.

Also of interest is the temperature dependence of the interaction parameters. Though the temperature dependence is weak, it is systematic. The physical implication, noted by Chen *et al*. (1982), is that the greater the absolute value of the difference in interaction parameters for a molecule-ion pair (e.g. $\left| \tau_{H_2O,K^+,CO_3^{2-}} - \tau_{K^+,CO_3^{2-},H_2O} \right|$) the greater the association of the ion pair. A lower degree of association between the ion pair at higher

118

temperatures is expected; thus, molecule-ion pair parameters should have positive temperature dependence and ion pair-molecule parameters should have negative temperature dependence. This trend is consistent with the values found in this work.

The equilibrium partial pressure of CO_2, $P_{CO_2}*$, reported by Tosh *et al*. (1959) was used to regress parameters for $KHCO_3/H_2O$ mixtures. Data for the mixed solvent system include 20 to 40 wt% K_2CO_3 with a range of conversions to $KHCO_3$ at 70 to 140°C. As with the previous regression, the interaction parameters obtained (Table 5.3) closely resemble behavior demonstrated by other electrolyte systems.

Figure 5.5 and Figure 5.6 show the equilibrium behavior of the mixed solvent at 20 and 40 wt% K_2CO_3 respectively and 70 to 130°C. The experimental data have a high degree of scatter, which is also noted by Chen *et al*. (1979) in an attempt to represent the data with an extended Pitzer model. Chen *et al*. also finds the addition of an ion-ion interaction parameter significantly improves model representation of the data, suggesting an equivalent parameter in the ENRTL model may improve the fit. Yet, the ENRTL model adequately represents the data set using only molecule-ion parameters, deviating by an average of 13.9% over the entire range of conditions.
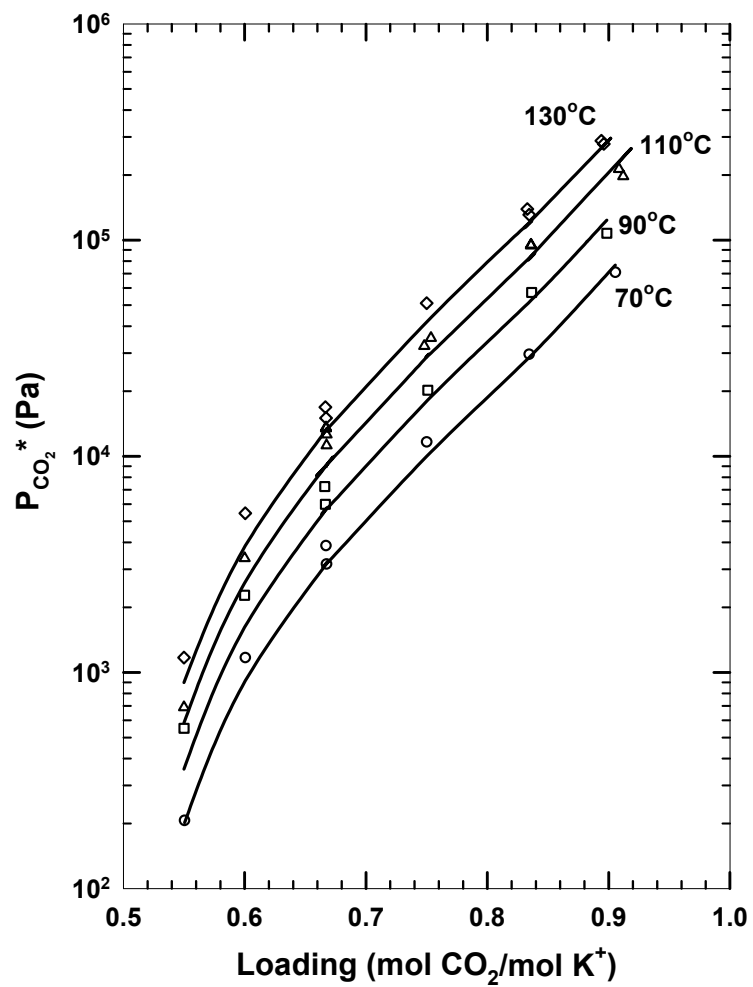
Figure 5.5. $P_{CO_2}^*$ in 20 wt% K_2CO_3, Points: Tosh *et al.* (1959), Lines: ENRTL
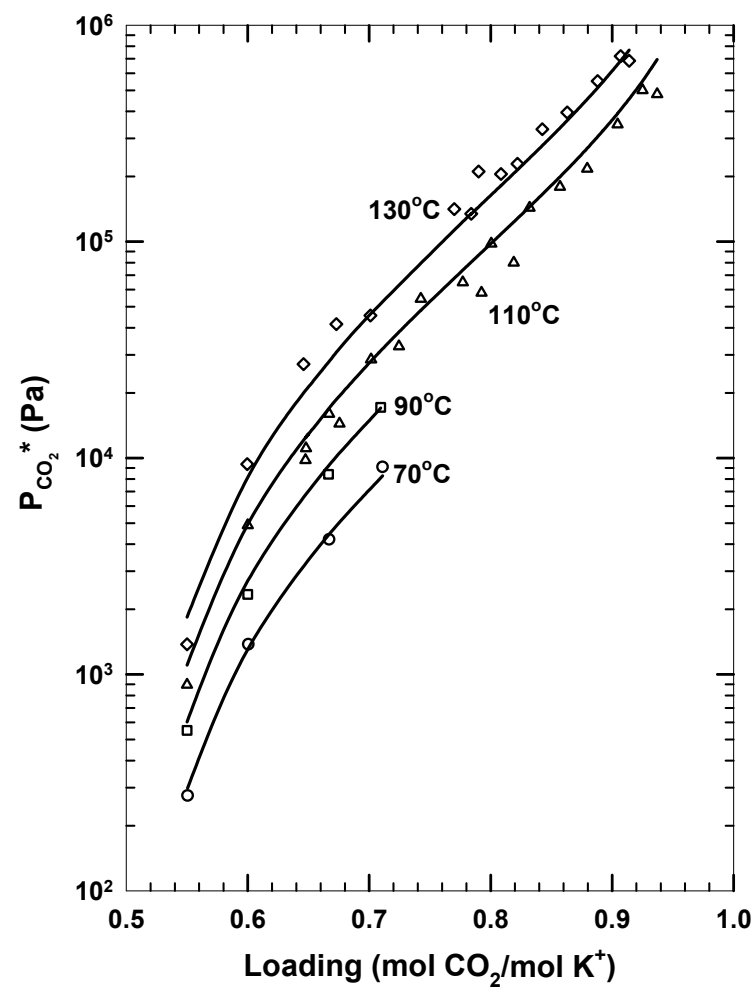
Figure 5.6. $P_{CO_2}^*$ in 40 wt% K_2CO_3, Points: Tosh *et al.* (1959), Lines: ENRTL

120

Data for $K_2CO_3/KHCO_3$ from Roy *et al*. (1984) and Simonson *et al*. (1987) were not used in the data regressions, but were modeled for comparison to the completed ENRTL model. Figure 5.7 shows the accuracy of the fit. A systematic deviation from experimental observations is shown. Regardless, the activity is represented well, deviating by a maximum of 4.2% over the full range of conditions (25 to 95°C).
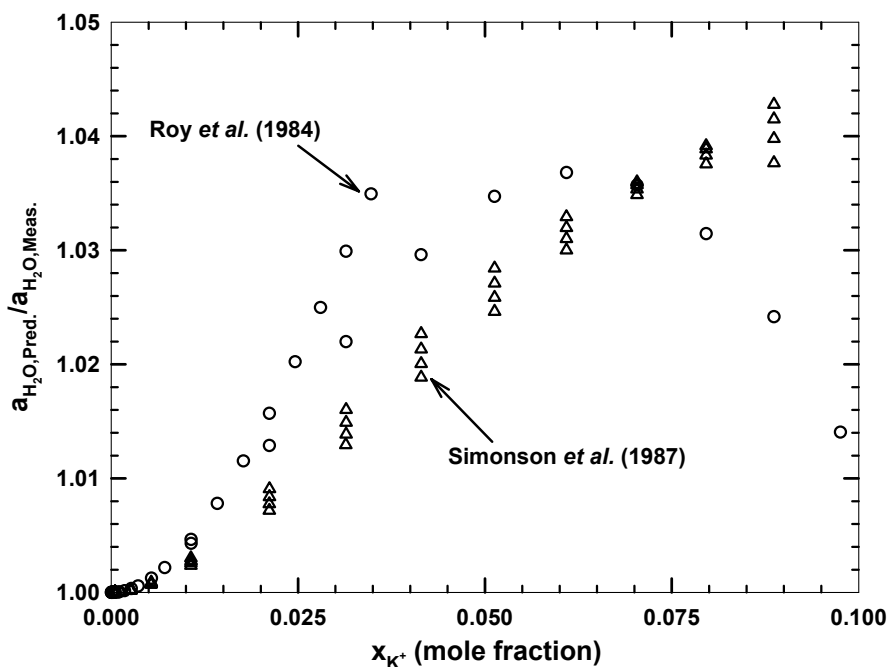
Figure 5.7. Error of ENRTL Predictions of a_{H_2O} in Aqueous $K_2CO_3/KHCO_3$

5.4. Aqueous Piperazine

5.4.1. Infinite Dilution Activity Coefficient and Solution Enthalpy

Data on the behavior of aqueous PZ are limited. The vapor pressure of PZ has been reported at high temperatures (112.8 and 198.8^{o}C) by Wilson and Wilding (1994). These data are derived from total pressure measurements, making the accuracy of points

important to dilute PZ questionable. Cabani *et al.* (1975) gives the Gibbs energy, enthalpy, and entropy of hydration of PZ (PZ(g) → PZ(aq)) at infinite dilution. This can be corrected by the vapor pressure of PZ to give γ_{PZ}^{∞}, but it is not apparent that the liquid behavior should be related by a liquid or solid vapor pressure (PZ is a solid at room temperature).

Given the lack of substantial data, predictions of PZ activity coefficient behavior were obtained from the UNIFAC model (Gmehling, 1982), a purely predictive model based on group contribution methods. UNIFAC bases its estimates for activity coefficients on similar structures that are liquids. This work, then, must assume a liquid reference state for PZ. UNIFAC is assumed accurate for liquid PZ from infinite dilution in water to the solid solubility limit between 25 and 80°C as reported by Bishnoi (2000).

Figure 5.8 shows the attempt to reproduce UNIFAC predictions with the fitted ENRTL model. The models predict a non-linear temperature dependence of γ_{PZ} at infinite dilution. The behavior suggested by UNIFAC is complex as the value of the activity coefficient varies by a factor of twenty over the given conditions. The ENRTL model does not match UNIFAC exactly with the given interaction parameters; however, the fit is acceptable because the accuracy of UNIFAC is unknown. From the ENRTL model, the infinite dilution activity coefficient of PZ can be represented by the equation

$$\ln \gamma_{PZ}^{\infty} = 318.1 - \frac{19779}{T(K)} - 44.42 \ln T(K). \tag{5.12}$$
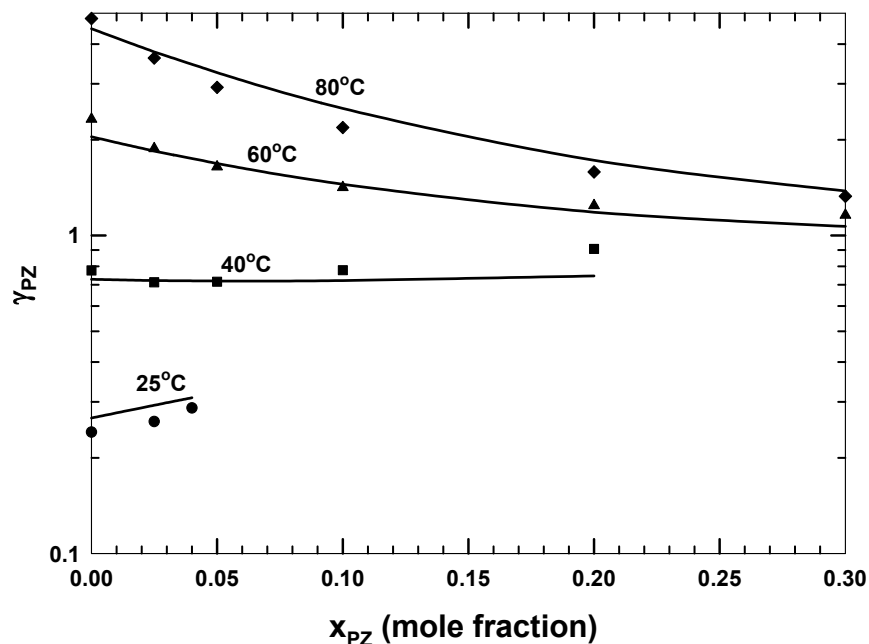
Figure 5.8. Activity Coefficient of Piperazine, Lines: ENRTL, Points: UNIFAC

Various enthalpies of phase change for PZ are reported in the literature and summarized in Table 5.7. Most sources are in close agreement, lending a degree of confidence to their findings. Of particular interest are the heat of fusion and the heat of dissolution, ΔH_{fus} and ΔH_{dis} respectively, whose values can be used to calculate a heat of solution, ΔH_{sol}. The heat of solution is related to the temperature dependence of the activity coefficient by

$$\ln\left(\frac{\gamma_{PZ,T_2}}{\gamma_{PZ,T_1}}\right) = \frac{\Delta H_{sol}}{R}\left(\frac{1}{T_2(K)} - \frac{1}{T_1(K)}\right). \tag{5.13}$$

The calculated value of ΔH_{sol} from literature in Table 5.7 has been compared to model predictions and data from Wilson and Wilding (1994). As shown in Table 5.8,

123

the comparison is favorable, indicating that the UNIFAC and ENRTL models are predicting a reasonable temperature dependence for γ_{PZ}^{∞} over a practical range. ΔH_{sol} is predicted to have a significant dependence on temperature.

Table 5.7. Enthalpies (kJ/mol) of Phase Change for Piperazine

ΔH_{vap}[a]	ΔH_{sub}[b]	ΔH_{fus}[c]	ΔH_{dis}[d]	T (K)	Source
43.93	-	-	-16.43	298.15	Enea and Berthon (1973)
43.25	-	-26.7	-	384.6	Steele *et al.* (1997)
50.1[e]	-	-22.2	-	298.15	
-	-	-22.15	-	381.8	Lee *et al.* (1997)
44.9	-	-	-	380.0	Yaws (1994)
-	72.1	-	-	298.15	Verevkin (1998)
-	72.85	-	-17.42	298.15	Cabani *et al.* (1975)

a. PZ(l) → PZ(g)
b. PZ(s) → PZ(g)
c. PZ(l) → PZ(s)
d. PZ(s) → PZ(aq)
e. Obtained from the an extrapolated Wager equation

Table 5.8. Enthalpy of Solution (kJ/mol) for PZ at Infinite Dilution in Water

ΔH_{sol}	T (K)	Source
-37.7[a]	386 to 471	Wilson and Wilding (1994)
-38.5 to -44.1[b]	-	Calculated Range
-65.9 to -28.4	298 to 353	UNIFAC Model
-54.4 to -34.1	298 to 353	Fitted E-NRTL Model

a. Average value over given temperature range.
b. Maximum and minimum from possible combinations in Table 5.7. Calculated as (ΔH_{dis} - ΔH_{fus}) for values given

5.4.2. Dissociation of Piperazine

Several researchers have reported data on the ionization constant of PZ in water (Equation (5.4)). A summary of these works is shown in Table 5.9. All four works that report values for pK_a give comparable results at 20 to 25°C. Only two works report data at higher temperatures, however, and the pK_a values show significant disagreement. This is shown graphically in Figure 5.9.

In addition to pK_a values, several researchers have reported data on the heat of protonation of PZ in water. Pagano *et al*. (1961) and Hetzer *et al*. (1968) calculate the ΔH based on the temperature dependence of pK_a. Paoletti *et al*. (1963) reports the ΔH from a calorimetric study. The values from Hetzer and Paoletti are consistent, differing slightly from the ΔH found by Pagano. Though the difference is small, extrapolation of the data to high temperatures would lead to significantly different pK_a values (Figure 5.9). Because the pK_a values and the ΔH are in agreement with other sources, this work assumes the data of Hetzer *et al*. best represent the pK_a of PZ.

Table 5.9. Summary of pK_a (Molarity-based, Infinite Dilution in Water) Investigations of Aqueous PZ

$pK_a^{20^oC}$	T (^{o}C)	ΔH^{25^oC} (kJ/mol)	$\Delta c_p^{25^oC}$ (J/mol-^{o}C)	Source
9.82	20	-	-	Schwarzenbach *et al*. (1952)
9.89	10 to 40	-38.91	-	Pagano *et al*. (1961)
9.72[a]	25	-42.55	-	Paoletti *et al*. (1963)
9.86	0 to 50	-42.87	75	Hetzer *et al*. (1968)
-	25	-	29	Cabani *et al*. (1976)

a. Value at 25°C.

In addition to enthalpy effects, the broad temperature range covered in this work requires the consideration of heat capacity and the potential change in ΔH as a function of temperature. Evaluation of the pK_a values from Hetzer *et al*. results in a Δc_p of 75 J/mol-^{o}C, consistent with values reported for primary and secondary alkanolamines (Oscarson *et al*., 1989b). Cabani *et al*. (1976) reports a heat capacity approximately 60% less (29 J/mol-^{o}C) based on calorimetric measurements of HCl addition to dilute aqueous PZ. It is difficult to assess the accuracy of these measurements due to the

correction for the partial molar heat capacity of HCl. Regardless, the effect of Δc_p is relatively small and will have no impact on conclusions derived from this work. Because Hetzer *et al*. is consistent with similar measurements and the ΔH reported agrees with other investigators, a value of 75 J/mol-^{o}C was chosen as the heat capacity. The resulting expression for the pK_a of PZ is Equation (5.4) in Table 5.1.
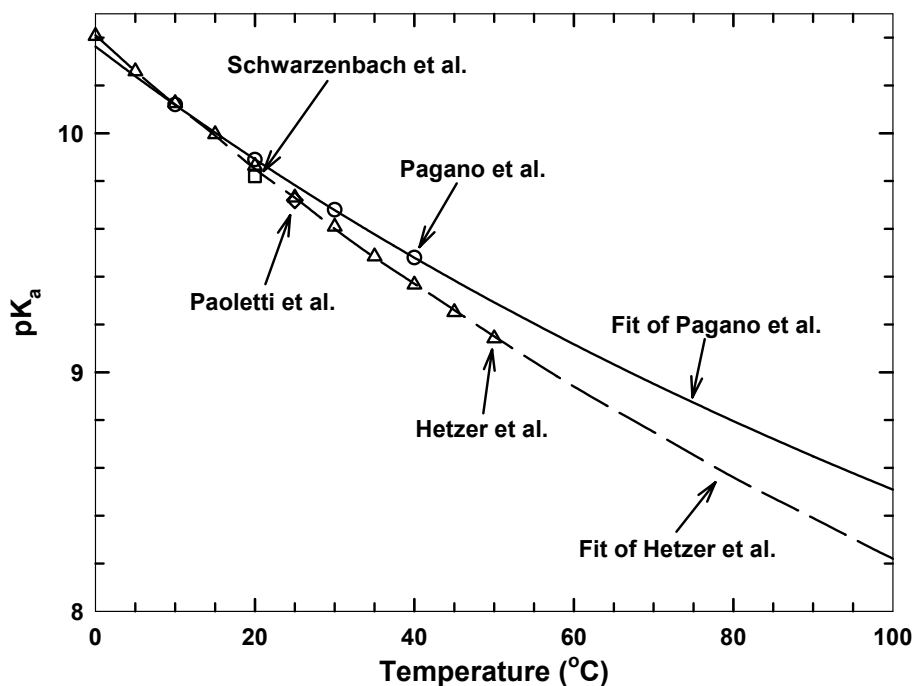
Figure 5.9. Correlation of the pK_a of Piperazine with Temperature

5.4.3. Regression of Parameters for Aqueous Piperazine

PZ speciation, total pressure, and P_{CO_2}* data were used to regress equilibrium constants (Table 5.10) and relevant τ parameters (Table 5.3) for the PZ/H_2O/CO_2 system. Note that the form of the equilibrium constant equations in Table 5.10 differs from that in Table 5.1, reducing correlation between regressed parameters.

126

Table 5.10. Regressed Equilibrium Constants in Electrolyte NRTL Model, Mole Fraction-Based

$$\ln K_i = A + B\left(\frac{1}{T(K)} - \frac{1}{298.15}\right) + C\ln\left(\frac{T(K)}{298.15}\right)$$

Eq. #	Equilibrium Constant	A	σ_A	B	σ_B	C^a
(5.5)	$K_{PZCOO^-} = \dfrac{a_{PZCOO^-} \cdot a_{H_3O^+}}{a_{PZ} \cdot a_{CO_2} \cdot a_{H_2O}}$	-10.15	0.17	21980	530	44.42
(5.6)	$K_{H^+PZCOO^-} = \dfrac{a_{PZCOO^-} \cdot a_{H_3O^+}}{a_{H^+PZCOO^-} \cdot a_{H_2O}}$	-25.91	0.14	-5700	440	0.0
(5.7)	$K_{PZ(COO^-)_2} = \dfrac{a_{PZ(COO^-)_2} \cdot a_{H_3O^+}}{a_{PZCOO^-} \cdot a_{CO_2} \cdot a_{H_2O}}$	-13.26	0.24	1990	710	0.0

a.   No parameters regressed. C parameter for K_{PZCOO^-} set by γ_{PZ}^{∞}.

The simultaneous determination of multiple parameters may introduce error into the regression if values are strongly correlated with one another. Of particular interest is the dependence of the infinite dilution equilibrium constants on the values of τ parameters. Because data cannot be taken at true infinite dilution, equilibrium constants may be particularly susceptible to interference from other parameters. To determine the potential for this type of error, a correlation matrix for the above regression was calculated and is presented in Table 5.11.   Calculations show that the equilibrium constants and τ parameters are only moderately correlated, suggesting the regressed values have little effect on each other and are largely independent.

Table 5.12 presents a comparison, referenced to infinite dilution in water, of the equilibrium constants (K_i) and heats of reaction found by several researchers. Bishnoi (2000) gives estimates based on limited vapor pressure and speciation data and on the

assumption that the ΔH_{rxn} for K_{PZCOO^-} is equal to that of $K_{PZ(COO^-)_2}$ (symmetrically normalized).

Table 5.11. Correlation Matrix for the Simultaneous Regression of Equilibrium Constants and τ Parameters in PZ/H₂O/CO₂

| | K_{PZCOO^-} | | $K_{PZ(COO^-)_2}$ | | $K_{H^+PZCOO^-}$ | | τ | | |
| | A | B | A | B | A | B | PZH⁺,PZCOO⁻,H₂O | H₂O, PZH⁺,HCO₃⁻ | H₂O, H⁺PZCOO⁻ |
	1	2	3	4	5	6	7	8	9
1	1.000								
2	0.175	1.000							
3	-0.065	-0.075	1.000						
4	-0.005	-0.505	0.621	1.000					
5	0.724	0.371	-0.273	-0.368	1.000				
6	0.147	0.752	-0.394	-0.615	0.396	1.000			
7	-0.606	0.520	-0.107	-0.272	-0.194	0.364	1.000		
8	0.507	-0.272	-0.061	0.081	0.115	-0.173	-0.650	1.000	
9	-0.430	0.402	0.131	-0.274	0.066	0.039	0.710	-0.780	1.000

Table 5.12. Equilibrium Constants and Temperature Dependences at 40°C (Mole Fraction-Based, Infinite Dilution in Water) from Four Studies

| Source | K_{PZH^+} | | $K_{H^+PZCOO^-}$ | | K_{PZCOO^-} | | $K_{PZ(COO^-)_2}$ | |
	Value	ΔH_{rxn}[a]	Value	ΔH_{rxn}[a]	Value	ΔH_{rxn}[a]	Value	ΔH_{rxn}[a]
Bishnoi (2000)[b]	6.21E-12	-36.0	6.96E-12	-32.9	4.53E-6	32.4	2.94E-7	77.2
Ermatchkov et al. (2003)[c]	7.70E-12	-42.8	1.13E-11	-29.0	9.24E-6	25.3	8.86E-7	6.2
Aroua and Salleh (2004)[b]	6.21E-12	-36.0	2.03E-14	-962.7	2.28E-5	283.3	2.02E-6	210.8
This Work[c]	7.70E-12	-44.0	1.40E-11	-47.4	7.47E-6	18.3	1.27E-6	16.5

a. Values given in kJ/mol.
b. Values obtained using Pagano et al. (1961) for pK$_a$ of PZ.
c. Values obtained using Hetzer et al. (1968) for pK$_a$ of PZ.

Ermatchkov et al. (2003) presents constants regressed from a large amount of ^{1}H NMR data using the Pitzer-Debye-Huckel model. The data are high enough in ionic strength that the omitted NRTL contributions may potentially alter the regression. The ΔH_{rxn} for the carbamate pK$_a$ is comparable to that obtained by Bishnoi, but is

128

substantially lower than the pK_a of PZ. The heats of reaction for the carbamates are substantially lower than those of Bishnoi, particularly for $K_{PZ(COO^-)_2}$.

Aroua and Salleh (2004) regress concentration-based equilibrium constants from VLE data at 20 to 50^oC and conclude that $PZCOO^-$ is not an important species in solution at high loading. All VLE data reported by Aroua and Salleh are above a loading of 0.8 where little $PZCOO^-$ would be expected to exist. The authors demonstrate an adequate fit of their model to their data, but the reported constants are not expected to apply outside of the high loading region or high temperatures. This is particularly evident in the ΔH_{rxn} values predicted by their regression, given that all non-idealities of the system are lumped into three equilibrium constants.

This work presents a composite of the previous works discussed. The combination of speciation and VLE data from multiple sources improves the significance of regressed parameters. The value of K_{PZCOO^-} is consistent with those found previously, but $K_{PZ(COO^-)_2}$ is approximately 50% higher than found by other researchers. The ΔH_{rxn} for the carbamates were found to be nearly equal ($\sim$17 kJ/mol). Likewise, the ΔH_{rxn} for the pK_a of $PZCOO^-$ is approximately equal to that of PZ as reported by Hetzer *et al*. (1968). Bishnoi (2000) and Ermatchkov *et al*. (2003) obtained or assumed substantially different values for ΔH_{rxn} of each constant.

5.4.4. Liquid Phase Equilibrium

Ermatchkov *et al*. (2003) presents a significant amount of data on the speciation of CO_2 loaded PZ over a broad range of conditions (0.1 to 1.5 m PZ and 20 to 60^oC). This provides the foundation for the regression of equilibrium constants presented in

Section 5.4.3. The resulting ENRTL model is able to calculate the presented speciation with an absolute error of ±5% (Figure 5.10).
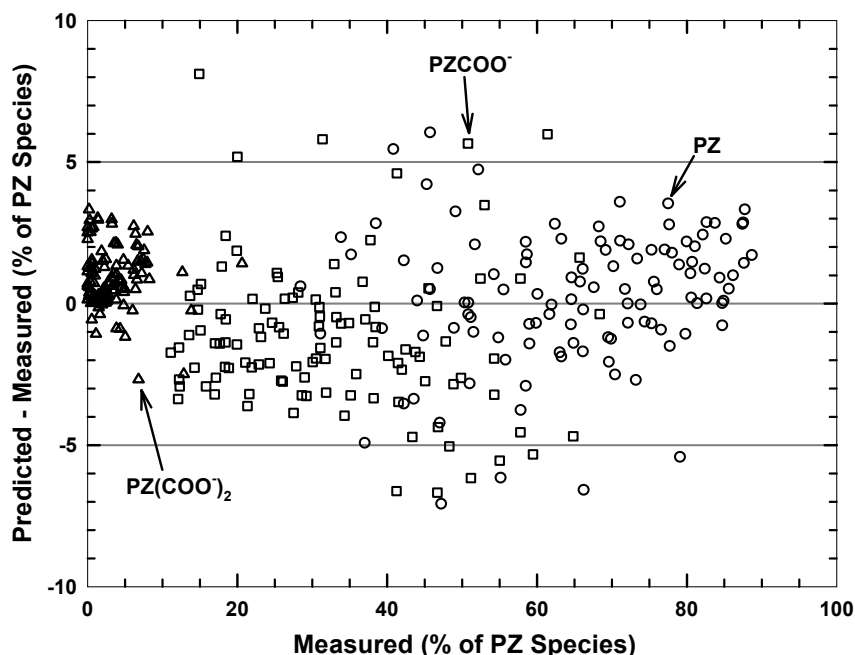
Figure 5.10. Absolute Error of ENRTL Model Predictions of Aqueous PZ Speciation, Data from Ermatchkov *et al.* (2003)

The predicted speciation of aqueous PZ is shown in Figure 5.11 to Figure 5.14. The effect of concentration on the speciation is trivial in that an increase in total amine increases the species proportionally. This is true at both low and high temperatures. In general, the model predicts the formation of some carbamate, but protonated species form preferentially. At low loadings, PZ/PZH^+ buffers the solution and at moderate loadings, $PZCOO^-/H^+PZCOO^-$ buffers the solution. $PZ(COO^-)_2$ is never a significant fraction of the PZ species; therefore, the regressed value of its equilibrium constant has more uncertainty. Bicarbonate does become important at high loadings, accounting for up to 50% of the total CO_2 at some conditions.
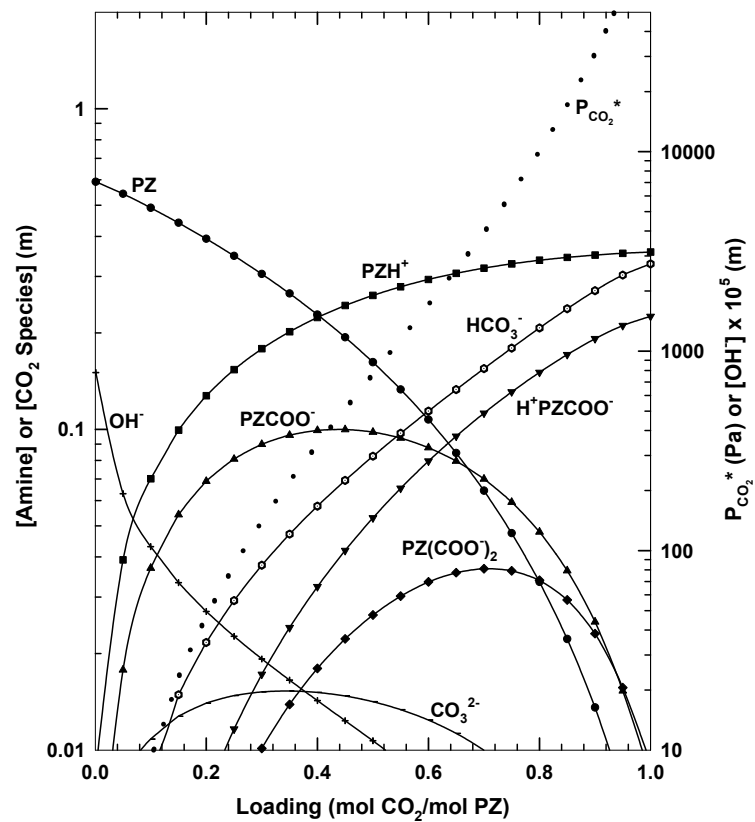
Figure 5.11. Speciation in 0.6 m PZ at 60°C
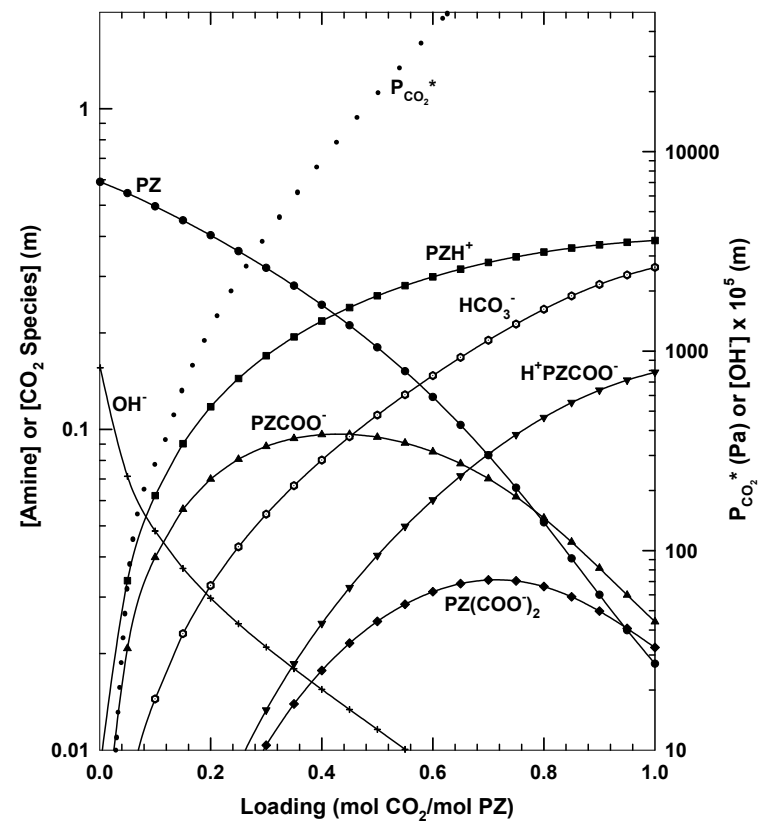
Figure 5.12. Speciation in 0.6 m PZ at 110°C

131
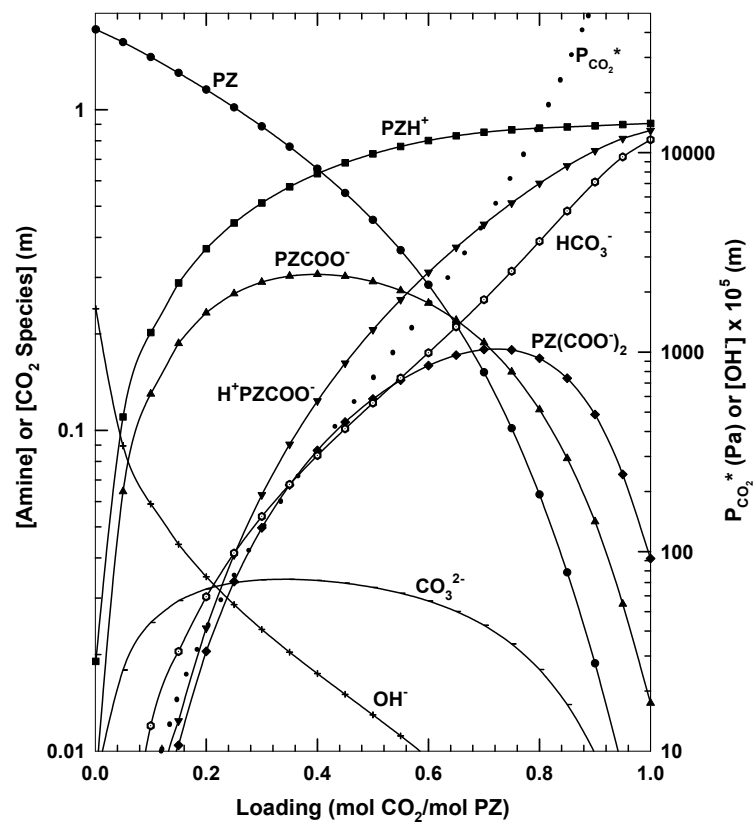
Figure 5.13. Speciation in 1.8 m PZ at 60°C
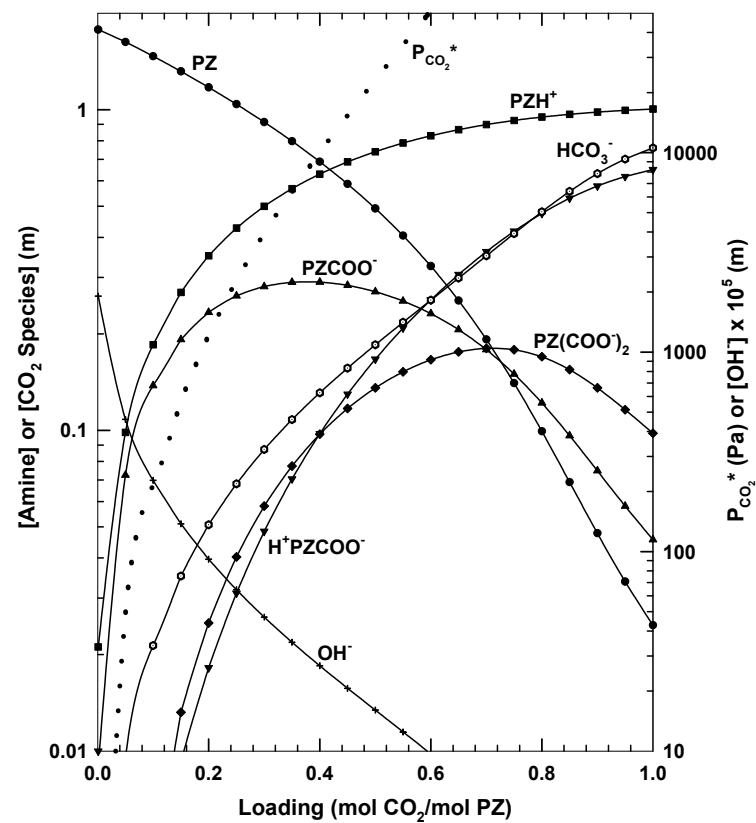
Figure 5.14. Speciation in 1.8 m PZ at 110°C

Another useful perspective for analyzing the speciation is based on the fraction of total amine present as a particular species (Figure 5.15). As the CO_2 concentration is increased in 1.8 m PZ at 60°C, an immediate reduction in the concentration of free amine occurs. At low loadings (0.25/P_{CO_2}* ~100 Pa), the main products are $PZCOO^-$ and PZH^+; approximately 45% of the total PZ has been converted. At intermediate loadings (0.54/~1,000 Pa), the solution is buffered with H^+PZCOO^-. The addition of CO_2 increases the concentration of protonated species, but very little of the carbamate or dicarbamate forms. At high loadings (0.77/~10,000 Pa), $PZ(COO^-)_2$ constitutes only 10% of the PZ and approximately 75% of the PZ is protonated.
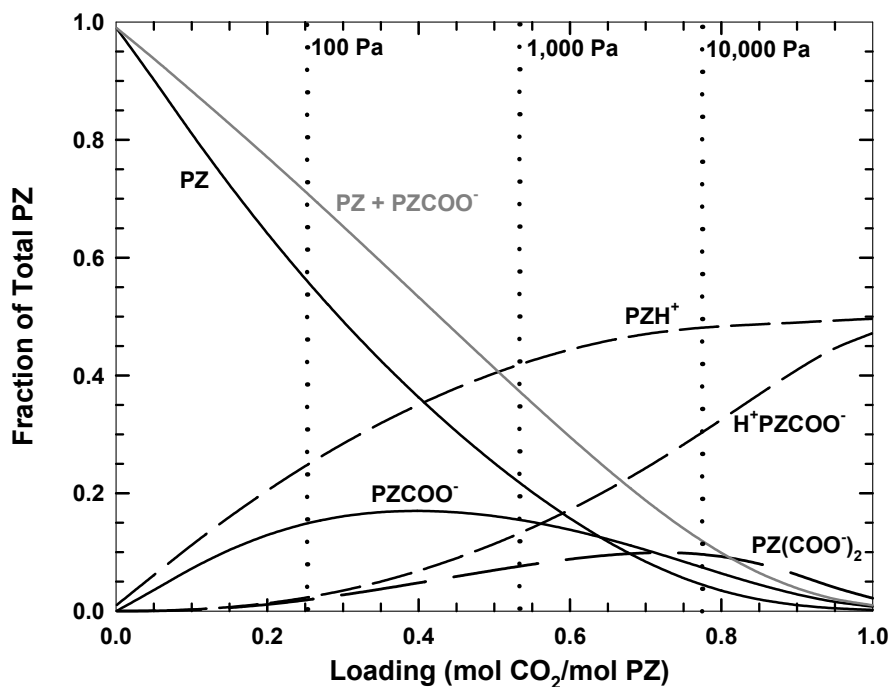
Figure 5.15. ENRTL Prediction of Speciation in 1.8 m PZ at 60°C

The predicted temperature dependence of the speciation is an important consequence of the model regression and is instrumental in calculating the correct VLE and rate at varying conditions. Figure 5.16 shows the model predictions in 1.8 m PZ with a loading of 0.275. As expected, the protonated species are less stable at high temperatures. In general, the carbamate species should be less stable, but the reduction of the protonated species results in a net increase in $PZ(COO^-)_2$. Overall, there is a net conversion of the carbamates to HCO_3^- as temperature increases.
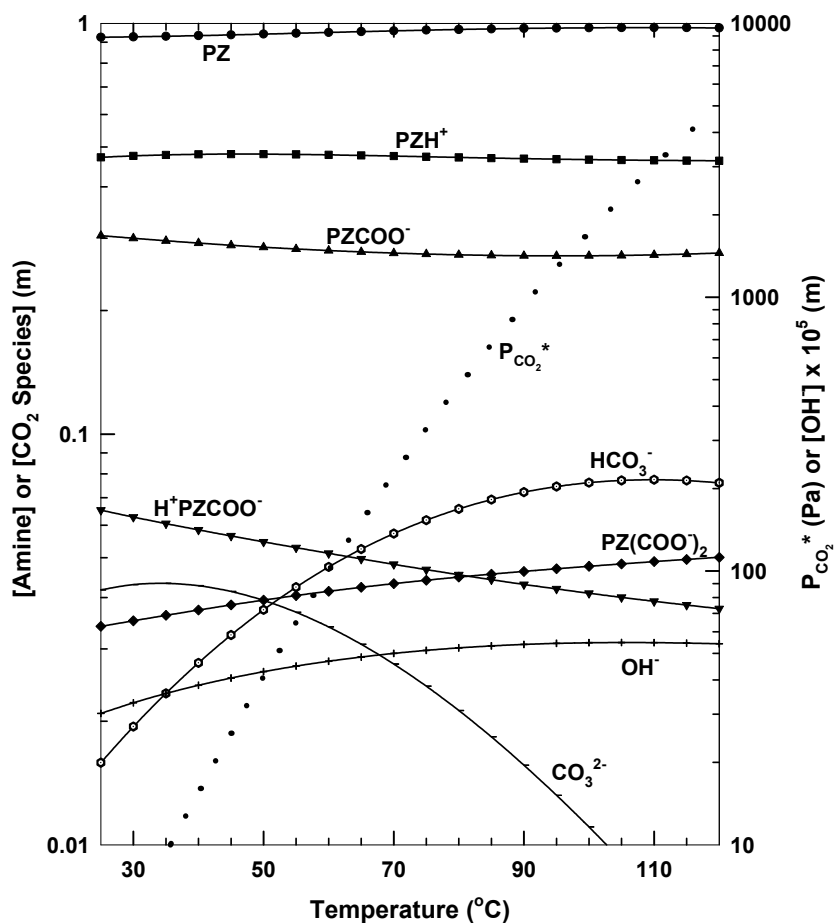
Figure 5.16. Temperature Dependence of Speciation in 1.8 m PZ, Loading = 0.275 (P_{CO_2}* = 100 Pa at 60°C)

5.4.5. Vapor-Liquid Equilibrium

In addition to speciation data, VLE measurements by Bishnoi and Rochelle (2002a) and Kamps *et al.* (2003) were used in the model regression. Bishnoi measured the VLE of 0.6 M PZ at 40 and 70°C by the same method presented in this work. Kamps *et al.* measured the total pressure over 2 to 4 M PZ at high CO_2 loadings. Some data, at extremes of P_{CO_2}* (>100,000) and loading (>1.0), are outside the useful range for this work and were not included in the regression of equilibrium constants.

The model is effective in correlating CO_2 equilibrium partial pressure as a function of loading. Figure 5.17 shows the comparison of experimental data from Bishnoi (2000) and model calculations for 0.6 M PZ. The average relative error of the model is 16%, within the expected accuracy of the VLE measurements. The temperature dependence is also replicated, implying a correct prediction of the heat of absorption, ΔH_{abs}, across the temperature range of the data.

Concentration may also be a significant variable in estimating P_{CO_2}*. As demonstrated in Figure 5.18, however, the total amine concentration has little effect on the predicted partial pressure at 60°C. Between the loadings of 0.2 and 0.7, the P_{CO_2}* for multiple PZ concentrations can be represented as a single curve with only a 10% error. Deviations occur at low and high loadings from complications introduced by significant hydroxide and bicarbonate concentrations. This simplification breaks down at 110°C due to differences in the heats of absorption; significant errors would be introduced by a similar approximation at high temperatures.

135
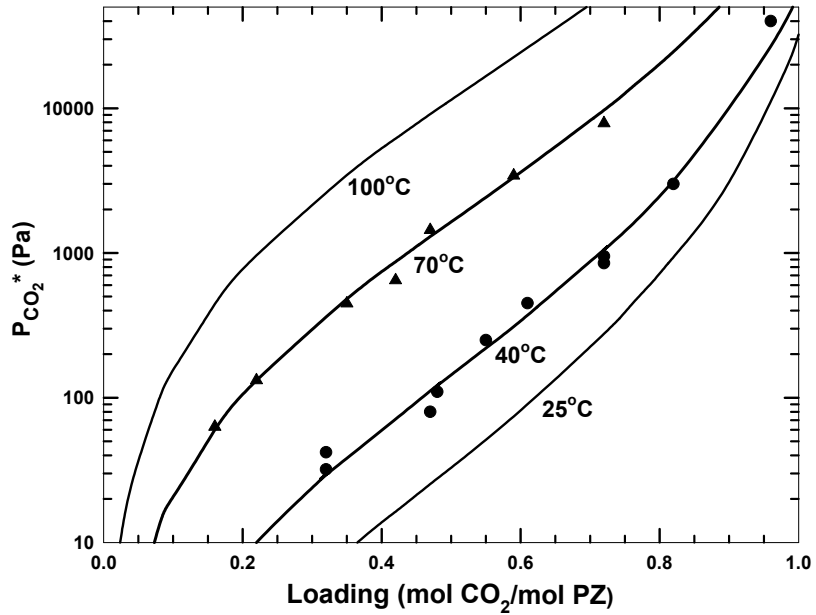
Figure 5.17. VLE of CO_2 in 0.6 M PZ, Points: Experimental (Bishnoi and Rochelle, 2000), Lines: ENRTL Model Predictions
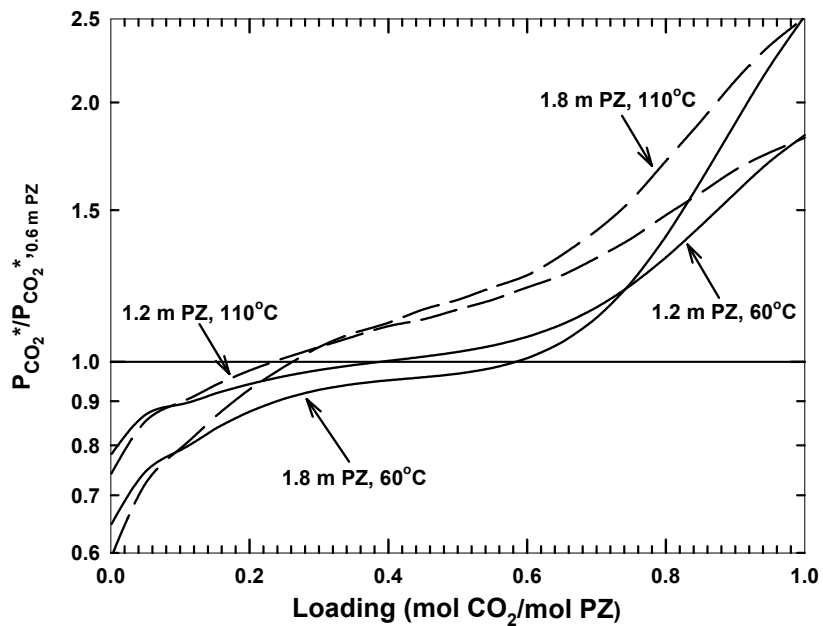
Figure 5.18. Effects of Concentration on $P_{CO_2}^*$ in Aqueous Piperazine Normalized to 0.6 m PZ

ENRTL predictions of PZ volatility are presented in Figure 5.19. At conditions representative of the top of an absorber (lean solution at 60°C), the predicted volatility of 1.8 m PZ is approximately 90 ppm. Volatility is a strong function of concentration and temperature, reaching a value of 700 ppm in 1.8 m PZ at 120°C. Lean solutions have a higher volatility than loaded solutions, where the free amine has been consumed by CO_2. Activity coefficients have a minimal and indirect effect on PZ concentration in the vapor phase because no parameters were regressed for PZ-ion interactions in aqueous solution.
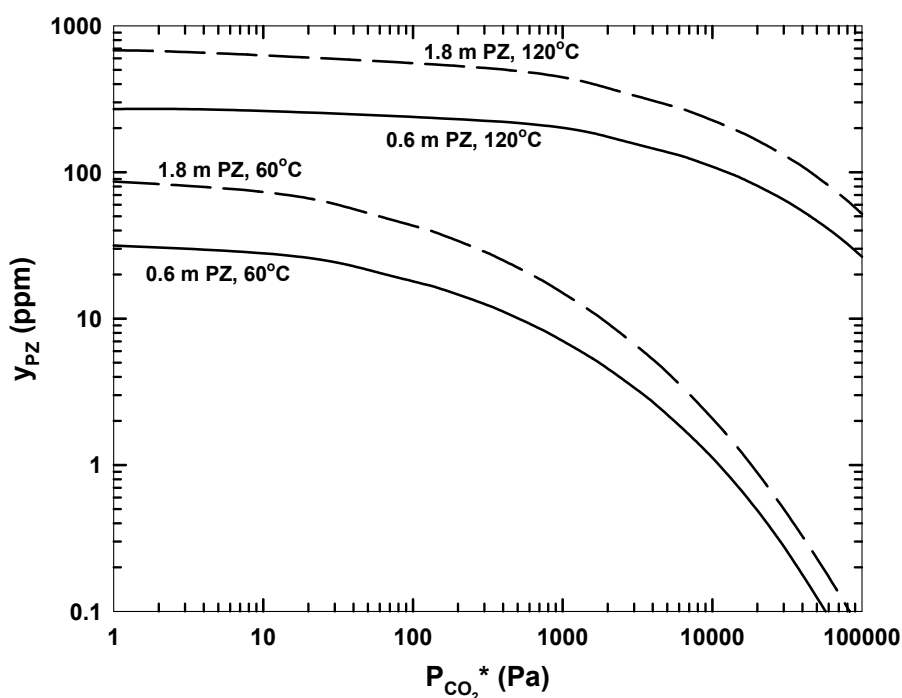
Figure 5.19. Volatility of PZ in Aqueous Solution Predicted by the ENRTL Model

5.5. Aqueous Potassium/Piperazine Mixtures

5.5.1. Liquid Phase Equilibrium

Proton NMR was used to collect speciation data on loaded K^+/PZ mixtures containing 3.5 to 6.2 m K^+ and 0.6 to 3.6 m PZ at 25 to 70°C (Table 5.13). Note that NMR does not distinguish between un-protonated and protonated forms of amines; therefore, the value reported is the sum of those species. These data were used in the regression of parameters describing the influence of salt on the solution. As shown in Figure 5.20, the model predicts the reported speciation within an absolute error of approximately 5%, comparable to the accuracy of model predictions in aqueous PZ (Figure 5.10). Detailed data can be found in Appendix B.

Table 5.13. Piperazine Speciation in K^+/PZ as Determined from ^{1}H NMR

[K^+] (m)	[PZ] (m)	T (K)	CO_2 Loading[a]	PZ + PZH^+ (%)[b]	$PZCOO^-$ + H^+PZCOO^- (%)[b]	$PZ(COO^-)_2$ (%)[b]
3.59	0.60	300	0.429	94.4	5.6	0.0
3.60	0.61	300	0.486	48.1	43.8	8.1
3.59	0.61	300	0.515	31.8	49.5	18.7
3.56	0.61	300	0.554	17.0	47.3	35.7
3.58	0.60	300	0.601	11.1	42.1	46.8
3.59	0.61	300	0.630	8.7	40.3	51.0
3.60	0.60	303	0.357	99.3	0.7	0.0
3.60	0.60	303	0.441	78.2	21.8	0.0
3.60	0.60	313	0.357	99.3	0.7	0.0
3.59	0.60	313	0.429	94.2	5.8	0.0
3.60	0.60	313	0.441	79.0	21.0	0.0
3.60	0.61	313	0.486	48.7	43.4	7.9
3.59	0.61	313	0.515	33.0	49.6	17.4
3.56	0.61	313	0.554	19.1	48.6	32.3
3.58	0.60	313	0.601	12.5	44.0	43.5
3.59	0.61	313	0.630	10.4	41.3	48.3
3.60	0.60	333	0.357	99.5	0.5	0.0
3.59	0.60	333	0.429	92.0	8.0	0.0
3.60	0.60	333	0.441	78.0	22.0	0.0
3.60	0.61	333	0.486	51.0	40.9	8.1
3.59	0.61	333	0.515	35.5	49.4	15.0
3.56	0.61	333	0.554	22.7	49.2	28.0
3.58	0.60	333	0.601	15.4	46.9	37.7
3.59	0.61	333	0.630	12.9	43.8	43.3

[K$^+$] (m)	[PZ] (m)	T (K)	CO$_2$ Loading[a]	PZ + PZH$^+$ (%)[b]	PZCOO$^-$ + H$^+$PZCOO$^-$ (%)[b]	PZ(COO$^-$)$_2$ (%)[b]
3.59	0.60	343	0.429	91.0	9.0	0.0
3.60	0.61	343	0.486	52.1	41.2	6.7
3.59	0.61	343	0.515	37.6	49.3	13.1
3.59	1.81	300	0.433	51.5	41.0	7.5
3.44	1.85	303	0.618	17.3	47.0	35.7
3.46	1.86	303	0.694	9.5	62.4	28.1
3.59	1.81	313	0.433	51.6	41.4	6.9
3.44	1.85	313	0.618	18.1	47.5	34.4
3.46	1.86	313	0.694	11.4	61.2	27.3
3.59	1.81	333	0.433	52.2	41.3	6.5
3.44	1.85	333	0.618	20.4	47.0	32.6
3.57	3.58	300	0.499	35.4	49.0	15.6
3.59	3.61	300	0.600	20.2	48.6	31.2
3.59	3.59	300	0.646	26.0	49.1	24.9
3.60	3.58	313	0.376	59.2	36.5	4.2
3.57	3.58	313	0.499	35.3	48.8	15.8
3.59	3.61	313	0.600	21.2	48.8	29.9
3.59	3.59	313	0.646	25.9	49.6	24.5
3.60	3.58	333	0.376	59.5	36.6	3.9
3.57	3.58	333	0.499	36.0	48.6	15.4
3.59	3.59	333	0.646	28.1	47.6	24.3
5.00	2.50	300	0.433	76.3	22.5	1.2
4.99	2.51	300	0.467	43.9	46.8	9.2
4.64	2.50	300	0.650	11.5	43.8	44.7
4.98	2.50	300	0.534	27.9	50.4	21.6
4.98	2.50	300	0.600	14.9	46.5	38.7
5.00	2.50	313	0.433	69.8	28.1	2.1
4.99	2.51	313	0.467	44.0	47.2	8.8
4.64	2.50	313	0.650	12.3	44.3	43.4
4.98	2.50	313	0.534	27.5	50.2	22.3
4.98	2.50	313	0.600	15.2	46.1	38.8
5.00	2.50	333	0.433	53.6	40.0	6.4
4.99	2.51	333	0.467	42.0	46.5	11.5
4.64	2.50	333	0.650	15.2	43.2	41.6
4.98	2.50	333	0.534	25.1	54.7	20.2
4.98	2.50	333	0.600	15.8	49.3	34.9
6.18	1.23	300	0.570	16.0	46.4	37.6
6.18	1.23	313	0.570	13.2	45.7	41.2
6.18	1.23	333	0.570	14.5	47.6	37.8
6.20	1.81	300	0.666	12.4	44.7	42.9
6.21	1.81	313	0.527	36.1	48.7	15.2
6.20	1.81	313	0.666	13.2	45.8	41.1
6.21	1.81	333	0.527	36.9	49.0	14.2
6.20	1.81	333	0.666	15.0	48.2	36.8

a. Loading = mol CO$_{2,TOT}$/(mol PZ + mol K$^+$).
b. Values reported as % of total PZ.
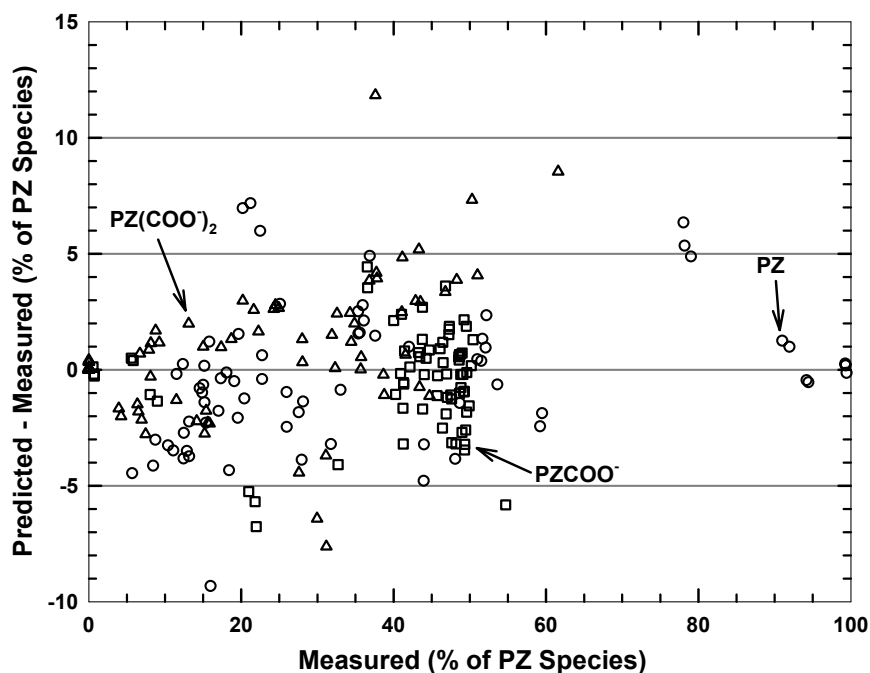
Figure 5.20. Absolute Error of ENRTL Model Predictions of K$^+$/PZ Speciation

The following figures, Figure 5.21 to Figure 5.26, show the speciation as calculated by the fitted ENRTL model for several solvents at 60°C and 110°C. Tabulated predictions of the ENRTL model are presented in Appendix D. With the addition of K$^+$, there is a substantial increase in apparent carbamate stability. Also, the solutions are at a higher pH, reducing the protonation of the amine. Carbonate and bicarbonate are present in significant quantities at all loadings. At 10,000 Pa, as much as 70% of the total CO$_2$ is present in an inorganic form in 3.6 m K$^+$/0.6 m PZ compared to 50% in aqueous PZ. In 5.0 m K$^+$/2.5 m PZ, inorganic CO$_2$ is reduced to 30% of the total due to the increased carbamate concentration. Thus, the buffering and bicarbonate formation is strongly dependent on the relative amounts of K$^+$ and PZ.
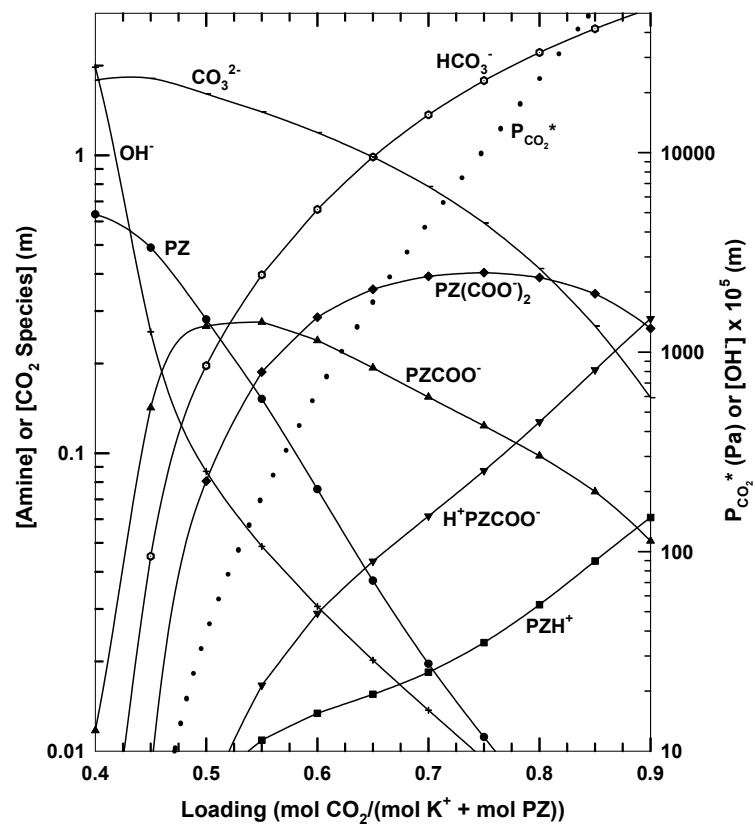
Figure 5.21. Speciation in 3.6 m K$^+$/0.6 m PZ at 60°C
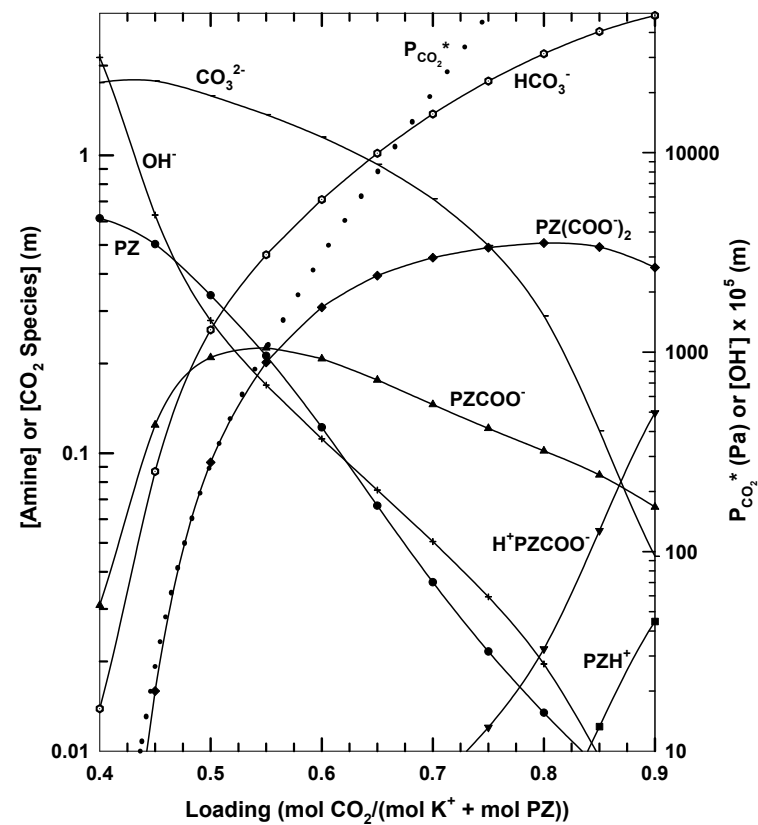
Figure 5.22. Speciation in 3.6 m K$^+$/0.6 m PZ at 110°C

141
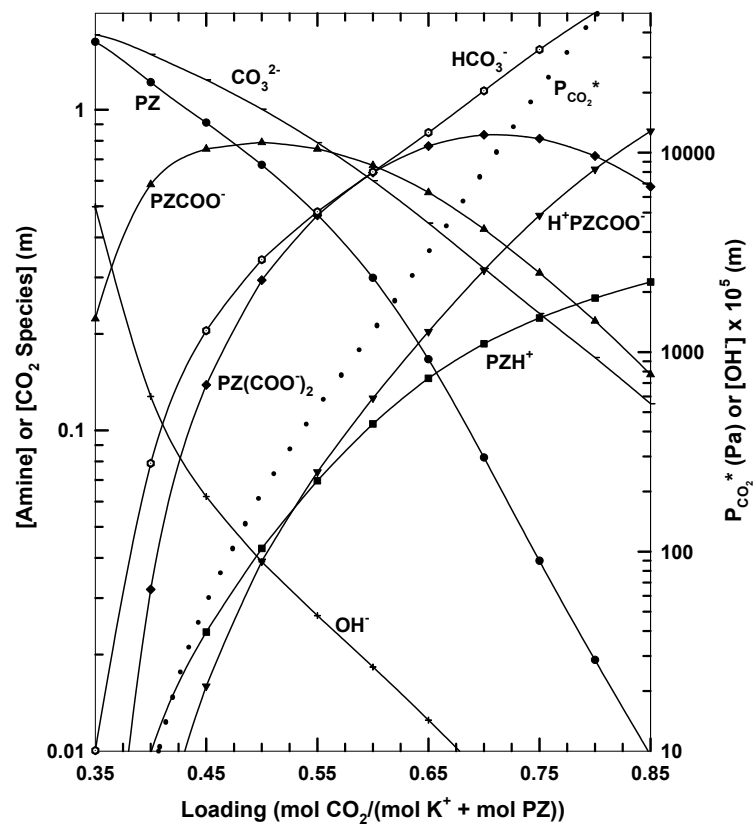
Figure 5.23. Speciation in 3.6 m K⁺/1.8 m PZ at 60°C
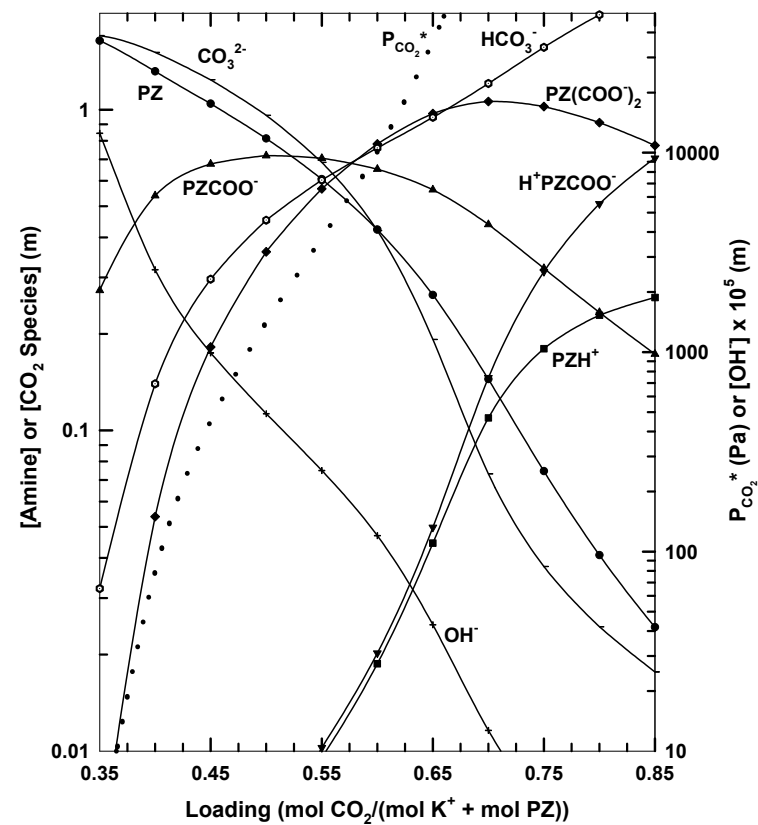
Figure 5.24. Speciation in 3.6 m K⁺/1.8 m PZ at 110°C
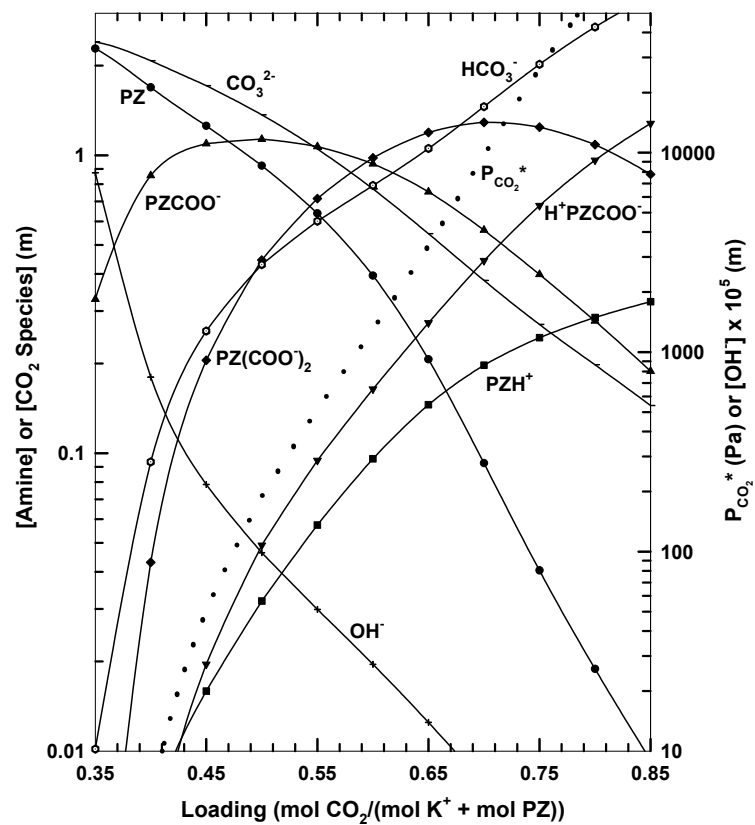
Figure 5.25. Speciation in 5.0 m K$^+$/2.5 m PZ at 60°C
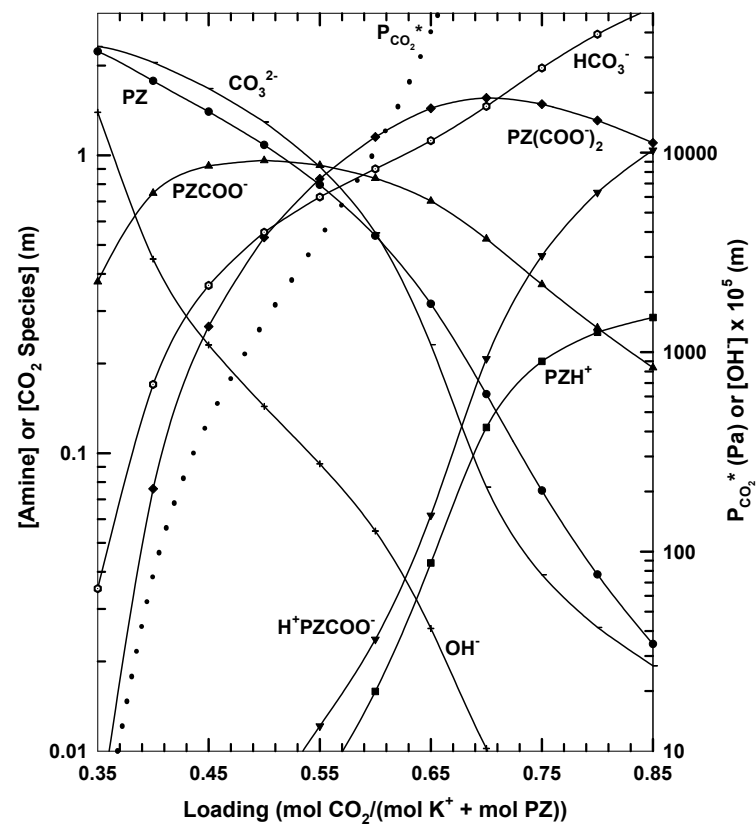
Figure 5.26. Speciation in 5.0 m K$^+$/2.5 m PZ at 110°C

143

Figure 5.27 shows speciation in 5.0 m K^+/2.5 m PZ at 60^oC in terms of fractional PZ content. The maximum concentrations of $PZCOO^-$ and $PZ(COO^-)_2$ can reach 50% of the total PZ species compared to 10 to 20% in solutions containing no K^+. The high concentration of CO_3^{2-}/HCO_3^- buffers the solution at a high pH, delaying the appearance of protonated PZ species until high loadings. Overall, there is a tradeoff between carbamate species and protonated species.

When considering the reactive forms of PZ ($PZ + PZCOO^-$), the advantages of the reduced protonation becomes apparent. Between 100 and 10,000 Pa, the reactive fraction of PZ varies from 85 to 25% compared to 70 to 15% in aqueous PZ. Despite the increased carbamate concentration, a greater amount of reactive PZ exists.
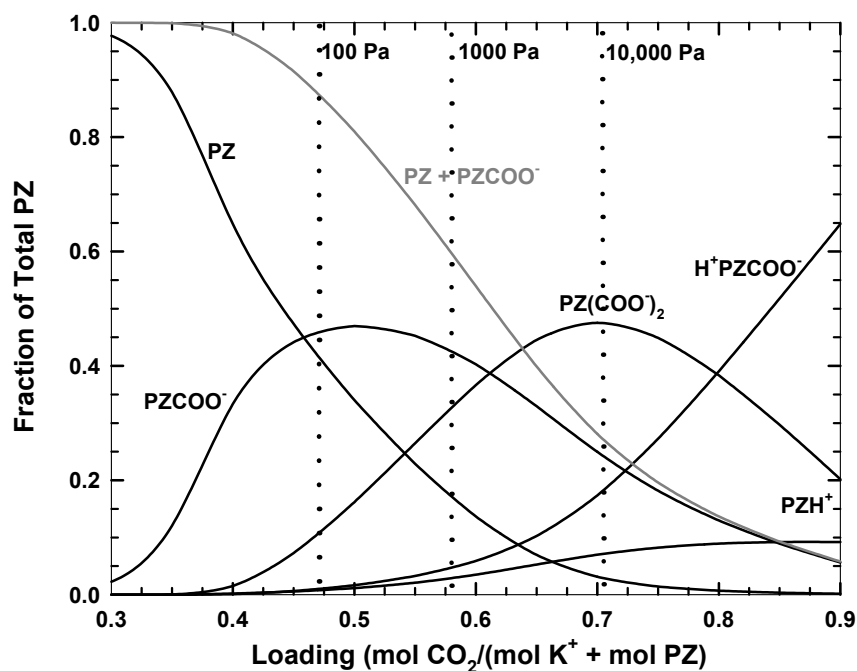
Figure 5.27. ENRTL Prediction of Speciation in 5.0 m K^+/2.5 m PZ at 60^oC

Figure 5.28 demonstrates the competing effects of buffering and carbamate stabilization more clearly. At a constant PZ concentration, an apparent maximum in the reactive species (PZ + PZCOO$^-$) concentration results when the K$^+$/PZ ratio is 2:1. At higher ratios, the PZ(COO$^-$)$_2$ concentration is expected to increase and reduce the total reactive PZ. At lower ratios, protonation of the amine will be more significant. The model does suggest that the reactive PZ concentration always increases with total PZ at a constant K$^+$ content. Effects are similar even as CO$_2$ content is varied between P_{CO_2}* = 300 to 3,000 Pa.
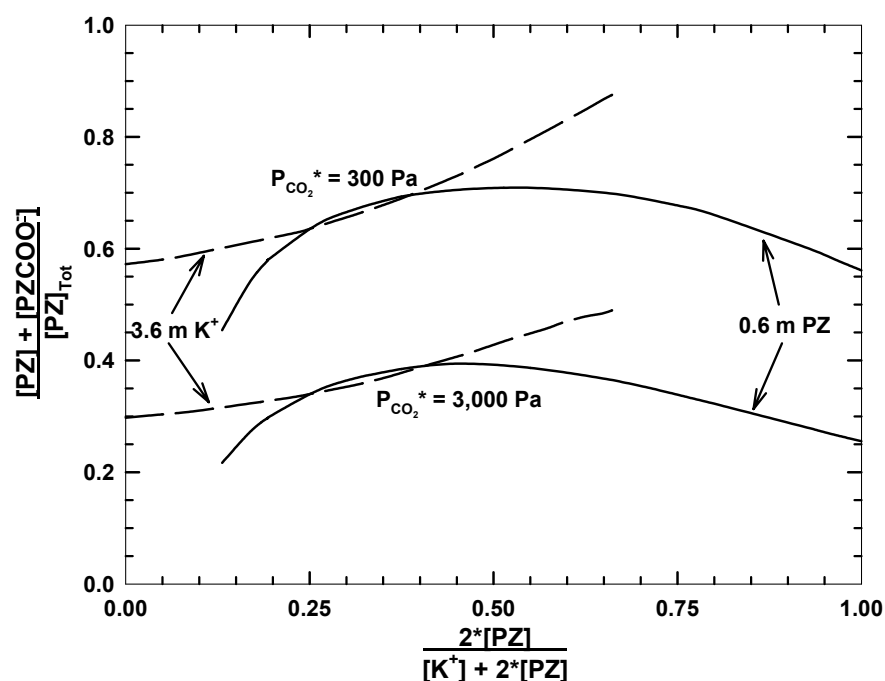
Figure 5.28. Total Reactive PZ Available in K$^+$/PZ Mixtures at 60°C

The temperature dependence of the speciation in K$^+$/PZ mixtures (Figure 5.29) gives trends similar to those observed in aqueous PZ (Figure 5.16). The stability of the protonated and carbamated PZ species decreases as temperature increases. A higher

free PZ concentration results from the temperature increase even though the bicarbonate concentration becomes more significant. The overall effect, then, is storage of more CO_2 as bicarbonate than as amine carbamate.
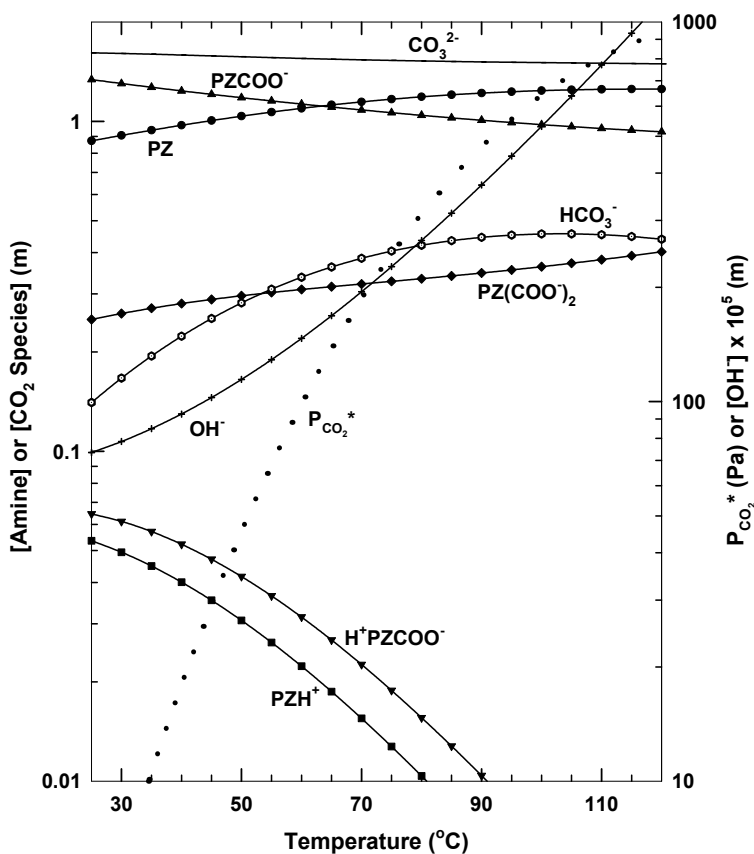
Figure 5.29. Temperature Dependence of Speciation in 5.0 m K^+/2.5 m PZ, P_{CO_2}* = 100 Pa at 60^oC, Loading = 0.473 mol CO_2/(mol K^+ + mol PZ)

To test the validity of the model as a rigorous thermodynamic representation of the proposed solvent, as opposed to an empirical regression, the activity coefficients were predicted from the completed model. Figure 5.30 shows the activity coefficients in 5.0 m K^+/2.5 m PZ at 60^oC. The model calculates reasonable trends, including stable

behavior for molecules and monovalent ions and a lower activity coefficient for divalent ions. The activity coefficient of water increases slightly throughout the loading range.
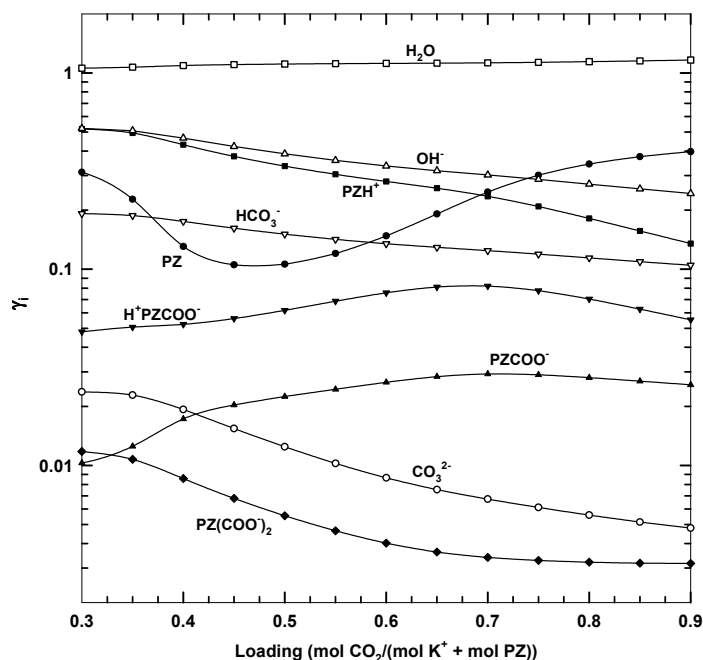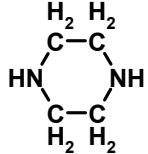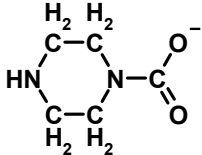
Figure 5.30. Activity Coefficient Predictions of the ENRTL Model for 5.0 m K$^+$/2.5 m PZ at 60°C

The carbamate stability constants for PZ and PZCOO$^-$ are reported and compared to other amines in Table 5.14. The stability of the carbamate species is generally related to the degree of steric hindrance imposed by the structure of the molecule. Hindered amines such as 2-amino-2-methyl-1-propanol (AMP) have very low carbamate stability; conversely, carbamates of primary amines are relatively stable. Piperazine, as measured in this work, is shown to be more stable than the typical secondary amine (e.g. diethanolamine (DEA)), likely due to the unique ring structure of the molecule. The PZCOO$^-$ stability is a factor of six less than free amine. In the presence of K_2CO_3, the carbamate stability constant is decreased slightly.

147

Table 5.14. Comparison of Concentration-based (Molarity) Carbamate Stability Constants at 40°C

Amine	Structure	Environment	K_{carb}[a]	Source
MEA	HO—CH$_2$—CH$_2$—N$\langle$ H / H	$x_{MEA} \to 0$	45.5	Austgen (1989)
		$x_{MEA} \to 0$	12.5	Sartori and Savage (1983)
AMP	HO—CH$_2$—C(CH$_3$)(CH$_3$)—N$\langle$ H / H	$x_{AMP} \to 0$	< 0.1	Sartori and Savage (1983)
DEA	HO—CH$_2$—CH$_2$ $\rangle$ N—H / HO—CH$_2$—CH$_2$	$x_{DEA} \to 0$	2.0	Austgen (1989)
		4 M MDEA	0.1	Bishnoi (2000)
PZ	(piperazine ring)	$x_{PZ} \to 0$	10.1	Bishnoi (2000)
		4 M MDEA	13.2	
		$x_{PZ} \to 0$	15.6	This Work
		2.5 m K$_2$CO$_3$	16.1	
PZCOO$^-$	(piperazine carbamate)	$x_{PZ} \to 0$	0.5	Bishnoi (2000)
		4 M MDEA	8.0	
		$x_{PZ} \to 0$	2.7	This Work
		2.5 m K$_2$CO$_3$	2.8	

a. $K_{carb} = \dfrac{\left[AmCOO^- \right]}{\left[Am \right]\left[HCO_3^- \right]}$

5.5.2. Vapor-Liquid Equilibrium

In addition to speciation data, vapor pressure of CO_2 over the mixed solvent system (2.5 to 6.2 m K$^+$ and 0.0 to 3.6 m PZ) was measured using the wetted-wall column. Data from 40 to 110°C are shown in Table 5.15 as well as model predictions. The data were used, in conjunction with the NMR speciation, to regress K$^+$-PZ interaction parameters. Detailed data are presented in Appendix C. Detailed model predictions are shown in Appendix D.

Table 5.15. Vapor Pressure of CO_2 over K^+/PZ Mixtures at 40 to 110°C

K^+ (m)	PZ (m)	T (K)	CO_2 Loading[a]	P_{CO_2}* (Pa)	$\sigma_{P_{CO_2}}$[b] (Pa)	P_{CO_2}* (Pa), Model	Loading, Model[c]
2.5	2.5	333.2	0.371	79	37	37	0.389
		333.3	0.416	120	-[d]	120	0.402
		333.6	0.500	919	92	733	0.510
		373.5	0.371	321	136	238	0.379
		372.5	0.425	1833	339	1386	0.433
		383.8	0.415	894	331	1324	0.402
		382.9	0.425	3714	449	1781	0.448
3.6	0.0	332.4	0.588	519	49	464	0.590
		333.1	0.776	10370	4990	9714	0.781
3.6	0.6	313.4	0.553	64	8	61	0.551
		313.2	0.698	1635	338	1602	0.698
		332.9	0.441	4	1	4	0.441
		332.5	0.553	279	27	211	0.562
		331.1	0.698	3539	1306	3944	0.691
		352.4	0.553	502	51	509	0.551
		351.5	0.698	10200	83	8763	0.706
		372.8	0.557	1069	36	1056	0.557
		374.1	0.643	5374	534	6325	0.633
		373.8	0.699	14340	2095	17010	0.688
		382.4	0.557	1693	31	1300	0.567
		382.4	0.643	6797	727	7572	0.636
		383.4	0.699	23000	4666	21090	0.703
3.6	1.8	314.6	0.610	156	-[d]	156	0.564
		334.8	0.610	1544	497	1769	0.603
		332.2	0.735	12830	4268	14300	0.730
		332.3	0.761	36710	1432	21590	0.789
		352.3	0.610	5590	271	4934	0.616
3.6	3.6	313.7	0.560	371	251	279	0.595
		314.2	0.684	1711	239	1513	0.704
		331.8	0.500	201	34	201	0.419
		333.7	0.560	1209	20	2034	0.509
		333.1	0.652	6868	682	5471	0.680
		351.8	0.554	7323	116	8492	0.537
		352.5	0.684	34570	4398	40150	0.679
4.8	0.6	313.4	0.717	2453	-[d]	2301	0.719
		333.5	0.717	6212	1072	6144	0.716
		352.0	0.717	14160	4894	12620	0.723
5.0	2.5	313.4	0.570	136	8	147	0.568
		312.4	0.680	1840	-[d]	1340	0.701
		314.0	0.716	3331	276	3169	0.723
		333.5	0.445	45	4	43	0.443
		333.1	0.472	56	51	95	0.451
		333.7	0.595	1642	216	1280	0.611

149

K^+ (m)	PZ (m)	T (K)	CO_2 Loading[a]	$P_{CO_2}^*$ (Pa)	$\sigma_{P_{CO_2}}$[b] (Pa)	$P_{CO_2}^*$ (Pa), Model	Loading, Model[c]
		333.0	0.602	1778	129	1388	0.618
		332.8	0.652	4081	293	3666	0.663
		332.3	0.703	9467	2586	9769	0.706
		352.9	0.689	25720	39	30650	0.684
		351.1	0.716	30460	4017	47900	0.698
		372.8	0.515	1071	199	1617	0.495
5.0	2.5	373.4	0.521	1059	21	1893	0.494
		373.6	0.579	4612	1605	6272	0.563
		373.9	0.579	4535	462	6321	0.562
		373.7	0.612	13150	958	13140	0.611
		383.5	0.521	2658	-[d]	2366	0.525
		383.4	0.570	5869	219	6464	0.564
		383.4	0.612	16300	961	17020	0.610
6.2	1.2	333.9	0.700	6014	605	5668	0.702
6.2	1.8	335.2	0.565	216	38	375	0.540

a. Loading = mol $CO_{2,TOT}$/(mol K^+ + mol PZ).
b. Standard deviation of points used to determine $P_{CO_2}^*$.
c. Loading calculated by the model from measured $P_{CO_2}^*$.
d. Only two points used to determine $P_{CO_2}^*$ (i.e. no standard deviation available).

Figure 5.31 and Table 5.15 include model predictions of $P_{CO_2}^*$ and loading. The prediction of loading gives the loading necessary to match the reported partial pressure exactly. The error in loading is on the order of 5 to 10% whereas the error in $P_{CO_2}^*$ is on the order of 20 to 50%. This means that small errors in loading can result in large errors in $P_{CO_2}^*$ calculations. Given this fact, most of the error associated with the predicted $P_{CO_2}^*$ is attributable to small differences in loading, not large discrepancies in measured partial pressure values or an inadequate model fit.
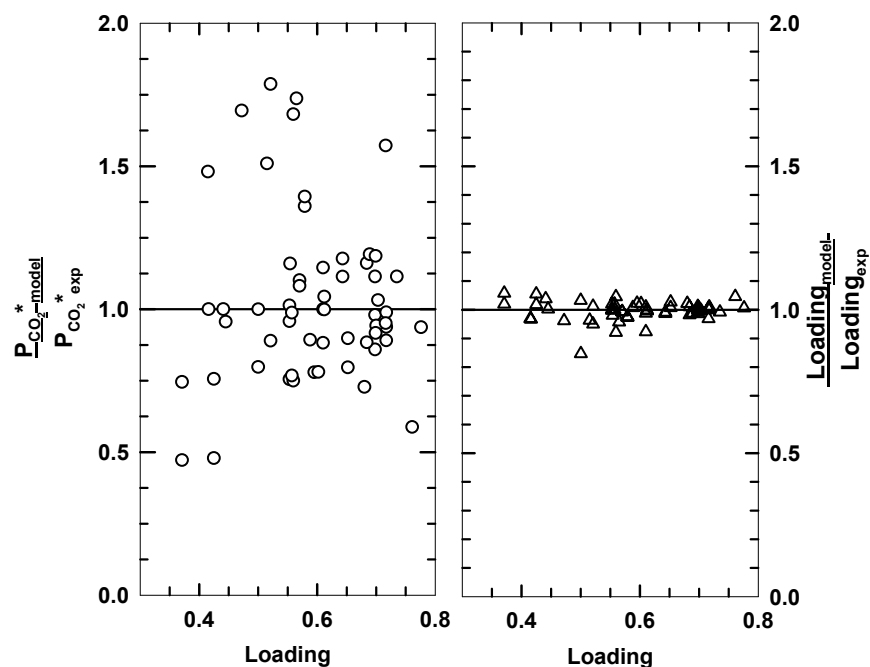
Figure 5.31. Error in the ENRTL Predictions of VLE Behavior in K^+/PZ Mixtures

A comparison of CO_2 equilibrium partial pressure in various solvents at 60^oC is presented in Figure 5.32 along with a representation of 7 m MEA from Dang (2001). ($P_{CO_2}*$ is also presented with the speciation in Figure 5.21 to Figure 5.26.) In comparison to the experimental points shown, it is apparent that the ENRTL model is successful in capturing the VLE behavior over a range of solvent concentrations.

In low solvent concentrations (e.g. 3.6 m K^+/0.6 m PZ), the VLE curve tends to rise faster with loading than in MEA. A higher CO_2 capacity is achieved with an increasing solvent concentration, reflected in the shallowing of the VLE curves. In more concentrated solvents, such as 5.0 m K^+/2.5 m PZ, the slope of the equilibrium line compares favorably with that of 7 m MEA at high $P_{CO_2}*$. At low $P_{CO_2}*$, the behavior is comparable to that of the dilute solvents.
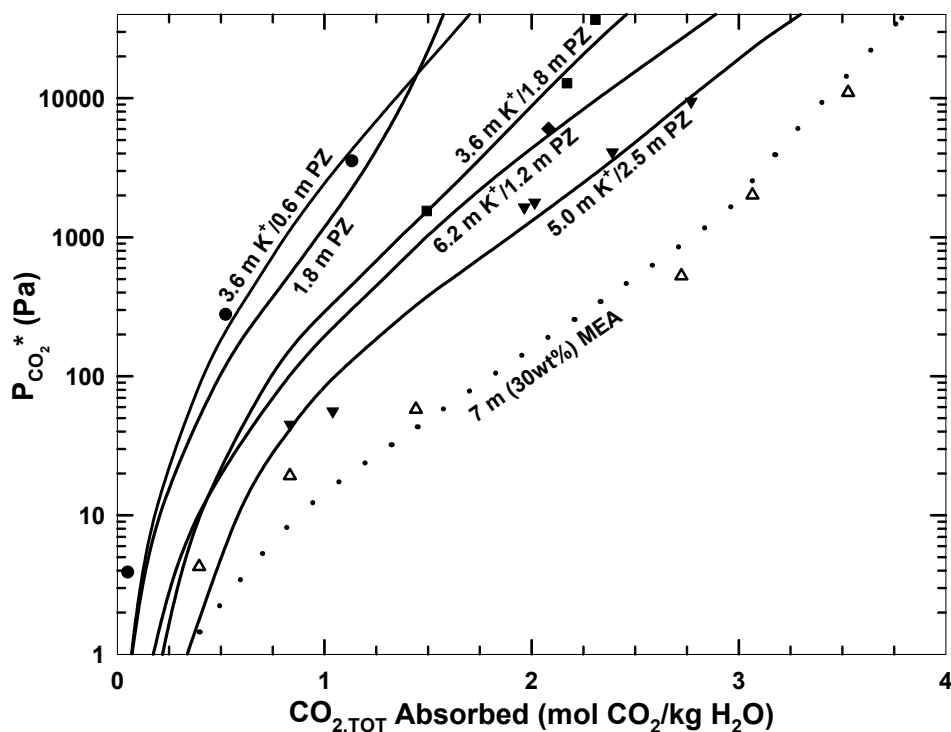
Figure 5.32. VLE of CO$_2$ in K$^+$/PZ Mixtures at 60°C, Points: Experimental, Lines: ENRTL Model Predictions, MEA Curve from Dang (2001)

Both experimental data and model predictions show the temperature dependence of P$_{CO_2}$* for three different solvents in Figure 5.33 to Figure 5.35. In each case, the model correlates the observed trends well. In comparison to the behavior of aqueous PZ, the VLE in K$^+$/PZ mixtures is much more linear throughout the range of interest. Also, the isotherms represented in the figures are nearly parallel throughout this range, indicating the heat of absorption is approximately constant with changes in loading. Total solvent concentration appears to have little effect in the temperature dependence displayed by the VLE.
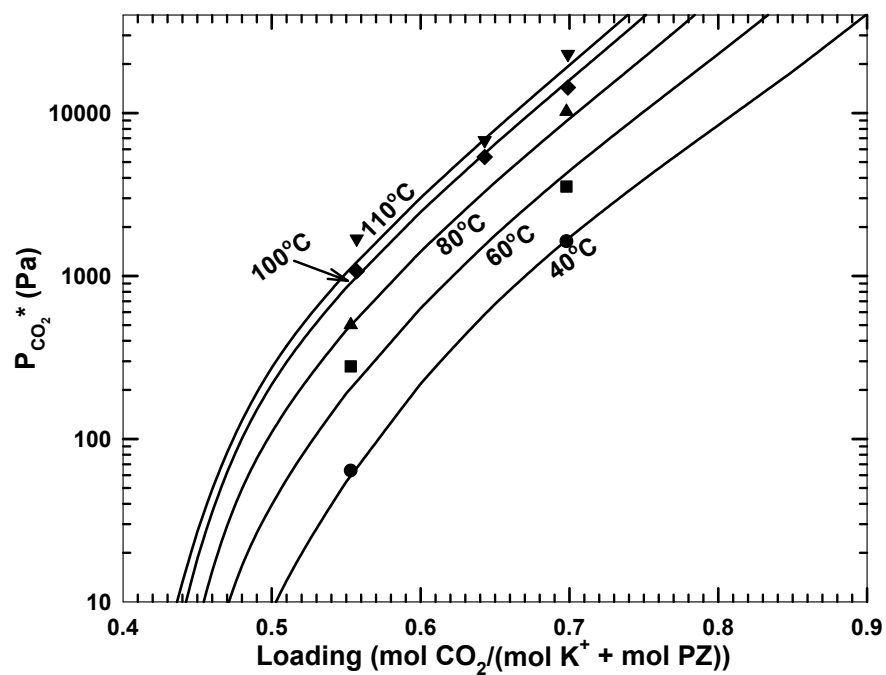
Figure 5.33. Temperature Dependence of $P_{CO_2}*$ in 3.6 m K^+/0.6 m PZ
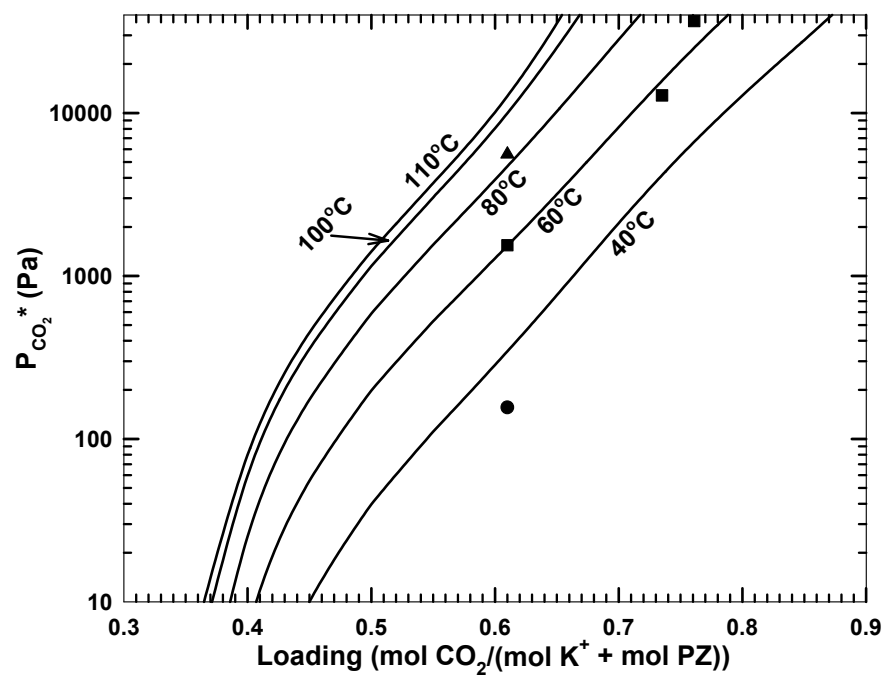
Figure 5.34. Temperature Dependence of $P_{CO_2}*$ in 3.6 m K^+/1.8 m PZ
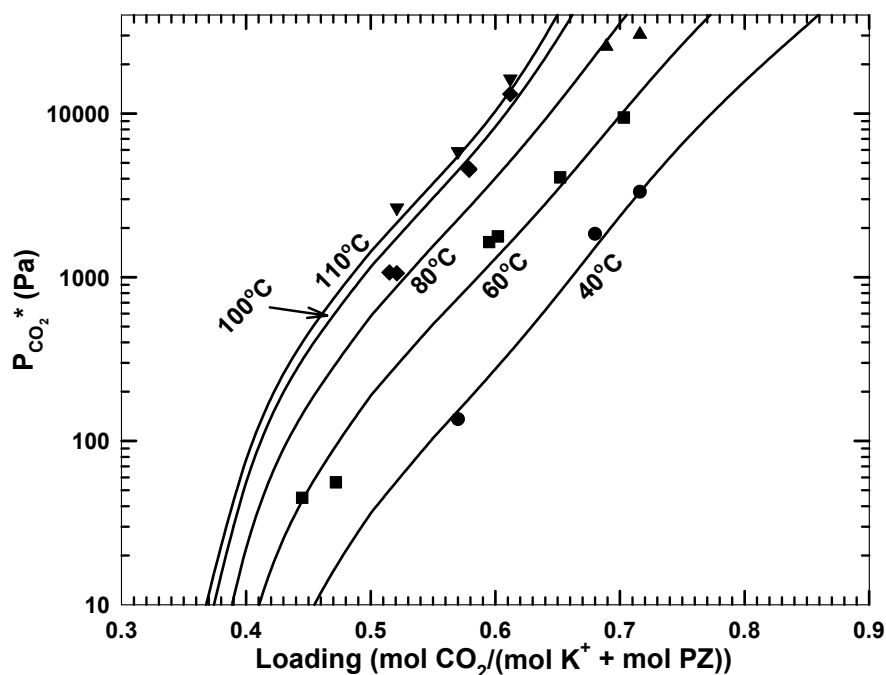
Figure 5.35. Temperature Dependence of $P_{CO_2}*$ in 5.0 m K^+/2.5 m PZ

Figure 5.36 shows the effect of solvent concentration on the representation of $P_{CO_2}*$. As with aqueous PZ, a simplification may be made. Mixed solvents containing the same ratio of K^+:PZ can be represented by the same equilibrium curve. $P_{CO_2}*$ for 3.6 m K^+/1.8 m PZ is essentially the same as 5.0 m K^+/2.5 m PZ at intermediate loadings. The same is true for 3.6 m K^+/0.6 m PZ and 5.0 m K^+/0.83 m PZ. Deviations of only ±10% can be expected by making this approximation.
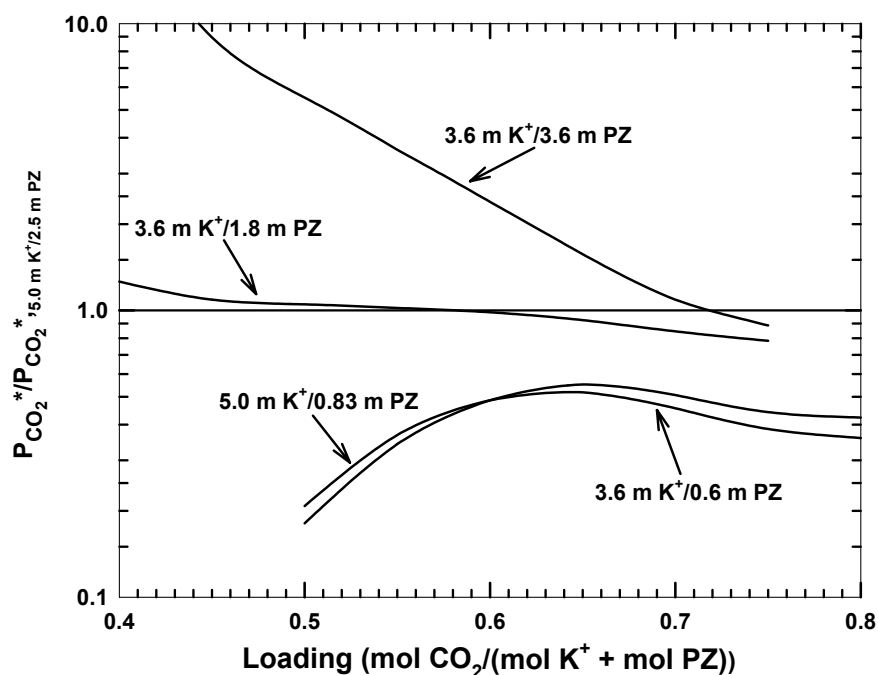
Figure 5.36. Effects of Concentration on $P_{CO_2}^*$ in Mixed Solvents at 60^oC Normalized to 5.0 m K^+/2.5 m PZ

The volatility of PZ in aqueous K^+/PZ mixtures was calculated with the ENRTL model and is presented in Figure 5.37. The volatility is much less than in aqueous PZ (Figure 5.19) due to the significant amount of CO_2 present in solution. At lean conditions, much of the PZ is present as the non-volatile carbamate ion. In 5.0 m K^+/2.5 m PZ, the volatility is predicted to be 9 ppm at 60^oC. Estimates for 3.6 m K^+/1.8 m PZ are similar, but lower in 3.6 m K^+/0.6 m PZ, showing that a larger proportion of CO_2 to PZ reduced the apparent volatility.

It should be emphasized that the estimates do not include the anticipated "salting out" of PZ as a result of ionic strength; no data were available to support the regression of the necessary ENRTL model parameters. The volatility is expected to increase in more concentrated salt solutions.

155
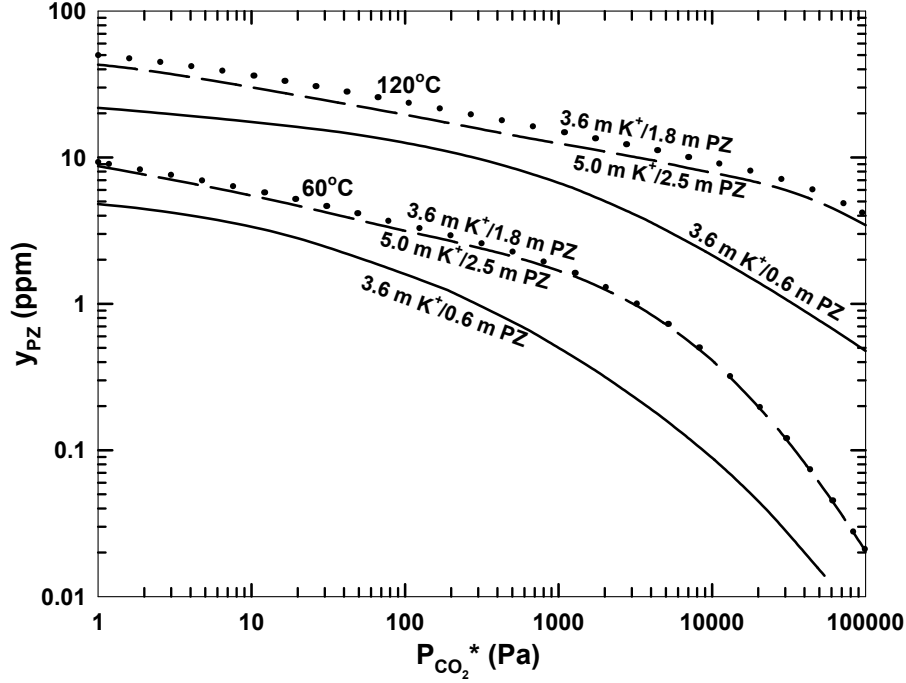
Figure 5.37. Volatility of PZ in K⁺/PZ Mixtures as Predicted by ENRTL Model

5.6. Capacity

The VLE of the solution was analyzed to determine the effect of solvent concentration and partial pressure limits on the capacity of mixed solvents. Capacity is defined as

$$Capacity\left(\frac{mol\ CO_2}{kg\ Solvent}\right) = \left(\alpha_{P^*_{CO_2,rich}} - \alpha_{P^*_{CO_2,lean}}\right)\left([K^+] + [PZ]\right), \qquad (5.14)$$

where α represents loading in mol CO_2/(mol K^+ + mol PZ) and the solvent concentration is given in mol/kg-solvent. This gives a molar quantity of CO_2 absorbed per kg of solvent over a given partial pressure range, $P_{CO_2}^*{}_{,rich}$ to $P_{CO_2}^*{}_{,lean}$.

In Figure 5.38, the effects of lean loading and concentration are demonstrated. One observation is that the capacity, regardless of the partial pressure range, is a nearly linear function of the total solution alkalinity. Another is that capacity increases with a decrease in lean loading, which is expected as more of the VLE curve is used. In comparison to 5 M MEA, the capacity of the K^+/PZ solvent is less competitive as the lean loading is decreased. This is a function of the shape of the VLE curves. From Figure 5.32, it is shown that MEA has a much shallower VLE curve at low $P_{CO_2}^*$, increasing its effective capacity. Operating at $P_{CO_2}^*$,lean = 100 Pa, a total alkalinity of 7 mol/kg is required to equal the capacity of 5 M MEA. At $P_{CO_2}^*$,lean = 10 Pa, MEA has a significant capacity advantage over even concentrated K^+/PZ blends.
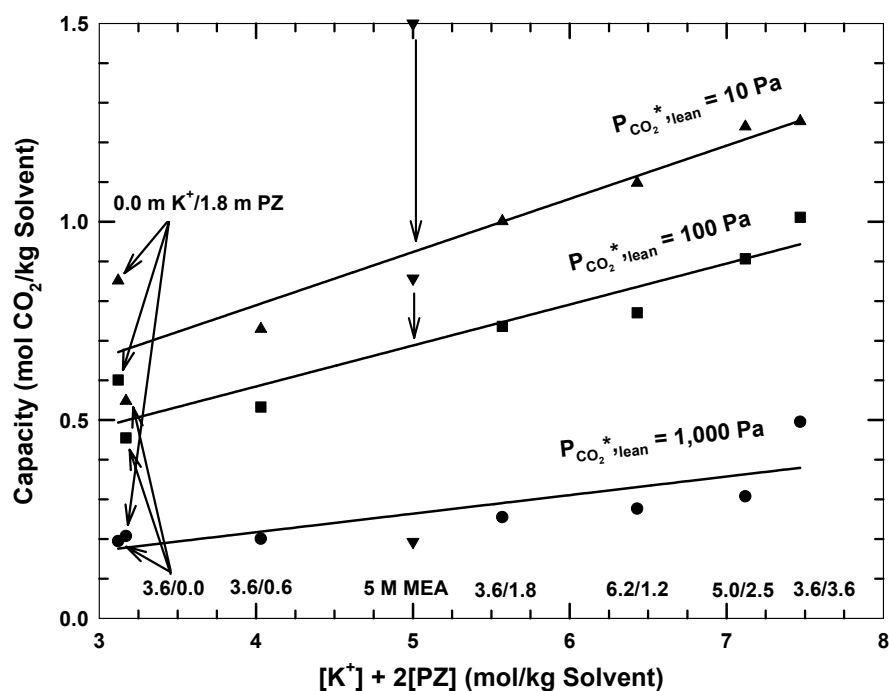
Figure 5.38. Capacity of K^+/PZ Solvents at 60°C, $P_{CO_2}^*$,rich = 3,000 Pa, Points: Calculated from ENRTL Model, Lines: Straight Line Fit of Points

Figure 5.39 gives a similar comparison, but with a fixed lean $P_{CO_2}^*$ of 100 Pa. Again, the capacity increases linearly with the total solvent alkalinity. Increasing the rich $P_{CO_2}^*$ has essentially the same effect as lowering the lean $P_{CO_2}^*$; however, the capacity benefits are greater for K^+/PZ than in 5 M MEA. This difference is due to the shallow VLE curve in K^+/PZ at higher $P_{CO_2}^*$. By utilizing the upper part of the curve, the capacity is increased over that of MEA, even in less concentrated solvents (e.g. 3.6 m K^+/1.8 m PZ).
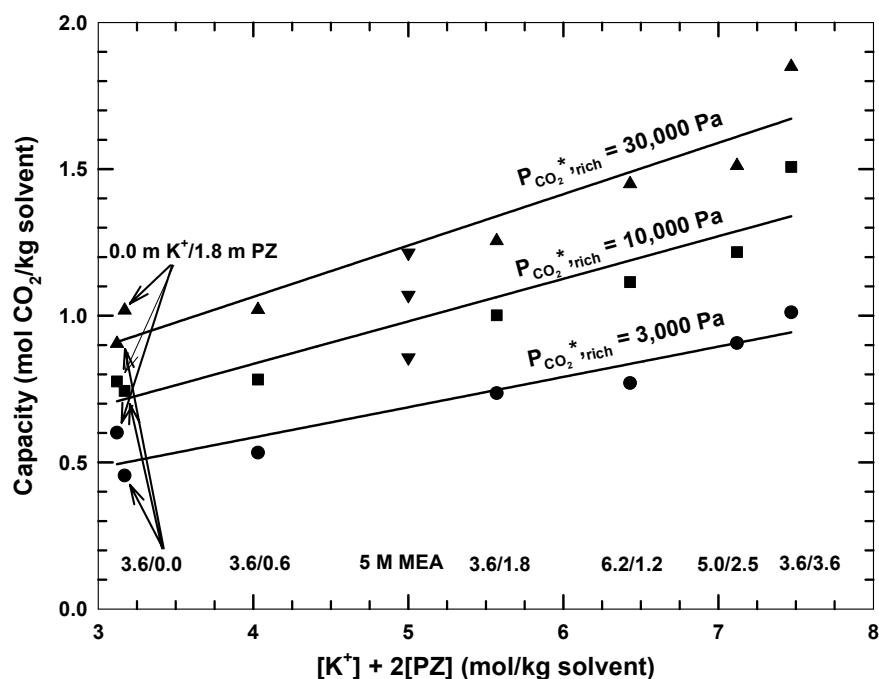
Figure 5.39. Capacity of K^+/PZ Solvents at 60°C, $P_{CO_2}^*$,lean = 100 Pa, Points: Calculated from ENRTL Model, Lines: Straight Line Fit of Points

It is also striking that the 10 to 3,000 Pa range gives nearly an identical capacity as the 100 to 10,000 Pa range in K^+/PZ. Thus, by increasing the partial pressure range by virtue of either the lean or rich end of the VLE curve, similar effects can be obtained.

158

It is a somewhat trivial conclusion that increasing the partial pressure range increases capacity. Given the previous two analyses, the direction of the most effective increase is not obvious. For K^+/PZ mixtures, additional capacity benefits above those found in MEA can be realized by increasing the rich P_{CO_2}*. Also, increasing the rich end has a larger impact on the capacity than an analogous decreasing of the lean end.

5.7. Heat of Absorption

The heat of CO_2 absorption into a solvent is an important parameter in that it describes the chemical energy released during the absorption process. Likewise, it represents the minimum energy needed to reverse the reaction and release CO_2 from solution. The heat of absorption of CO_2 into aqueous PZ and K^+/PZ blends has been estimated using VLE calculations from the ENRTL model according to the equation

$$\Delta H_{abs} = R \cdot \frac{\partial \ln P_{CO_2}^*}{\partial \left(\dfrac{1}{T} \right)}.$$ (5.15)

The calculated heat of absorption for aqueous PZ is shown in Figure 5.40 as a function of loading. At low to intermediate loadings, the calculated average of ΔH_{abs} between 40 and 70°C is constant at -80 kJ/mol. The small perturbation at loadings less than 0.05 is caused by absorption by hydroxide. As loading increases above 0.5, the formation of bicarbonate becomes more significant, decreasing the ΔH_{abs} sharply. As loading increases past 1.0, ΔH_{abs} should approach that of physical absorption (~ -20 kJ/mol). This trend with loading is similar to experimental observations for alkanolamines, such as DGA and DEA (Oscarson *et al.*, 1989a).

A temperature dependence of ΔH_{abs}, a heat capacity of absorption ($\Delta c_{p,abs}$), is predicted by the ENRTL model. A substantial decrease in ΔH_{abs} accompanies an increase in temperature, contradicting previous work (Oscarson *et al.*, 1989b). Partial pressure data are a poor predictor of derived properties such as Δc_P, particularly over a narrow temperature range as is available in this work, and should not be the sole basis for such extrapolations. An average value spanning the range of available experimental data (40 to 70°C) is recommended for estimating ΔH_{abs}.
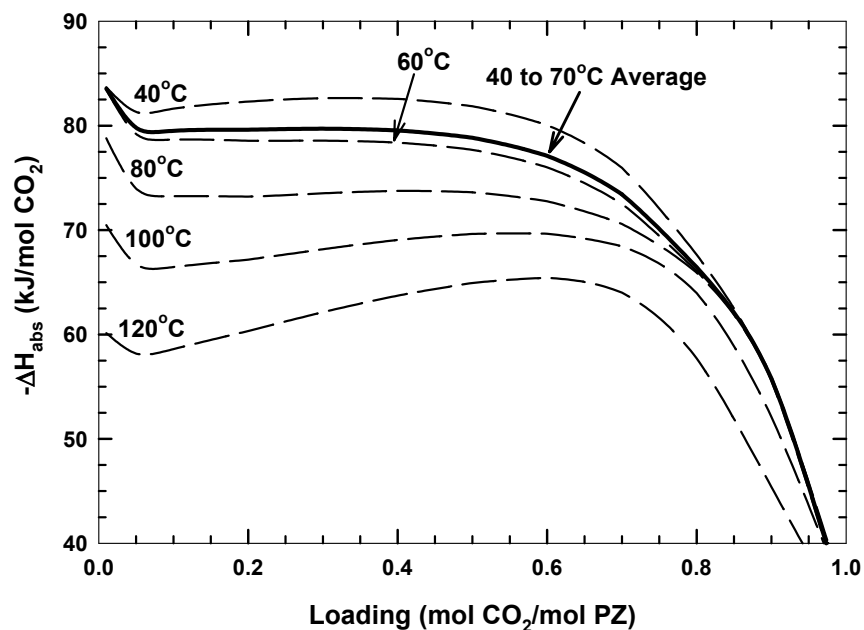
Figure 5.40. Heats of Absorption of CO_2 in 1.8 m PZ

The ΔH_{abs} was also calculated for mixed solvents to determine the effect of K^+ on the overall heat of reaction. Figure 5.41 shows the ENRTL predictions for 5.0 m K^+/2.5 m PZ. The behavior is strikingly different from aqueous PZ. Using the 40 to

$70^{\circ}C$ average, the ΔH_{abs} is nearly constant as a function of loading, suggesting that the larger quantity of CO_3^{2-}, relative to PZ, effectively lowers the overall energy requirement. The ΔH_{abs} is 20% less than in aqueous PZ. The model predicts a similarly unexpected dependence of ΔH_{abs} on temperature.
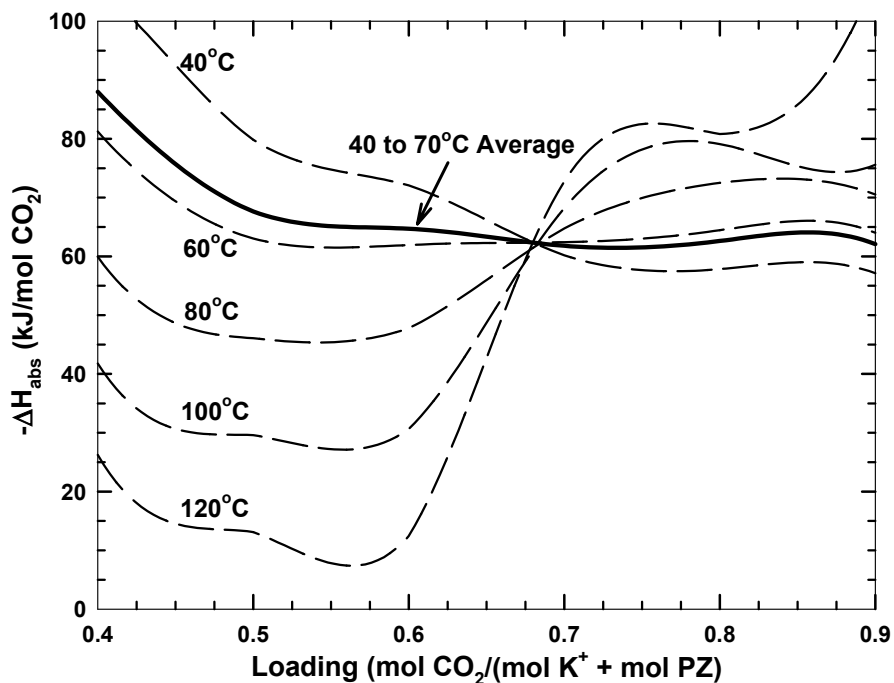
Figure 5.41. Heat of Absorption of CO_2 in 5.0 m K^+/2.5 m PZ

Figure 5.42 demonstrates the effect of the relative amounts of K^+ and PZ on the heat of absorption. At low fractions of PZ, the dominating contribution of the CO_3^{2-} /HCO_3^- buffer drives the ΔH_{abs} down. At high fractions, the ΔH_{abs} behaves more like aqueous amines where protonation and carbamate formation drive the reaction enthalpy. This behavior is also independent of total concentration at most conditions. This generalization breaks down at a high fractional PZ content due to differences in

161

speciation at a given partial pressure. Overall, the ΔH_{abs} of the solvent may be selectable when considering process requirements and other tradeoffs.
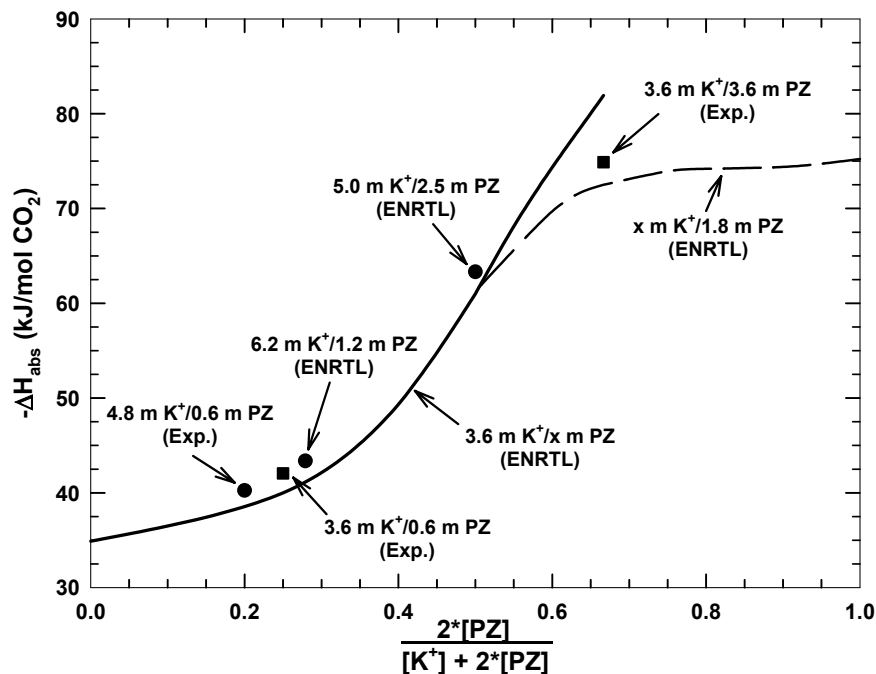
Figure 5.42. The Effect of K^+/PZ Ratio on the Heat of Absorption (40 to 70°C Average) at P_{CO_2}* = 3,000 Pa

5.8. Stoichiometry and Enthalpy

Examining the stoichiometry of the reactions provides a better look at contributions to the reaction enthalpy and highlights species controlling thermodynamic behavior at a given loading. The stoichiometry was calculated numerically by the ENRTL model as the change in moles of each species resulting from a small differential in loading.

Reaction stoichiometry for 1.8 m PZ at 25°C is shown in Figure 5.43. The loading can be broken down into three sections: low loading (< 0.4), medium loading

162

(0.4 to 0.8), and high loading (> 0.8). At low loadings, PZH^+ and $PZCOO^-$ are the main reaction products. PZ accounts for a majority of the reactant through nearly the entire loading range (up to 0.7). At medium loadings, $PZCOO^-$ is actually consumed as H^+PZCOO^- buffers the solution. At high loadings, bicarbonate becomes the buffering species and the main product. Aqueous CO_2 becomes important also and will be the main product at loadings greater than 1.0. $PZ(COO^-)_2$, though never an important species at most conditions, is consumed in this region. Stoichiometry was found to be a weak function of temperature.
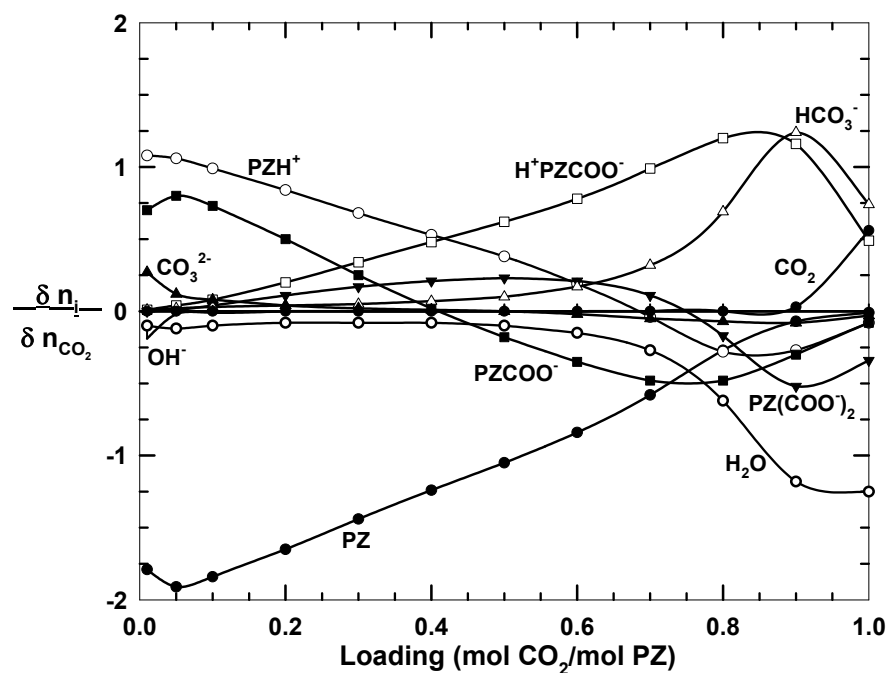
Figure 5.43. Reaction Stoichiometry in 1.8 m PZ at 25°C

The stoichiometry for 5.0 m K^+/2.5 m PZ at 25°C is given in Figure 5.44. PZ is still the main reactant and $PZCOO^-$ the main product at low loadings (< 0.5); however, CO_3^{2-} also contributes to the reaction. At intermediate loadings (0.5 to 0.7), bicarbonate

and $PZ(COO^-)_2$ form while PZ, $PZCOO^-$, and CO_3^{2-} are consumed. Interestingly, at high loadings, $PZ(COO^-)_2$ is the main PZ reactant. The buffering of the solution by CO_3^{2-} and HCO_3^- is significant at all loadings, as expected, and protonated species are less important.
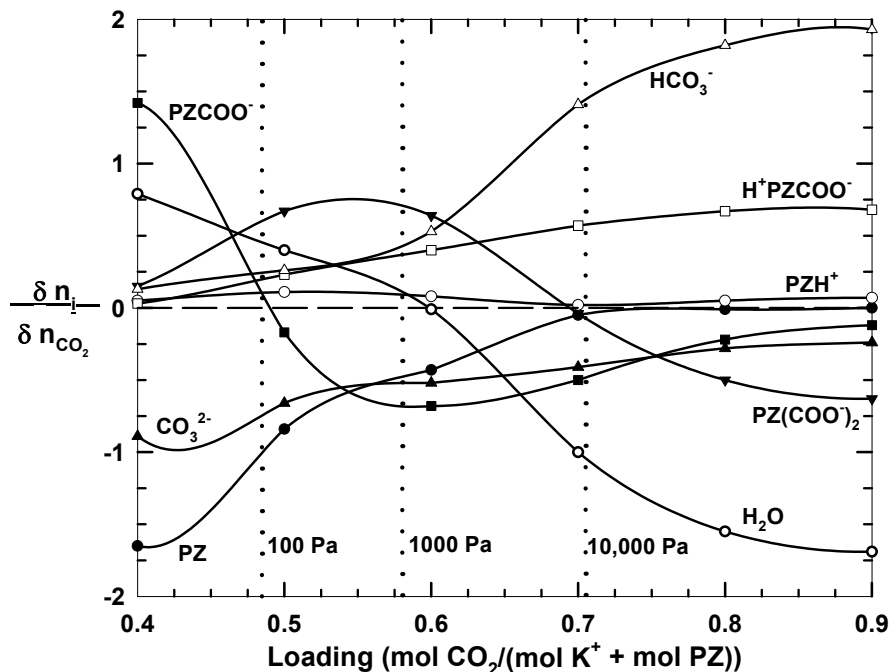
Figure 5.44. Reaction Stoichiometry in 5.0 m K^+/2.5 m PZ at $25^{\circ}C$, CO_2 and OH^- Changes Negligible Under Given Conditions

The apparent change of ΔH_{abs} with temperature is based on contributions of equilibrium constants and activity coefficients to the solution enthalpy, which is the sum of the enthalpy of formation (ΔH_f) and the excess enthalpy (ΔH^{ex}). The sum over all species in solution represents the total solution enthalpy.

$$\Delta H_{abs} = \sum \frac{\partial n_i}{\partial n_{CO_2}} \left[\Delta H_{f,i} + \Delta H_i^{ex} \right] \tag{5.16}$$

164

The enthalpies are multiplied by the stoichiometry to normalize values to CO_2. To simplify the analysis, stoichiometry is assumed constant over a small differential in temperature.

The enthalpies of formation for each PZ species have been calculated using the regressed equilibrium constants and literature values for common molecules. ΔH_f for PZ(l) was estimated as the ΔH_f for PZ(s), -45.6 kJ/mol, minus the enthalpy of fusion, 22.2 kJ/mol (DIPPR, 2004). Values are reported at standard state conditions at 25°C in Table 5.16. ΔH_i^{ex} is calculated as

$$\Delta H_i^{ex} = R \cdot \frac{\partial \ln \gamma_i}{\partial \left(\frac{1}{T}\right)} \cdot \qquad (5.17)$$

Table 5.16. Calculated Heats of Formation at 25°C

Species	ΔH_f^o (kJ/mol)	Source
H_2O (l)	-285.83	
H_3O^+ (aq)	-285.83	
OH^- (aq)	-230.02	CRC (2000)
CO_2 (aq)	-413.26	
CO_3^{2-} (aq)	-675.23	
HCO_3^- (aq)	-689.93	
PZ (l)	-67.8	DIPPR (2004)
PZH^+ (aq)	-110.55	
$PZCOO^-$ (aq)	-542.14	This Work
H^+PZCOO^- (aq)	-589.50	
$PZ(COO^-)_2$ (aq)	-971.93	

Figure 5.45 demonstrates that the sum of enthalpies from activity coefficients and equilibrium constants is indeed equivalent to the ΔH_{abs} predicted by differentiating the $\ln(P_{CO_2}{}^*)$ with respect to inverse temperature. Excess enthalpy is relatively small at

$25^{\circ}C$, accounting for approximately 20% of the total enthalpy at low loadings. Between 25 and $100^{\circ}C$, the ΔH_f changes by 60 kJ/mol at a loading of 0.5 whereas the ΔH^{ex} changes by 10 kJ/mol. The dramatic difference at low loadings is the result of heat capacities included in the symmetric equilibrium constants. Specifically, it is a result of the strong non-linear temperature dependence from the UNIFAC estimation of γ_{PZ}, which produces unusual predictions for temperature behavior. Information on γ^{∞}_{PZ} and calorimetric data of the mixed solvent is needed to clarify this trend and correct the model predictions.
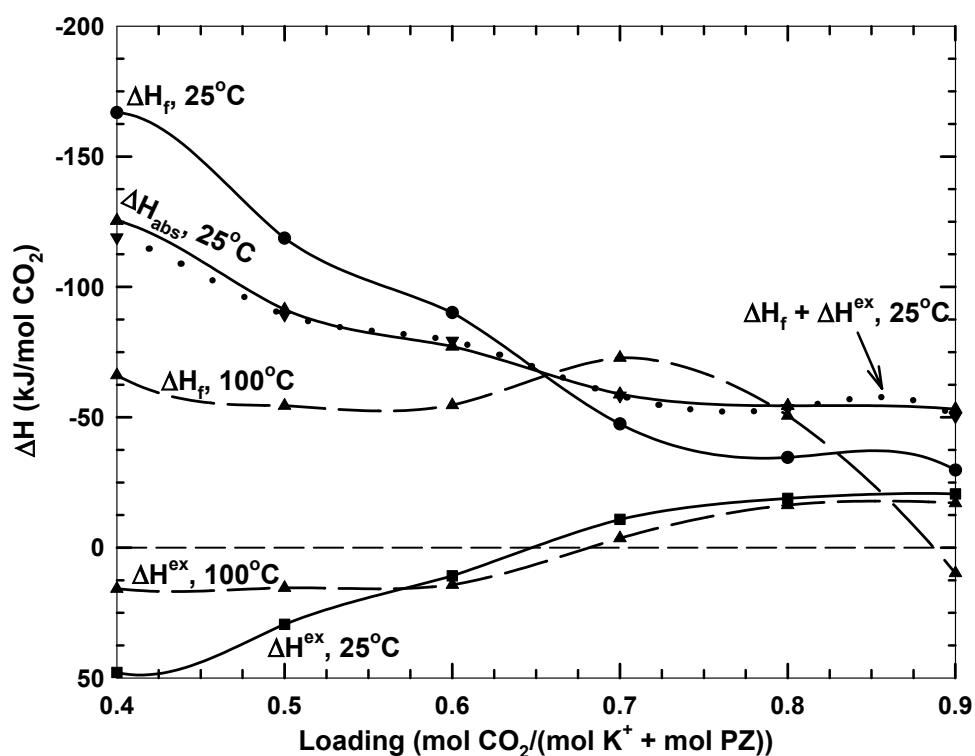
Figure 5.45. Calculation and Comparison of Contributing Enthalpies in 5.0 m K⁺/2.5 m PZ at 25°C and 100°C

5.9. Solid Solubility

One practical limit of operation is the solid solubility of the components in the K^+/PZ mixtures. The results of solid solubility measurements of K_2CO_3/PZ and $KHCO_3$/PZ are presented in Table 5.17 and Table 5.18 respectively at 25 and 40^oC. The challenge is recognizing the competing effects of PZ salting out by ionic strength and an apparent salting in by reaction with CO_2.

Figure 5.46 shows the results of the experiments at 25^oC. At this temperature, it is believed that the solid form of PZ is actually a hexahydrate, $PZ\text{-}6\cdot H_2O$ (Bishnoi, 2000). The addition of K_2CO_3 to aqueous PZ significantly decreases the solid solubility. In 2 mol K^+/kg-solution, the solubility of PZ is reduced by 65%. At high salt concentrations, PZ is nearly insoluble. At 4 m K^+, the PZ solubility is < 0.1 mol/kg-solution, consistent with a further salting out of the organic hydrate. Likewise, it is apparent that small amounts of PZ reduce the solid solubility of K_2CO_3 by greater than 50%. This is due the consumption of water as PZ forms the hexahydrate solid, increasing the apparent concentration of K_2CO_3.

$KHCO_3$ has a markedly different effect on the solubility. As the excess CO_2 reacts with PZ to form soluble ionic species, such as $PZCOO^-$, PZH^+, and $PZ(COO^-)_2$, the apparent solubility of PZ and $KHCO_3$ actually increases. This effect is observed at both high PZ and high $KHCO_3$ concentrations. The result is a significant difference in soluble concentrations in loaded ($KHCO_3$) and unloaded (K_2CO_3) solutions.

Table 5.17. Phase Behavior in K_2CO_3/PZ at 25 and 40°C

T (°C)	Nominal Conc. (mol/kg-solution)		Measured Conc. (mol/kg-solution)				Observations
	[K+]	[PZ]	[K+]	[PZ]	[CO2]	K+:CO2	
25	0.20	2.00	0.53	1.45	0.256	0.48	no precipitate in a yellow liquid
	0.19	2.32	0.55	1.47	0.269	0.49	Thick yellowish suspension, yellow liquid extracted
	0.39	1.95	1.13	1.09	0.497	0.44	Thick white suspension, yellow liquid extracted
	0.46	2.23	1.30	1.02	0.664	0.51	Thick white solid; very little yellow liquid extracted
	0.63	2.17	1.87	0.66	0.925	0.49	Thick white solid, some yellow liquid extracted
	0.72	2.15	2.11	0.57	0.991	0.47	Thick white suspension, yellow liquid extracted
	1.34	1.68	3.88	0.09	1.821	0.47	Fluffy white solid over small amount of clear liquid
	1.84	1.53	5.07	0.04	2.883	0.57	Thick white suspension, clear liquid extracted
	2.20	1.69	5.90	0.01	3.774	0.64	Fluffy white solid over in clear liquid
	3.51	0.88	7.61	0.01	4.261	0.56	Solid floating layer, white liquid underneath
	3.65	0.46	7.48	0.03	3.355	0.45	Solid floating layer, white liquid underneath
	3.39	1.27	7.59	0.02	3.569	0.47	Solid floating layer, white liquid underneath
	3.27	1.63	7.60	0.02	3.894	0.51	Solid floating layer, white liquid underneath
40	0.22	4.60	0.51	4.57	0.143	0.28	2 liquid layer, yellow liquid on top
			2.88	2.27	2.265	0.79	2 liquid layer, small clear bottom layer
	0.28	4.55	0.51	4.71	0.087	0.17	2 liquid layer, yellow liquid on top
			4.08	1.21	2.680	0.66	2 liquid layer, small clear bottom layer
	1.01	4.15	0.39	5.68	0.042	0.11	2 liquid layer, yellow liquid on top
			6.44	0.11	4.234	0.66	2 liquid layer, small clear bottom layer
	1.79	3.57	0.37	6.54	0.319	0.86	2 liquid layer, yellow liquid on top
			7.15	0.11	3.934	0.55	2 liquid layer, small clear bottom layer
	2.38	3.18	7.47	0.11	3.346	0.45	Viscous, white liquid
	3.65	0.46	7.45	0.09	3.569	0.48	Floating white precipitate, milky solution
	3.51	0.88	7.61	0.09	4.040	0.53	Floating, solid yellow layer, clear liquid w/ white powder ppt.
	3.39	1.27	7.65	0.11	4.800	0.63	Floating, solid yellow layer, clear liquid w/ white powder ppt.
	3.27	1.63	7.68	0.08	3.485	0.45	Floating, solid yellow layer, clear liquid w/ white powder ppt.

Table 5.18. Phase Behavior in KHCO$_3$/PZ at 25 and 40°C

T (°C)	Nominal Conc. (mol/kg-solution)		Measured Conc. (mol/kg-solution)				Observations
	[K$^+$]	[PZ]	[K$^+$]	[PZ]	[CO$_2$]	K$^+$:CO$_2$	
25	0.34	3.38	0.49	1.92	0.717	1.46	Thick white solution, little yellow liquid extracted
	0.65	3.29	1.27	1.88	2.029	1.60	White slush, yellow liquid extracted
	1.23	3.07	1.82	2.00	1.729	0.95	White slush, yellow liquid extracted
	2.19	2.71	2.45	2.27	2.912	1.19	Yellowish slush, thick yellow liquid extracted
	2.39	2.66	2.53	2.35	2.270	0.90	Clear liquid on top of thick suspension, yellow liquid extracted
	2.71	2.17	2.51	2.03	2.326	0.93	Clear liquid with white granular ppt.
	3.65	0.30	2.97	0.32	2.546	0.86	Clear liquid with white granular ppt.
	3.56	0.59	2.94	0.62	2.682	0.91	Clear liquid with white granular ppt.
	3.39	1.13	3.20	1.09	3.451	1.08	Clear liquid with white granular ppt.
	3.23	1.62	3.07	1.43	2.992	0.97	Clear liquid with white granular ppt.
	3.16	1.84	2.87	1.60	2.520	0.88	Clear liquid with white granular ppt.
	2.95	2.46	2.54	2.15	2.458	0.97	Clear liquid with white granular ppt.
	2.83	2.83	2.47	2.58	2.244	0.91	Clear liquid with white granular ppt.
	3.89	1.46	3.24	1.28	3.309	1.02	Yellow liquid with white granular ppt.
40	0.21	6.59	0.57	6.54	0.208	0.36	Opaque yellow solution with a white ppt.
	0.51	5.10	1.03	4.86	0.218	0.21	Yellow liquid with ppt.
	0.97	4.85	1.67	4.37	0.834	0.50	Yellow liquid with ppt.
	1.92	3.83	1.74	3.64	1.668	0.96	White viscous liquid
	3.89	1.46	3.33	1.21	3.265	0.98	Yellow liquid with white powder ppt.
	3.21	3.21	1.97	2.75	2.032	1.03	Thick white suspension, filtered to a yellow liquid
	4.27	1.71	3.54	1.16	3.667	1.04	Yellow liquid over a white ppt.
	4.11	2.06	3.00	1.55	2.843	0.95	Yellow liquid over a white ppt.
	3.72	2.97	2.24	3.15	2.225	0.99	Yellow liquid over a white ppt.
	4.72	1.57	3.23	1.28	3.526	1.09	Yellow liquid over a white ppt.
	5.96	0.37	3.15	0.62	2.395	0.76	Clear solution white ppt.
	5.77	0.72	3.46	1.08	2.297	0.66	Clear solution white ppt.
	5.60	1.05	3.50	1.14	2.331	0.67	Clear solution white ppt.
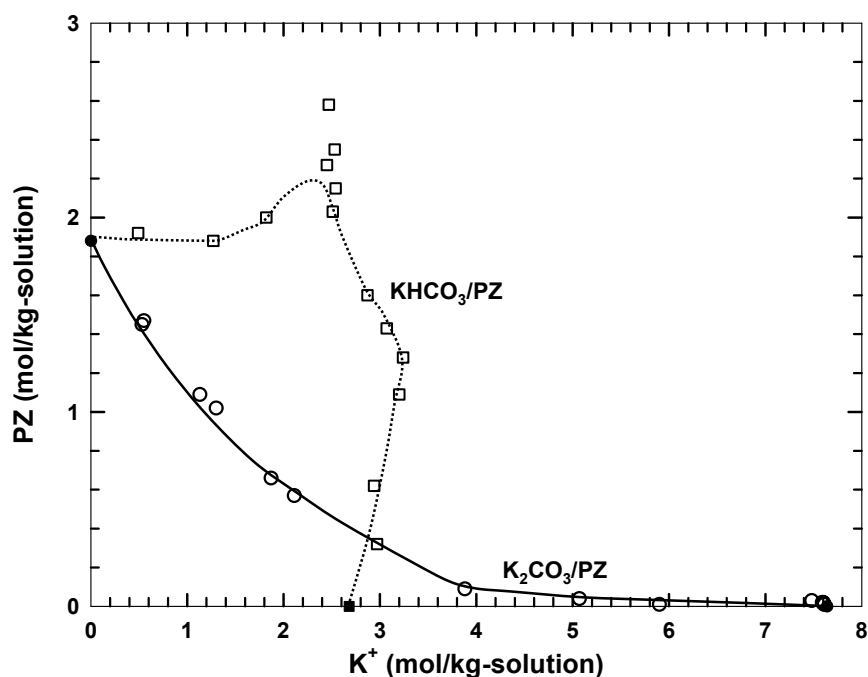
Figure 5.46. Solubility of K⁺/PZ at 25°C, Open Points: This Work, Closed Points: Aqueous PZ from Bishnoi (2000) and K₂CO₃ and KHCO₃ from Linke (1966)

In Figure 5.47, the results of experiments at 40°C are shown. A dramatic difference in PZ solubility is noted and is explained by the melting of the hexahydrate, which occurs at approximately 43°C (Schwarzenbach, 1968). Salting out of the PZ still occurs with the additions of K_2CO_3, though the solubility is significantly higher up to 6 mol K⁺/kg-solution. Also, the difference between solubilities in K_2CO_3 and $KHCO_3$ is reduced. At the higher PZ concentrations, more CO_2 than is available from $KHCO_3$ would be required to increase the apparent solubility. Thus, the ionic strength salts out PZ and the behavior is similar to that of K_2CO_3 up to 3 mol K⁺/kg-solution.

170

It should be recognized that at $40^{\circ}C$ with K_2CO_3, the solution often does not precipitate a solid, but instead forms two liquid phases. The two layers are thought to be an organic phase, with little salt, and a salt phase, with some PZ. At $25^{\circ}C$, phase splitting occurs at similar conditions, but the organic phase is a solid. The molten organic phase is possible due to the melting of the hexahydrate near $40^{\circ}C$.
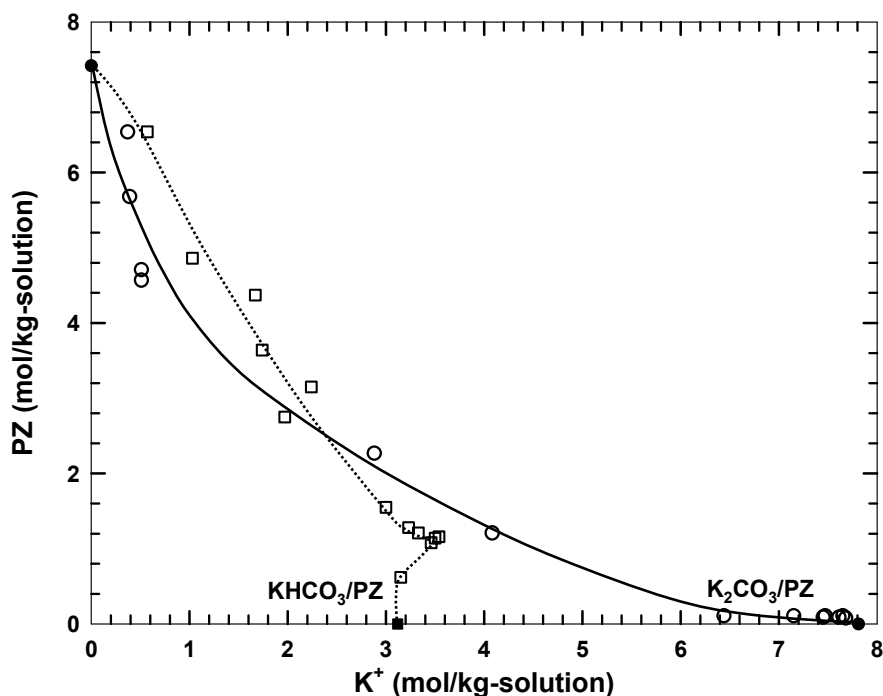
Figure 5.47. Solubility of K^+/PZ at $40^{\circ}C$, Open Points: This Work, Closed Points: Aqueous PZ from Bishnoi (2000) and K_2CO_3 and $KHCO_3$ from Linke (1966)

A K^+:CO_2 ratio is also included in the tables as an estimate of CO_2 distribution between phases. If the ratio is near 0.5 in a solution dominated by K^+, the solid precipitate is likely a potassium carbonate salt. Similarly, if the ratio is near 1.0, a potassium bicarbonate salt is expected. In general, the CO_2 tends to pair with the potassium salt as opposed to the aqueous PZ.

171

5.10. Conclusions

The ENRTL model adequately predicts the activity of water and $P_{CO_2}^*$ in aqueous K_2CO_3 and $KHCO_3$ solutions at various temperatures. The fit was achieved using four τ parameters each with a small, linear temperature dependence. Future inclusion of ion pair-ion pair interactions may improve inaccuracies at high salt concentrations.

The ENRTL was fit to the UNIFAC predictions for γ_{PZ}. The model shows a strong, non-linear dependence of γ_{PZ} on temperature and PZ concentration. Behavior at infinite dilution in water gives a heat of solution that compares favorably with literature values.

Relevant equilibrium constants for the reaction of CO_2 with PZ have been regressed as well as for the protonation of $PZCOO^-$. The heats of reaction for the formation of $PZCOO^-$ and $PZ(COO^-)_2$ are similar, 18.3 and 16.5 kJ/mol, as would be expected by an analysis of structure. Likewise, the heat of reaction for the protonation of $PZCOO^-$ is comparable to the heat of PZ protonation, at a value of -47.4 kJ/mol.

The fitted ENRTL model is able to represent aqueous PZ and K^+/PZ speciation to within an absolute error of 5%. VLE behavior is fairly well represented, deviating by an apparent 25%. Most of the error, however, has been identified as in the solution loading. A 10% error in loading can result in a 30% "error" in $P_{CO_2}^*$. VLE behavior suggests the solvent capacity increases as a linear function of solvent equivalents.

The speciation of PZ shows significant differences between aqueous PZ and K^+/PZ mixtures. In aqueous PZ, the carbamate species are never more than 20% of the total PZ concentration. In contrast, each can account for as much as 50% with the addition of K^+. Protonation represents a significant amount of product from the addition of CO_2 to aqueous PZ. A high K^+ concentration increases the prevalence of the CO_3^{2-}/HCO_3^- buffer and delays protonation of the amine to high loadings. Thus, carbamation of amines will increase in the presence of K^+ to an extent related to the carbamate stability. This effect is countered by the reduction of protonation afforded by the strong buffer. The overall effect is an increase in reactive PZ concentration.

Model predictions show that the maximum reactive PZ concentration (PZ + $PZCOO^-$) occurs when the PZ concentration is maximized and K^+ is added in a 2:1 ratio of K^+:PZ. The maximum concentration will be defined by the solid solubility limit under any given condition.

VLE curves are depressed as total solution concentration increases, indicating improved CO_2 capacity in concentrated solvents. The addition of potassium improves the VLE behavior of aqueous PZ.

The ΔH_{abs}, at 40 to 70^oC, is calculated to be -80 kJ/mol for aqueous PZ and -65 kJ/mol for K^+/PZ mixtures, a reduction of 20%. Stoichiometry shows that the lower enthalpy is obtained due to significant contribution of CO_3^{2-} and the reduction in protonation in mixed solvent reactions. Additionally, the ΔH_{abs} may be "tuned" simply by variation of the K^+ to PZ ratio.

ΔH_{abs} is predicted to be a strong function of temperature and is a result of the heat capacity predicted by UNIFAC for γ_{PZ}^{∞}. The model is therefore limited in extrapolating second-order temperature effects, such as enthalpies, over broad ranges and should be used with care to predict heats of CO_2 absorption at extreme temperature. Gathering experimental data for γ_{PZ} and Δc_P for the solution at various loadings should be considered to correct this shortcoming.

Chapter 6: Rate and Kinetics of Potassium Carbonate, Piperazine and Carbon Dioxide Mixtures

This chapter presents experimental data and modeling results on CO_2 absorption into K^+/PZ mixtures. The absorption rate of CO_2 was measured in a wetted-wall column in 0.45 to 3.6 m piperazine (PZ) and 0.0 to 3.1 m potassium carbonate (K_2CO_3) at 25 to 110^oC. A rigorous kinetic model was used to interpret diffusivities and rate constants. The kinetics of important reactions were interpreted with the termolecular mechanism. The rate constants were found to follow correlations provided by base catalysis theory. The effect of neutral salts on the absorption rate in aqueous PZ was also measured and accounted for within the rigorous model. Approximations were developed to represent the absorption rate from the range of pseudo-first order to instantaneous behavior. Limitations to the approximations and to the performance of K^+/PZ mixtures as applied at industrial conditions are discussed.

6.1. Model Description

The rigorous rate model is made up of several reactions as discussed in Section 4.2.3. The reactions include $PZCOO^-$ formation, $PZ(COO^-)_2$ formation, and base-catalyzed bicarbonate formation. The reactions of PZ with CO_2 are considered termolecular according to previous experience and include effects of catalyzing bases.

Experimental data on the absorption rate were collected and used to sequentially regress rate constants for aqueous PZ and K^+/PZ mixtures, satisfying the imposed reactive conditions. The results of the regressions are shown in Table 6.1 and discussed throughout the chapter.

Table 6.1. Regressed Constants for Modeling CO_2 Absorption into K^+/PZ

i	$pK_{a,Am-i}$ [a]	$i \times 10^{-3}$ [b]	$\sigma \times 10^{-3}$ [c]	Relation for ln(i)
$k^o_{PZ-H_2O}$ [d]	-1.74	0.6	0.09	Regressed from aqueous PZ
$k^o_{PZ-PZCOO^-}$	9.51	48.9	-	$= \ln k^o_{PZ-PZ} + 0.457\left(pK_{a,PZCOO^-} - pK_{a,PZ}\right)$
k^o_{PZ-PZ}	10.30	70.1	9.6	Regressed from aqueous PZ
$k^o_{PZ-CO_3^{2-}}$	10.33	145.1	-	Regressed from K^+/PZ
$k^o_{PZ-OH^-}$	15.74	1857	486	Regressed from aqueous PZ
$k^o_{PZCOO^- -H_2O}$	-1.74	0.4	-	$= \ln k^o_{PZCOO^- -CO_3^{2-}} + 0.457\left(pK_{a,H_2O} - pK_{a,CO_3^{2-}}\right)$
$k^o_{PZCOO^- -PZCOO^-}$	9.51	66.3	-	$= \ln k^o_{PZCOO^- -CO_3^{2-}} + 0.457\left(pK_{a,PZCOO^-} - pK_{a,CO_3^{2-}}\right)$
$k^o_{PZCOO^- -PZ}$	10.30	95.1	-	$= \ln k^o_{PZCOO^- -CO_3^{2-}} + 0.457\left(pK_{a,PZ} - pK_{a,CO_3^{2-}}\right)$
$k^o_{PZCOO^- -CO_3^{2-}}$	10.33	96.7	-	Regressed from K^+/PZ
ΔH_a	-	35.02	2.0	Regressed from aqueous PZ
ξ [e]	-	0.00151	-	Regressed from K^+/PZ

a. pK_a of the extracting base.
b. Rate constants given as $m^6/kmol^2$-s. ΔH_a given as kJ/kmol.
c. Standard deviation of the regressed value.
d. Regressed as pseudo-first order rate constant with $[H_2O] = 55.55$ kmol/m^3.
e. Parameter for diffusivity correction.

6.2. Aqueous Piperazine

6.2.1. Rate Constants

Bishnoi and Rochelle (2000) measured the rate of CO_2 absorption into 0.2 and 0.6 M PZ at 25 to $60^{\circ}C$ and zero loading and reported a rate constant assuming first-order rate dependence on PZ. The reported rate constant is 53,700 m^3/kmol-s at $25^{\circ}C$ with an activation energy of 33.6 kJ/mol. In this work, the absorption rate was measured in 0.45 to 1.5 mol-PZ/kg-H_2O (m) at 25 and $60^{\circ}C$ and zero loading. Data were also obtained in 0.6 m PZ containing 0.15 m KOH. Table 6.2 provides a summary of the experiments.

All data on aqueous PZ are represented as an apparent second-order rate constant, $k_{2,app}$, in Figure 6.1. This is equivalent to a pseudo-first order simplification in which the rate is first-order with PZ. The dependence of $k_{2,app}$ on PZ concentration shows that the reaction is not first-order with PZ as had been previously assumed. As PZ concentration is increased above a concentration of 0.5 M, the reaction order approaches 2. The curvature at low PZ concentrations is due to contributions of water as the dominant catalyzing base at low PZ concentrations.

In addition to the second-order dependence on the amine, a significant rate enhancement is observed with hydroxide in solution. With 0.15 m KOH, the flux increases by a factor of two in 0.6 m PZ solution. This suggests that strong bases contribute to the overall reaction rate and must be included in the rate expression, consistent with the termolecular mechanism.

Table 6.2. Absorption rate of CO_2 into Aqueous PZ

T (°C)	[PZ] (m)	Loading (mol-CO_2/mol-PZ)	$P_{CO_2,b}$ (Pa)[a]	$k_g \times 10^9$ (kmol/m²-Pa-s)	$k_l^o \times 10^5$ (m/s)	K_G/k_g (%)	CO_2 Removal (%)	$H_{CO_2} \times 10^{-6}$ (m³-Pa/kmol)	$D_{CO_2} \times 10^9$ (m²/s)	$N_{CO_2} \times 10^7$ (kmol/m²-s) Measured	$N_{CO_2} \times 10^7$ (kmol/m²-s) Predicted
25	0.45	0.008	51	2.99	7.9	50.8	40.1	3.01	1.83	0.78	0.66
		0.008	98	3.01	8.0	44.5	36.1	3.03	1.84	1.31	1.26
		0.008	167	2.98	8.0	40.1	32.8	3.04	1.85	2.00	2.14
	0.68	0.012	448	2.61	9.0	51.0	38.9	3.35	1.85	5.86	6.15
		0.012	65	2.58	9.0	58.5	39.3	3.35	1.85	0.82	0.89
		0.012	356	2.59	8.9	53.1	40.3	3.35	1.85	4.78	4.87
	1.20	0.008	34	2.54	8.7	58.0	43.6	3.12	1.43	0.47	0.53
		0.010	64	2.70	8.7	61.3	46.4	3.14	1.44	1.06	1.02
		0.013	287	2.89	8.7	58.0	44.3	3.18	1.46	4.78	4.76
		0.016	93	2.53	8.9	60.4	46.2	3.25	1.49	1.39	1.43
		0.019	247	2.71	8.7	59.5	45.5	3.25	1.50	3.95	3.93
	1.50	0.007	50	2.53	8.2	66.6	49.4	3.49	1.46	0.84	0.82
		0.007	302	2.59	8.2	67.0	48.8	3.49	1.46	5.24	4.98
		0.007	93	2.48	8.2	69.9	50.2	3.49	1.46	1.60	1.49
		0.005	422	2.61	8.2	64.3	46.9	3.49	1.46	7.09	7.02
	0.60[b]	0.000	55	2.23	9.5	80.8	54.4	3.22	1.82	0.90	0.88
		0.000	287	2.21	9.5	72.4	51.7	3.22	1.82	4.52	4.57
		0.000	181	2.22	9.5	75.2	53.5	3.24	1.83	2.95	2.90
		0.000	87	2.23	9.6	79.4	54.8	3.25	1.84	1.45	1.40
60	1.20	0.009	32	2.73	11.7	60.3	47.5	6.40	3.28	0.53	0.61
		0.010	58	2.73	11.8	73.0	54.0	6.51	3.36	1.16	1.10
		0.012	215	3.04	12.0	66.9	50.9	6.65	3.45	4.38	4.36
		0.015	334	3.45	11.8	62.1	47.3	6.62	3.43	7.14	7.28
		0.017	238	3.40	11.9	65.3	48.9	6.72	3.50	5.29	5.16

a. Log mean average of bulk partial pressure of CO_2.
b. Solution also contains 0.15 m KOH.
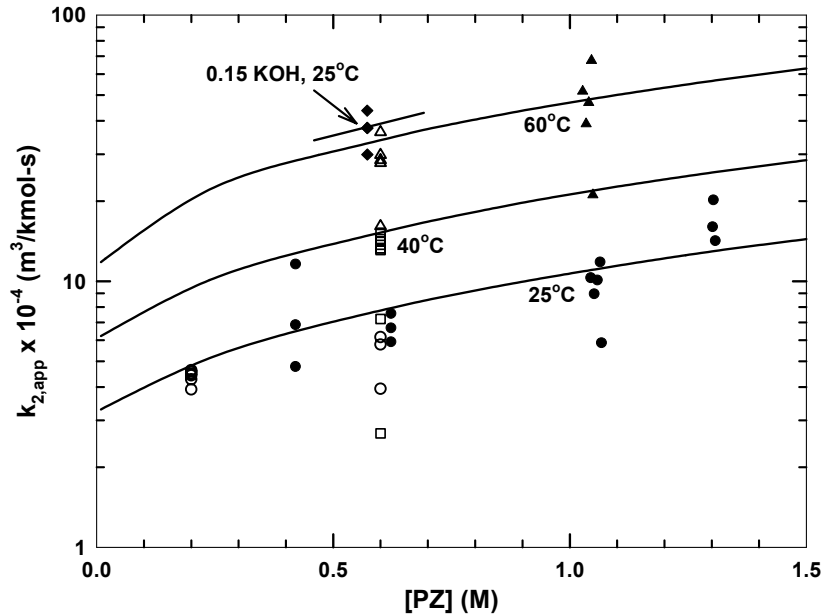
Figure 6.1. Apparent Second-Order Rate Constant for CO_2 Absorption into Aqueous PZ, Lines: Model ($P_{CO_2,i}$ = 100 Pa, k_l^o = 1×10^{-4} m/s), Open Points: Bishnoi and Rochelle (2000), Filled Points: This Work

Data on aqueous PZ from Bishnoi (2000) and this work were combined in a regression of PZ rate constants for CO_2 absorption into aqueous PZ. The regressed constants, reported in Table 6.1, are k_{PZ-PZ}, k_{PZ-H_2O}, k_{PZ-OH}, and ΔH_a. Calculated values of the flux (Table 6.2), were within approximately 20% of the measured values. The value of the rate constant for PZ found in this work is consistent with previous work at similar concentrations. In 0.6 M PZ, the overall rate constant is 61,320 s^{-1} compared to 53,700 s^{-1} as given by Bishnoi. The activation energies were assumed equal for all rate constants, with a regressed value of 33.0 kJ/mol, comparable to Bishnoi (33.6 kJ/mol).

The curves in Figure 6.1 represent a model correlation of $k_{2,app}$ under typical experimental conditions. The model correlation of the experimental flux data deviates

179

by less than 25% on average. The model captures the non-first-order behavior displayed by the experimental data and the addition of k_{PZ-OH} effectively compensates for the accelerated rate in the presence of excess hydroxide. The activation energy provides an adequate fit between 25 and 60°C.

A comparison between overall rate constants of several amines at 1.0 M and 25°C is shown in Table 6.3. The fact that piperazine has the highest rate constant may be attributed to the moderately high pK_a. Also, the cyclic diamine structure yields rates faster than would be expected from simple chemical classifications or pK_a correlations. These characteristics are also observable in diamines such as ethylenediamine and heterocycles such as piperidine and morpholine.

Table 6.3. Overall Rate Constants for 1.0 M Amines at 25°C

Amine	Source[a] (Rate/pK_a)	pK_a	Rate Constant[b] (s^{-1})	ΔH_r (kJ/mol)
Piperazine	This Work	9.73	102.2×10^3	35.0
Monoethanolamine	1/2	9.55	5.9×10^3	41.2
Diethanolamine	1/2	8.88	1.3×10^3	53.1
Diglycolamine	3/4	9.46	4.52×10^3	39.4
	5/4		6.7×10^3	40.1
Ethylenediamine	6/2	9.91	15.1×10^3	-
Piperidine	7/2	11.12	93.3×10^3	-
	8/2		60.3×10^3	-
Morpholine	3/2	8.49	20.6×10^3	-
	7/2		20.0×10^3	-
	5/2		22.3×10^3	23.3

a. 1. Hikita *et al.* (1977). 2. Perrin *et al.* (1981). 3. Alper (1990a). 4. Littel *et al.* (1990a).   5. Al-Juaied (2004).   6. Jensen and Christensen (1955). 7. Sharma (1965). 8. Jensen *et al.* (1952).

b. Overall rate constant ($k = k_{Am}[Am]$ **or** $k_{Am-Am}[Am]^2 + k'_{Am-H_2O}[Am]$) assuming 25°C, negligible loading, and negligible hydroxide contributions.

The sensitivity of the model to the regressed parameters, i, is presented as $\dfrac{d \ln k_g'}{d \ln i}$

in Figure 6.2 for 1.8 m PZ at 60°C and typical experimental conditions. Parameters with sensitivities under 0.05 have been omitted.

Kinetics are the dominant contributor to k_g' at low $P_{CO_2}^*$ (< 1,000 Pa). Specifically, the self-catalysis of PZ is most significant. The contribution of water to the reaction is also important, signifying a potential change in observed reaction orders as the PZ concentration varies. Because $PZCOO^-$ is also an important species in loaded solutions, there is an associated sensitivity to it as a reactant and a base.
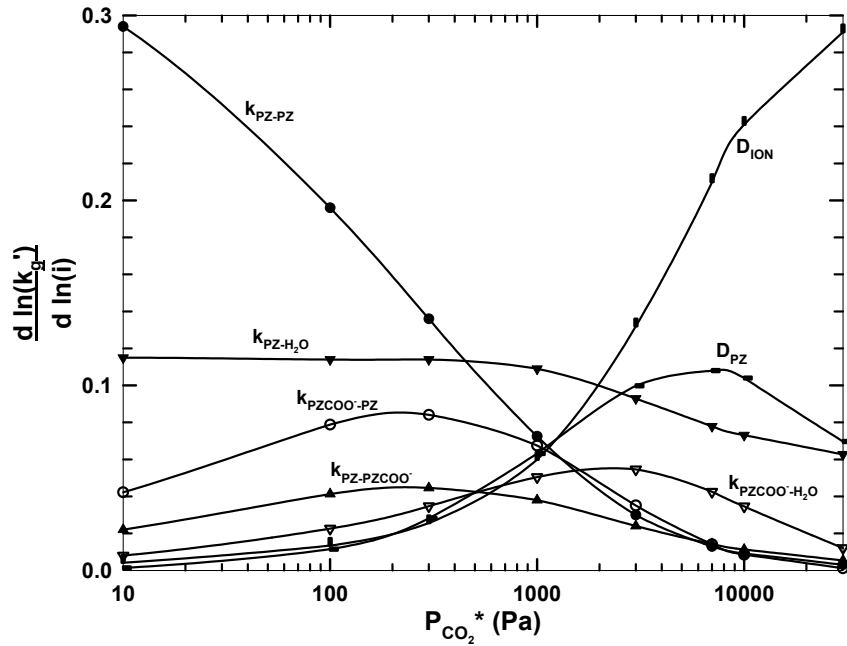
Figure 6.2. Sensitivity of Model Parameters in 1.8 m PZ at 60°C, $k_l^{\circ} = 1.0\times10^{-4}$ m/s, $P_{CO_2,i} = 1.5\times P_{CO_2}^*$

At high $P_{CO_2}^*$ (> 1,000 Pa), the dominant effect on rate is the diffusion of ions in solution (all ions have the same diffusivity). Physically, this is either the diffusion of

products away from the interface, or the diffusion of PZCOO⁻ reactant to the interface. Because PZ is of diminished in importance to the reaction mechanism at high loadings, its diffusion coefficient has a marginal effect on the rate.

6.2.2. Absorption Rate of Carbon Dioxide

The absorption rate of CO_2 into aqueous PZ is given in Figure 6.3 as normalized flux, k_g'. The rate in the aqueous amine decreases sharply as $P_{CO_2}^*$ increases, as expected, due to the consumption of reactive amine. The effect of PZ concentration is more pronounced at low $P_{CO_2}^*$, likely the result of increased pH, than at high $P_{CO_2}^*$. The model accurately represents data in loaded 0.64 m PZ as reported by Bishnoi (2000), though the points were not included in the regression. (These points rely on rate constants determined by the regression of K^+/PZ data presented in Section 6.3.1.)
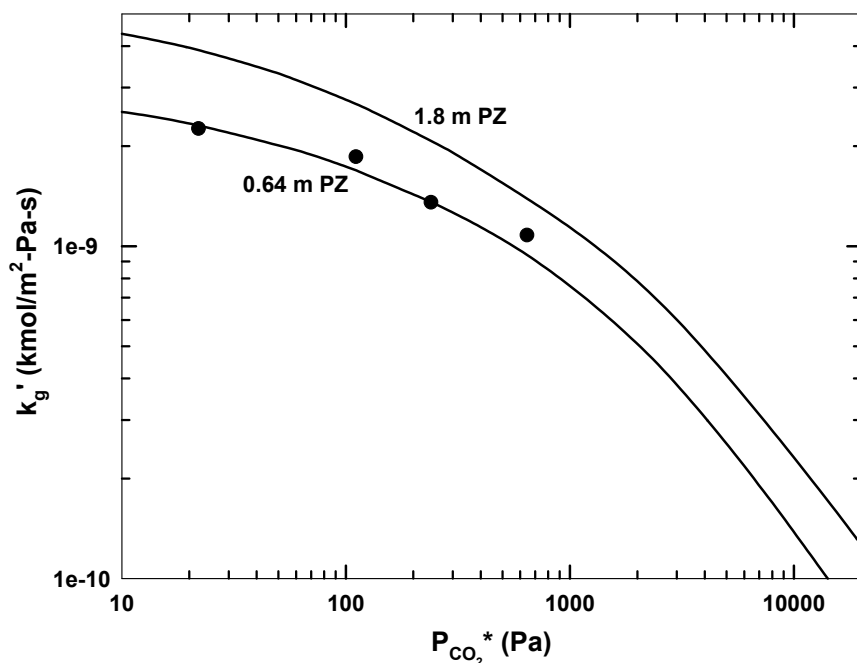
Figure 6.3. Normalized Flux in Aqueous PZ at 40°C, Points: Data from Bishnoi (2000), Lines: Model Predictions ($k_l^0 = 1 \times 10^{-4}$ m/s, $P_{CO_2,i} = 3.0 \times P_{CO_2}^*$)

182

The temperature dependence of absorption rate in 1.8 m PZ is shown in Figure 6.4. At low temperatures, there is a marked distinction between absorption rates, reflecting the influence of temperature on the kinetics. At high temperatures, the normalized flux at 100°C and 110°C are nearly equal; the physical solubility of CO_2 effectively limits the rate increases associated with temperature.
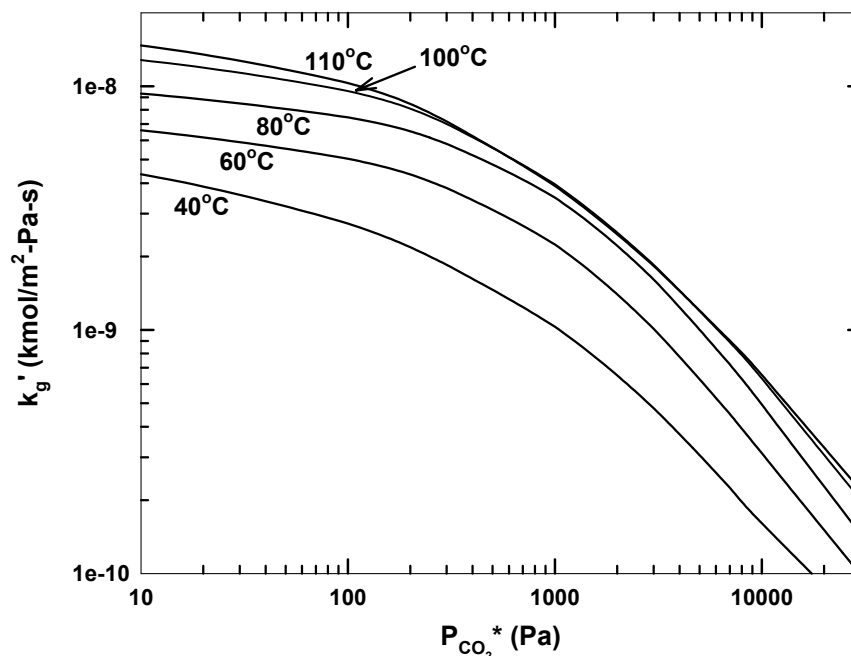
Figure 6.4. Temperature Dependence of Normalized Flux of 1.8 m PZ, Lines: Model Prediction ($k_l^o = 1 \times 10^{-4}$ m/s, $P_{CO_2,i} = 3.0 \times P_{CO_2}*$)

6.2.3. Neutral Salt Effects

The potential for ionic strength to alter reaction rates through primary and secondary salt effects has been recognized in many types of reactions (Section 2.3.2.). To quantify the influence of salt on CO_2 absorption into aqueous PZ, the absorption rate has been measured in 0.6 m PZ with various salts at 25 and 60°C. The data are

presented in Table 6.4. For modeling neutral salts, the Henry's constant of CO_2 was estimated by the model of Weisenberger and Schumpe (1996).

The salt effect is commonly represented by a function (Brønsted, 1928) so that

$$\ln k = \ln k^\infty + bI \tag{6.1}$$

where b is a constant and I is the ionic strength. The rigorous rate model has been run with rate constants of the form shown in Equation (6.1) to interpret the effect of neutral salts. The average value of b was found to be 0.45 ± 0.10. The constant b can be specific to both the ion and the reaction involved; the limited data presented here prevent a rigorous interpretation of its value for individual species.

Other studies on ionic strength effects show similar acceleration of reaction rates. French (1928) studied the iodine-catalyzed decomposition of hydrogen peroxide. The influence of up to 2 M of several neutral salts increased reaction rates by as much as factor of two. As interpreted through Equation (6.1), reported values of b include 0.32 for LiCl, 0.13 for NaCl, and 0.08 for KCl. Grube and Schmid (1926) determined the effect of concentrated neutral salts on the hydrolysis of cyanamide. The authors conclude that the value of b ranges from 0.16 in KNO_3 to 0.40 in $Mg(NO_3)_2$. Again, the reaction rates in 2 M ionic strength increase by a factor of two.

Neutral salts have also been shown to positively influence the absorption rate of CO_2 into amines. Data from Danckwerts and Sharma (1966) give a value for b of approximately 0.4 for CO_2 absorption into ammonia with NaCl. Laddha and Danckwerts (1982) suggest 0.4 and 0.6 for Na_2SO_4 and K_2SO_4 in DEA respectively.

Table 6.4. Absorption rate of CO_2 into 0.6 m PZ at High Ionic Strength

T (°C)	Salt	[Salt] (M)	$P_{CO_2,b}$ (Pa)	$k_g \times 10^9$ (kmol/cm²-Pa-s)	$k_l^o \times 10^5$ (m/s)	K_G/k_g (%)	CO_2 Removal (%)	$N_{CO_2} \times 10^7$ Measured (kmol/m²-s)	Avgerage γ_{CO_2} [a]	Estd. $k_2 \times 10^{-4}$ (m³/kmol-s) [b]
25	KHCO₂	1.81	57	2.85	9.01	47.6	42.7	0.80	1.93	23.6
			103	2.81	8.97	44.3	39.8	1.31		
			59	2.80	8.97	44.1	40.3	0.75		
			38	2.82	8.97	43.4	40.4	0.49		
	NaCl	2.81	117	2.54	6.78	52.6	37.7	1.57	2.06	34.8
			157	2.53	6.80	51.1	37.0	2.03		
			90	2.50	6.83	53.6	38.2	1.20		
			68	2.51	6.84	53.5	38.2	0.91		
			43	2.46	6.84	52.2	37.7	0.56		
	KCl	3.04	66	2.27	10.2	76.0	54.2	1.02	1.92	81.4
			311	2.25	10.2	68.9	54.4	4.70		
			195	2.71	10.3	68.0	52.3	3.48		
			80	2.73	10.3	72.0	52.9	1.44		
			219	2.92	10.3	62.6	49.4	3.87		
60	K₂SO₄	1.38	113	3.31	10.8	49.9	43.0	1.88	1.55	68.4
			155	3.32	10.8	47.8	41.5	2.47		
			203	3.06	10.7	50.5	43.3	3.14		
			66	2.97	10.8	49.5	43.1	0.98		
			36	2.98	10.8	54.4	46.5	0.59		
			87	3.01	10.8	50.5	43.6	1.33		
	KCl	1.78	54	2.38	12.6	72.3	55.1	0.93	1.33	98.3
			15	2.37	12.5	71.8	55.4	0.28		
			28	2.33	12.6	74.8	56.3	0.49		
			111	2.37	12.9	68.8	52.9	1.82		
			167	2.41	12.7	59.6	51.5	2.68		
			187	2.39	12.8	59.7	51.1	2.96		
			283	2.38	12.8	60.1	49.7	4.34		
			299	2.41	12.9	59.4	49.1	4.57		
	KHCO₂	1.75	31	2.79	11.0	55.1	51.1	0.55	1.75	132.3
			67	2.79	11.0	54.9	48.5	1.10		
			248	2.84	11.0	54.6	46.3	3.91		
			183	2.82	11.0	54.7	46.7	2.90		
			131	2.84	11.0	54.7	47.1	2.11		
			101	2.79	11.0	56.1	48.4	1.66		

a. Estimated from the model of Weisenberger and Schumpe (1996). KHCO₂ assumed to be the same as KHCO₃.
b. Estimated from pseudo-first order analysis.

Pohorecki *et al.* (1988) quantified the effect of KCl addition on CO_2 absorption into K_2CO_3-promoted ethylaminoethanol. Interpreting the results in terms of Equation (6.1), a value of 0.31 is obtained for b. Because K_2CO_3 constitutes a significant portion of the ionic strength and similar results for KCl have been found in other studies, the contribution to ionic strength effects by K_2CO_3 must be similar to that of neutral salts.

A comparable effect is expected to apply to CO_2 absorption by concentrated K^+/PZ. Assigning a definitive value in this instance is difficult due to the reactive nature of the carbonate, its contribution to the reaction mechanism, and complications arising from speciation of the amine, though some effort has been made to reconcile the ionic strength effect with kinetics.

From the conclusions of previous studies, a value of 0.3 was chosen for b for use in this work. This value is the most consistent, and moderate, choice based on the wide range of b values presented in the literature.

Figure 6.5 illustrates the influence of neutral salts in 0.6 m PZ on the apparent rate constant and important physical parameters, represented as $\sqrt{D_{CO_2}}/H_{CO_2}$. Experiments show that the apparent rate constant is elevated by ionic strength. The addition of 1.8 M ionic strength increases the $k_{2,app}$ by a factor of 2.5 at $25^{\circ}C$ and $60^{\circ}C$. With 3 M KCl, the apparent rate constant increases by a factor of 15. The rate model for K^+/PZ shows similar results and suggests the value of 0.3 for b is a reasonable estimate for the ionic strength contribution to PZ reactions.

It is important to recognize that ionic strength also changes the effective diffusion coefficient and physical solubility of CO_2; therefore, the interpretation of a

rate constant strongly depends on the ability to estimate $\sqrt{D_{CO_2}}/H_{CO_2}$. In 3 M K_2CO_3, the parameter decreases by 70%. The normalized flux, k_g', is only a weak function of ionic strength. The competing effects of kinetics and changes in D_{CO_2} and H_{CO_2} result in a diminishing absorption rate when not considering the catalytic benefit of carbonate.
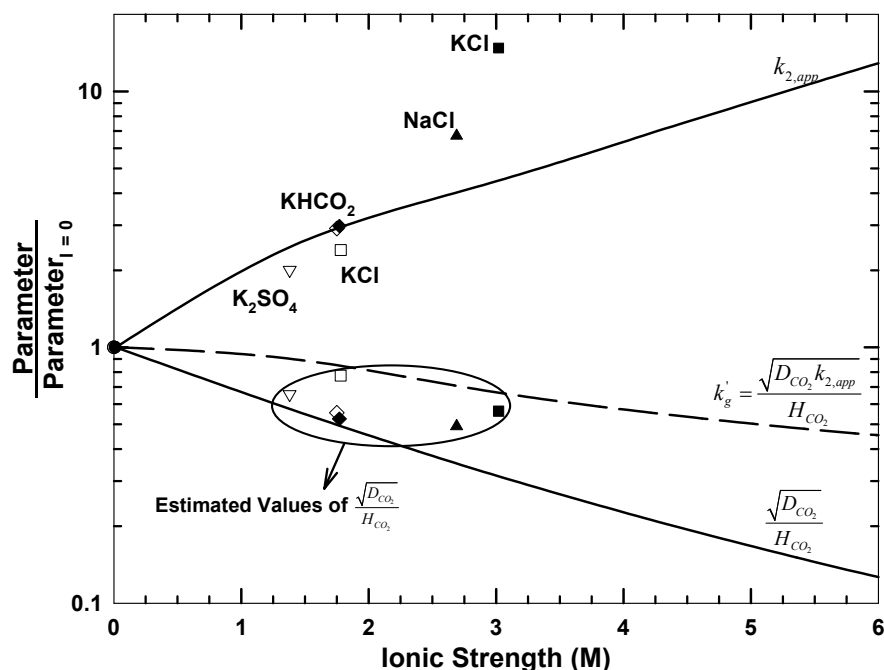
Figure 6.5. Effect of Ionic Strength on the Apparent Rate Constant and Physical Parameters in 0.6 m PZ, Closed Points: 25°C Experiments, Open Points: 60°C Experiments, Lines: Model for K_2CO_3/PZ ($k_{2,app}$ excludes CO_3^{2-} catalysis effect)

6.3. Aqueous Potassium Carbonate/Piperazine

The absorption rate of CO_2 into K^+/PZ mixtures was measured in the wetted-wall column. This study includes 2.5 to 6.2 m K^+, 0.6 to 3.6 m PZ, and 40 to 110°C. All data points collected are presented in Appendix C. Predictions of absorption rate and concentration profiles are tabulated in Appendix D.

6.3.1. Parameter Regression and Correlation

The data were used to regress rate constants and a correction to the diffusion coefficient of ions. The heats of activation were assumed to be the same as in aqueous PZ. Table 6.1 shows the specific rate constant regressed for each parameter as well as the correlation used, if applicable.

Recall from Section 2.3.1. that the rate constant for a reaction catalyzed by a base may be written in a logarithmic form

$$\ln k_{b_1} = x + \chi \, pK_{a,b_1} . \tag{6.2}$$

From the regression of rate constants in aqueous PZ ($k_{PZ\text{-}PZ}$, $k_{PZ\text{-}H_2O}$, $k_{PZ\text{-}OH}$), the slope of the Brønsted relationship, χ, was found to be 0.457. This value was used to correlate several of the rate constants for the K^+/PZ data according to differences in base strength.

$$\ln k_{Am-b_2} = \ln k_{Am-b_1} + \chi \left(pK_{a,b_2} - pK_{a,b_1} \right) \tag{6.3}$$

Because base catalysis has been widely recognized as a contributing factor in the reaction of some amines with CO_2 (Sharma, 1965), the correlation of unknown rate constants to regressed rate constants is thought to be a reasonable approximation of kinetic behavior.

Independent regression of all necessary rate constants proved to be statistically unachievable. Figure 6.6 illustrates the relationship of base strength with rate, showing the slope of 0.457 with both regressed and correlated values.

A representation of the pK_a of H_2O and OH^- was calculated from assuming

$$pK_w = -\log_{10} \left(\left[H^+ \right] \left[OH^- \right] \right) = 14 . \tag{6.4}$$

Thus,

$$pK_{a,OH^-} = -\log_{10}\left(\frac{\left[H^+\right]\left[OH^-\right]}{\left[H_2O\right]}\right) = 15.74\,, \tag{6.5}$$

and

$$pK_{a,H_2O} = pK_{a,w} - pK_{a,OH^-} = -1.74\,. \tag{6.6}$$
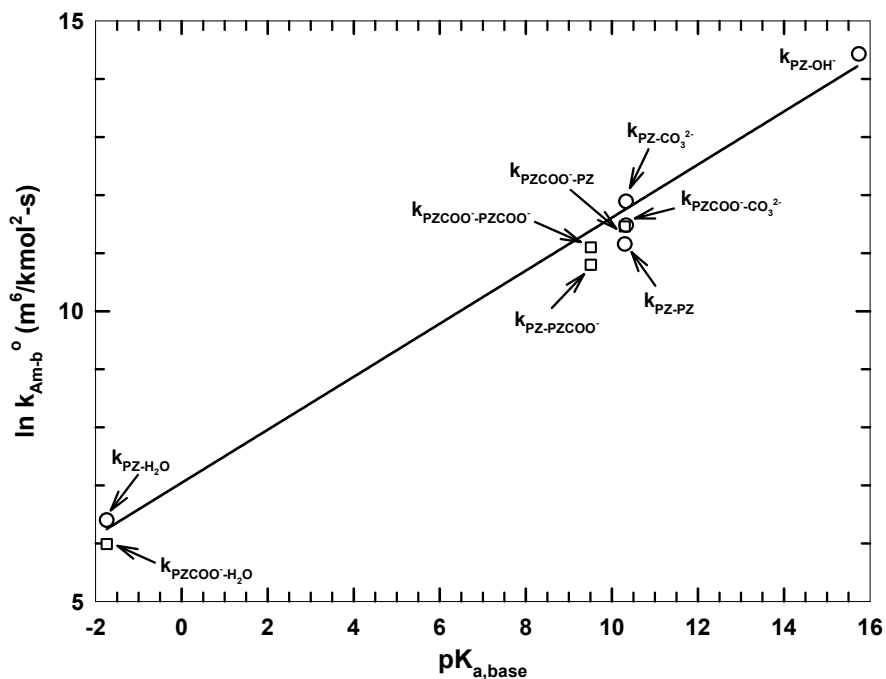
Figure 6.6. Fit of Specific Rate Constants to Brønsted Theory of Acid-Basic Catalysis, Circles: Independently Regressed, Squares: Correlated by Slope

This type of approximation is supported by previous work on other amines. Data on CO_2 absorption into aqueous morpholine (MOR), diethanolamine (DEA), and diisopropanolamine (DIPA) have been reanalyzed in terms of a termolecular mechanism to give rate constants for comparison to PZ in this work. The rate constants are presented in Figure 6.7 and Table 6.5.

189

As the analysis shows, the effect of base strength on the rate is nearly proportional for the given amines (i.e. $\chi \sim 0.5$). It is also striking that the effect does not depend on the type of molecule, only the pK_a; thus, water and hydroxide can be represented by the same correlation used for amines. Deviations from the correlation, as observed for TEA, can be explained in terms of steric effects.

The vertical displacement is also a function of base strength and steric effects. DEA and DIPA are of approximately the same pK_a, but are differentiated by structure. In constrast, MOR and PZ have similar structures, but the PZ has a higher pK_a and, consequently, a larger rate constant.
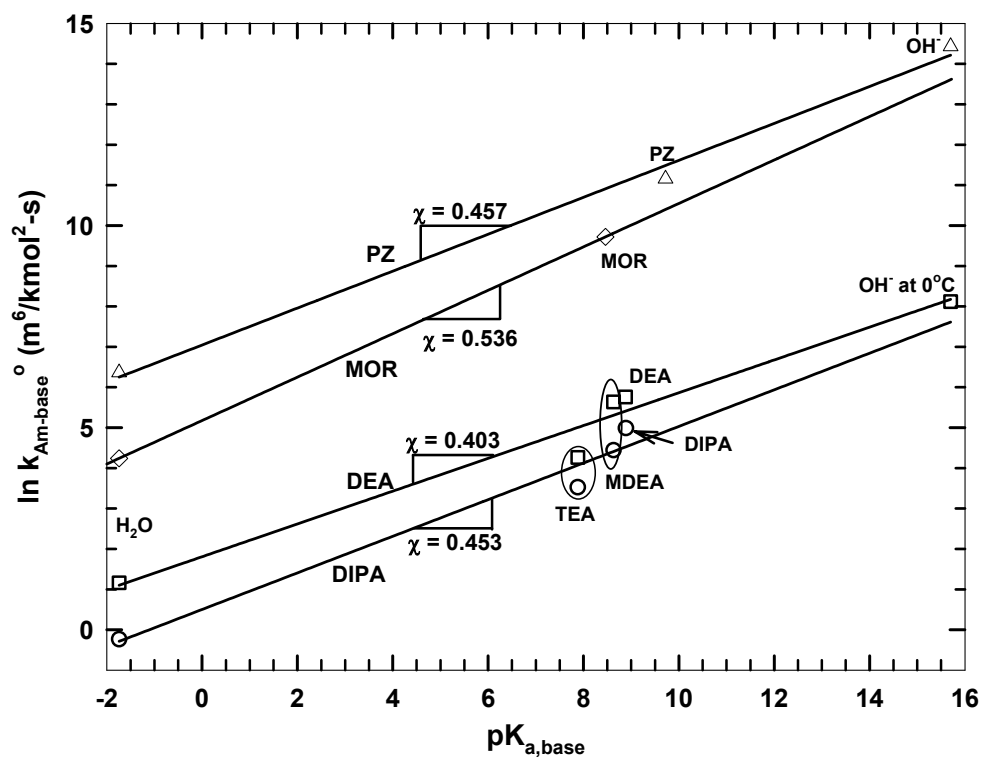
Figure 6.7. Correlation of Rate Constants to Base Strength for Four Secondary Amines Given by the Termolecular Mechanism at 25°C

Table 6.5. Termolecular Rate Constants ($k_{Am\text{-}base}$ ($m^6/kmol^2$-s)) for Four Secondary Amines Interpreted from Previous Work at 25^oC

		base						
	H_2O	TEA	MOR	MDEA	DEA	DIPA	PZ	OH⁻
pK_a	-1.74	7.88	8.49	8.63	8.88	8.89	9.73	15.74
MOR[1]	1.2	-	1715	-	-	-	-	-
DEA[2]	3.2	70.7	-	281	315	-	-	3.38×10^3 [a]
DIPA[3]	0.8	33.8	-	85.3	-	147	-	-
PZ[4]	550	-	-	-	-	-	70.1×10^3	1.86×10^6

(The leftmost label **Am** spans the four rows MOR, DEA, DIPA, PZ.)

1. Alper (1990a) 2. Jorgensen (1956) per Danckwerts (1979), Blauwhoff *et al.* (1984), Littel *et al.* (1992a), Versteeg and Oyevaar (1989) 3. Blauwhoff *et al.* (1984), Littel *et al.* (1992a), Versteeg and van Swaaij (1988a) 4. This Work
a. Point given by Danckwerts (1979) as interpreted from Jorgensen (1956) data at 0^oC.

As previously mentioned, a correction to the diffusion coefficient representing ions in solution was regressed in addition to the kinetic parameters. The correction was added to the diffusion coefficient estimate so that

$$D_{Am} = \beta D_{Am}^{\infty} \left(\frac{\eta_w}{\eta_{Sol}} \right). \tag{6.7}$$

β was found to be 1.51, correcting for discrepancies in the correlation used for diffusion coefficients of ions and for k_l^o in the calculation of film thickness. Only the coefficient for ions was adjusted; molecular diffusion coefficients remained unchanged.

The incorporation of the above parameters into the model results in a good representation of the experimental data. Of the predictions of flux, 91% fall within $\pm 30\%$ of the experimental data and 79% fall within $\pm 20\%$. Figure 6.8 illustrates the ability of the model to correlate the flux under the given conditions.

191
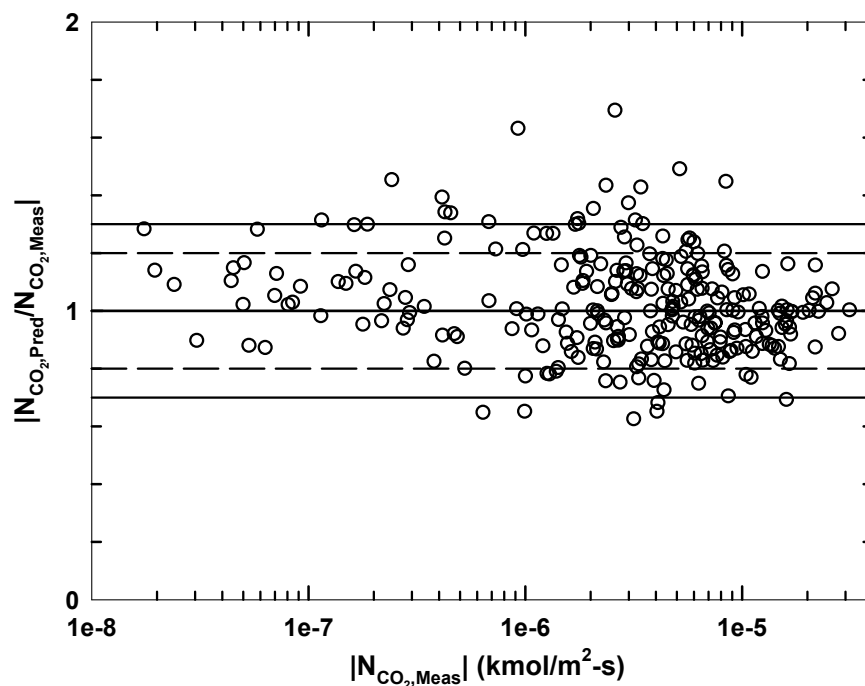
Figure 6.8. Model Correlation of CO_2 Flux into K^+/PZ

Figure 6.9 shows the sensitivity of the model to variations in parameter i

$(\frac{d \ln k_g^{'}}{d \ln i})$ in 5.0 m K^+/2.5 m PZ at 60^oC. The conditions represent values typical of

experiments in this work. Parameters with sensitivities under 0.05 have been omitted.

In the region of low P_{CO_2}* (< 300 Pa), kinetics dominate the model sensitivity.

Specifically, the catalysis of the PZ reaction by CO_3^{2-} is the most significant parameter.

While the self-catalysis of PZ is important, the reaction of CO_2 with $PZCOO^-$ is

impacting the absorption rate, even at the low loadings.

Between P_{CO_2}* of 300 and 3,000 Pa, the kinetics are still the major determinant

of the absorption rate though the diffusion of ions is now a contributing factor.

Carbonate is still the most influential catalyst for reaction, but the main reactant is

192

PZCOO⁻ rather than PZ. The self-catalysis of PZCOO⁻, represented by $k_{PZCOO^- - PZCOO^-}$, is also important.
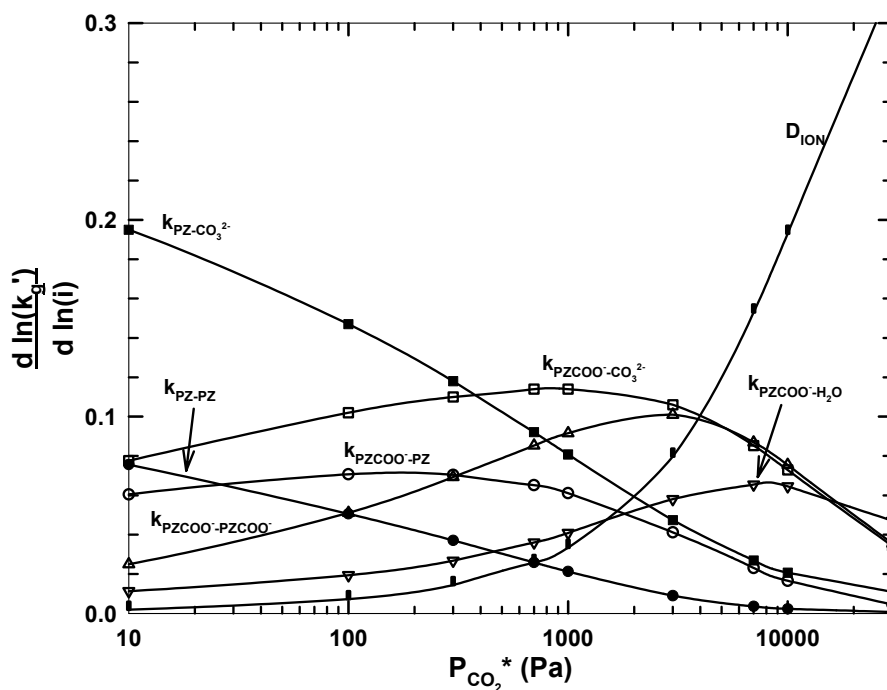
Figure 6.9. Sensitivity of Model Parameters in 5.0 m K⁺/2.5 m PZ at 60°C, $k_l^o =$ 1.0×10⁻⁴ m/s, $P_{CO_2,i} = 1.5 \times P_{CO_2}*$

Above a $P_{CO_2}*$ of 3,000 Pa, the diffusion of the ions has the greatest effect on absorption rate. It is expected that, under these conditions, there will be a significant accumulation of products at the gas-liquid interface as the diffusion coefficients limit the reaction rate. Nearly all of the PZ has been consumed and PZCOO⁻ is the main reactant. While the catalysis by CO_3^{2-} is still significant, H_2O also contributes to the rate through $k_{PZCOO^- - H_2O}$. As the pH decreases, $k_{PZCOO^- - CO_3^{2-}}$ diminishes in importance as CO_3^{2-} is converted to HCO_3^-.

In addition to discerning common trends for model sensitivity, Figure 6.9 also highlights the complexity of regressing parameters within a multi-parameter reaction mechanism. It is typical for several parameters to have approximately the same significance under similar conditions. In these cases, independent regression of these parameters is difficult and a method of correlating the values may be justified.

6.3.2. Absorption Rate of Carbon Dioxide

Given the ability of the model to represent the experimental data accurately, it is useful to compare model correlations to arrive at conclusions concerning solvent performance at various conditions. Solvent concentrations and temperature dependence are of particular interest as these properties often dictate overall performance.

The normalized flux (k_g') of several K^+/PZ solvents is shown in Figure 6.10. In promoted K_2CO_3 (i.e. 3.6 m K^+/0.6 m PZ), the absorption rate is fast, though 20 to 30% less than 5 M MEA under similar conditions. More concentrated solvents, such as 3.6 m K^+/1.8 m PZ, have absorption rates a factor of 2 higher than the promoted solvent and a factor of 1.5 higher than 5 M MEA. The 3.6 m K^+/3.6 m PZ solvent has an absorption rate 2 to 3 times that of 5 M MEA. From Section 5.6, this solvent is expected to have a high capacity; however, volatility may prevent concentrated PZ solvents from being commercially viable.

Interestingly, 5.0 m K^+/2.5 m PZ has a normalized flux nearly identical to 3.6 m K^+/1.8 m PZ. The similarity can be explained by two mechanisms. First, in the concentrated solvents, the viscosity is higher, leading to smaller diffusion coefficients. Second, the physical solubility of CO_2 is less in the higher ionic strength environment.

The competing effects of kinetics and diffusivity and solubility appear to play a significant role in determining the absorption rate in some concentrated solvents.
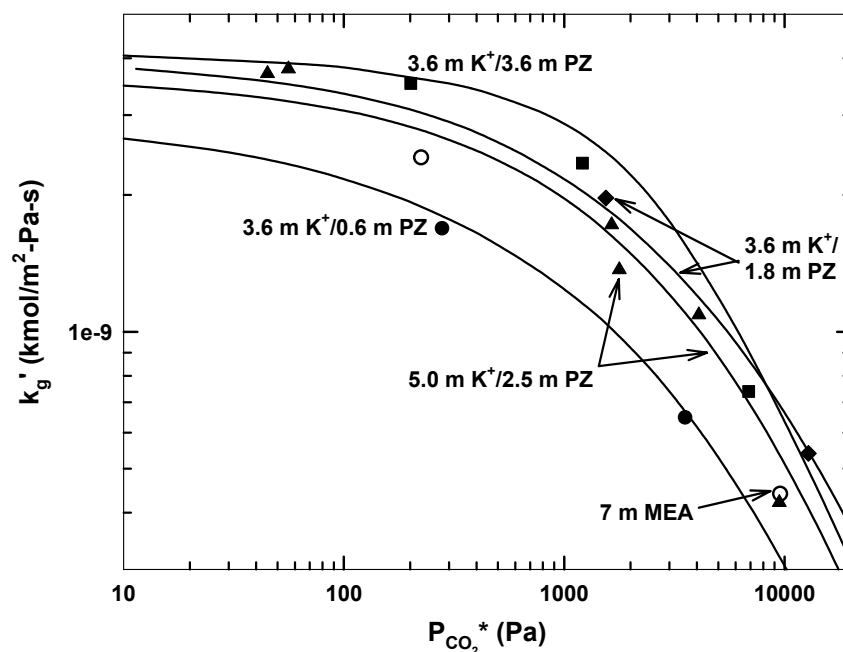
Figure 6.10. Normalized Flux in K$^+$/PZ Mixtures at 60°C, Points: Experimental Data (MEA from Dang (2001)), Lines: Model Prediction ($k_l^o = 1\times10^{-4}$ m/s, $P_{CO_2,i} = 3.0\times P_{CO_2}^*$)

The relative impact of K$^+$ and PZ on the absorption rate is compared in Figure 6.11. The two lines demonstrate the changing ratio of K$^+$:PZ where one component is constant. As the amount of PZ increases relative to the K$^+$ concentration, an increase in the rate of absorption is observed in both the cases of constant K$^+$ and constant PZ. From a K$^+$:PZ ratio of 8:1 to 1:1, the normalized flux increases by a factor of three.

As suggested previously, more concentrated solvents do not necessarily yield faster absorption rates. This is somewhat unexpected since previous investigations of speciation suggest more reactive species are present at higher total solvent

195

concentrations (Cullinane and Rochelle, 2004). The predictions of absorption rate of 5.0 m K^+/2.5 m PZ and 6.2 m K^+/1.2 m PZ in Figure 6.11 clearly demonstrate that, though the amount of PZ is high, other effects, such as diffusion coefficients and physical solubility, contribute to the absorption rate. Over the concentration ranges considered, the K^+:PZ ratio is more significant in determining the absorption rate than the total PZ concentration.
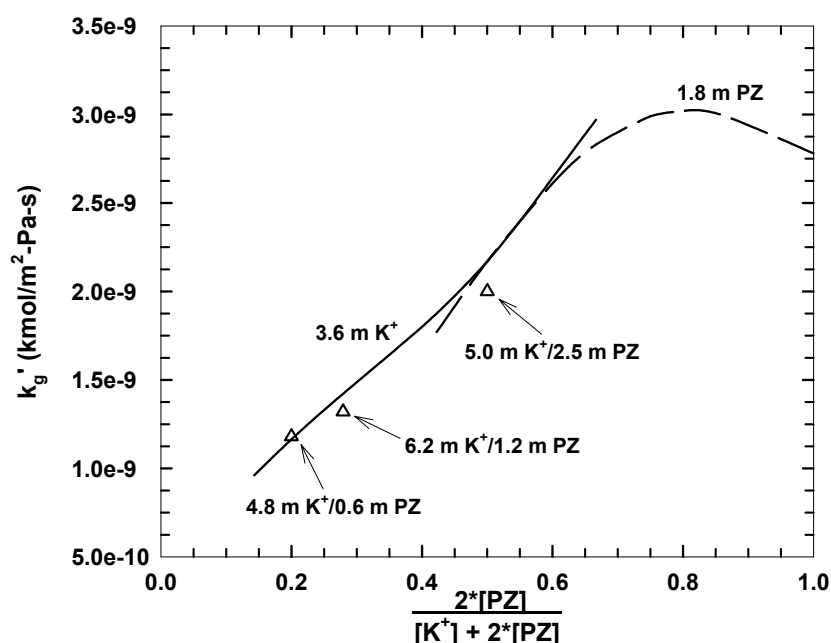
Figure 6.11. The Effect of K^+/PZ Ratio on the Absorption Rate of CO_2 at 60^oC and $P_{CO_2}* = 1,000$ Pa, $k_l^o = 1.0 \times 10^{-4}$ m/s, $P_{CO_2,i} = 1.05 \times P_{CO_2}*$

The absorption rate of K^+/PZ mixtures is compared to other promoted-K_2CO_3 solvents in Figure 6.12. The solvents included in the comparison are from Exxon (Sartori and Savage, 1983). (In the preferred embodiment of the DEA- and hindered amine-promoted solvents, the absorber/stripper would be operated at high temperature, leading to the high temperature comparison.) The absorption rate of 3.6 m K^+/0.6 m PZ

196

at 60°C is nearly equivalent to the hindered amine-promoted solvent at 90°C. At 90°C the 3.6 m K^+/0.6 m PZ has an absorption rate slightly faster, though the rate declines faster at high loadings. This effect can be attributed to the formation of stable piperazine carbamates. The 5.0 m K^+/2.5 m PZ gives 2 to 4 times faster at 60°C and 90°C. The concentrated solvent exhibits much faster absorption rates at high loadings, demonstrating the advantage of using a diamine promoter in large quantities.
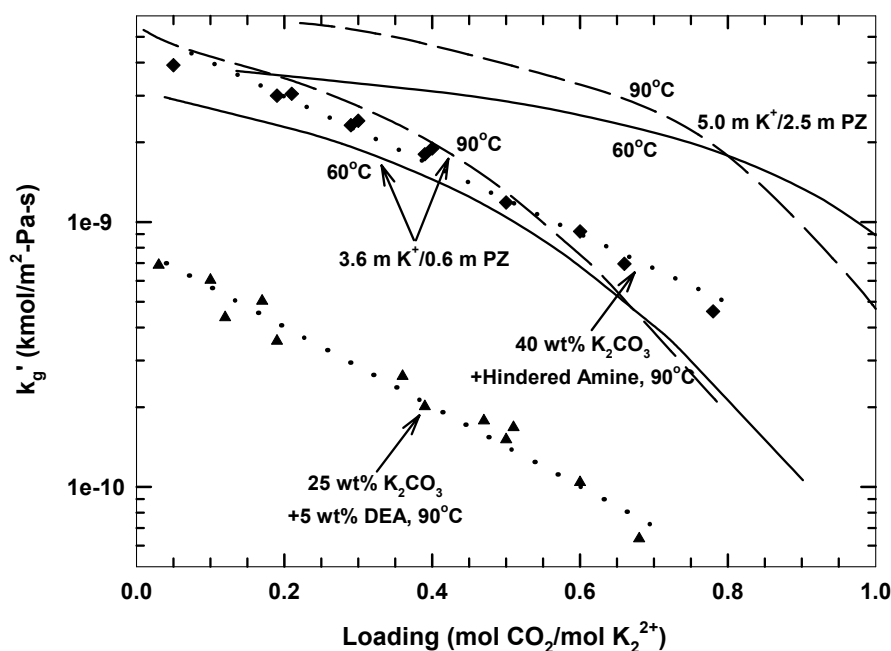
Figure 6.12. Normalized Flux Comparison of PZ to Other Promoters in K₂CO₃, Points: Experimental Data, Lines for K^+/PZ: Model

Figure 6.13 to Figure 6.15 illustrate the dependence of normalized flux on temperature. At low to moderate temperatures (40 to 80°C), an increase in k_g' is observed with temperature at constant $P_{CO_2}*$. This corresponds to increasing kinetics and mass transfer properties that accompany a higher temperature. This is also

observed at 100 to 110°C and low $P_{CO_2}*$. At the high temperatures and high $P_{CO_2}*$, a relatively small difference in k_g' is observed. This indicates an approach to instantaneous behavior, where the diffusion of reactants and products becomes limiting.
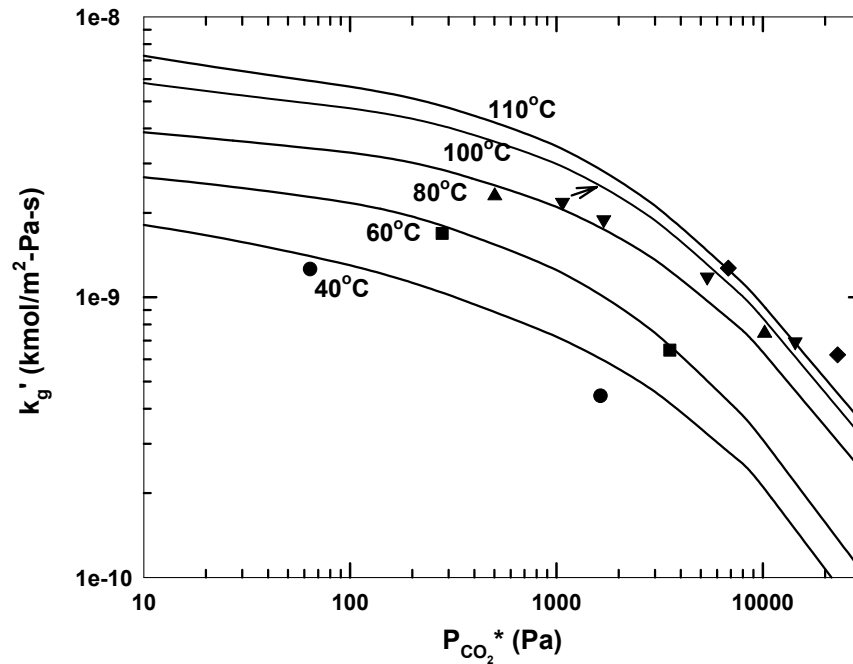
Figure 6.13. Temperature Dependence of k_g' of 3.6 m K^+/0.6 m PZ, Points: Experimental Data, Lines: Model Prediction ($k_l^o = 1 \times 10^{-4}$ m/s, $P_{CO_2,i} = 3.0 \times P_{CO_2}*$)

Conclusions are markedly different when viewed at constant loading as in Figure 6.16. With a constant CO_2 concentration, k_g' increases by a factor of 3 as the temperature increases from 40 to 110°C at low loadings. At high loadings, however, an increasing temperature brings about a similarly large reduction in absorption rate with increasing temperature. This occurs because the relative increase in $P_{CO_2}*$ with temperature is greater than in changes in speciation. Over the loading range of 0.55 to 0.65, k_g' is nearly independent of temperature.

198
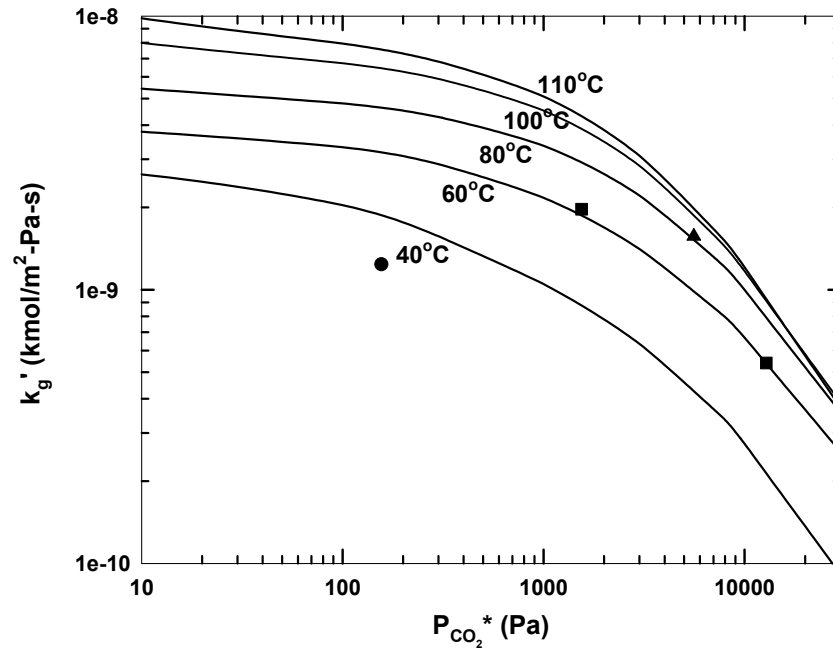
Figure 6.14. Temperature Dependence of k_g' of 3.6 m K^+/1.8 m PZ, Points: Experimental Data, Lines: Model Prediction ($k_l^0 = 1 \times 10^{-4}$ m/s, $P_{CO_2,i} = 3.0 \times P_{CO_2}^*$)
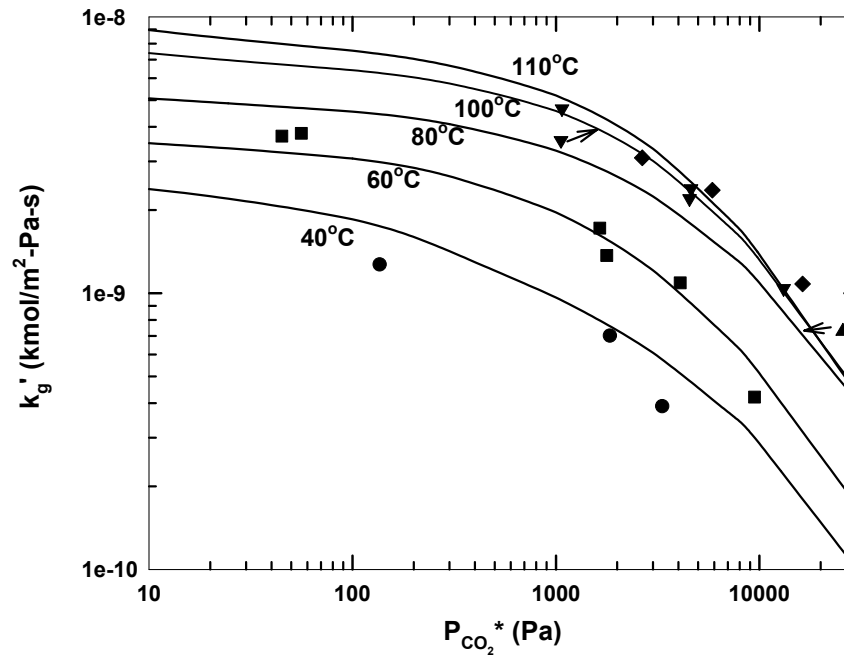
Figure 6.15. Temperature Dependence of k_g' of 5.0 m K^+/2.5 m PZ, Points: Experimental Data, Lines: Model Prediction ($k_l^0 = 1 \times 10^{-4}$ m/s, $P_{CO_2,i} = 3.0 \times P_{CO_2}^*$)

199

It is this viewpoint that will be of utility when describing absorber/stripper processes. When transferring solvent from the absorber to the stripper, the solution will be heated at a constant high loading. Thus, based on a constant driving force, k_g' at the top of the stripper is expected to be less than at the bottom of the absorber. Likewise, the rate in the bottom of the stripper will be faster than in the top of the absorber.
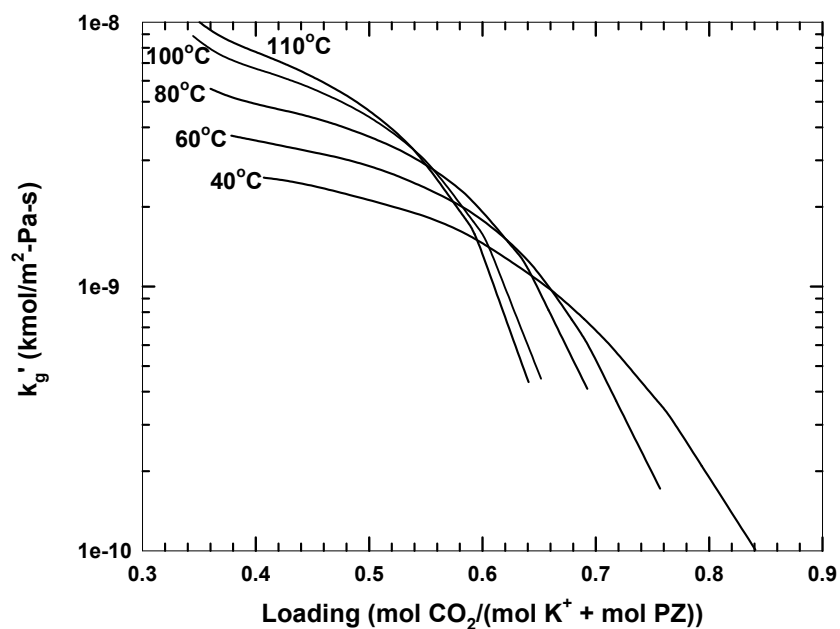
Figure 6.16. Temperature Dependence of k_g' of 5.0 m K^+/2.5 m PZ at Constant Loading, Points: Experimental Data, Lines: Model Prediction ($k_l^o = 1 \times 10^{-4}$ m/s, $P_{CO_2,i} = 3.0 \times P_{CO_2}^*$)

6.3.3. Approximations

As previously discussed, approximate solutions to the rigorous model have advantages in that simple calculations based on bulk properties are possible. Additionally, simple models aid the understanding of complex physical phenomena. In

light of these advantages, solvent performance at typical experimental conditions was analyzed to determine the validity of the proposed expressions.

Figure 6.17 shows various representations of normalized flux at 60°C with a low driving force ($P_{CO_2,i} = 1.05 \times P_{CO_2}*$). At low loadings, the normalized flux, k_g', is described well by pseudo-first order approximation, $k_g'_{,PFO}$. At high loadings, the reaction approaches an instantaneous condition and deviates from simple kinetic considerations. The values of $k_g'_{,PZ,INST}$ and $k_g'_{,GBL,INST}$ are approximately equal at low loadings, but diverge at high loadings, indicating an increase in the contribution of bicarbonate formation to the overall absorption rate relative to the reaction with PZ species. A simple, series addition of the pseudo-first order approximation and the PZ-instantaneous condition provides a good representation of actual rate performance over the entire loading range.

$$\frac{1}{k_{g,SR}'} = \frac{1}{k_{g,PFO}'} + \frac{1}{k_{g,PZ,INST}'} \tag{6.8}$$

As shown in Figure 6.18, the behavior of the absorption rate at 110°C is similar, but the loading ranges in which approximations are valid change considerably. The pseudo-first order approximation is less likely to apply. In this case, $k_g'_{,PFO}$ would give a 40% error in predicting k_g' at a loading of 0.5. At high loadings, the reaction is much closer to an instantaneous condition though kinetics still play a significant role in determining the absorption rate. An 80% error would be obtained by assuming the absorption rate is instantaneous at a loading of 0.6. Also at the higher temperature, $k_g'_{,PZ,INST}$ and $k_g'_{,GBL,INST}$ no longer diverge at high loadings. This suggests that

reactions to form bicarbonate are sufficiently fast due to increased temperature that they may be considered instantaneous.
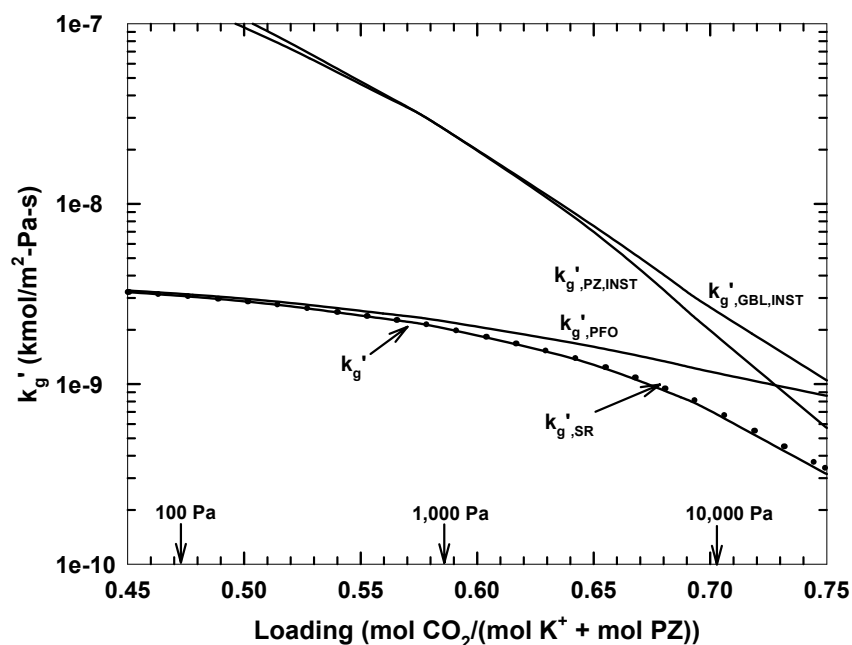
Figure 6.17. Approximate Solutions to Normalized Flux in 5.0 m K$^+$/2.5 m PZ at 60°C, $k_l^o = 1.0 \times 10^{-4}$ m/s, $P_{CO_2,i} = 1.05 \times P_{CO_2}$*

The previous examples illustrate the usefulness of approximations under low driving force conditions. With the imposition of a large driving force, the transport of species becomes less empirical and simple representations may break down. Figure 6.19 demonstrates that the simple, series resistance model is not a satisfactory representation at higher driving forces. Much of the inaccuracies fall in the high loading region where equilibrium effects, not pseudo-first order conditions, must change across the boundary layer.
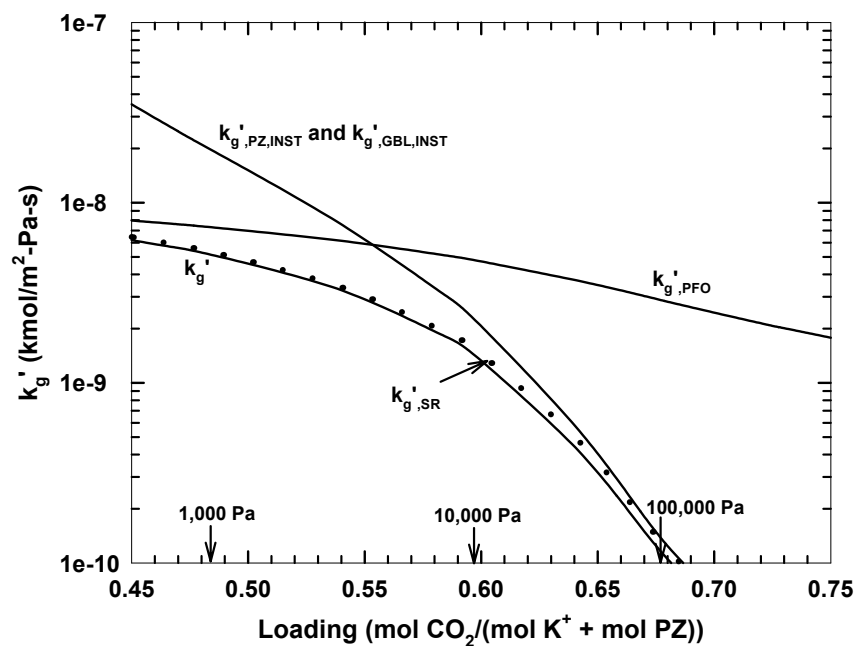
Figure 6.18. Approximate Solutions to Normalized Flux in 5.0 m K$^+$/2.5 m PZ at 110°C, k$_l^o$ = 1.0×10^{-4} m/s, P$_{CO_2,i}$ = 1.05×P$_{CO_2}$*
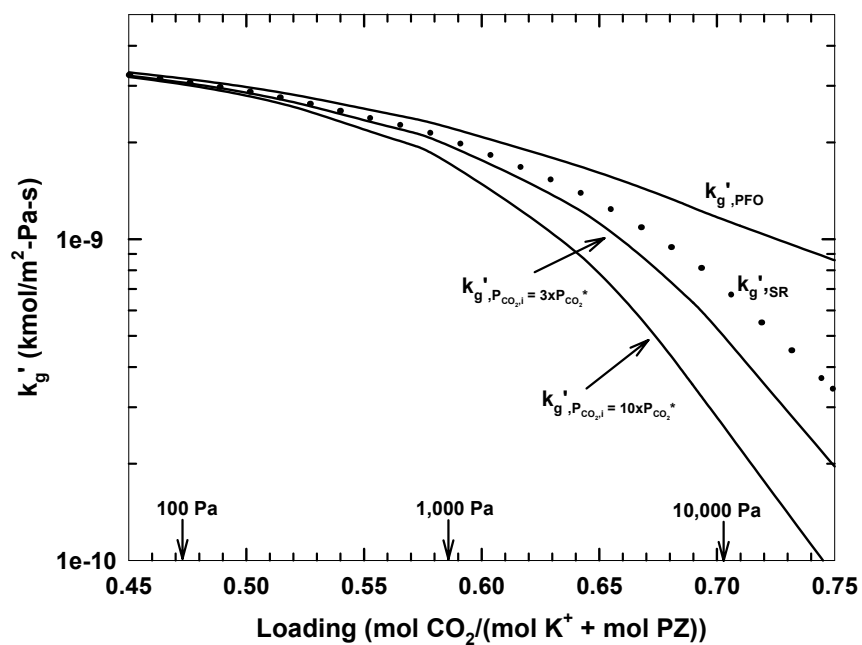
Figure 6.19. Effect of Driving Force on Approximate Solutions to Normalized Flux in 5.0 m K$^+$/2.5 m PZ at 60°C, k$_l^o$ = 1.0×10^{-4} m/s

The analysis presented in Table 6.6 shows the difficulty. The ability to represent the absorption rate empirically based on bulk solution properties rests on the change in species concentrations across the interface. At low loadings and low and high temperatures, the absorption rate can be still described by the pseudo-first order approximation even with a factor of 10 driving force. At $110^{\circ}C$ and a loading of 0.473, the concentrations of PZ and $PZCOO^-$ change by less than 5% across the boundary layer; however, substantial differences in the buffering species carbonate and bicarbonate are predicted. This indicates a changing equilibrium across the boundary layer and shows that an equilibrium representation of instantaneous behavior is not sufficient.

Table 6.6. Concentration ($kmol/m^3$) Across the Liquid Boundary Layer in 5.0 m K^+/2.5 m PZ, $k_l^o = 1.0x10^{-4}$ m/s

	$P_{CO2,i} = 10.0 \times P_{CO2}*$, T = $60^{\circ}C$				$P_{CO2,i} = 0.1 \times P_{CO2}*$, T = $110^{\circ}C$			
Loading[a]	0.473		0.586		0.473		0.586	
$P_{CO2}*$ (Pa)	100		1,000		810		7,600	
	Interface	Bulk	Interface	Bulk	Interface	Bulk	Interface	Bulk
CO_3^{2-}	1.155	1.179	0.518	0.633	1.161	1.118	0.644	0.479
HCO_3^-	0.281	0.258	0.663	0.548	0.299	0.340	0.469	0.624
PZ	0.810	0.831	0.26	0.344	0.965	0.931	0.547	0.447
PZH^+	0.019	0.017	0.07	0.062	0.002	0.002	0.006	0.009
$PZCOO^-$	0.863	0.859	0.671	0.733	0.700	0.711	0.659	0.638
H^+PZCOO^-	0.027	0.024	0.143	0.106	0.003	0.003	0.008	0.014
$PZ(COO^-)_2$	0.248	0.237	0.771	0.679	0.268	0.286	0.682	0.781

a. Loading given in mol CO_2/(mol K^+ + mol PZ)

At high loadings, substantial differences in concentrations are obtained for most of the species; simple models based on bulk solution equilibrium will not describe the absorption rate. At $60^{\circ}C$, PZ and $PZCOO^-$ are depleted by 24% and 9% respectively. Also, an accumulation (or depletion) of $PZ(COO^-)_2$ occurs at the interface. Although

PZH$^+$ and H$^+$PZCOO$^-$ are accumulating to a notable extent, most of the buffering still occurs with the CO$_3$$^{2-}$/HCO$_3$$^-$.

Figure 6.20 illustrates changes in the liquid boundary layer as a result of approaching instantaneous behavior. Under kinetically controlled conditions (60°C and P$_{CO_2,i}$ = 10.0×P$_{CO_2}$*), the influence of chemical reaction is apparent in the large region of nonlinear approach to the interface concentration of CO$_2$ near the interface (r < 0.01). Further away (r > 0.01), the profile is linear, extending to the equilibrium concentration of CO$_2$ in the bulk solution, [CO$_2$]$_b$. Only 10% of the mass transfer occurs in the linear diffusion region, whereas 90% occurs as a result of reaction with amines near the interface.
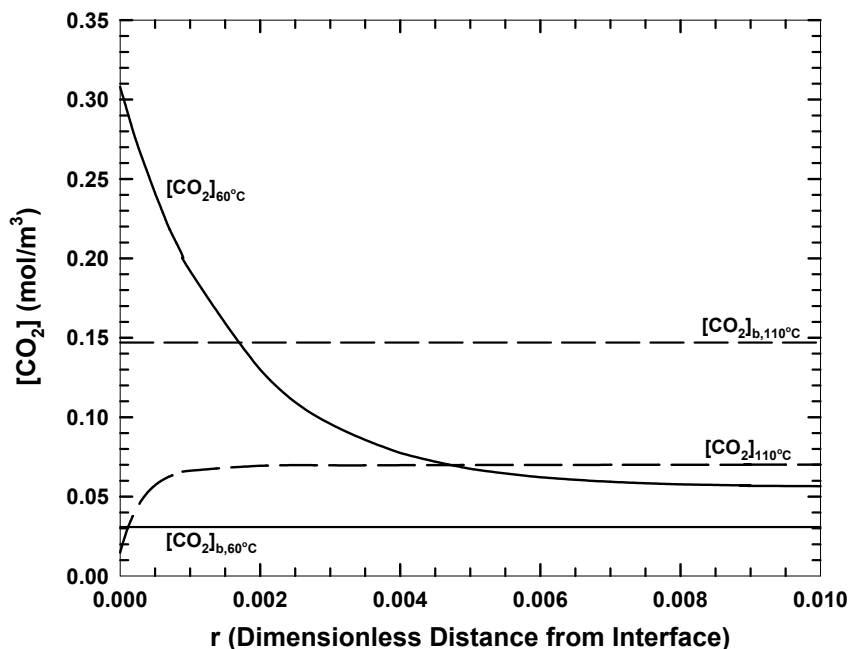
Figure 6.20. Concentration Profile in 5.0 m K$^+$/2.5 m PZ, Loading = 0.586 mol CO$_2$/(mol K$^+$ + mol PZ), (P$_{CO_2}$* = 1,000 Pa at 60°C), k$_l$^{o} = 1.0×10^{-4} m/s, Solid Line: P$_{CO_2,i}$ = 10.0×P$_{CO_2}$* and T = 60°C, Dashed Line: P$_{CO_2,i}$ = 0.1×P$_{CO_2}$* and T = 110°C

The mass transfer characteristics change dramatically at high temperatures as instantaneous conditions are approached. At 110^oC and $P_{CO_2,i} = 0.1 \times P_{CO_2}*$, the zone of chemical reaction is much closer to the interface, terminating at r = 0.001. Now, 58% of the mass transfer occurs in the diffusion boundary layer and 42% in the reaction zone. In this case, diffusion of reactants and products has become much more significant in determining the absorption rate.

6.3.4. Applications

A useful function of the fundamental modeling provided by this work is its application to estimating the behavior of the K^+/PZ solvent under typical industrial conditions. As an exercise, the solvent performance was analyzed under conditions that may be encountered in treating flue gas from a coal-fired power plant.

Figure 6.21 shows the calculated k_g' with a low driving force and a variation of k_l^o. The wetted-wall column in this work typically operates at a k_l^o of 10^{-4} m/s, which is in the pseudo-first order region under most conditions. Low values of k_l^o, as would be typical of quiescent liquids, result in a sharply decreasing k_g' as the reaction moves into the instantaneous region. At 60^oC, the transition occurs at approximately 2×10^{-5} m/s. The difference in k_g' with temperature in the instantaneous region is a function of equilibrium at the given conditions. Increasing the value of k_l^o from pseudo-first order conditions yields a transition to physical absorption. This occurs at very large k_l^o (i.e. > 0.1 m/s) indicative of rapid mixing of the fluid. The difference in temperature in the physical mass transfer region is a result of the physical solubility of CO_2.

206

In general, industrial conditions give larger liquid film mass transfer coefficients than the wetted-wall column used in this work. It is expected that kinetics will play a larger role in determining the absorption rate in industrial absorbers. It is also important to recognize that the influence of kinetics at stripper conditions will increase.
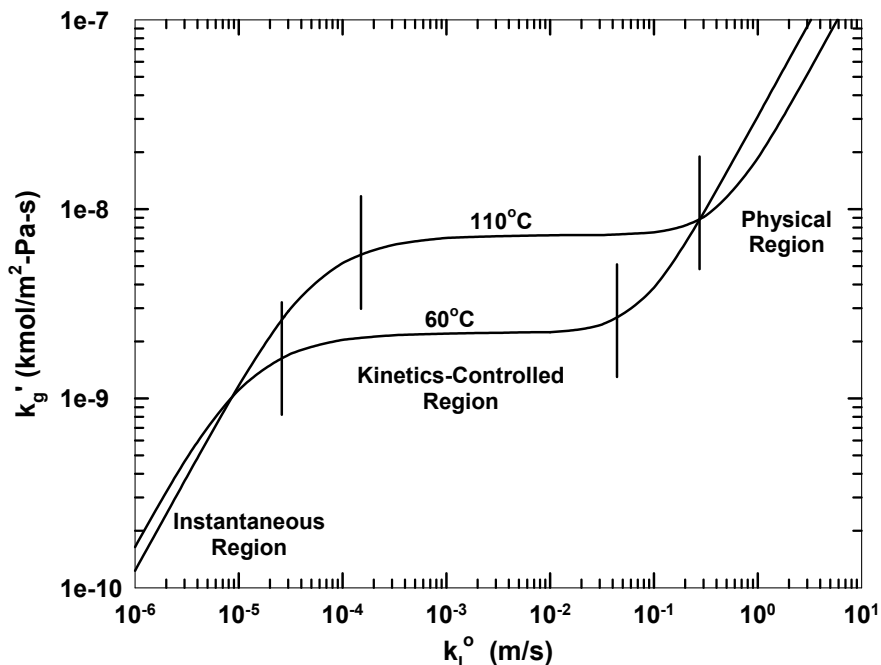
Figure 6.21. Model Sensitivity to k_l^o for 5.0 m K^+/2.5 m PZ, $P_{CO_2,i} = 1.05 \times P_{CO_2}^*$, $P_{CO_2}^* = 1,000$ Pa

Another important parameter influencing mass transfer is the gas film resistance, k_g. The percent gas film resistance, defined as the ratio of the gas film resistance to the overall resistance (i.e. K_G/k_g), provides an estimate of the importance of the kinetics in determining the absorption or stripping rate of CO_2 from K^+/PZ mixtures. Figure 6.22 shows the predicted contribution of gas film resistance under industrially significant

conditions. The mass transfer coefficients were previously estimated by Bishnoi (2000) and are applied here as representative of commercial conditions.

Gas film resistance is significant at low loadings, due to the fast reaction rates at low $P_{CO_2}*$. This is particularly important at high temperatures where gas film resistance can be up to 90% of the total resistance at 100 Pa. At high loadings, kinetics become increasingly important as $P_{CO_2}*$ increases and the effective absorption rate decreases. The K_G/k_g at 10,000 Pa ranges from 30 to 40% at 60 to 110°C. In general, gas film resistance is expected to be significant at the top of the absorber and the bottom of the stripper; conversely, kinetics will determine the mass transfer rate at the bottom of the absorber and the top of the stripper.
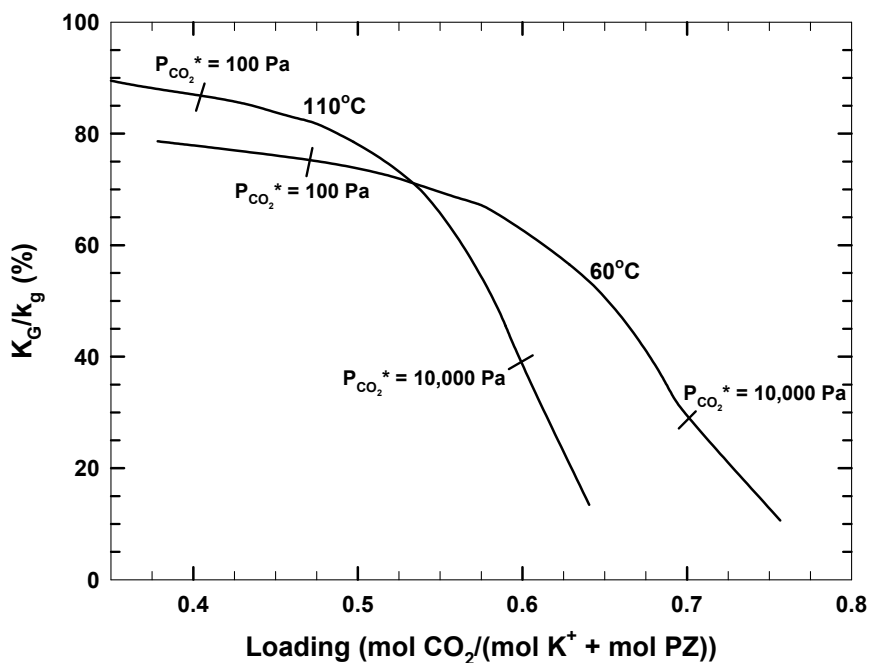
Figure 6.22. Contribution of Gas Film Resistance to Overall Mass Transfer in 5.0 m K$^+$/2.5 m PZ, $P_{CO_2,i} = 3.0 \times P_{CO_2}*$, $k_l^o = 6 \times 10^{-5}$ m/s, $k_g = 1.0 \times 10^{-9}$ kmol/m^2-Pa-s

6.4. Conclusions

Investigations on the rate of CO_2 absorption into aqueous PZ reveal that the reaction can approach second-order with respect to PZ. The addition of 0.15 m KOH increases the absorption rate in 0.6 m PZ by a factor of 2, suggesting that strong bases must be included in the reaction mechanism. The kinetics can be represented by both the "zwitterion" and termolecular mechanisms.

The rigorous rate model was used to regress rate constants to describe aqueous PZ. The values are consistent with the Brønsted theory of base catalysis and with behavior of other amine studies. The apparent rate constant of 1 M PZ is a factor of 20 greater than MEA and a factor of 100 greater than DEA. The rapid reaction of the PZ with CO_2 can be attributed to its unique, cyclic diamine structure.

Neutral salts in aqueous PZ significantly influence the reaction rate; the addition of 1.8 M KCl increases the apparent rate constant by a factor of 2.5 at 60°C. This neutral salt effect suggests that amine-promoted K_2CO_3 exhibits kinetics above what would be expected. A correction for the rate constants in K^+/PZ was introduced to account for promotion from ionic strength. The correction results in increases similar to those observed from neutral salts. While the rate constants increase, an opposite effect is observed for the diffusion coefficient and Henry's constant, resulting in a net decrease on the overall absorption rate.

Data on K^+/PZ show that strong bases, such as carbonate or other amines, accelerate the absorption rate of CO_2. Based on the experimental data, the rate constants, though correlated, were in agreement with work on aqueous PZ in that base

strength adequately correlates the rate constants of additional bases. PZ, PZCOO⁻, and CO_3^{2-} are recognized as significant rate contributors.

The sensitivity of the model to changes in kinetic and mass transfer parameters indicates that, at low CO_2 loadings, kinetics determine the absorption rate. The most significant reactions involve PZ-CO_3^{2-} and PZCOO⁻-CO_3^{2-}. At higher loadings, the diffusion of ions across the reaction boundary layer dictates the rate. The diffusion of PZ to the gas-liquid interface is not a significant parameter under the tested conditions.

With typical experimental conditions, concentrated K^+/PZ mixtures have absorption rates 2 to 3 times faster than 5 M MEA at constant P_{CO_2}*. Evidence also suggests that the ratio of K^+:PZ influences the absorption rate more than total solvent concentration. With 1.8 m PZ and P_{CO_2}* = 1,000 Pa, k_g' increases by 50% when the K^+ concentration is reduced from 3.6 m to 0.9 m. The absorption rate into 3.6 m K^+/1.8 m PZ solvent is nearly equivalent to that into 5.0 m K^+/2.5 m PZ, explainable through the competing effects of kinetics and CO_2 solubility and diffusivity.

At constant P_{CO_2}*, normalized flux is a significant function of temperature between 40 and 100°C, reflecting faster kinetics at these conditions. At 100 to 110°C, little temperature dependence is observed suggesting a significant approach to instantaneous behavior at high temperatures. This is also observed with increasing P_{CO_2}* at all temperatures as the rate becomes limited by diffusion processes.

At many conditions, empirical approximations are sufficient to express the absorption rate in K^+/PZ mixtures. At low loadings, a pseudo-first order assumption is usually suitable, even at high temperatures and driving forces. At high loadings and

high temperatures, a rate expression assuming instantaneous reaction with the amine can be used to describe the absorption with minimal error. A global instantaneous model does not appear to be effective at low temperatures as the formation of bicarbonate limits the instantaneous rate. Normalized flux at moderate conditions can be approximated with a simple series addition of the pseudo-first order and amine-instantaneous calculations. At extreme driving forces, solution equilibrium can differ across the boundary layer, causing equilibrium-based approximations to be in error.

Given the k_l^o of the gas-liquid contactor used in this work, most data were collected in a kinetically controlled region. At high temperatures, measurements in the wetted-wall column approach the instantaneous region, although kinetics still play a significant role in the absorption rate. In industrial contactors, where the k_l^o is expected to be somewhat higher, reaction kinetics would be more important.

When considering reasonable industrial conditions for the application of the K^+/PZ solvent, the gas film accounts for significant resistance at low loadings. At some conditions, the gas film may constitute >85% of the total resistance. The resistance is more pronounced at higher temperatures. At high loadings, the gas film resistance is only 20 to 30%.

Chapter 7: Conclusions and Recommendations

This chapter presents a summary of the important findings in this work. The completed work contributes to the experimental foundation of thermodynamics and kinetics in aqueous amine systems, specifically heterocyclic diamines. The work also presents detailed information on amine behavior in concentrated salt solutions. A method of modeling absorption into complex, reactive systems was developed and validated. Recommendations for future work are presented.

7.1. Summary

Experimental data were presented for K^+/PZ mixtures at 25 to 110°C with P_{CO_2}* of 10 to 30,000 Pa, encompassing conditions of CO_2 absorption from combustion flue gas. Data sets include speciation measurements by ^{1}H NMR, P_{CO_2}* and absorption rate measurements from a wetted-wall column, physical CO_2 solubility, solid solubility, and

other physical properties. The performance of this solvent was compared to other solvents using standard criteria: capacity, heat of absorption, and rate of absorption.

A rigorous thermodynamic model was developed using experimental data to regress equilibrium constants and binary interaction parameters. Values of equilibrium constants and enthalpies were compared to those of other amines. An adequate representation of the vapor-liquid equilibrium of CO_2 and the equilibrium speciation of thirteen molecular species was obtained over a broad range of conditions. The model was used to calculate and predict capacities and heats of absorption.

The rate of CO_2 absorption into K^+/PZ was simulated using a rigorous boundary layer model. Rates for twelve parallel reactions were considered along with the required diffusion coefficients for describing transport across a liquid film. From data of CO_2 absorption into K^+/PZ, nine rate constants were quantified by regression and correlation. The impact of neutral salts on the absorption rate was treated independently. The model was applied to predict solvent performance under typical experimental and industrial conditions. The model also aided the development and validation of approximate solutions to mass transfer under limited conditions.

7.2. Conclusions

7.2.1. Thermodynamics

In aqueous PZ loaded with CO_2, $PZCOO^-$ and $PZ(COO^-)_2$ are only minor components in solution, representing 10 to 20% of the total PZ. Most of the CO_2 absorption results in protonation of the PZ. With K^+, the concentration of $PZCOO^-$ and $PZ(COO^-)_2$ can each account for up to 50% of the total PZ concentration. The solution

is buffered at high pH and protonation is only significant at high $P_{CO_2}*$. Thus, the increased carbamate concentration is countered by a reduced presence of protonated species, giving a higher reactive PZ concentration. A maximum fraction of reactive PZ (PZ + PZCOO⁻) exists at a 2:1 ratio of K^+:PZ, independent of the total concentration.

Measurements of the equilibrium CO_2 partial pressure indicate improved VLE behavior in K^+/PZ. Correlations suggest that solvents containing the same K^+:PZ ratio can be represented by the same curve versus loading. Most of the error associated with the VLE measurements has been identified as in the solution loading. A 10% error in loading can result in a 30% apparent error in $P_{CO_2}*$.

Equilibrium constants, based on the NMR and VLE work, were regressed giving a concentration-based, carbamate stability constant, K_{carb}, of 15.6 for PZ, comparable to the value of 12.5 for MEA. The stability constant of PZCOO⁻, 2.7, suggests a less stable product, behaving more like a secondary amine such as DEA ($K_{carb} = 2.0$). The regression gives similar heats of reaction for PZCOO⁻ and PZ(COO⁻)₂ formation, 18.3 and 16.5 kJ/mol. The heat of protonation for PZCOO⁻, -47.4 kJ/mol, is comparable to the value for PZ by Hetzer *et al.* (1968) at 40°C, -44.0 kJ/mol.

At 25°C, the apparent physical solubility of CO_2 in aqueous PZ (31.60 atm-L/mol) was found to be nearly equivalent to the Henry's constant in water (29.65 atm-L/mol), a difference of less than 10%. The apparent solubility is a strong function of ionic strength. In K_2CO_3 with 3.5 M ionic strength, it is 65.89 atm-L/mol. Likewise, in 1.07 M PZ with a nominal ionic strength of 3.2 M added as K_2CO_3, it is 62.03 atm-L/mol, demonstrating that an adequate representation of CO_2 solubility in K_2CO_3/PZ

mixtures can be achieved with empirical models of K_2CO_3. The effect is ion specific; loaded solutions may be estimated from models of $KHCO_3$.

The capacity of concentrated K^+/PZ solvents at 60^oC was comparable to or better than MEA over various ranges of $P_{CO_2}*$. With a rich $P_{CO_2}*$ of 3,000 Pa and a lean $P_{CO_2}*$ of 100 Pa, 5.0 m $K^+/2.5$ m PZ has a capacity of 0.90 mol CO_2/kg-solvent compared to 0.85 in 5.0 M MEA. Increasing the rich $P_{CO_2}*$ to 10,000 Pa gave a capacity of 1.2 for the K^+/PZ mixture and 1.1 for MEA. By expanding the partial pressure range, a large capacity increase can be realized, particularly by raising the rich $P_{CO_2}*$. The capacity is a nearly linear function of total solvent concentration in K^+/PZ.

At a constant $P_{CO_2}*$, the addition of K^+ to aqueous PZ reduces the ΔH_{abs} of CO_2. The ΔH_{abs} strongly depends on the K^+:PZ ratio, but not the absolute solvent concentration. In 5.0 m $K^+/2.5$ m PZ, the ΔH_{abs} is reduced from -80 kJ/mol to -65 kJ/mol. In 3.6 m $K^+/0.6$ m PZ, the ΔH_{abs} is -40 kJ/mol, a reduction of 50% over aqueous PZ. For comparison, the ΔH_{abs} of MEA is approximately -80 to -85 kJ/mol. The ENRTL model predicts an unexpected variation of ΔH_{abs} with temperature. It is believed that this is a result of the temperature dependence of the UNIFAC predictions of γ_{PZ}^∞.

Studies of the solid solubility show that at ambient conditions (25^oC), PZ solubility is reduced from 1.8 mol/kg-solution in aqueous PZ to 0.3 mol/kg-solution in 3.0 mol K^+/kg-solution, consistent with a "salting out" effect. The apparent solubility was increased in $KHCO_3/PZ$ mixtures as the reaction of PZ with excess CO_2 reduced

the concentration in solution. Based on experimental results and laboratory experience, solvent concentrations of 5.0 m K^+/2.5 m PZ, 3.6 m K^+/3.6 m PZ, and 6.2 m K^+/1.2 m PZ can be made and stored at ambient conditions as rich solutions. At 40°C, the soluble PZ concentration increases to 7.5 mol/kg-solution with no salt. At this temperature both K_2CO_3 and $KHCO_3$ reduce the solubility of PZ. At 25 and 40°C, the bicarbonate salt will likely be the limiting solid at rich conditions.

7.2.2. Kinetics

Concentrated K^+/PZ solvents, such as 5.0 m K^+/2.5 m PZ, give absorption rates 2 to 3 times faster than 5.0 M MEA at constant P_{CO_2}*. This work also shows that the absorption rate is 2 to 3 times faster than promoted-K_2CO_3. At constant P_{CO_2}*, the absorption rate is a strong function of temperature between 40 and 100°C, but not between 100 and 110°C, indicating diffusion and solubility limitations. At constant loading, the absorption rate does not appear to be strongly dependent on temperature.

Given a constant P_{CO_2}*, the maximum absorption rate occurs at a K^+:PZ ratio of 1:2. This effect has more influence on the rate than even the total solvent concentration. The consideration of only speciation would suggest a ratio of 2:1. This behavior reflects the tradeoff between increased kinetics by the addition of ionic strength and carbonate and decreased CO_2 solubility and diffusivity in concentrated salts.

Studies of aqueous PZ show that the reaction with CO_2 approaches second-order with respect to PZ. The apparent rate constant of 1 M PZ is 102,200 s^{-1}, a factor of 20 higher than MEA (5,900 s^{-1}) and a factor of 100 higher than DEA (1,300 s^{-1}). The

addition of 0.15 m KOH catalyzes the absorption rate, suggesting a termolecular mechanism is appropriate.

The regression of rate constants within the rigorous rate model demonstrates that all bases play a role in the reaction mechanism. The most significant acting bases in K^+/PZ are PZ, PZCOO$^-$ and CO_3^{2-}. This work succeeded in identifying the contribution of nine components to the kinetics through regression and correlation, in contrast to previous work which generally considers only two or three bases in simpler mixed solvent systems (i.e. DEA/MDEA, DEA/K_2CO_3). This work validates the suitability of a Brønsted-type correlation for estimating the base contributions to reaction rates.

Neutral salts increase the apparent rate constants of amine/CO_2 reactions. The addition of 2 M ionic strength increases the apparent rate constant of the reaction with PZ by a factor of 3. This increase in rate has been suggested in literature, but never quantified in terms of an identifiable kinetic contribution. In this work, the acceleration is represented as linear function of ionic strength, so that

$$\ln k = \ln k^\infty + 0.3I \tag{7.1}$$

It is significant that this catalysis occurs with a reaction between two molecules, not two charged species as typical in transition state theory. Ionic strength also decreases the diffusivity and increases the Henry's constant to an equal and opposite extent. The net effect of neutral salts in aqueous PZ appears to be a 50% reduction of absorption rate at 5 M ionic strength.

The absorption rate in the absorber may be estimated by pseudo-first order approximations, but both kinetics and mass transfer must be considered in rate models

217

of the stripper. A pseudo-first order approximation for describing the absorption rate is usually suitable at low loadings, even at high temperatures and driving forces. At high loadings and high temperatures, the absorption rate is no longer pseudo-first order and approaches a PZ-instantaneous condition. At these conditions, with low a driving force, the normalized flux can be approximated with a series addition of the pseudo-first order and amine-instantaneous calculations. At moderate to high driving forces, a rigorous model is required.

Under typical industrial conditions, gas film resistance may account for >85% of the total mass transfer resistance at low loadings and high temperatures. At high loadings, the gas film resistance is only 20 to 30%. In general, the bottom of the stripper and top of the absorber may be gas film controlled, whereas the top of the stripper and bottom of the absorber will likely be liquid film controlled.

7.2.3. Potassium Carbonate/Piperazine as a Unique Solvent for CO_2 Capture

The rate of CO_2 absorption into K^+/PZ solvents has been shown to be 1.5 to 4 times that of 5 M MEA and some promoted-K_2CO_3 solvents. This advantage is realized from the high kinetics of the PZ-CO_2 reaction. The ratio of K^+:PZ is an important variable and can account for large changes in the reaction rate.

The heat of absorption has been shown to be somewhat lower than other aqueous amines. Additionally, this study suggests that changing the ratio of K^+ to PZ allows for the "tuning" of the heat of absorption. This characteristic is not noted in the open literature for any other solvent system. The change in ΔH_{abs} is directly related to the rate of absorption. As the heat of absorption increases (with a decreasing K^+:PZ

218

ratio), the reaction rate also increases; therefore, there is a tradeoff between a low ΔH_{abs} and a high reaction rate. A process model will be required to optimize the solution composition for given process configurations.

The capacity of this solvent is generally comparable to 30 wt% MEA given a favorable $P_{CO_2}^*$ range. One advantage of the K^+/PZ solvent appears to be a proclivity for high capacity at high equilibrium partial pressures. The VLE curves suggest that concentrated K^+/PZ gives capacities 10 to 30% higher than 30 wt% MEA given a $P_{CO_2}^*$ range of 100 to 10,000 Pa.

Though the capacity of this solvent is largely comparable to other amine solvents such as MEA, a unique feature is that the CO_2 can largely be stored in an inorganic form rather than an organic complex with the amine. Speciation studies show that, at rich loadings, as much as 70% of the CO_2 present is stored as carbonate and bicarbonate in some K^+/PZ solvents compared to 50% in an aqueous PZ solvent. An even lower percentage is expected in a mono-amine solvent. The level of storage is strongly dependent on the relative amount of K^+ and PZ in solution and is directly related to the heat of absorption.

The solvent does have a limitation in that the potassium salts and PZ are solids at ambient temperature. This may result in a maximum solvent concentration as discussed in Chapter 5. At higher temperatures, however, the PZ solubility increases dramatically and many formulations of the solvent become viable options.

7.3. Recommendations for Future Studies

7.3.1. Thermodynamics

The vapor phase partial pressure of PZ should be measured with aqueous PZ and aqueous K^+/PZ. This data would provide valuable information on the activity coefficient of PZ in the liquid phase. Also, knowing the volatility of PZ will be critical in estimating solvent losses in an absorber/stripper and in designing the process to circumvent the potential atmospheric release. The vapor pressure is expected to be relatively low at moderate temperatures, particularly in rich K^+ solvents due to ionization of the amine. It is recommended that these measurements be carried out at high temperatures (80 to 110°C) where accuracy would be expected to improve.

The equilibrium partial pressure of CO_2 as determined in this work spans a broad range of temperatures and solvent concentrations. It provides a good estimate of the equilibrium behavior between 40 and 110°C and 100 to 10,000 Pa. It would be useful to reinforce the current measurements with expanded conditions as follows:

1. The VLE at low partial pressures may be important, but current data do not define VLE well below 100 Pa. Equilibrium should be measured between 10 and 100 Pa.

2. More experiments should be performed at high temperatures (80 to 120°C).

3. A well-designed, batch VLE method may be advisable, as opposed to a wetted-wall column. Difficulties of temperature control and gas saturation at high temperatures could be substantially reduced.

Additional measurements of PZ speciation are advisable. Experiments on low K^+-high PZ concentration would allow a better extrapolation of carbamate equilibrium constants to infinite dilution in water.

The current ENRTL model of PZ and K^+/PZ solvents relies on VLE and speciation measurements for prediction of behavior. Predictions and extrapolations could be markedly improved with the inclusion of calorimetric measurements:

1. Direct measurement of heats of absorption by integral measurements, similar to those by Oscarson *et al.* (1989a, 1989b), could improve heats of reaction and temperature dependences of τ parameters.

2. The heat capacity of the solution should be measured to improve calorimetric dependent properties. This will be particularly important over the broad temperature range of the absorber/stripper process. Also, knowing the heat capacity will aid in the design of more efficient heat recovery systems.

3. The heats of mixing of various solutions would provide information on activity coefficients of PZ species, particularly in loaded solutions.

7.3.2. Kinetics

While the understanding of PZ kinetics with CO_2 has been improved in this work, additional experiments would be beneficial to verify the reaction order and rate constants. A rate investigation of PZ in a non-aqueous solvent, such as methanol or ethanol, may clarify the reaction order by eliminating complications from the kinetic

contributions of water (or hydroxide). Also, higher PZ concentrations are attainable in the alcohols than in water.

From this work, independent values of rate constants for several species were undeterminable. Rate studies at additional conditions may clarify their contributions.

1. Experiments on loaded, aqueous PZ would eliminate the contribution of carbonate in the kinetic expression and allow a better determination of the $PZCOO^-$ rate constants.

2. In K^+/PZ mixtures, experiments on very rich solutions would also eliminate carbonate. It may also show that the weak bases bicarbonate and monoprotonated PZ are important to the kinetics.

3. Experiments on low K^+-high PZ solutions would buffer the solution somewhat and isolate contributions of PZ to the rate.

It would also be of interest to better define the diffusion coefficient of rate limiting species under instantaneous conditions. The values could be determined by rate measurements under high driving force conditions. The same effect may be achieved with an apparatus with a lower k_l^o, such as laminar jet.

The effect of neutral salts on the kinetics of CO_2-PZ reactions should be investigated more thoroughly. More absorption experiments with more salts should be performed. Speciation of loaded PZ with neutral salts should be determined with NMR to determine equilibrium constants as a function of ionic strength, showing if the neutral salt effects are primary or secondary in nature. This would allow subsequent modeling to focus on either thermodynamic or kinetic corrections for explaining increased rates.

7.3.3. General

The experiments in this work are idealized in that clean components (pure gas and chemicals) were used. In an industrial process, impurities may alter the performance; therefore, effects of impurities should be quantified. Important impurities include SO_x, NO_x, iron, vanadium, and copper. The absorption rate and VLE of H_2S and mercaptans should be quantified to determine the applicability of this solvent to natural gas treating.

Foaming is another performance-hindering characteristic that may be encountered during industrial application. Given the complex nature of foaming and the potentially expensive prevention methods employed in other solvent systems, some effort should be made to identify key contributors to this effect. Surface tension is an important parameter and will likely be significantly different than aqueous amine solvents due to the high concentration of ionic components. Also, impurities such as copper, vanadium, and iron may contribute to the development of foam. Bench-scale studies on the effect of these parameters on foaming may help anticipate and eliminate problems encountered in pilot- or commercial-scale processes.

Amine degradation and equipment corrosion are also significant process concerns. These characteristics will determine the amount of make-up amine required and the material of construction for the process. The degradation rate should be quantified and corrosion of materials should be examined to determine process limitations.

Before applying this solvent to industrial use, environmental hazards should be assessed. Concerns include the environmental fate of released chemicals and the transport of the chemicals through the atmosphere and groundwater.

1. Inhalation and exposure hazards should be quantified to assess possible risks to humans. The toxicity should also be investigated.

2. Biological degradation of amines should be investigated to circumvent potential accumulation in the environment.

3. Studies on the transport of amines through the environment should include the atmospheric chemistry and mobility in groundwater.

Appendix A: Density and Viscosity Results

This appendix contains results of density and viscosity experiments outlined in Section 3.4. Both the measured and predicted values are listed in the tables. Kinematic viscosity is converted to dynamic viscosity using the predicted density.

A.1. Density Results

Table A.1. Density of K_2CO_3 and $KHCO_3$ at 25 and 40°C

T (^{o}C)	[K^+] (m)	Loading (mol CO_2/mol K^+)	ρ_{meas} (g/cm^3)	ρ_{pred} (g/cm^3)
	1.5	0.950	1.085	1.084
	3.0	0.950	1.159	1.156
25	3.0	0.850	1.154	1.156
	6.0	0.500	1.283	1.281
	12.0	0.500	1.466	1.473
	1.5	0.950	1.087	1.077
	3.0	0.950	1.152	1.150
40	3.0	0.850	1.152	1.149
	6.0	0.500	1.275	1.275
	12.0	0.500	1.461	1.467

Table A.2. Density of Aqueous PZ at 25 and 40°C at Zero Loading

T (^{o}C)	[PZ] (m)	ρ_{meas} (g/cm^3)	ρ_{pred} (g/cm^3)
25	0.5	0.999	0.999
	1.0	1.001	1.000
	1.5	1.003	1.001
	1.8	1.004	1.001
40	0.5	0.994	0.992
	1.0	0.996	0.993
	1.5	0.997	0.994
	1.8	0.999	0.995

Table A.3. Density of K$^+$/PZ Mixtures at 25 and 40°C

T (^{o}C)	[K$^+$] (m)	[PZ] (m)	Loading (mol CO_2/mol K$^+$ + mol PZ)	ρ_{meas} (g/cm^3)	ρ_{pred} (g/cm^3)
25	1.0	1.0	0.250	1.053	1.054
	1.0	1.0	0.500	1.067	1.057
	1.0	2.5	0.286	1.065	1.058
	2.5	2.5	0.500	1.138	1.134
	3.0	0.3	0.455	1.152	1.153
	3.0	0.3	0.909	1.163	1.157
	3.0	0.9	0.769	1.165	1.157
	5.0	2.5	0.667	1.237	1.247
40	1.0	1.0	0.250	1.047	1.048
	1.0	1.0	0.500	1.059	1.050
	1.0	2.5	0.143	1.046	1.050
	1.0	2.5	0.285	1.057	1.051
	2.5	2.5	0.250	1.108	1.125
	2.5	2.5	0.500	1.132	1.127
	5.0	0.5	0.455	1.228	1.235
	5.0	0.5	0.909	1.236	1.239
	5.0	2.5	0.667	1.227	1.240

A.2. Viscosity Results

Table A.4. Viscosity of Aqueous PZ at 25 to 70°C

T (^{o}C)	[PZ] (m)	v_{exp} (cSt)	ρ_{model} (g/cm^3)	μ_{meas} (cP)	μ_{pred} (cP)
25	0.5	1.09	0.999	1.09	1.09
	1.0	1.29	1.000	1.28	1.30
	1.5	1.52	1.001	1.52	1.52
	1.8	1.66	1.001	1.66	1.66
40	0.5	0.78	0.992	0.78	0.78
	1.0	0.91	0.993	0.91	0.91
	1.5	1.04	0.994	1.03	1.04
	1.8	1.13	0.995	1.13	1.13
60	0.5	0.55	0.983	0.54	0.54
	1.0	0.61	0.984	0.60	0.61
	1.5	0.69	0.985	0.68	0.68
	1.8	0.74	0.986	0.73	0.73
70	0.5	0.46	0.979	0.45	0.46
	1.0	0.52	0.980	0.51	0.51
	1.5	0.58	0.981	0.57	0.57
	1.8	0.61	0.981	0.60	0.60

Table A.5. Viscosity of K$^+$/PZ Mixtures at 25 to 70°C

T (^{o}C)	[K$^+$] (m)	[PZ] (m)	Loading (mol CO$_2$/mol K$^+$ + mol PZ)	N$_{meas}$ (cSt)	ρ_{pred}	μ_{meas} (cP)	μ_{pred} (cP)
25	3.0	0.0	1.000	1.14	1.157	1.32	1.39
	5.0	0.0	0.500	1.53	1.241	1.90	1.91
	0.5	1.0	0.167	1.35	1.028	1.39	1.40
	0.5	1.0	0.334	1.35	1.029	1.39	1.39
	1.0	2.0	0.333	2.00	1.057	2.11	2.03
	1.0	1.0	0.250	1.40	1.054	1.48	1.50
	1.0	1.0	0.500	1.40	1.057	1.48	1.50
	1.0	2.0	0.167	2.02	1.056	2.13	2.04
	2.0	1.0	0.333	1.58	1.105	1.74	1.74
	2.0	1.0	0.667	1.53	1.108	1.70	1.73
	2.0	2.0	0.500	2.17	1.109	2.40	2.36
	3.6	3.6	0.500	4.13	1.187	4.90	4.71
	4.0	2.0	0.667	2.59	1.203	3.12	3.21
	5.0	2.5	0.667	3.33	1.247	4.15	4.35
40	1.0	1.0	0.250	1.01	1.048	1.06	1.05
	1.0	2.0	0.167	1.35	1.049	1.42	1.38
	1.0	2.0	0.333	1.35	1.050	1.41	1.38
	2.0	1.0	0.333	1.12	1.099	1.23	1.22
	2.0	1.0	0.667	1.11	1.102	1.22	1.22
	2.0	2.0	0.500	1.48	1.102	1.64	1.60
	3.0	1.0	0.375	1.25	1.147	1.43	1.42
	3.6	3.6	0.500	2.64	1.180	3.12	3.01
	4.0	2.0	0.667	1.79	1.196	2.14	2.17
	5.0	2.5	0.667	2.23	1.240	2.77	2.88
60	0.5	1.0	0.167	0.65	1.012	0.66	0.66
	0.5	1.0	0.334	0.64	1.014	0.65	0.66
	1.0	1.0	0.250	0.68	1.039	0.71	0.71
	1.0	1.0	0.500	0.68	1.041	0.71	0.71
	1.0	2.0	0.167	0.87	1.040	0.90	0.89
	1.0	2.0	0.333	0.87	1.042	0.91	0.88
	2.0	1.0	0.333	0.76	1.090	0.83	0.83
	2.0	1.0	0.667	0.75	1.093	0.82	0.82
	2.0	2.0	0.500	0.96	1.093	1.05	1.03
	3.6	3.6	0.500	1.60	1.171	1.87	1.81
	4.0	2.0	0.667	1.16	1.188	1.38	1.39
	5.0	2.5	0.667	1.42	1.231	1.75	1.80
70	1.0	1.0	0.250	0.57	1.034	0.59	0.60
	1.0	2.0	0.167	0.70	1.036	0.73	0.73
	1.0	2.0	0.333	0.72	1.037	0.74	0.73
	2.0	1.0	0.333	0.64	1.085	0.69	0.70
	2.0	1.0	0.667	0.63	1.088	0.69	0.69
	2.0	2.0	0.500	0.79	1.089	0.87	0.85
	3.0	1.0	0.375	0.71	1.133	0.80	0.81
	3.6	3.6	0.500	1.27	1.167	1.49	1.45
	4.0	2.0	0.667	0.96	1.183	1.13	1.15
	5.0	2.5	0.667	1.16	1.227	1.42	1.47

Appendix B: Detailed ^{1}H NMR Data

This appendix archives all ^{1}H NMR data collected by the procedure outline in Section 3.2. Most data were included in the regression in Chapter 5, though some were discarded. All loadings (α) are given in mol CO_2/(mol K^+ + mol PZ). The original scans are available from Gary Rochelle at the University of Texas at Austin.

B.1. ^{1}H NMR Data

Table B.1. 3.60 m K^+/0.60 m PZ, α = 0.357

T (^{o}C)	Species	Chem Shift (ppm)	Intensity	Peak Area
30	PZCOO$^-$	-	-	269.7
	PZ	2.7189	416.30	
	PZ(COO$^-$)$_2$	-	-	-
	PZCOO$^-$	~3.3	~4.0	1.0
40	PZCOO$^-$	-	-	287.1
	PZ	2.7174	415.59	
	PZ(COO$^-$)$_2$	-	-	-
	PZCOO$^-$	~3.3	~4.0	1.0
60	PZCOO$^-$	-	-	355.3
	PZ	2.7152	412.66	
	PZ(COO$^-$)$_2$	-	-	-
	PZCOO$^-$	~3.29	~3.0	1.0

Table B.2. 3.59 m K$^+$/0.60 m PZ, $\alpha = 0.429$

T (^{o}C)	Species	Chem Shift (ppm)	Intensity	Peak Area
27	PZCOO$^-$	2.5685	2.04	1.36
		2.5756	1.49	
		2.5793	1.74	
	PZ	2.5890	2.46	
		2.6172	206.63	32.96
		2.6565	2.77	0.59
	PZ(COO$^-$)$_2$	-	-	-
	PZCOO$^-$	3.1752	1.76	1.00
		3.1856	1.92	
		3.1958	1.70	
40	PZCOO$^-$	2.6759	2.08	1.49
		2.6863	2.86	
		2.6965	2.51	
	PZ	2.7244	210.99	31.52
		2.7643	2.39	0.35
	PZ(COO$^-$)$_2$	-	-	-
	PZCOO$^-$	3.2782	1.93	1.00
		3.2887	1.99	
		3.2988	1.81	
60	PZCOO$^-$	2.8361	2.49	1.13
		2.8431	1.56	
		2.8465	2.34	
	PZ	2.8568	2.67	
		2.8834	210.35	22.30
		2.9227	2.98	0.42
	PZ(COO$^-$)$_2$	-	-	-
	PZCOO$^-$	3.4324	2.82	1.00
		3.4427	2.44	
		3.4530	2.24	
70	PZCOO$^-$	2.9154	2.40	1.14
		2.9256	2.91	
		2.9360	2.82	
	PZ	2.9623	205.86	19.66
		3.0017	3.89	0.41
	PZ(COO$^-$)$_2$	-	-	-
	PZCOO$^-$	3.5086	2.56	1.00
		3.5190	2.41	
		3.5293	2.21	

Table B.3. 3.60 m K$^+$/0.60 m PZ, $\alpha = 0.441$

T (^{o}C)	Species	Chem Shift (ppm)	Intensity	Peak Area
30	PZCOO$^-$	2.6807	7.74	1.061
		2.6909	8.64	
		2.7012	9.07	
	PZ	2.7367	208.62	7.386
	PZ(COO$^-$)$_2$	-	-	-
	PZCOO$^-$	3.2912	8.68	1.000
		3.3017	8.86	
		3.3118	7.93	
40	PZCOO$^-$	2.6788	7.31	0.959
		2.6890	7.44	
		2.6995	7.97	
	PZ	2.7329	207.82	7.378
	PZ(COO$^-$)$_2$	-	-	-
	PZCOO$^-$	3.2856	8.83	1.000
		3.2961	8.15	
		3.3064	7.89	
60	PZCOO$^-$	2.6759	6.19	1.083
		2.6863	7.40	
		2.6873	7.31	
	PZ	2.7263	206.56	7.400
	PZ(COO$^-$)$_2$	-	-	-
	PZCOO$^-$	3.2839	3.46	1.000
		3.2869	6.96	
		3.2972	6.75	

231

Table B.4. 3.60 m K$^+$/0.61 m PZ, $\alpha = 0.486$

T (^{o}C)	Species	Chem Shift (ppm)	Intensity	Peak Area
27	PZCOO$^-$	2.5934	1.46	1.002
		2.6036	1.57	
		2.6140	1.52	
	PZ	2.6818	13.18	2.199
	PZ(COO$^-$)$_2$	3.1805	2.60	0.372
	PZCOO$^-$	3.1953	1.47	1.000
		3.2057	1.57	
		3.2159	1.39	
40	PZCOO$^-$	2.6999	1.34	0.979
		2.7101	1.43	
		2.7105	1.45	
	PZ	2.7795	13.24	2.218
	PZ(COO$^-$)$_2$	3.2865	2.39	0.359
	PZCOO$^-$	3.2980	1.40	1.000
		3.3084	1.46	
		3.3186	1.33	
60	PZCOO$^-$	2.8575	1.06	1.032
		2.8677	1.14	
		2.8782	1.13	
	PZ	2.9275	13.16	2.532
	PZ(COO$^-$)$_2$	3.4438	1.69	0.402
	PZCOO$^-$	3.4503	1.17	1.000
		3.4608	1.17	
		3.4711	1.03	
70	PZCOO$^-$	2.9359	0.94	1.000
		2.9461	1.12	
		2.9565	1.03	
	PZ	3.0011	13.12	2.526
	PZ(COO$^-$)$_2$	3.5226	1.39	
	PZCOO$^-$	3.5259	1.33	1.325
		3.5368	1.17	
		3.5470	0.92	

Table B.5. 3.59 m K$^+$/0.61 m PZ, $\alpha = 0.515$

T (^{o}C)	Species	Chem Shift (ppm)	Intensity	Peak Area
27	PZCOO$^-$	2.6200	2.34	0.992
		2.6301	2.58	
		2.6406	2.48	
	PZ	2.7374	13.00	1.278
	PZ(COO$^-$)$_2$	3.1859	7.80	0.752
	PZCOO$^-$	3.2155	2.42	1.000
		3.2259	2.62	
		3.2361	2.23	
40	PZCOO$^-$	2.7236	2.21	0.994
		2.7338	2.42	
		2.7443	2.34	
	PZ	2.8293	13.09	1.328
	PZ(COO$^-$)$_2$	3.2932	6.89	0.698
	PZCOO$^-$	3.3166	2.30	1.000
		3.3270	2.47	
		3.3373	2.15	
60	PZCOO$^-$	2.8760	1.95	0.960
		2.8862	2.37	
		2.8966	2.08	
	PZ	2.9644	13.03	1.409
	PZ(COO$^-$)$_2$	3.4507	4.74	0.595
	PZCOO$^-$	3.4654	2.21	1.000
		3.4759	2.45	
		3.4860	1.94	
70	PZCOO$^-$	2.9527	2.06	1.000
		2.9625	2.84	
		2.9728	2.28	
	PZ	3.0326	12.98	1.525
	PZ(COO$^-$)$_2$	3.5300	4.01	
	PZCOO$^-$	3.5397	2.92	1.532
		3.5501	3.01	
		3.5604	2.06	

Table B.6. 3.56 m K$^+$/0.61 m PZ, $\alpha = 0.554$

T (^{o}C)	Species	Chem Shift (ppm)	Intensity	Peak Area
27	PZCOO$^-$	2.7840	1.80	1.007
		2.7943	2.00	
		2.8048	1.92	
	PZ	2.9330	7.02	0.781
	PZ(COO$^-$)$_2$	3.2957	12.88	1.454
	PZCOO$^-$	3.3663	1.95	1.000
		3.3769	2.09	
		3.3872	1.82	
40	PZCOO$^-$	2.7577	2.04	0.988
		2.7679	2.37	
		2.7784	2.19	
	PZ	2.8969	7.82	0.800
	PZ(COO$^-$)$_2$	3.2896	13.00	1.306
	PZCOO$^-$	3.3422	2.25	1.000
		3.3527	2.48	
		3.3630	2.08	
60	PZCOO$^-$	2.7373	5.56	4.68
		2.7461	4.41	
	PZ	2.8425	10.42	4.32
	PZ(COO$^-$)$_2$	3.2822	12.95	
	PZCOO$^-$	3.3137	4.91	10.00
		3.3228	5.95	

Table B.7. 3.58 m K$^+$/0.60 m PZ, α = 0.601

T (^{o}C)	Species	Chem Shift (ppm)	Intensity	Peak Area
27	PZCOO$^-$	2.7573	1.39	0.992
		2.7673	1.76	
		2.7779	1.45	
	PZ	2.8905	3.17	0.524
	PZ(COO$^-$)$_2$	3.1984	12.98	2.212
	PZCOO$^-$	3.3145	1.46	1.000
		3.3250	1.78	
		3.3351	1.36	
40	PZCOO$^-$	2.8318	1.45	0.978
		2.8419	1.89	
		2.8523	1.52	
	PZ	2.9707	3.43	0.560
	PZ(COO$^-$)$_2$	3.3035	12.92	1.955
	PZCOO$^-$	3.3949	1.57	1.000
		3.4054	1.91	
		3.4155	1.40	
60	PZCOO$^-$	2.9635	4.11	0.961
	PZ	3.0843	3.94	0.643
	PZ(COO$^-$)$_2$	3.4643	12.85	1.578
	PZCOO$^-$	3.5316	4.25	1.000

Table B.8. 3.59 m K$^+$/0.61 m PZ, $\alpha = 0.630$

T (^{o}C)	Species	Chem Shift (ppm)	Intensity	Peak Area
27	PZCOO$^-$	2.7986	1.16	0.987
		2.8088	1.50	
		2.8193	1.24	
	PZ	2.9131	2.32	0.431
	PZ(COO$^-$)$_2$	3.1978	13.06	2.517
	PZCOO$^-$	3.3426	1.25	1.000
		3.3531	1.52	
		3.3633	1.15	
40	PZCOO$^-$	2.8687	1.28	0.992
		2.8788	1.79	
		2.8889	1.38	
	PZ	2.9982	2.40	0.501
	PZ(COO$^-$)$_2$	3.3046	13.13	2.328
	PZCOO$^-$	3.4205	1.43	1.00
		3.4307	1.81	
		3.4408	1.26	
60	PZCOO$^-$	2.9912	3.82	0.928
	PZ	3.1134	2.75	0.567
	PZ(COO$^-$)$_2$	3.4662	12.88	1.907
	PZCOO$^-$	3.5496	4.08	1.000

Table B.9. 3.59 m K$^+$/1.81 m PZ, $\alpha = 0.433$

T (^{o}C)	Species	Chem Shift (ppm)	Intensity	Peak Area
27	PZCOO$^-$	2.5735	1.79	10.00
		2.5832	2.03	
		2.5938	1.50	
	PZ	2.6491	12.98	24.81
	PZ(COO$^-$)$_2$	3.1683	2.20	3.59
	PZCOO$^-$	3.1683	2.20	9.77
		3.1805	1.84	
		3.1907	2.02	
40	PZCOO$^-$	2.6911	1.41	10.00
		2.7013	1.45	
		2.7117	1.48	
	PZ	2.7612	13.05	25.07
	PZ(COO$^-$)$_2$	3.2846	2.37	3.36
	PZCOO$^-$	3.2938	1.45	10.11
		3.3043	1.48	
		3.3145	1.36	
60	PZCOO$^-$	2.8633	1.23	10.00
		2.8735	1.41	
		2.8840	1.33	
	PZ	2.9270	13.12	25.27
	PZ(COO$^-$)$_2$	3.4547	1.77	
	PZCOO$^-$	3.4602	1.43	13.15
		3.4707	1.44	
		3.4809	1.22	

Table B.10. 3.44 m K$^+$/1.85 m PZ, α = 0.618

T (^{o}C)	Species	Chem Shift (ppm)	Intensity	Peak Area
30	PZCOO$^-$	2.7340	2.35	9.79
		2.7441	3.13	
		2.7545	2.61	
	PZ	2.8721	7.18	7.30
	PZ(COO$^-$)$_2$	3.2045	13.07	15.06
	PZCOO$^-$	3.3024	2.50	10.00
		3.3129	3.15	
		3.3229	2.44	
40	PZCOO$^-$	2.8148	2.66	9.64
		2.8240	3.95	
		2.8333	3.17	
	PZ	2.9512	7.22	7.47
	PZ(COO$^-$)$_2$	3.2952	13.09	14.24
	PZCOO$^-$	3.3836	2.98	10.00
		3.3929	4.00	
		3.4022	2.90	
60	PZCOO$^-$	2.9861	7.20	9.85
	PZ	3.1042	7.25	8.61
	PZ(COO$^-$)$_2$	3.4810	13.03	13.74
	PZCOO$^-$	3.5499	8.01	10.00

Table B.11. 3.46 m K$^+$/1.86 m PZ, α = 0.694

T (^{o}C)	Species	Chem Shift (ppm)	Intensity	Peak Area
30	PZCOO$^-$ / PZ	2.9546	12.80	13.04
	PZ(COO$^-$)$_2$	3.1363	8.07	9.02
	PZCOO$^-$	3.4258	11.19	10.00
40	PZCOO$^-$ / PZ	3.0392	12.82	13.73
	PZ(COO$^-$)$_2$	3.2229	5.05	8.92
	PZCOO$^-$	3.5045	7.98	10.00

Table B.12. 3.60 m K$^+$/3.58 m PZ, $\alpha = 0.376$

T (^{o}C)	Species	Chem Shift (ppm)	Intensity	Peak Area
40	PZCOO$^-$	2.6914	1.56	10.00
		2.7017	1.71	
		2.7121	1.66	
	PZ	2.7532	13.03	32.20
	PZ(COO$^-$)$_2$	3.2913	1.84	2.30
	PZCOO$^-$	3.3000	1.60	9.87
		3.3104	1.73	
		3.3206	1.53	
60	PZCOO$^-$	2.8774	1.34	10.00
		2.8876	1.55	
		2.8980	1.48	
	PZ	2.9361	13.18	32.52
	PZ(COO$^-$)$_2$	3.4743	1.43	
	PZCOO$^-$	3.4798	1.50	12.15
		3.4903	1.57	
		3.5005	1.32	

Table B.13. 3.57 m K$^+$/3.58 m PZ, $\alpha = 0.499$

T (^{o}C)	Species	Chem Shift (ppm)	Intensity	Peak Area
27	PZCOO$^-$	2.5837	2.65	10.00
		2.5939	2.92	
		2.6044	2.66	
	PZ	2.6946	12.92	14.57
	PZ(COO$^-$)$_2$	3.1575	6.60	6.43
	PZCOO$^-$	3.1874	2.69	10.17
		3.1978	2.95	
		3.2080	2.49	
40	PZCOO$^-$	2.7126	2.55	10.00
		2.7229	2.91	
		2.7333	2.59	
	PZ	2.8177	13.10	14.65
	PZ(COO$^-$)$_2$	3.2850	6.04	6.57
	PZCOO$^-$	3.3122	2.66	10.24
		3.3226	2.99	
		3.3328	2.44	
60	PZCOO$^-$	2.9064	4.28	10.00
	PZ	2.9923	12.86	14.78
	PZ(COO$^-$)$_2$	3.4670	4.67	16.33
	PZCOO$^-$	3.4991	4.58	

Table B.14. 3.59 m K$^+$/3.61 m PZ, $\alpha = 0.600$

T (^{o}C)	Species	Chem Shift (ppm)	Intensity	Peak Area
27	PZCOO$^-$	2.6794	2.79	10.08
		2.6886	3.40	
		2.6989	2.33	
	PZ	2.7948	6.84	8.37
	PZ(COO$^-$)$_2$	3.0914	9.21	12.92
	PZCOO$^-$	3.2313	2.89	10.08
		3.2409	3.37	
		3.2508	2.24	
40	PZCOO$^-$	2.7987	4.06	10.00
	PZ	2.9061	7.81	8.90
	PZ(COO$^-$)$_2$	3.2075	9.18	12.56
	PZCOO$^-$	3.3495	4.12	10.48

Table B.15. 3.60 m K$^+$/3.60 m PZ, $\alpha = 0.646$

T (^{o}C)	Species	Chem Shift (ppm)	Intensity	Peak Area
27	PZCOO$^-$	2.6168	2.93	10.00
		2.6263	3.36	
		2.6371	2.33	
	PZ	2.7579	9.10	10.61
	PZ(COO$^-$)$_2$	3.1243	8.11	10.18
	PZCOO$^-$	3.1996	2.98	10.05
		3.2097	3.32	
		3.2198	2.24	
40	PZCOO$^-$	2.7353	2.36	10.00
		2.7454	3.06	
		2.7557	2.47	
	PZ	2.8718	9.05	10.61
	PZ(COO$^-$)$_2$	3.2441	7.52	10.01
	PZCOO$^-$	3.3151	2.47	10.27
		3.3254	3.10	
		3.3355	2.36	
60	PZCOO$^-$	2.9243	6.01	10.00
	PZ	3.0401	9.07	11.81
	PZ(COO$^-$)$_2$	3.4250	6.86	20.19
	PZCOO$^-$	3.4920	6.58	

Table B.16. 5.00 m K$^+$/2.50 m PZ, $\alpha = 0.433$

T (^{o}C)	Species	Chem Shift (ppm)	Intensity	Peak Area
30	PZCOO$^-$	2.4226	4.35	11.71
		2.4328	8.40	
		2.4428	4.68	
	PZ	2.5290	128.63	76.31
	PZ(COO$^-$)$_2$	2.9939	3.00	1.49
	PZCOO$^-$	3.0251	4.55	10.50
		3.0351	8.20	
		3.0451	4.24	
40	PZCOO$^-$	2.4232	6.58	14.29
		2.4331	12.66	
		2.4429	7.84	
	PZ	2.5157	149.53	69.47
	PZ(COO$^-$)$_2$	3.0022	5.79	2.62
	PZCOO$^-$	3.0249	6.62	13.62
		3.0348	12.52	
		3.0446	6.94	
60	PZCOO$^-$	2.4289	10.14	20.28
		2.4391	17.26	
		2.4492	9.91	
	PZ	2.4881	120.13	53.55
	PZ(COO$^-$)$_2$	3.0243	15.52	
	PZCOO$^-$	3.0296	10.56	26.17
		3.0398	17.00	
		3.0499	9.04	

Table B.17. 4.99 m K$^+$/2.51 m PZ, $\alpha = 0.467$

T (^{o}C)	Species	Chem Shift (ppm)	Intensity	Peak Area
30	PZCOO$^-$	2.4821	13.58	23.22
		2.4923	25.97	
		2.5024	16.01	
	PZ	2.5628	127.54	43.93
	PZ(COO$^-$)$_2$	3.0739	32.02	10.95
	PZCOO$^-$	3.0885	13.08	21.90
		3.0987	25.13	
		3.1087	14.00	
40	PZCOO$^-$	2.4821	13.19	23.19
		2.4922	25.75	
		2.5023	16.49	
	PZ	2.5579	126.08	43.62
	PZ(COO$^-$)$_2$	3.0738	30.37	10.70
	PZCOO$^-$	3.0856	13.42	22.48
		3.0963	24.36	
		3.1060	14.79	
60	PZCOO$^-$	2.4818	16.28	23.34
		2.4921	28.74	
		2.5023	15.53	
	PZ	2.5487	136.76	42.76
	PZ(COO$^-$)$_2$	3.0735	35.09	
	PZCOO$^-$	3.0809	17.35	33.90
		3.0911	28.51	
		3.1013	14.26	

Table B.18. 4.98 m K$^+$/2.50 m PZ, $\alpha = 0.534$

T (^{o}C)	Species	Chem Shift (ppm)	Intensity	Peak Area
30	PZCOO$^-$	2.5137	21.68	25.44
		2.5240	37.22	
		2.5342	23.55	
	PZ	2.6314	126.98	27.93
	PZ(COO$^-$)$_2$	3.0769	95.72	21.97
	PZCOO$^-$	3.1111	23.40	24.66
		3.1213	36.72	
		3.1314	21.49	
40	PZCOO$^-$	2.5138	24.47	25.65
		2.5240	46.42	
		2.5341	28.49	
	PZ	2.6234	145.13	27.22
	PZ(COO$^-$)$_2$	3.0807	109.50	22.50
	PZCOO$^-$	3.1098	26.82	24.63
		3.1198	46.08	
		3.1298	26.58	
60	PZCOO$^-$	2.5236	62.34	25.44
	PZ	2.6069	124.83	26.53
	PZ(COO$^-$)$_2$	3.0862	95.69	23.03
	PZCOO$^-$	3.1151	61.45	25.00

243

Table B.19. 4.98 m K⁺/2.50 m PZ, α = 0.600

T (°C)	Species	Chem Shift (ppm)	Intensity	Peak Area
30	PZCOO⁻	2.5851	15.09	22.97
		2.5954	27.55	
		2.6056	16.58	
	PZ	2.7241	53.53	14.96
	PZ(COO⁻)₂	3.0876	127.60	39.32
	PZCOO⁻	3.1633	16.35	22.76
		3.1735	27.17	
		3.1837	15.00	
40	PZCOO⁻	2.5853	18.80	23.13
		2.5952	34.02	
		2.6052	20.20	
	PZ	2.7206	144.81	15.04
	PZ(COO⁻)₂	3.0954	60.42	38.71
	PZCOO⁻	3.1633	20.25	23.13
		3.1733	34.32	
		3.1830	17.60	
60	PZCOO⁻	2.5958	14.24	23.37
	PZ	2.7109	10.03	16.84
	PZ(COO⁻)₂	3.1079	9.07	36.67
	PZCOO⁻	3.1696	14.07	23.12

Table B.20. 4.64 m K⁺/2.50 m PZ, α = 0.650

T (°C)	Species	Chem Shift (ppm)	Intensity	Peak Area
27	PZCOO⁻			18.88
	PZ	-	-	10.0
	PZ(COO⁻)₂	-	-	38.80
	PZCOO⁻	-	-	19.11
40	PZCOO⁻	-	-	17.53
	PZ	-	-	10.00
	PZ(COO⁻)₂	-	-	35.18
	PZCOO	-	-	18.35
60	PZCOO	-	-	13.94
	PZ	-	-	10.00
	PZ(COO⁻)₂	-	-	27.37
	PZCOO⁻	-	-	14.54

Table B.21. 6.18 m K$^+$/1.23 m PZ, $\alpha = 0.570$

T (^{o}C)	Species	Chem Shift (ppm)	Intensity	Peak Area
27	PZCOO$^-$	2.7870	1.83	9.82
		2.7972	2.21	
		2.8077	1.91	
	PZ	2.9324	5.95	6.82
	PZ(COO$^-$)$_2$	3.2865	13.00	16.06
	PZCOO$^-$	3.3658	2.01	10.00
		3.3764	2.28	
		3.3866	1.83	
40	PZCOO$^-$	2.7504	1.74	9.62
		2.7606	2.15	
		2.7710	1.79	
	PZ	2.8868	4.26	5.65
	PZ(COO$^-$)$_2$	3.2812	13.00	17.67
	PZCOO$^-$	3.3344	1.89	10.00
		3.3448	2.21	
		3.3550	1.70	
60	PZCOO$^-$	2.7279	3.55	9.52
	PZ	2.8315	3.80	5.96
	PZ(COO$^-$)$_2$	3.2727	13.09	15.50
	PZCOO$^-$	3.3043	3.33	10.00
		3.3123	3.80	

Table B.22. 6.20 m K$^+$/1.81 m PZ, $\alpha = 0.527$

T (^{o}C)	Species	Chem Shift (ppm)	Intensity	Peak Area
40	PZCOO$^-$	-	-	6.73
	PZ	-	-	10.00
	PZ(COO$^-$)$_2$	-	-	4.21
	PZCOO$^-$	-	-	6.76
60	PZCOO$^-$	-	-	10.00
	PZ	-	-	6.40
	PZ(COO$^-$)$_2$	-	-	15.69
	PZCOO$^-$	-	-	10.54

Table B.23. 6.20 m K$^+$/1.81 m PZ, $\alpha = 0.667$

T (^{o}C)	Species	Chem Shift (ppm)	Intensity	Peak Area
27	PZCOO$^-$	2.6150	1.51	10.00
		2.6248	1.75	
		2.6354	1.24	
	PZ	2.7548	3.01	5.59
	PZ(COO$^-$)$_2$	3.1289	9.17	19.28
	PZCOO$^-$	3.1960	1.55	10.09
		3.2062	1.76	
		3.2164	1.17	
40	PZCOO$^-$	2.7030	1.25	10.00
		2.7132	1.48	
		2.7237	1.29	
	PZ	2.8349	3.12	5.82
	PZ(COO$^-$)$_2$	3.2304	9.17	18.16
	PZCOO$^-$	3.2843	1.31	10.23
		3.2947	1.50	
		3.3050	1.22	
60	PZCOO$^-$	2.8460	2.60	10.00
	PZ	2.9510	2.66	6.40
	PZ(COO$^-$)$_2$	3.3805	9.07	15.69
	PZCOO$^-$	3.4258	2.76	10.54

B.2. Samples Not Used

Table B.24. 3.56 m K$^+$/0.61 m PZ, $\alpha = 0.554$, 100% D$_2$O

T (^{o}C)	Species	Chem Shift (ppm)	Intensity	Peak Area
27	PZCOO$^-$	2.7024	1.37	0.988
		2.7126	1.63	
		2.7231	1.43	
	PZ	2.8469	4.65	0.715
	PZ(COO$^-$)$_2$	3.2059	12.57	1.499
	PZCOO$^-$	3.2784	1.69	1.000
		3.2889	1.79	
		3.2992	1.57	
40	PZCOO$^-$	2.8021	1.75	0.980
		2.8123	2.16	
		2.8228	1.85	
	PZ	2.9383	5.97	0.778
	PZ(COO$^-$)$_2$	3.3240	12.70	1.317
	PZCOO$^-$	3.3799	2.09	1.000
		3.3903	2.34	
		3.4006	1.96	
60	PZCOO$^-$	2.9636	5.52	0.935
	PZ	3.0687	9.22	0.864
	PZ(COO$^-$)$_2$	3.4989	12.55	2.000
	PZCOO$^-$	3.5426	5.96	

Table B.25. 3.33 m K/0.57 m PZ, $\alpha = 0.699$

T (^{o}C)	Species	Chem Shift (ppm)	Intensity	Peak Area
27	PZCOO$^-$	2.9865	1.14	0.998
		2.9966	1.65	
		3.0068	1.28	
	PZ	3.0512	1.87	0.409
	PZ(COO$^-$)$_2$	3.3007	13.00	2.435
	PZCOO$^-$	3.5040	1.29	1.000
		3.5144	1.71	
		3.5245	1.20	
60	PZCOO$^-$	2.8787	4.04	4.83
	PZ	2.9768	3.07	
	PZ(COO$^-$)$_2$	3.2904	12.97	10.00
	PZCOO$^-$	3.3920	4.71	

<p style="text-align:center">Table B.26. 5.72 m K⁺/0.56 m PZ, $\alpha = 0.526$</p>

Table B.26. 5.72 m K$^+$/0.56 m PZ, $\alpha = 0.526$

T (^{o}C)	Species	Chem Shift (ppm)	Intensity	Peak Area
40	PZCOO$^-$	2.6440	2.26	9.77
		2.6542	2.80	
		2.6647	2.45	
	PZ	2.7732	8.10	7.89
	PZ(COO$^-$)$_2$	3.1961	13.05	12.49
	PZCOO$^-$	3.2328	2.54	10.00
		3.2431	2.90	
		3.2534	2.35	
60	PZCOO$^-$	2.7734	2.85	10.00
		2.7836	3.57	
		2.7940	3.04	
	PZ	2.8751	10.21	9.01
	PZ(COO$^-$)$_2$	3.3428	13.00	
	PZCOO$^-$	3.3613	3.30	21.05
		3.3718	3.72	
		3.3820	2.91	
80	PZCOO$^-$	2.9056	5.37	10.86
	PZ	2.9735	8.93	
	PZ(COO$^-$)$_2$ PZCOO$^-$	3.4761	12.83	10.00

Table B.27. 5.83 m K$^+$/0.57 m PZ, $\alpha = 0.697$

T (^{o}C)	Species	Chem Shift (ppm)	Intensity	Peak Area
40	PZCOO-	2.8974	1.34	13.48
	PZ	2.9616	0.61	
	PZ(COO$^-$)$_2$	3.2174	12.63	37.66
	PZCOO-	3.4164	1.35	10.00
60	PZCOO- PZ	2.9838	1.97	10.00
	PZ(COO$^-$)$_2$	3.3696	13.05	32.83
	PZCOO-	3.4954	2.21	

B.3. Example Spectra

Current Data Parameters
NAME   36K06PZL2
EXPNO   1
PROCNO   1

F2 - Acquisition Parameters
Date   830224
Time   7.21
PULPROG   zgpr
SOLVENT   D2O
AQ   2.7197640 sec
FIDRES   0.183841 Hz
DW   83.0 usec
RG   8
NUCLEUS   1H
HL1   3 dB
D12   0.0000200 sec
HL2   68 dB
P1B   2000000.0 usec
D13   0.0000030 sec
P1   2.0 usec
DE   132.8 usec
SFO1   499.8784650 MHz
SWH   6024.10 Hz
TD   32768
NS   32
DS   2

F2 - Processing parameters
SI   32768
SF   499.8760807 MHz
WDW   EM
SSB   0
LB   0.10 Hz
GB   0
PC   1.00

1D NMR plot parameters
CX   20.00 cm
F1P   3.500 ppm
F1   1749.57 Hz
F2P   2.500 ppm
F2   1249.69 Hz
PPMCM   0.05000 ppm/cm
HZCM   24.99380 Hz/cm

TEMP = 300K

2.7573
2.7673
2.7779

2.8905

3.1984

3.3145
3.3250
3.3351

0.992

0.524

2.212

1.000

2.6   2.8   3.0   3.2   3.4   ppm

Figure B.1. ^{1}H NMR Spectrum of 3.6 m K^{+}/0.6 m PZ, a = 0.600, T = 27°C
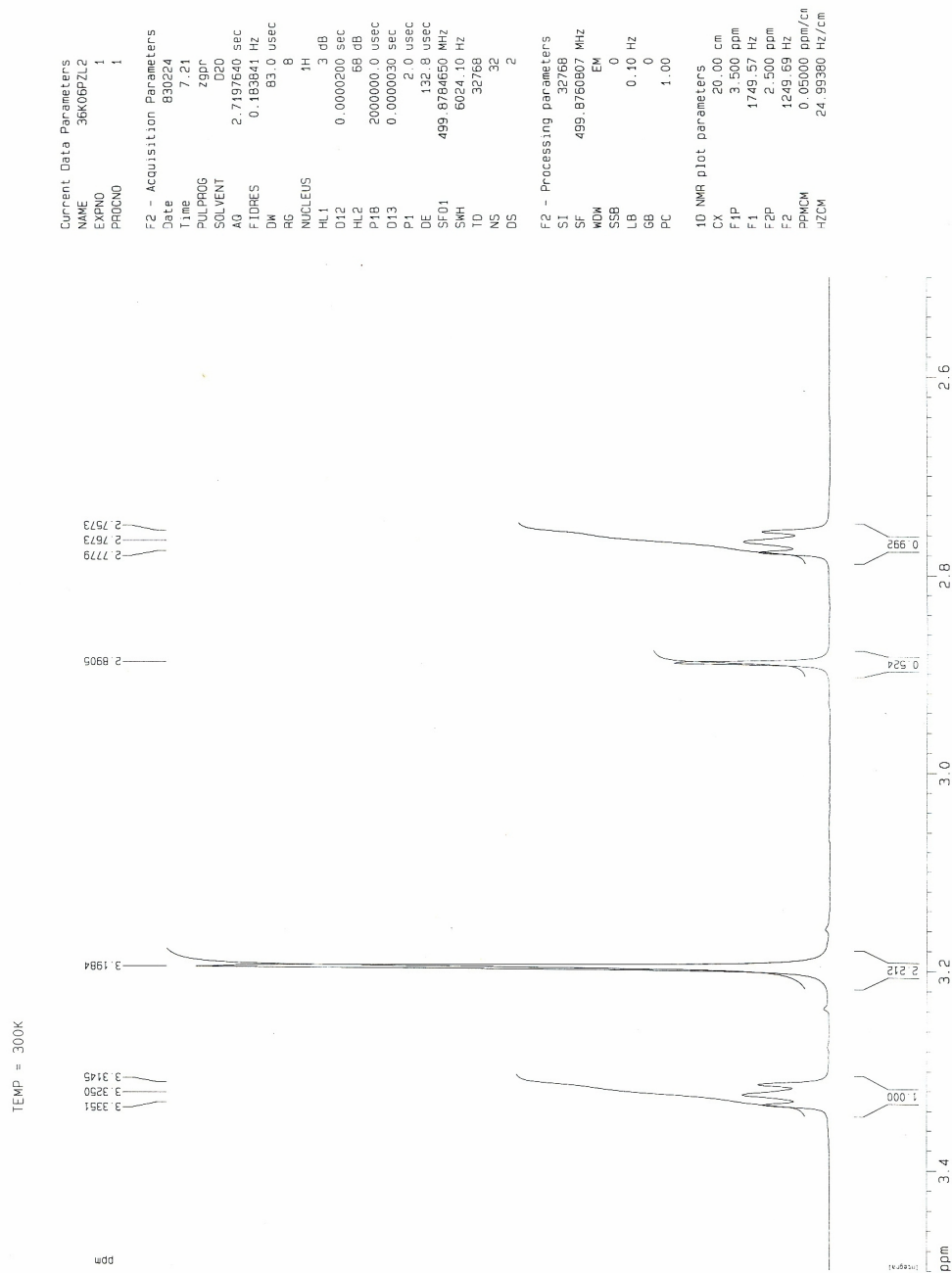
Figure B.2. ^{1}H NMR Spectrum of 3.6 m K$^+$/0.6 m PZ, a = 0.600, T = 40°C
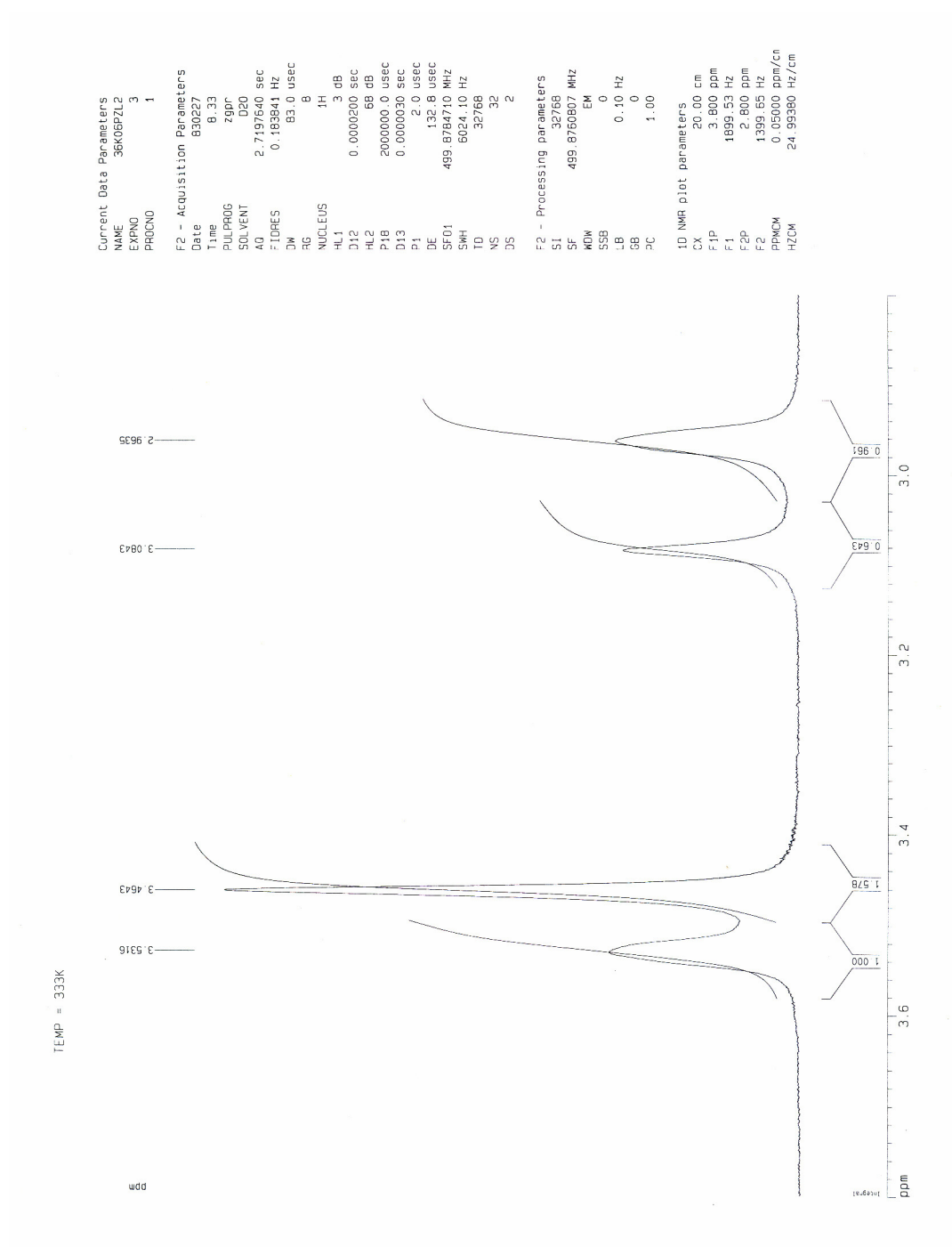
Figure B.3. ^{1}H NMR Spectrum of 3.6 m K$^+$/0.6 m PZ, a = 0.600, T = 60°C

Appendix C: Detailed Wetted-Wall Column Data

This appendix presents the detailed results of the wetted-wall column experiments used to calculate the equilibrium partial pressure and the absorption rate of CO_2 in K^+/PZ mixtures. An asterisk indicates points that were used for modeling the absorption rate; these points typically have a moderate driving force and CO_2 removal. The temperature is an average of the inlet and outlet liquid temperatures; ΔT across the column was typically no more than 1 to 3^oC. A predicted loading is also presented, indicating the loading required for the ENRTL model to match the measured $P_{CO_2}^*$ exactly. The predicted flux is based on rigorous rate model calculations with the predicted loading, relying on the measured partial pressure driving force to eliminate errors associated with loading and thermodynamic estimates.

Table C.1. Experimental Results for Wetted-Wall Column

	T (^{o}C)	Loading, Meas.	Loading, Pred.	$k_g \times 10^9$ (kmol/Pa -m^2-s)	$k_l^o \times 10^4$ (m/s)	$P_{CO_2,b}$ (Pa)	$P_{CO_2}*$ (Pa)	K_G/k_g (%)	CO_2 Removal (%)	$N_{CO_2} \times 10^7$ Measured (kmol/m^2-s)	$N_{CO_2} \times 10^7$ Predicted (kmol/m^2-s)
2.5 m K$^+$/2.5 m PZ											
*	60.0	0.262	0.309	2.26	0.83	180	1	70.8	56.5	2.86	2.76
	59.4	0.262	0.309	2.13	0.84	122	1	77.7	60.1	2.01	1.79
	59.9	0.262	0.309	2.15	0.84	99	1	81.1	61.9	1.72	1.46
	60.4	0.262	0.308	2.14	0.83	36	1	95.5	67.3	0.71	0.52
	60.2	0.262	0.308	2.15	0.83	16	1	111.9	71.7	0.35	0.22
	59.7	0.262	0.309	2.12	0.83	8	1	137.4	76.0	0.20	0.10
*	59.6	0.416	0.337	3.61	0.84	7532	7	54.1	44.5	146.77	146.32
*	60.8	0.416	0.335	3.58	0.82	11613	7	50.9	42.2	211.52	221.02
*	59.7	0.416	0.336	3.53	0.78	15406	7	47.9	39.9	260.22	280.87
*	59.9	0.416	0.336	3.57	0.78	19267	7	45.5	38.0	312.85	344.50
*	59.8	0.416	0.336	3.59	0.78	13581	7	44.7	37.9	217.54	252.73
*	59.7	0.416	0.336	3.55	0.78	9962	7	45.9	39.2	162.54	188.48
*	60.3	0.416	0.336	3.45	0.77	2497	7	56.0	46.1	48.14	48.14
*	60.3	0.416	0.336	3.46	0.77	4023	7	52.3	43.7	72.78	78.01
*	60.5	0.416	0.335	3.48	0.78	5249	7	49.6	41.9	90.45	101.61
*	60.2	0.416	0.336	3.44	0.80	1540	7	50.2	42.5	26.49	30.12
	59.0	0.416	0.337	3.49	0.79	0	7	16.9	<-100	-0.04	-0.04
*	60.4	0.416	0.335	3.46	0.79	575	7	58.2	47.0	11.42	11.28
*	60.0	0.416	0.336	3.46	0.79	1186	7	52.8	43.9	21.49	23.26
*	60.1	0.416	0.336	3.46	0.80	1689	7	50.0	42.2	29.14	33.11
	60.1	0.416	0.336	3.45	0.80	10	7	72.8	<-100	-2.77	0.06
	60.1	0.416	0.336	3.46	0.80	1115	7	53.7	44.4	20.57	21.88
*	59.8	0.371	0.390	3.50	0.83	2081	79	61.3	47.7	42.98	38.07
*	60.3	0.371	0.389	3.49	0.83	8625	79	55.4	44.6	165.45	155.54
*	60.0	0.371	0.390	3.48	0.83	6575	79	56.9	45.6	128.72	119.54
*	60.0	0.371	0.390	3.49	0.83	821	79	59.5	44.7	15.43	14.23
*	60.0	0.371	0.390	3.52	0.82	3826	79	60.1	47.4	79.24	70.67
*	60.1	0.500	0.513	2.70	0.86	2256	919	63.7	34.6	22.97	18.98
*	60.3	0.500	0.512	2.69	0.85	1218	919	65.4	16.5	5.26	4.28
*	59.7	0.500	0.515	2.99	0.84	4499	919	54.8	38.4	58.78	51.96
*	61.2	0.500	0.506	2.96	0.84	12387	919	44.9	36.4	152.52	155.41

253

	T (°C)	Loading, Meas.	Loading, Pred.	$k_g \times 10^9$ (kmol/Pa-m²-s)	$k_l^o \times 10^4$ (m/s)	$P_{CO_2,b}$ (Pa)	$P_{CO_2}^*$ (Pa)	K_G/k_g (%)	CO_2 Removal (%)	$N_{CO_2} \times 10^7$ Measured (kmol/m²-s)	$N_{CO_2} \times 10^7$ Predicted (kmol/m²-s)
*	60.3	0.500	0.511	2.96	0.86	21099	919	34.1	29.3	203.67	248.33
*	61.0	0.500	0.507	2.95	0.85	18654	919	32.4	28.1	169.37	169.40
*	101.1	0.371	0.372	3.82	1.23	2048	319	75.0	49.4	49.53	42.48
*	100.5	0.371	0.372	3.83	1.23	5296	319	70.1	50.4	133.47	118.98
*	100.9	0.371	0.372	3.72	1.22	8836	319	68.5	50.2	217.21	194.24
*	100.1	0.371	0.373	3.73	1.22	12312	319	62.4	47.1	278.93	263.46
*	99.8	0.371	0.373	3.78	1.22	3302	319	66.2	47.4	74.76	71.61
	100.0	0.371	0.373	3.76	1.22	23	319	76.2	< -100	-8.47	-7.28
*	100.0	0.425	0.430	3.74	1.12	744	1833	32.8	-68.4	-13.36	-21.41
	98.2	0.425	0.432	3.62	1.09	2020	1833	41.0	4.0	2.78	3.50
*	98.8	0.425	0.432	3.58	1.10	3048	1833	40.0	15.8	17.40	22.33
*	101.1	0.425	0.429	3.74	1.12	3867	1833	26.5	13.9	20.14	38.06
	100.3	0.425	0.430	3.76	1.10	2554	1833	23.0	6.7	6.24	13.76
*	100.2	0.425	0.430	3.78	1.11	4478	1833	31.3	17.9	31.26	48.95
*	110.8	0.415	0.396	4.20	1.30	1955	894	73.2	34.3	32.62	26.29
*	110.9	0.415	0.396	4.17	1.32	6522	894	62.8	43.2	147.20	130.44
*	110.0	0.415	0.396	4.75	1.30	7482	894	54.1	39.0	169.49	158.74
*	109.7	0.415	0.396	4.81	1.30	4459	894	52.9	35.7	90.70	91.05
*	109.6	0.415	0.397	4.55	1.30	3319	894	50.8	32.3	56.10	61.34
*	109.5	0.415	0.397	4.62	1.30	47	894	60.3	< -100	-23.59	-22.69
*	110.2	0.425	0.447	4.06	1.18	3118	3714	45.0	-9.5	-10.90	-9.89
	110.6	0.425	0.447	4.19	1.17	4331	3714	10.9	1.6	2.80	10.15
*	109.1	0.425	0.448	4.17	1.17	1741	3714	30.7	-44.6	-25.26	-34.25
*	109.6	0.425	0.447	4.12	1.17	2353	3714	26.4	-17.6	-14.80	-23.10
*	109.5	0.425	0.448	4.09	1.17	1130	3714	30.8	<-100	-32.56	-45.23
*	109.8	0.425	0.447	4.06	1.17	5257	3714	39.3	11.4	24.59	24.23

3.6 m K^+/0.6 m PZ

	T (°C)	Loading, Meas.	Loading, Pred.	$k_g \times 10^9$ (kmol/Pa-m²-s)	$k_l^o \times 10^4$ (m/s)	$P_{CO_2,b}$ (Pa)	$P_{CO_2}^*$ (Pa)	K_G/k_g (%)	CO_2 Removal (%)	$N_{CO_2} \times 10^7$ Measured (kmol/m²-s)	$N_{CO_2} \times 10^7$ Predicted (kmol/m²-s)
*	38.7	0.553	0.558	2.00	0.75	127	64	39.6	20.6	0.50	0.51
*	41.0	0.553	0.553	2.34	0.77	298	64	39.6	30.2	2.17	2.10
*	41.7	0.553	0.551	2.07	0.77	453	64	35.9	30.0	2.89	3.35
*	40.8	0.553	0.553	2.01	0.77	243	64	31.9	24.0	1.15	1.50
*	39.7	0.553	0.556	2.02	0.76	1	64	35.8	< -100	-0.45	-0.52
	39.7	0.553	0.556	2.01	0.76	76	64	20.4	3.8	0.05	0.10
*	39.8	0.698	0.698	3.26	0.77	11	1636	13.8	< -100	-7.31	-8.86
*	39.8	0.698	0.698	3.18	0.77	12085	1636	11.6	10.1	38.57	44.44

254

	T (°C)	Loading, Meas.	Loading, Pred.	$k_g \times 10^9$ (kmol/Pa-m²-s)	$k_l^o \times 10^4$ (m/s)	$P_{CO_2,b}$ (Pa)	$P_{CO_2}^*$ (Pa)	K_G/k_g (%)	CO_2 Removal (%)	$N_{CO_2} \times 10^7$ Measured (kmol/m²-s)	$N_{CO_2} \times 10^7$ Predicted (kmol/m²-s)
*	40.4	0.698	0.696	3.33	0.78	17730	1636	11.9	10.7	63.88	63.25
*	40.2	0.698	0.697	3.30	0.78	5559	1636	15.4	11.1	19.97	19.27
*	40.3	0.698	0.696	3.28	0.77	2751	1636	11.3	4.9	4.13	5.80
	58.8	0.373	0.430	2.28	0.92	30	0	92.9	66.5	0.64	0.38
	59.0	0.373	0.430	2.29	0.92	93	0	75.2	58.6	1.60	1.20
*	59.2	0.373	0.430	2.54	0.92	267	0	61.2	50.5	4.15	3.66
*	59.3	0.373	0.430	2.57	0.92	309	0	61.3	50.5	4.85	4.26
*	59.5	0.373	0.430	2.55	0.92	180	0	59.7	50.0	2.73	2.48
*	59.6	0.441	0.459	2.34	0.95	22	4	47.3	35.9	0.20	0.23
*	59.6	0.441	0.459	2.29	0.96	43	4	49.6	40.3	0.44	0.49
*	59.9	0.441	0.458	2.34	0.95	82	4	50.1	42.0	0.92	0.99
*	59.9	0.441	0.458	2.35	0.94	123	4	49.2	41.8	1.37	1.52
*	59.8	0.441	0.459	2.35	0.94	163	4	48.6	41.6	1.82	2.03
*	59.9	0.553	0.565	1.63	0.96	187	280	47.4	-32.6	-0.71	-0.80
*	59.2	0.553	0.567	2.05	0.95	549	280	43.1	21.8	2.38	2.57
	59.3	0.553	0.566	1.91	0.95	291	280	5.7	0.3	0.01	0.10
*	59.4	0.553	0.566	1.91	0.95	457	280	43.8	18.1	1.49	1.64
*	59.3	0.553	0.567	1.74	0.95	6	280	39.5	< -100	-1.87	-2.43
*	58.0	0.698	0.692	2.86	0.93	30	3539	17.4	< -100	-17.44	-22.95
*	58.5	0.698	0.691	2.84	0.94	6796	3539	23.1	11.3	21.31	18.78
*	57.7	0.698	0.693	3.31	0.93	18846	3539	11.1	9.0	56.26	70.78
	57.7	0.698	0.693	3.37	0.93	2997	3539	46.6	-9.6	-8.50	-3.42
*	57.8	0.698	0.693	3.88	0.93	10481	3539	12.6	8.5	33.86	38.42
*	79.1	0.553	0.555	2.06	1.08	428	502	55.4	-11.7	-0.84	-0.83
	78.5	0.553	0.556	2.03	1.08	525	502	7.4	0.4	0.04	0.26
*	79.5	0.553	0.554	2.67	1.08	462	502	59.2	-6.1	-0.63	-0.51
*	79.7	0.553	0.554	2.61	1.08	279	502	50.2	-59.4	-2.93	-2.87
*	78.2	0.553	0.556	3.34	1.04	4347	502	41.6	32.9	53.50	51.62
*	79.4	0.553	0.554	3.37	1.08	13274	502	37.3	31.7	160.51	155.55
*	79.7	0.553	0.554	3.58	1.06	21725	502	28.6	25.2	217.69	232.66
	79.8	0.553	0.553	3.52	1.06	21	502	91.4	< -100	-15.47	-7.13
*	77.1	0.698	0.711	3.33	1.11	82	10197	17.7	< -100	-59.57	-67.11
*	79.1	0.698	0.707	3.36	1.13	17936	10197	15.9	6.9	41.43	37.49
*	78.8	0.698	0.708	3.39	1.13	6159	10197	19.6	-14.9	-26.88	-24.35
	78.3	0.698	0.709	3.37	1.13	11911	10197	19.8	3.0	11.43	9.21

	T (°C)	Loading, Meas.	Loading, Pred.	$k_g \times 10^9$ (kmol/Pa-m²-s)	$k_l^o \times 10^4$ (m/s)	$P_{CO_2,b}$ (Pa)	$P_{CO_2}^*$ (Pa)	K_G/k_g (%)	CO$_2$ Removal (%)	$N_{CO_2} \times 10^7$ Measured (kmol/m²-s)	$N_{CO_2} \times 10^7$ Predicted (kmol/m²-s)
*	78.5	0.698	0.708	3.43	1.15	3427	10197	19.6	-52.4	-45.57	-43.37
*	99.3	0.557	0.561	3.95	1.27	949	1069	34.3	-4.8	-1.63	-2.06
*	99.6	0.557	0.561	3.89	1.27	1772	1069	35.6	14.1	9.73	11.92
*	99.8	0.557	0.560	3.91	1.28	2495	1069	35.9	19.8	20.05	24.09
*	99.7	0.557	0.560	3.97	1.27	1406	1069	31.9	7.9	4.26	5.79
*	99.7	0.557	0.560	3.96	1.27	560	1069	33.7	-39.0	-6.79	-8.88
*	101.2	0.643	0.639	4.10	1.20	2252	5374	22.4	-39.9	-28.68	-36.19
*	101.1	0.643	0.639	4.11	1.22	3501	5374	23.1	-14.2	-17.79	-21.20
*	101.1	0.643	0.639	5.05	1.21	4681	5374	24.8	-4.9	-8.69	-8.01
*	101.0	0.643	0.639	3.72	1.22	7613	5374	27.8	8.3	23.15	22.72
*	101.0	0.643	0.639	3.94	1.22	11697	5374	24.4	12.9	60.67	60.17
*	100.4	0.643	0.640	3.92	1.22	15016	5374	24.2	15.0	91.45	85.76
*	100.6	0.643	0.640	3.95	1.21	13128	5374	21.3	12.3	65.39	71.36
*	101.5	0.699	0.692	3.81	1.23	10294	14341	16.3	-7.0	-25.10	-26.68
	100.3	0.699	0.694	3.86	1.23	15892	14341	24.4	2.5	14.64	9.15
*	100.0	0.699	0.694	3.96	1.24	18886	14341	14.8	3.6	26.56	25.67
*	100.7	0.699	0.693	4.02	1.23	24569	14341	15.2	6.2	62.42	53.07
	100.6	0.699	0.693	3.97	1.24	19875	14341	8.6	2.4	18.83	31.05
*	100.6	0.699	0.693	3.95	1.24	12063	14341	19.5	-4.0	-17.53	-14.47
*	109.1	0.557	0.573	3.66	1.41	1332	1693	34.2	-10.6	-4.53	-6.05
*	108.2	0.557	0.573	3.69	1.41	3899	1693	33.9	18.6	27.62	35.74
*	108.4	0.557	0.573	3.74	1.41	2533	1693	34.9	11.7	10.95	13.98
*	108.5	0.557	0.573	3.73	1.41	2014	1693	35.4	5.9	4.24	5.39
*	109.5	0.557	0.572	3.67	1.42	754	1693	36.4	-63.4	-12.54	-16.03
*	111.7	0.557	0.571	3.62	1.44	3109	1693	28.9	13.2	14.80	23.68
*	109.6	0.643	0.642	4.86	1.29	13862	6797	20.9	10.2	71.70	68.30
*	109.0	0.643	0.643	4.95	1.28	11439	6797	24.3	9.5	55.76	46.75
	109.0	0.643	0.643	4.91	1.28	8295	6797	13.4	2.5	9.84	16.07
*	109.2	0.643	0.643	4.97	1.28	4406	6797	17.3	-10.3	-20.60	-28.04
*	109.2	0.643	0.643	4.91	1.27	9084	6797	21.0	5.3	23.56	24.07
*	109.3	0.643	0.643	4.95	1.28	3252	6797	18.3	-23.2	-32.18	-42.66
	110.5	0.699	0.708	3.86	1.34	26156	22998	20.2	2.5	24.60	14.99
	110.3	0.699	0.708	3.86	1.34	20309	22998	18.1	-2.5	-18.80	-13.70
	110.2	0.699	0.708	3.88	1.34	27986	22998	16.5	2.9	31.94	23.19
	110.4	0.699	0.708	3.84	1.34	24182	22998	4.3	0.2	1.96	5.81

	T (^{o}C)	Loading, Meas.	Loading, Pred.	k_g x 10^9 (kmol/Pa-m^2-s)	k_l^o x 10^4 (m/s)	$P_{CO_2,b}$ (Pa)	P_{CO_2}* (Pa)	K_G/k_g (%)	CO_2 Removal (%)	N_{CO_2} x 10^7 Measured (kmol/m^2-s)	N_{CO_2} x 10^7 Predicted (kmol/m^2-s)
*	110.2	0.699	0.709	3.84	1.33	18545	22998	14.9	-3.8	-25.54	-23.34
*	110.4	0.699	0.708	3.86	1.34	14760	22998	10.9	-6.7	-34.80	-45.81
3.6 m K$^+$/1.8 m PZ											
*	41.3	0.610	0.563	3.33	0.66	4401	157	32.3	28.7	45.64	49.08
*	41.7	0.610	0.561	3.34	0.66	13843	157	27.1	24.7	124.10	141.77
*	41.2	0.610	0.563	3.30	0.67	3	157	32.6	< -100	-1.65	-1.87
*	41.5	0.610	0.562	3.31	0.67	9196	157	28.8	26.2	86.18	98.76
*	41.5	0.610	0.562	3.35	0.67	6738	157	29.7	26.9	65.56	74.43
*	60.3	0.610	0.610	3.09	0.81	9499	1544	42.5	31.8	104.36	81.95
*	61.7	0.610	0.605	3.07	0.82	4933	1544	36.4	23.8	37.81	38.08
*	61.6	0.610	0.605	3.04	0.82	27	1544	36.3	< -100	-16.74	-18.07
*	63.0	0.610	0.600	3.30	0.84	13565	1544	37.9	30.0	150.20	126.57
*	59.1	0.735	0.727	3.03	0.77	94	12829	16.1	< -100	-62.16	-66.90
*	59.4	0.735	0.726	3.03	0.77	25739	12829	14.5	7.2	56.68	43.10
	59.1	0.735	0.727	2.95	0.76	12034	12829	-24.1	1.7	5.66	-3.24
*	58.8	0.735	0.728	2.94	0.76	19702	12829	12.8	4.6	25.91	24.62
*	59.2	0.735	0.727	2.96	0.76	29217	12829	14.3	7.9	69.48	51.39
*	59.1	0.761	0.787	3.15	0.77	20819	36714	7.6	-6.3	-38.17	-31.95
	59.3	0.761	0.786	3.14	0.76	34830	36714	5.3	-0.3	-3.11	-3.10
	59.4	0.761	0.785	3.11	0.77	46321	36714	2.1	0.4	6.32	14.38
	58.9	0.761	0.788	3.00	0.76	53645	36714	4.6	1.4	23.20	23.14
	59.2	0.761	0.786	2.84	0.76	60056	36714*	8.2	3.0	54.30	30.24
*	78.9	0.610	0.623	3.25	1.00	14758	5590	31.7	18.8	94.65	83.40
	79.1	0.610	0.622	3.25	1.00	5382	5590	51.2	-2.2	-3.46	-2.11
*	79.0	0.610	0.622	3.22	1.00	10218	5590	28.9	13.1	43.18	44.97
*	79.6	0.610	0.621	3.17	1.00	76	5590	29.9	< -100	-52.27	-62.23
*	79.4	0.610	0.621	3.27	1.00	7744	5590	30.7	8.8	21.61	21.91
3.6 m K$^+$/3.6 m PZ											
*	40.1	0.560	0.579	2.78	0.58	2247	371	52.5	38.6	27.35	20.51
*	40.1	0.560	0.579	2.77	0.58	1005	371	38.7	23.9	6.80	7.02
*	40.5	0.560	0.575	2.74	0.59	4967	371	47.9	38.7	60.45	49.26
*	40.9	0.560	0.571	2.77	0.59	16183	371	38.2	33.1	167.54	153.76
*	41.1	0.560	0.570	2.74	0.59	10636	371	41.4	35.3	116.36	105.86
*	42.0	0.684	0.681	2.55	0.60	8814	1711	34.7	26.3	63.00	47.05
*	41.0	0.684	0.687	2.56	0.59	2636	1711	41.9	15.0	9.93	6.46

257

	T (^{o}C)	Loading, Meas.	Loading, Pred.	k_g x 10^9 (kmol/Pa -m^2-s)	k_l^o x 10^4 (m/s)	$P_{CO_2,b}$ (Pa)	P_{CO_2}* (Pa)	K_G/k_g (%)	CO_2 Removal (%)	N_{CO_2} x 10^7 Measured (kmol/m^2-s)	N_{CO_2} x 10^7 Predicted (kmol/m^2-s)
*	41.2	0.684	0.686	2.60	0.60	1146	1711	43.5	-27.4	-6.38	-4.08
*	40.3	0.684	0.690	2.95	0.58	19567	1711	19.7	17.2	103.62	96.90
*	40.8	0.684	0.688	2.97	0.59	13620	1711	22.5	19.0	79.55	72.21
	58.4	0.500	0.421	2.17	0.72	216	201	35.3	2.8	0.11	0.20
*	58.0	0.500	0.422	2.16	0.72	237	201	68.5	11.5	0.53	0.48
*	58.2	0.500	0.421	2.10	0.72	146	201	60.4	-30.7	-0.70	-0.72
*	59.4	0.500	0.418	2.18	0.73	371	201	60.1	27.4	2.23	2.29
*	59.0	0.500	0.419	2.17	0.73	460	201	60.7	32.6	3.42	3.46
*	59.2	0.500	0.418	2.16	0.72	420	201	59.3	30.1	2.80	2.93
*	60.8	0.560	0.506	2.70	0.75	5084	1209	57.8	38.7	60.45	51.65
*	60.5	0.560	0.508	2.72	0.75	1444	1209	59.3	10.3	3.79	3.23
*	61.0	0.560	0.505	2.64	0.75	2542	1209	58.5	29.1	20.58	17.92
*	60.6	0.560	0.507	2.69	0.75	10696	1209	48.4	37.5	123.46	120.87
*	60.2	0.560	0.510	2.67	0.75	16249	1209	47.5	37.8	191.02	182.37
*	60.4	0.560	0.509	2.70	0.75	13336	1209	48.3	38.0	158.34	151.39
	59.2	0.652	0.674	2.86	0.74	5979	6869	22.8	-3.8	-5.81	-6.72
	59.6	0.652	0.672	2.88	0.74	8872	6869	20.7	5.0	11.97	14.85
	59.6	0.652	0.672	2.88	0.74	7411	6869	25.7	2.0	4.03	4.14
*	60.4	0.652	0.667	2.96	0.75	14372	6869	20.1	10.7	44.72	53.28
*	60.5	0.652	0.666	2.96	0.74	20047	6869	20.7	13.4	80.66	86.82
*	60.8	0.652	0.665	2.94	0.74	17416	6869	18.5	11.2	57.27	72.42
	77.7	0.554	0.545	2.64	0.88	6676	7323	27.7	-3.0	-4.73	-6.85
*	78.0	0.554	0.543	2.63	0.89	3615	7323	30.7	-42.1	-29.92	-40.88
*	79.5	0.554	0.534	2.64	0.89	12730	7323	30.2	13.0	43.06	54.94
*	79.1	0.554	0.536	2.63	0.89	18628	7323	34.1	19.9	101.38	108.42
*	78.9	0.554	0.538	2.83	0.88	15024	7323	23.6	12.3	51.55	77.88
*	79.1	0.684	0.679	2.92	0.86	10461	34574	11.9	-34.7	-84.23	-123.45
*	79.1	0.684	0.679	2.88	0.85	19868	34574	13.0	-10.7	-55.14	-66.87
	79.2	0.684	0.678	3.66	0.87	29142	34574	18.6	-4.7	-37.03	-23.41
	79.7	0.684	0.675	2.95	0.87	37965	34574	17.8	1.6	17.77	13.37
*	79.7	0.684	0.675	2.88	0.87	50856	34574	13.8	4.3	64.68	57.12
4.8 m K$^+$/0.6 m PZ											
*	41.1	0.717	0.716	3.33	0.69	4946	2453	15.6	8.1	12.93	10.15
*	41.0	0.717	0.716	3.31	0.68	10222	2453	11.1	8.6	28.69	28.12
	39.9	0.717	0.720	3.41	0.69	2845	2453	15.2	2.2	2.03	1.63

258

	T (°C)	Loading, Meas.	Loading, Pred.	$k_g \times 10^9$ (kmol/Pa-m²-s)	$k_l^o \times 10^4$ (m/s)	$P_{CO_2,b}$ (Pa)	$P_{CO_2}^*$ (Pa)	K_G/k_g (%)	CO_2 Removal (%)	$N_{CO_2} \times 10^7$ Measured (kmol/m²-s)	$N_{CO_2} \times 10^7$ Predicted (kmol/m²-s)
*	39.9	0.717	0.720	3.35	0.68	15393	2453	8.8	7.5	38.15	41.38
*	39.6	0.717	0.721	3.44	0.67	20106	2453	7.4	6.5	45.16	51.30
	60.1	0.717	0.718	3.22	0.84	5392	6212	6.6	-1.1	-1.74	-3.79
*	60.1	0.717	0.718	3.18	0.84	16190	6212	12.9	8.0	40.90	36.97
*	60.3	0.717	0.717	3.20	0.84	3365	6212	17.9	-17.9	-16.30	-13.92
*	60.8	0.717	0.716	3.20	0.85	10709	6212	15.5	6.7	22.28	18.93
*	60.7	0.717	0.717	3.33	0.83	20680	6212	11.5	8.0	55.21	49.49
*	60.1	0.717	0.718	3.24	0.84	83	6212	14.3	< -100	-28.48	-32.31
	77.7	0.717	0.728	3.51	0.99	10296	14161	6.7	-2.7	-9.04	-16.55
	79.0	0.717	0.725	3.48	1.01	20234	14161	11.4	3.5	24.17	22.09
	78.9	0.717	0.725	3.46	1.00	15556	14161	3.2	0.3	1.55	5.57
*	79.1	0.717	0.725	3.47	1.00	3600	14161	14.2	-57.2	-52.05	-53.68
*	79.6	0.717	0.724	3.44	1.02	22806	14161	13.2	5.0	39.27	30.53

5.0 m K⁺/2.5 m PZ

	T (°C)	Loading, Meas.	Loading, Pred.	$k_g \times 10^9$ (kmol/Pa-m²-s)	$k_l^o \times 10^4$ (m/s)	$P_{CO_2,b}$ (Pa)	$P_{CO_2}^*$ (Pa)	K_G/k_g (%)	CO_2 Removal (%)	$N_{CO_2} \times 10^7$ Measured (kmol/m²-s)	$N_{CO_2} \times 10^7$ Predicted (kmol/m²-s)
*	40.0	0.570	0.564	3.18	0.64	3336	136	32.0	28.8	32.54	34.24
*	39.8	0.570	0.565	3.16	0.64	1403	136	39.1	32.5	15.66	13.71
*	40.3	0.570	0.562	3.16	0.65	831	136	45.6	34.7	10.02	7.65
*	40.0	0.570	0.564	3.17	0.64	2015	136	34.5	30.1	20.54	20.33
*	40.0	0.570	0.564	3.17	0.64	2551	136	32.6	29.0	24.99	26.00
	39.9	0.570	0.564	3.21	0.64	514	136	56.6	37.2	6.89	4.16
*	40.0	0.570	0.564	2.45	0.65	63	136	32.4	-56.0	-0.58	-0.73
*	40.4	0.570	0.562	2.48	0.64	194	136	35.2	11.5	0.50	0.59
	40.2	0.570	0.563	2.47	0.64	150	136	30.5	3.3	0.11	0.14
*	40.3	0.570	0.562	2.46	0.64	111	136	38.6	-10.9	-0.24	-0.25
*	39.0	0.680	0.692	2.82	0.64	20488	1840	20.9	18.2	109.99	84.44
*	38.8	0.680	0.693	2.83	0.64	14244	1840	24.6	20.5	86.35	60.39
*	39.8	0.680	0.689	2.82	0.64	17679	1840	19.9	17.4	88.92	76.04
*	39.2	0.680	0.691	2.83	0.66	5353	1840	31.8	20.5	31.62	19.59
	39.7	0.680	0.690	2.86	0.67	1935	1840	31.5	1.7	0.85	0.57
*	41.9	0.716	0.710	3.02	0.64	8251	3331	17.9	11.0	26.58	23.83
*	42.1	0.716	0.709	3.00	0.64	5398	3331	19.5	7.9	12.06	10.49
*	42.5	0.716	0.708	2.97	0.62	2541	3331	20.1	-7.1	-4.70	-4.21
*	39.8	0.716	0.717	2.96	0.61	17398	3331	14.0	11.3	58.24	55.19
*	37.9	0.716	0.724	2.95	0.60	23696	3331	11.5	9.8	69.10	68.99
*	59.1	0.445	0.449	1.92	0.75	187	45	65.2	44.5	1.78	1.69

259

	T (°C)	Loading, Meas.	Loading, Pred.	$k_g \times 10^9$ (kmol/Pa-m²-s)	$k_l^o \times 10^4$ (m/s)	$P_{CO_2,b}$ (Pa)	$P_{CO_2}^*$ (Pa)	K_G/k_g (%)	CO_2 Removal (%)	$N_{CO_2} \times 10^7$ Measured (kmol/m²-s)	$N_{CO_2} \times 10^7$ Predicted (kmol/m²-s)
*	60.2	0.445	0.446	1.88	0.76	114	45	61.9	36.2	0.81	0.82
*	60.4	0.445	0.446	1.92	0.74	138	45	63.9	40.4	1.14	1.12
	60.8	0.445	0.445	1.91	0.74	44	45	40.0	-1.5	-0.01	-0.01
*	60.5	0.445	0.445	1.89	0.75	27	45	50.0	-52.4	-0.17	-0.21
*	61.5	0.445	0.443	1.89	0.75	22	45	71.6	-134.8	-0.31	-0.28
*	59.6	0.472	0.454	2.96	0.81	3675	56	61.5	49.0	65.89	54.21
*	59.5	0.472	0.454	2.95	0.81	1850	56	63.0	49.5	33.33	27.00
*	59.6	0.472	0.454	2.98	0.81	6455	56	58.5	47.2	111.43	95.04
*	59.9	0.472	0.454	2.99	0.81	8292	56	57.3	46.4	141.29	121.93
*	60.6	0.472	0.452	2.97	0.82	4314	56	60.6	48.5	76.68	64.36
*	60.5	0.472	0.452	2.96	0.81	2438	56	62.5	49.4	44.02	36.18
*	61.9	0.595	0.606	2.63	0.81	7699	1642	46.2	33.0	73.55	60.61
*	60.3	0.595	0.611	3.02	0.80	4349	1642	42.0	25.1	34.32	28.42
*	60.3	0.595	0.611	3.02	0.80	10878	1642	37.3	29.2	104.06	90.78
*	60.3	0.595	0.611	3.01	0.81	2579	1642	35.9	13.5	10.12	10.02
*	60.4	0.595	0.611	3.03	0.80	13045	1642	35.9	28.8	124.02	109.93
*	60.1	0.595	0.612	3.05	0.80	7683	1642	38.7	28.4	71.29	61.25
*	59.3	0.602	0.619	3.04	0.78	1452	1778	24.4	-6.3	-2.42	-3.38
*	60.4	0.602	0.615	3.01	0.78	4343	1778	32.4	19.1	25.04	26.37
*	59.3	0.602	0.619	3.03	0.77	914	1778	34.9	-44.4	-9.12	-9.00
*	59.6	0.602	0.618	3.02	0.78	6620	1778	32.6	23.1	47.70	47.83
*	59.9	0.602	0.617	3.05	0.77	10681	1778	31.3	24.7	84.99	84.82
*	60.8	0.602	0.614	3.04	0.78	8456	1778	29.3	22.3	59.48	66.45
*	59.5	0.652	0.660	2.95	0.79	16845	4081	24.6	18.1	92.50	86.37
*	59.8	0.652	0.659	3.03	0.79	21243	4081	30.8	23.1	160.11	111.49
*	60.4	0.652	0.657	2.98	0.77	26130	4081	25.1	20.0	165.11	135.31
*	59.5	0.652	0.660	2.96	0.80	2866	4081	29.8	-15.1	-10.71	-9.86
*	59.1	0.652	0.662	2.97	0.79	5562	4081	32.2	9.0	14.19	11.46
*	59.8	0.652	0.659	2.98	0.79	13720	4081	28.4	19.3	81.46	68.41
	59.4	0.703	0.701	3.14	0.74	11394	9467	7.0	1.3	4.25	9.84
	59.3	0.703	0.701	3.17	0.73	8381	9467	7.5	-1.1	-2.57	-5.79
	59.3	0.703	0.701	3.10	0.75	14135	9467	10.8	3.7	15.66	22.85
*	59.0	0.703	0.702	2.83	0.76	21772	9467	14.2	8.2	49.52	53.69
*	59.2	0.703	0.702	3.11	0.76	25674	9467	12.1	7.6	60.98	68.33
*	58.9	0.703	0.702	3.12	0.77	27982	9467	11.3	7.4	65.00	75.85

260

	T (^{o}C)	Loading, Meas.	Loading, Pred.	$k_g \times 10^9$ (kmol/Pa-m^2-s)	$k_l^o \times 10^4$ (m/s)	$P_{CO_2,b}$ (Pa)	$P_{CO_2}^*$ (Pa)	K_G/k_g (%)	CO_2 Removal (%)	$N_{CO_2} \times 10^7$ Measured (kmol/m^2-s)	$N_{CO_2} \times 10^7$ Predicted (kmol/m^2-s)
	79.3	0.689	0.688	2.67	0.93	28494	25715	24.6	2.3	18.28	10.74
	79.5	0.689	0.687	2.69	0.93	31356	25715	20.1	3.4	30.55	21.19
*	80.3	0.689	0.685	2.69	0.94	34614	25715	18.3	4.3	43.63	32.57
*	79.5	0.689	0.687	2.67	0.94	19559	25715	24.6	-7.9	-40.47	-26.23
	80.2	0.689	0.685	2.69	0.95	22398	25715	24.5	-3.6	-21.86	-13.81
*	77.9	0.716	0.699	2.94	0.92	22940	30461	18.5	-6.6	-40.90	-27.71
*	77.1	0.716	0.701	3.34	0.90	25521	30461	14.3	-2.9	-23.49	-17.41
	78.4	0.716	0.698	3.36	0.91	30803	30461	8.5	0.1	0.97	1.15
	78.0	0.716	0.699	3.38	0.90	33079	30461	22.2	1.8	19.67	8.64
	78.4	0.716	0.698	3.47	0.91	34712	30461	21.5	2.6	31.83	13.97
*	101.0	0.521	0.495	3.67	1.01	8560	1059	55.6	40.6	152.86	144.38
*	101.1	0.521	0.494	3.65	1.01	14974	1059	48.4	37.6	245.98	245.98
*	100.4	0.521	0.495	3.59	1.00	10429	1059	47.9	36.8	161.35	175.00
*	99.5	0.521	0.496	3.59	1.00	5227	1059	51.5	35.8	77.07	80.40
*	99.9	0.521	0.496	3.62	1.01	50	1059	50.5	< -100	-18.46	-20.33
*	100.1	0.521	0.496	3.58	1.00	2752	1059	51.0	28.9	30.91	33.29
*	99.5	0.515	0.497	3.55	1.10	2014	1071	62.7	27.5	20.98	18.66
*	99.5	0.515	0.497	3.11	1.10	4485	1071	65.3	41.9	69.33	61.83
*	100.2	0.515	0.496	3.08	1.12	7243	1071	60.4	43.0	114.79	110.27
*	100.6	0.515	0.496	3.15	1.10	242	1071	66.2	< -100	-17.30	-15.58
*	100.7	0.515	0.495	3.10	1.11	7705	1071	60.5	43.1	124.19	118.82
*	100.1	0.515	0.496	3.13	1.07	3627	1071	59.6	36.8	47.66	46.68
*	101.4	0.579	0.569	3.81	1.04	1423	4535	36.7	< -100	-43.49	-48.63
*	101.2	0.579	0.569	3.82	1.05	3431	4535	31.8	-11.6	-13.40	-16.89
	100.9	0.579	0.569	3.81	1.05	4429	4535	44.2	-1.1	-1.78	-1.59
*	100.3	0.579	0.570	3.73	1.06	5348	4535	30.5	4.8	9.25	12.03
*	100.2	0.579	0.570	3.81	1.06	5913	4535	35.0	8.3	18.36	20.44
	100.8	0.579	0.570	3.81	1.06	4010	4535	23.2	-3.3	-4.64	-7.92
*	100.0	0.579	0.571	3.58	1.06	14000	4611	40.9	25.2	137.53	122.69
*	100.5	0.579	0.571	3.50	1.04	9824	4611	38.6	19.7	70.49	70.73
	99.9	0.579	0.572	3.49	1.03	4277	4611	-36.6	3.0	4.26	-4.78
*	99.9	0.579	0.572	3.46	1.03	7487	4611	41.8	15.9	41.63	39.59
*	100.4	0.579	0.571	3.51	1.05	2884	4611	55.0	-43.2	-33.34	-25.40
*	100.6	0.579	0.571	3.45	1.06	11937	4611	36.5	21.2	92.29	97.12
*	100.3	0.612	0.620	3.73	1.02	9900	13153	21.4	-7.6	-26.05	-28.47

261

	T (°C)	Loading, Meas.	Loading, Pred.	$k_g \times 10^9$ (kmol/Pa-m²-s)	$k_l^o \times 10^4$ (m/s)	$P_{CO_2,b}$ (Pa)	$P_{CO_2}^*$ (Pa)	K_G/k_g (%)	CO$_2$ Removal (%)	$N_{CO_2} \times 10^7$ Measured (kmol/m²-s)	$N_{CO_2} \times 10^7$ Predicted (kmol/m²-s)
	100.6	0.612	0.619	3.86	1.03	12406	13153	-8.6	0.5	2.49	-6.27
	100.9	0.612	0.619	3.92	1.04	16285	13153	17.1	3.0	21.04	25.73
*	100.4	0.612	0.620	3.87	1.02	6305	13153	21.1	-26.4	-56.04	-64.30
*	100.8	0.612	0.619	3.82	1.03	7619	13153	20.4	-16.3	-43.01	-51.04
*	100.2	0.612	0.620	3.83	1.05	3076	13153	21.5	-104.6	-82.88	-100.50
	109.8	0.521	0.532	3.78	1.08	3515	2658	83.8	19.7	27.15	15.88
*	110.4	0.521	0.532	3.73	1.08	11380	2658	45.9	30.9	149.25	148.76
*	110.7	0.521	0.531	3.81	1.09	16375	2658	43.1	31.3	225.44	224.79
*	110.5	0.521	0.531	3.86	1.07	6760	2658	37.9	21.6	59.89	74.37
*	110.2	0.521	0.532	3.86	1.08	110	2658	48.6	< -100	-47.86	-49.43
*	110.5	0.570	0.573	3.94	1.12	2766	5869	38.7	-58.8	-47.36	-47.76
*	110.8	0.570	0.573	4.46	1.13	3836	5869	32.6	-19.9	-29.55	-32.42
*	110.0	0.570	0.573	4.42	1.12	4478	5869	31.2	-10.7	-19.18	-21.72
	110.2	0.570	0.573	4.44	1.12	5419	5869	31.0	-2.7	-6.21	-6.85
*	110.1	0.570	0.573	4.43	1.12	4781	5869	30.4	-7.6	-14.67	-16.90
*	110.0	0.570	0.573	4.41	1.12	3338	5869	29.4	-26.5	-32.74	-40.21
*	109.9	0.612	0.619	4.62	1.09	11906	16300	16.1	-6.3	-32.60	-37.14
	110.2	0.612	0.619	4.36	1.10	15970	16300	15.2	-0.3	-2.18	-2.42
*	110.7	0.612	0.618	4.39	1.09	20809	16300	18.5	4.0	36.58	32.88
*	110.5	0.612	0.618	4.62	1.09	8256	16300	20.2	-22.8	-75.15	-72.75
*	110.2	0.612	0.619	4.54	1.09	4426	16300	20.0	-76.1	-107.69	-114.71
*	110.1	0.612	0.619	4.54	1.09	5802	16300	17.7	-40.1	-84.60	-98.79
6.2 m K$^+$/1.2 m PZ											
	59.2	0.700	0.707	2.97	0.78	6918	6014	33.0	4.6	8.84	4.62
*	60.4	0.700	0.705	3.10	0.79	20286	6014	14.3	10.0	63.25	61.25
*	61.0	0.700	0.703	2.98	0.80	3590	6014	19.7	-15.5	-14.23	-13.57
	61.3	0.700	0.703	2.88	0.80	13520	6014	17.8	10.0	38.58	36.02
*	61.0	0.700	0.703	2.90	0.80	54	6014	19.2	< -100	-33.07	-35.20
*	61.4	0.700	0.702	2.90	0.80	24400	6014	16.5	12.1	87.65	75.69
6.2 m K$^+$/1.8 m PZ											
*	62.4	0.565	0.542	2.68	0.68	5182	216	49.2	40.8	65.43	59.33
*	61.8	0.565	0.544	2.66	0.67	10858	216	42.4	36.6	119.99	120.46
*	62.4	0.565	0.542	2.66	0.68	2478	216	50.1	40.1	30.19	27.45
*	61.5	0.565	0.545	2.62	0.67	1129	216	58.3	41.1	13.91	10.96
*	62.0	0.565	0.543	2.42	0.67	8749	216	46.3	39.5	95.83	94.53

262

Appendix D: Tabulated Model Predictions

D.1. P_{CO_2}* and Speciation Predictions

This section presents ENRTL model predictions of bulk solution equilibrium as determined from ^{1}H NMR and P_{CO_2}* experiments outlined in Chapter 5. The data represent model results given the nominal solution conditions listed in the captions. The equilibrium partial pressure is reported in Pa and the liquid concentrations are given in mol/kg-H_2O (m). Loading is given in mol CO_2/(mol K^+ + mol PZ).

Table D.1. Speciation in 1.8 m PZ at 40°C

Loading	P_{CO_2}* (Pa)	PZ	PZH$^+$	PZCOO$^-$	H$^+$PZCOO$^-$	PZ(COO$^-$)$_2$	HCO$_3^-$	CO$_3^{2-}$	OH$^-$
0.00	0.0	1.782	0.017	0.001	0.000	0.000	0.000	0.001	1.41E-02
0.10	1.2	1.455	0.205	0.132	0.006	0.003	0.007	0.029	1.35E-03
0.20	6.4	1.143	0.372	0.240	0.028	0.018	0.017	0.039	5.98E-04
0.30	20.2	0.869	0.513	0.303	0.072	0.045	0.032	0.044	3.35E-04
0.40	50.7	0.631	0.627	0.324	0.139	0.081	0.050	0.045	2.05E-04
0.50	118.3	0.427	0.715	0.309	0.231	0.121	0.075	0.044	1.29E-04
0.60	285.9	0.257	0.776	0.265	0.347	0.159	0.112	0.041	7.81E-05
0.70	805.7	0.127	0.806	0.196	0.493	0.184	0.172	0.035	4.24E-05
0.80	3031.0	0.046	0.804	0.115	0.668	0.177	0.284	0.026	1.87E-05
0.90	16376.8	0.011	0.786	0.046	0.856	0.116	0.482	0.013	5.89E-06
1.00	154136.3	0.001	0.781	0.008	1.002	0.029	0.708	0.003	9.29E-07

Table D.2. Speciation in 1.8 m PZ at 60°C

Loading	P_{CO_2}* (Pa)	PZ	PZH$^+$	PZCOO$^-$	H$^+$PZCOO$^-$	PZ(COO$^-$)$_2$	HCO$_3^-$	CO$_3^{2-}$	OH$^-$
0.00	0.0	1.780	0.019	0.001	0.000	0.000	0.000	0.001	1.65E-02
0.10	7.4	1.459	0.202	0.130	0.005	0.004	0.012	0.025	1.73E-03
0.20	41.2	1.155	0.369	0.233	0.024	0.020	0.030	0.032	7.48E-04
0.30	129.8	0.887	0.512	0.290	0.063	0.050	0.054	0.034	4.07E-04
0.40	325.2	0.654	0.632	0.307	0.124	0.087	0.083	0.034	2.45E-04
0.50	745.8	0.453	0.728	0.291	0.206	0.125	0.122	0.032	1.52E-04
0.60	1727.4	0.284	0.802	0.249	0.311	0.159	0.175	0.029	9.25E-05
0.70	4447.8	0.152	0.850	0.188	0.439	0.179	0.255	0.025	5.20E-05
0.80	14087.6	0.063	0.876	0.116	0.589	0.168	0.389	0.018	2.49E-05
0.90	59101.3	0.019	0.891	0.052	0.745	0.112	0.595	0.010	9.08E-06
1.00	334328.1	0.004	0.906	0.014	0.862	0.040	0.806	0.003	2.20E-06

Table D.3. Speciation in 1.8 m PZ at 80°C

Loading	P_{CO_2}* (Pa)	PZ	PZH$^+$	PZCOO$^-$	H$^+$PZCOO$^-$	PZ(COO$^-$)$_2$	HCO$_3^-$	CO$_3^{2-}$	OH$^-$
0.00	0.0	1.778	0.020	0.001	0.000	0.000	0.000	0.001	1.80E-02
0.10	35.0	1.465	0.195	0.132	0.004	0.005	0.017	0.017	2.03E-03
0.20	195.0	1.167	0.360	0.230	0.021	0.023	0.043	0.021	8.52E-04
0.30	615.8	0.904	0.506	0.282	0.056	0.053	0.074	0.021	4.53E-04
0.40	1541.6	0.675	0.631	0.295	0.111	0.091	0.113	0.020	2.67E-04
0.50	3503.0	0.477	0.735	0.278	0.186	0.129	0.161	0.019	1.64E-04
0.60	7900.9	0.309	0.818	0.238	0.282	0.160	0.226	0.017	9.97E-05
0.70	19192.6	0.174	0.880	0.182	0.398	0.176	0.319	0.014	5.72E-05
0.80	54331.5	0.080	0.924	0.117	0.531	0.163	0.460	0.010	2.89E-05
0.90	185870.3	0.029	0.956	0.058	0.663	0.114	0.657	0.006	1.21E-05
1.00	674122.6	0.009	0.979	0.023	0.759	0.056	0.838	0.003	4.32E-06

Table D.4. Speciation in 1.8 m PZ at 110°C

Loading	P_{CO_2}* (Pa)	PZ	PZH$^+$	PZCOO$^-$	H$^+$PZCOO$^-$	PZ(COO$^-$)$_2$	HCO$_3^-$	CO$_3^{2-}$	OH$^-$
0.00	0.2	1.777	0.021	0.001	0.000	0.000	0.000	0.000	1.91E-02
0.10	216.0	1.468	0.185	0.138	0.004	0.005	0.021	0.006	2.27E-03
0.20	1221.5	1.174	0.350	0.233	0.018	0.025	0.051	0.008	9.16E-04
0.30	3941.3	0.915	0.500	0.281	0.048	0.058	0.087	0.007	4.69E-04
0.40	10054.8	0.689	0.630	0.290	0.098	0.097	0.131	0.007	2.68E-04
0.50	23079.9	0.492	0.740	0.271	0.167	0.136	0.185	0.006	1.60E-04
0.60	51744.6	0.325	0.829	0.231	0.255	0.166	0.255	0.005	9.67E-05
0.70	120834.3	0.192	0.899	0.179	0.361	0.180	0.350	0.004	5.62E-05
0.80	303187.8	0.099	0.949	0.122	0.475	0.170	0.481	0.003	3.06E-05
0.90	766628.7	0.048	0.983	0.075	0.578	0.136	0.632	0.002	1.61E-05
1.00	1698848.3	0.025	1.005	0.046	0.651	0.098	0.760	0.002	8.99E-06

Table D.5. Speciation in 3.6 m K$^+$/0.6 m PZ at 40°C

Loading	P$_{CO_2}$* (Pa)	PZ	PZH$^+$	PZCOO$^-$	H$^+$PZCOO$^-$	PZ(COO$^-$)$_2$	HCO$_3^-$	CO$_3^{2-}$	OH$^-$
0.45	0.2	0.471	0.005	0.160	0.001	0.006	0.025	1.819	9.18E-03
0.50	8.7	0.231	0.014	0.306	0.012	0.080	0.140	1.620	1.43E-03
0.55	54.1	0.101	0.020	0.294	0.032	0.195	0.322	1.423	5.32E-04
0.60	217.8	0.040	0.022	0.232	0.055	0.293	0.588	1.226	2.44E-04
0.65	677.0	0.017	0.023	0.174	0.079	0.351	0.935	1.030	1.26E-04
0.70	1736.1	0.008	0.026	0.132	0.107	0.373	1.331	0.838	7.04E-05
0.75	3959.0	0.005	0.030	0.102	0.143	0.370	1.755	0.656	4.11E-05
0.80	8533.5	0.003	0.038	0.078	0.191	0.343	2.196	0.487	2.40E-05
0.85	18267.4	0.002	0.049	0.057	0.256	0.292	2.650	0.336	1.37E-05
0.90	41220.3	0.001	0.063	0.038	0.340	0.217	3.113	0.208	7.18E-06
0.95	112728.1	0.000	0.080	0.020	0.441	0.122	3.576	0.101	3.05E-06

Table D.6. Speciation in 3.6 m K$^+$/0.6 m PZ at 60°C

Loading	P$_{CO_2}$* (Pa)	PZ	PZH$^+$	PZCOO$^-$	H$^+$PZCOO$^-$	PZ(COO$^-$)$_2$	HCO$_3^-$	CO$_3^{2-}$	OH$^-$
0.45	1.8	0.490	0.002	0.142	0.001	0.008	0.045	1.813	1.26E-02
0.50	39.0	0.281	0.007	0.267	0.006	0.081	0.197	1.608	2.52E-03
0.55	189.6	0.152	0.011	0.276	0.017	0.187	0.397	1.399	1.06E-03
0.60	635.2	0.076	0.013	0.239	0.029	0.286	0.658	1.192	5.31E-04
0.65	1792.1	0.037	0.016	0.193	0.043	0.355	0.987	0.987	2.86E-04
0.70	4476.3	0.020	0.018	0.154	0.062	0.393	1.368	0.785	1.60E-04
0.75	10376.4	0.011	0.023	0.124	0.087	0.404	1.781	0.593	9.11E-05
0.80	23462.1	0.007	0.031	0.098	0.127	0.389	2.214	0.417	5.07E-05
0.85	53914.7	0.004	0.043	0.074	0.190	0.343	2.660	0.267	2.68E-05
0.90	130304.5	0.002	0.061	0.051	0.283	0.262	3.112	0.154	1.32E-05

Table D.7. Speciation in 3.6 m K^+/0.6 m PZ at 80°C

Loading	P_{CO_2}* (Pa)	PZ	PZH^+	$PZCOO^-$	H^+PZCOO^-	$PZ(COO^-)_2$	HCO_3^-	CO_3^{2-}	OH^-
0.40	0.0	0.629	0.000	0.016	0.000	0.000	0.005	1.779	2.75E-01
0.45	6.9	0.503	0.001	0.129	0.000	0.010	0.064	1.804	2.06E-02
0.50	109.4	0.318	0.003	0.237	0.003	0.082	0.237	1.599	4.88E-03
0.55	465.8	0.191	0.005	0.254	0.008	0.186	0.448	1.384	2.19E-03
0.60	1421.0	0.106	0.006	0.231	0.013	0.286	0.704	1.169	1.15E-03
0.65	3797.0	0.057	0.008	0.195	0.020	0.364	1.021	0.955	6.31E-04
0.70	9379.0	0.032	0.010	0.161	0.030	0.414	1.389	0.745	3.53E-04
0.75	22358.4	0.019	0.013	0.133	0.045	0.440	1.792	0.540	1.94E-04
0.80	54560.2	0.011	0.019	0.109	0.072	0.440	2.217	0.350	9.99E-05
0.85	143351.9	0.007	0.031	0.085	0.128	0.403	2.653	0.196	4.63E-05

Table D.8. Speciation in 3.6 m K^+/0.6 m PZ at 110°C

Loading	P_{CO_2}* (Pa)	PZ	PZH^+	$PZCOO^-$	H^+PZCOO^-	$PZ(COO^-)_2$	HCO_3^-	CO_3^{2-}	OH^-
0.40	0.7	0.614	0.000	0.031	0.000	0.001	0.014	1.754	3.00E-01
0.45	26.7	0.503	0.000	0.124	0.000	0.016	0.087	1.776	4.87E-02
0.50	274.2	0.339	0.001	0.209	0.001	0.093	0.259	1.586	1.44E-02
0.55	1050.1	0.212	0.001	0.226	0.002	0.202	0.464	1.370	6.84E-03
0.60	3049.0	0.122	0.001	0.207	0.003	0.309	0.710	1.152	3.67E-03
0.65	8022.9	0.067	0.002	0.176	0.005	0.394	1.016	0.933	2.03E-03
0.70	20072.2	0.037	0.002	0.146	0.008	0.453	1.376	0.714	1.12E-03
0.75	49998.9	0.022	0.003	0.121	0.012	0.490	1.774	0.498	5.93E-04
0.80	137208.6	0.013	0.005	0.102	0.022	0.507	2.192	0.289	2.73E-04
0.85	490629.7	0.009	0.012	0.085	0.055	0.492	2.603	0.119	9.35E-05

267

Table D.9. Speciation in 3.6 m K$^+$/1.8 m PZ at 40°C

Loading	P$_{CO_2}$* (Pa)	PZ	PZH$^+$	PZCOO$^-$	H$^+$PZCOO$^-$	PZ(COO$^-$)$_2$	HCO$_3^-$	CO$_3^{2-}$	OH$^-$
0.40	0.9	1.176	0.017	0.626	0.004	0.023	0.044	1.497	4.41E-03
0.45	10.0	0.833	0.042	0.818	0.026	0.123	0.132	1.267	1.20E-03
0.50	39.7	0.577	0.074	0.844	0.066	0.277	0.235	1.062	5.45E-04
0.55	110.8	0.370	0.111	0.783	0.125	0.448	0.348	0.881	2.93E-04
0.60	284.6	0.206	0.148	0.667	0.202	0.613	0.493	0.719	1.63E-04
0.65	762.7	0.096	0.177	0.522	0.304	0.739	0.709	0.575	8.82E-05
0.70	2111.6	0.040	0.199	0.380	0.433	0.791	1.031	0.450	4.68E-05
0.75	5478.6	0.017	0.219	0.269	0.590	0.759	1.452	0.348	2.57E-05
0.80	12823.5	0.008	0.241	0.186	0.769	0.664	1.939	0.265	1.48E-05
0.85	28022.5	0.004	0.265	0.124	0.961	0.528	2.467	0.195	8.72E-06
0.90	61693.9	0.002	0.292	0.076	1.161	0.368	3.021	0.131	4.90E-06
0.95	160115.3	0.001	0.319	0.037	1.359	0.198	3.582	0.070	2.27E-06

Table D.10. Speciation in 3.6 m K$^+$/1.8 m PZ at 60°C

Loading	P$_{CO_2}$* (Pa)	PZ	PZH$^+$	PZCOO$^-$	H$^+$PZCOO$^-$	PZ(COO$^-$)$_2$	HCO$_3^-$	CO$_3^{2-}$	OH$^-$
0.35	0.1	1.628	0.002	0.223	0.000	0.001	0.010	1.714	5.36E-02
0.40	6.6	1.218	0.010	0.585	0.003	0.032	0.079	1.489	6.00E-03
0.45	55.3	0.911	0.024	0.754	0.016	0.139	0.205	1.239	1.89E-03
0.50	198.3	0.673	0.043	0.791	0.039	0.294	0.341	1.004	8.89E-04
0.55	527.3	0.471	0.070	0.755	0.074	0.468	0.481	0.789	4.78E-04
0.60	1283.3	0.299	0.105	0.670	0.126	0.637	0.640	0.600	2.64E-04
0.65	3174.5	0.167	0.145	0.552	0.203	0.770	0.849	0.443	1.43E-04
0.70	8188.8	0.082	0.186	0.424	0.316	0.835	1.145	0.320	7.55E-05
0.75	20705.5	0.039	0.224	0.310	0.468	0.812	1.540	0.232	4.05E-05
0.80	48393.9	0.019	0.259	0.219	0.652	0.717	2.007	0.169	2.28E-05
0.85	105636.6	0.010	0.290	0.149	0.857	0.575	2.518	0.121	1.33E-05
0.90	229124.0	0.005	0.320	0.094	1.071	0.408	3.049	0.081	7.54E-06

Table D.11. Speciation in 3.6 m K⁺/1.8 m PZ at 80ᵒC

Loading	P_{CO_2}* (Pa)	PZ	PZH⁺	PZCOO⁻	H⁺PZCOO⁻	PZ(COO⁻)₂	HCO₃⁻	CO₃²⁻	OH⁻
0.35	0.6	1.621	0.001	0.230	0.000	0.002	0.018	1.697	6.93E-02
0.40	25.2	1.253	0.005	0.549	0.002	0.039	0.111	1.479	9.86E-03
0.45	174.1	0.970	0.011	0.704	0.008	0.151	0.261	1.218	3.41E-03
0.50	587.9	0.744	0.021	0.747	0.019	0.310	0.416	0.962	1.64E-03
0.55	1554.9	0.546	0.036	0.728	0.037	0.491	0.571	0.718	8.65E-04
0.60	3900.5	0.372	0.061	0.664	0.068	0.672	0.736	0.498	4.51E-04
0.65	10232.4	0.227	0.101	0.565	0.124	0.821	0.936	0.319	2.21E-04
0.70	28243.8	0.122	0.155	0.444	0.224	0.897	1.211	0.198	1.04E-04
0.75	75327.9	0.062	0.209	0.328	0.376	0.876	1.582	0.128	5.16E-05
0.80	181141.6	0.032	0.254	0.235	0.568	0.776	2.028	0.088	2.78E-05
0.85	396139.4	0.017	0.291	0.163	0.780	0.629	2.512	0.062	1.61E-05

Table D.12. Speciation in 3.6 m K⁺/1.8 m PZ at 110ᵒC

Loading	P_{CO_2}* (Pa)	PZ	PZH⁺	PZCOO⁻	H⁺PZCOO⁻	PZ(COO⁻)₂	HCO₃⁻	CO₃²⁻	OH⁻
0.35	3.7	1.640	0.000	0.273	0.000	0.005	0.032	1.702	1.25E-01
0.40	79.6	1.317	0.001	0.540	0.001	0.054	0.140	1.510	2.59E-02
0.45	451.2	1.044	0.003	0.677	0.002	0.182	0.296	1.239	9.91E-03
0.50	1421.1	0.813	0.005	0.719	0.005	0.361	0.452	0.961	4.91E-03
0.55	3731.7	0.607	0.010	0.706	0.010	0.567	0.603	0.685	2.55E-03
0.60	10177.4	0.423	0.019	0.652	0.020	0.782	0.760	0.420	1.20E-03
0.65	36056.7	0.264	0.045	0.563	0.050	0.973	0.947	0.192	4.30E-04
0.70	157384.9	0.144	0.109	0.439	0.146	1.061	1.207	0.073	1.27E-04
0.75	521187.6	0.075	0.180	0.320	0.313	1.023	1.565	0.038	5.05E-05
0.80	1306073.9	0.041	0.229	0.233	0.509	0.912	1.976	0.024	2.64E-05
0.85	2725772.3	0.024	0.260	0.173	0.706	0.774	2.384	0.018	1.62E-05

Table D.13. Speciation in 5.0 m K$^+$/2.5 m PZ at 40°C

Loading	P$_{CO_2}$* (Pa)	PZ	PZH$^+$	PZCOO$^-$	H$^+$PZCOO$^-$	PZ(COO$^-$)$_2$	HCO$_3^-$	CO$_3^{2-}$	OH$^-$
0.40	0.6	1.634	0.010	0.920	0.004	0.029	0.049	2.082	5.94E-03
0.45	8.5	1.146	0.029	1.203	0.031	0.178	0.163	1.736	1.42E-03
0.50	36.2	0.792	0.056	1.231	0.084	0.414	0.295	1.425	6.11E-04
0.55	104.2	0.503	0.095	1.134	0.161	0.680	0.434	1.152	3.16E-04
0.60	275.2	0.272	0.139	0.955	0.267	0.937	0.609	0.917	1.70E-04
0.65	782.0	0.117	0.178	0.731	0.410	1.137	0.884	0.714	8.82E-05
0.70	2361.1	0.044	0.207	0.517	0.601	1.216	1.326	0.547	4.44E-05
0.75	6534.2	0.017	0.233	0.357	0.839	1.160	1.924	0.419	2.36E-05
0.80	15738.7	0.008	0.261	0.245	1.113	1.007	2.622	0.320	1.35E-05
0.85	34589.5	0.004	0.291	0.164	1.410	0.795	3.382	0.238	8.03E-06
0.90	75831.9	0.002	0.324	0.100	1.721	0.550	4.184	0.162	4.59E-06
0.95	197670.6	0.001	0.357	0.049	2.032	0.291	5.006	0.087	2.15E-06

Table D.14. Speciation in 5.0 m K$^+$/2.5 m PZ at 60°C

Loading	P$_{CO_2}$* (Pa)	PZ	PZH$^+$	PZCOO$^-$	H$^+$PZCOO$^-$	PZ(COO$^-$)$_2$	HCO$_3^-$	CO$_3^{2-}$	OH$^-$
0.35	0.1	2.282	0.001	0.329	0.000	0.001	0.010	2.400	7.92E-02
0.40	5.2	1.691	0.006	0.856	0.004	0.043	0.093	2.077	7.50E-03
0.45	50.6	1.256	0.016	1.093	0.020	0.205	0.257	1.713	2.17E-03
0.50	189.1	0.923	0.032	1.133	0.049	0.445	0.429	1.368	9.86E-04
0.55	516.6	0.638	0.057	1.069	0.095	0.716	0.601	1.050	5.13E-04
0.60	1302.8	0.395	0.096	0.936	0.164	0.980	0.792	0.771	2.72E-04
0.65	3431.3	0.207	0.146	0.754	0.274	1.193	1.054	0.546	1.39E-04
0.70	9696.4	0.093	0.197	0.561	0.443	1.290	1.457	0.380	6.89E-05
0.75	26459.9	0.040	0.244	0.398	0.678	1.243	2.019	0.271	3.54E-05
0.80	64085.2	0.019	0.285	0.278	0.963	1.086	2.695	0.198	1.98E-05
0.85	140992.7	0.009	0.323	0.188	1.279	0.863	3.436	0.145	1.16E-05
0.90	305352.0	0.005	0.357	0.118	1.609	0.606	4.212	0.099	6.72E-06

Table D.15. Speciation in 5.0 m K$^+$/2.5 m PZ at 80°C

Loading	P$_{CO_2}$* (Pa)	PZ	PZH$^+$	PZCOO$^-$	H$^+$PZCOO$^-$	PZ(COO$^-$)$_2$	HCO$_3^-$	CO$_3^{2-}$	OH$^-$
0.35	0.4	2.275	0.001	0.336	0.000	0.002	0.019	2.383	9.61E-02
0.40	22.1	1.741	0.003	0.799	0.002	0.056	0.136	2.070	1.17E-02
0.45	167.7	1.340	0.007	1.008	0.010	0.227	0.330	1.695	3.84E-03
0.50	578.5	1.019	0.015	1.053	0.024	0.472	0.525	1.326	1.81E-03
0.55	1553.3	0.738	0.028	1.011	0.046	0.753	0.711	0.973	9.32E-04
0.60	4035.8	0.488	0.054	0.907	0.086	1.037	0.907	0.651	4.65E-04
0.65	11473.5	0.281	0.100	0.751	0.165	1.273	1.154	0.391	2.11E-04
0.70	35549.7	0.138	0.167	0.570	0.319	1.386	1.524	0.227	9.10E-05
0.75	103675.0	0.064	0.233	0.407	0.558	1.338	2.056	0.143	4.26E-05
0.80	259400.7	0.031	0.285	0.286	0.855	1.170	2.707	0.099	2.28E-05
0.85	573646.4	0.016	0.324	0.197	1.182	0.938	3.417	0.072	1.34E-05

Table D.16. Speciation in 5.0 m K$^+$/2.5 m PZ at 110°C

Loading	P$_{CO_2}$* (Pa)	PZ	PZH$^+$	PZCOO$^-$	H$^+$PZCOO$^-$	PZ(COO$^-$)$_2$	HCO$_3^-$	CO$_3^{2-}$	OH$^-$
0.35	2.8	2.232	0.000	0.376	0.000	0.005	0.035	2.320	1.59E-01
0.40	76.7	1.777	0.001	0.747	0.001	0.076	0.170	2.050	2.92E-02
0.45	455.7	1.401	0.002	0.921	0.003	0.266	0.366	1.676	1.09E-02
0.50	1433.8	1.083	0.004	0.961	0.006	0.530	0.552	1.294	5.34E-03
0.55	3745.0	0.796	0.007	0.926	0.012	0.834	0.724	0.915	2.75E-03
0.60	10347.6	0.537	0.016	0.837	0.024	1.152	0.900	0.549	1.27E-03
0.65	40407.2	0.317	0.043	0.702	0.062	1.437	1.119	0.231	4.12E-04
0.70	213715.7	0.158	0.122	0.524	0.207	1.559	1.460	0.077	1.03E-04
0.75	777016.9	0.075	0.203	0.369	0.460	1.484	1.963	0.039	3.92E-05
0.80	2036563.0	0.039	0.255	0.263	0.750	1.309	2.548	0.026	2.05E-05
0.85	4414678.9	0.023	0.285	0.194	1.040	1.101	3.130	0.019	1.29E-05

D.2. $P_{CO_2}^*$ and Normalized Flux

The following tables present model predictions for $P_{CO_2}^*$ and k_g' as a function of loading. $P_{CO_2}^*$ is in units of Pa. The normalized flux is in units of kmol/m^2-Pa-s as was calculated at two driving forces, $P_{CO_2,i} = 1.05 \times P_{CO_2}^*$ and $P_{CO_2,i} = 3.0 \times P_{CO_2}^*$, as indicated in parenthesis. The liquid film coefficient, k_l^o, was 1.0×10^{-4} m/s.

Table D.17. Partial Pressure and Rate Predictions in Aqueous PZ at 40°C

Loading	0.6 m PZ			1.8 m PZ		
	$P_{CO_2}^*$ (Pa)	k_g' (1.05)	k_g' (3.0)	$P_{CO_2}^*$ (Pa)	k_g' (1.05)	k_g' (3.0)
0.00	0.0	31.64	31.62	0.0	58.82	58.82
0.05	0.3	29.74	29.74	0.3	55.73	55.72
0.10	1.5	28.28	28.27	1.2	53.27	53.26
0.15	3.9	26.89	26.88	3.1	50.83	50.81
0.20	8.0	25.49	25.46	6.4	48.26	48.22
0.25	14.4	24.05	24.00	11.8	45.51	45.45
0.30	24.3	22.55	22.46	20.2	42.58	42.48
0.35	39.1	20.99	20.86	32.5	39.48	39.33
0.40	61.2	19.37	19.19	50.7	36.22	36.00
0.45	94.2	17.69	17.43	77.6	32.81	32.50
0.50	143.7	15.94	15.59	118.3	29.27	28.85
0.55	219.6	14.14	13.66	181.9	25.61	25.05
0.60	338.2	12.26	11.63	285.9	21.84	21.10
0.65	529.2	10.33	9.52	466.8	17.98	17.02
0.70	847.1	8.35	7.37	805.7	14.07	12.85
0.75	1398.5	6.36	5.27	1496.6	10.17	8.74
0.80	2405.1	4.47	3.41	3031.0	6.52	5.08
0.85	4380.7	2.81	1.97	6716.7	3.53	2.47
0.90	8735.6	1.53	1.03	16376.8	1.60	1.07
0.95	20485.6	0.71	0.51	46014.4	0.65	0.48
1.00	59452.4	0.34	0.29	154136.3	0.31	0.27

Table D.18. Partial Pressure and Rate Predictions in Aqueous PZ at 60°C

Loading	0.6 m PZ			1.8 m PZ		
	P_{CO2}* (Pa)	k_g' (1.05)	k_g' (3.0)	P_{CO2}* (Pa)	k_g' (1.05)	k_g' (3.0)
0.00	0.1	40.35	40.34	0.1	78.05	78.05
0.05	2.2	37.57	37.55	1.6	73.11	73.09
0.10	9.3	35.33	35.26	7.4	69.18	69.10
0.15	23.4	33.19	33.03	19.5	65.31	65.12
0.20	47.1	30.99	30.70	41.2	61.23	60.85
0.25	84.2	28.69	28.21	76.3	56.89	56.23
0.30	140.0	26.28	25.54	129.8	52.29	51.25
0.35	222.1	23.75	22.70	209.2	47.44	45.93
0.40	341.6	21.11	19.72	325.2	42.37	40.31
0.45	515.5	18.39	16.63	494.7	37.11	34.46
0.50	769.8	15.62	13.54	745.8	31.70	28.48
0.55	1145.7	12.85	10.57	1127.1	26.20	22.52
0.60	1710.9	10.18	7.87	1727.4	20.73	16.83
0.65	2579.8	7.69	5.55	2717.8	15.44	11.68
0.70	3953.9	5.50	3.71	4447.8	10.62	7.42
0.75	6205.7	3.69	2.35	7670.0	6.61	4.26
0.80	10070.6	2.31	1.42	14087.6	3.66	2.23
0.85	17134.4	1.35	0.82	27753.7	1.82	1.09
0.90	31231.5	0.73	0.47	59101.3	0.84	0.53
0.95	62496.4	0.39	0.28	137741.7	0.39	0.27
1.00	132683.4	0.23	0.19	334328.1	0.22	0.18

Table D.19. Partial Pressure and Rate Predictions in Aqueous PZ at 80°C

Loading	0.6 m PZ			1.8 m PZ		
	P_{CO2}* (Pa)	k_g' (1.05)	k_g' (3.0)	P_{CO2}* (Pa)	k_g' (1.05)	k_g' (3.0)
0.00	0.7	52.20	52.18	0.4	105.03	105.00
0.05	10.5	47.07	46.88	7.8	96.14	95.94
0.10	43.4	42.21	41.59	35.0	88.03	87.32
0.15	107.0	37.48	36.19	92.5	79.71	78.04
0.20	212.6	32.73	30.64	195.0	70.90	67.86
0.25	375.8	28.04	25.15	361.2	61.79	57.15
0.30	618.1	23.50	20.01	615.8	52.65	46.53
0.35	970.0	19.24	15.43	992.8	43.79	36.61
0.40	1475.2	15.36	11.58	1541.6	35.45	27.84
0.45	2197.8	11.94	8.46	2338.0	27.83	20.45
0.50	3234.3	9.02	6.04	3503.0	21.09	14.51
0.55	4733.1	6.62	4.22	5239.1	15.34	9.91
0.60	6929.1	4.71	2.88	7900.9	10.63	6.49
0.65	10204.9	3.25	1.93	12137.3	6.97	4.07
0.70	15204.2	2.17	1.27	19192.6	4.29	2.44
0.75	23050.7	1.41	0.83	31550.7	2.48	1.40
0.80	35788.1	0.89	0.54	54331.5	1.35	0.78
0.85	57275.6	0.55	0.35	98285.6	0.72	0.44
0.90	94853.7	0.35	0.24	185870.3	0.39	0.26

Table D.20. Partial Pressure and Rate Predictions in Aqueous PZ at 100°C

Loading	0.6 m PZ			1.8 m PZ		
	P_{CO2}* (Pa)	k_g' (1.05)	k_g' (3.0)	P_{CO2}* (Pa)	k_g' (1.05)	k_g' (3.0)
0.00	2.7	65.92	65.69	1.7	140.71	140.49
0.05	38.7	52.63	50.98	28.3	119.35	117.61
0.10	156.6	40.40	36.85	125.5	97.46	92.42
0.15	382.4	30.84	26.15	332.3	77.21	68.76
0.20	755.7	23.31	18.37	703.6	59.41	49.03
0.25	1330.6	17.47	12.87	1310.7	44.68	34.11
0.30	2181.3	12.97	9.01	2247.7	33.02	23.46
0.35	3411.6	9.56	6.31	3643.6	24.06	16.04
0.40	5168.5	6.98	4.42	5683.2	17.28	10.91
0.45	7664.4	5.05	3.10	8644.5	12.22	7.37
0.50	11211.9	3.61	2.16	12963.1	8.47	4.93
0.55	16279.5	2.56	1.51	19351.3	5.74	3.25
0.60	23582.0	1.79	1.05	29018.2	3.78	2.11
0.65	34226.3	1.24	0.73	44090.9	2.41	1.34
0.70	49946.5	0.86	0.51	68419.0	1.49	0.84
0.75	73464.0	0.59	0.37	109059.1	0.90	0.52
0.80	108982.0	0.41	0.27	178726.2	0.54	0.33

Table D.21. Partial Pressure and Rate Predictions in Aqueous PZ at 120°C

Loading	0.6 m PZ			1.8 m PZ		
	P_{CO2}* (Pa)	k_g' (1.05)	k_g' (3.0)	P_{CO2}* (Pa)	k_g' (1.05)	k_g' (3.0)
0.00	8.1	75.67	73.94	5.1	178.83	177.09
0.05	111.5	45.43	39.77	79.0	123.44	114.37
0.10	448.9	27.39	21.59	350.7	79.62	66.32
0.15	1097.8	17.73	12.94	937.3	51.52	38.97
0.20	2176.0	11.92	8.20	2006.4	33.64	23.56
0.25	3845.1	8.20	5.39	3780.7	22.26	14.67
0.30	6326.7	5.72	3.63	6557.1	14.91	9.36
0.35	9927.8	4.03	2.49	10742.4	10.08	6.09
0.40	15078.9	2.86	1.73	16917.5	6.84	4.01
0.45	22390.0	2.03	1.22	25946.4	4.64	2.65
0.50	32733.9	1.45	0.86	39165.7	3.13	1.76
0.55	47362.1	1.03	0.62	58714.3	2.09	1.17
0.60	68061.5	0.74	0.45	88108.1	1.38	0.78
0.65	97341.5	0.54	0.34	133209.2	0.90	0.52

Table D.22. Partial Pressure and Rate Predictions in K$^+$/PZ at 40°C

Loading	3.6 m K$^+$/0.6 m PZ			3.6 m K$^+$/1.8 m PZ		
	P_{CO2}* (Pa)	k$_g$' (1.05)	k$_g$' (3.0)	P_{CO2}* (Pa)	k$_g$' (1.05)	k$_g$' (3.0)
0.40	-	-	-	0.9	28.72	28.72
0.45	0.2	21.92	21.92	9.9	26.44	26.43
0.50	8.7	18.35	18.34	39.5	23.58	23.55
0.55	54.1	14.61	14.57	110.6	20.08	19.99
0.60	217.8	11.17	11.04	284.5	16.09	15.89
0.65	677.0	8.47	8.19	765.9	11.96	11.58
0.70	1736.1	6.37	5.89	2135.3	8.23	7.57
0.75	3959.0	4.60	3.97	5569.7	5.22	4.33
0.80	8533.5	3.05	2.39	13067.6	2.98	2.15
0.85	18267.4	1.75	1.22	28567.4	1.51	0.96
0.90	41220.3	0.80	0.51	62867.9	0.66	0.40

Table D.23. Partial Pressure and Rate Predictions in K$^+$/PZ at 60°C

Loading	3.6 m K$^+$/0.6 m PZ			3.6 m K$^+$/1.8 m PZ		
	P_{CO2}* (Pa)	k$_g$' (1.05)	k$_g$' (3.0)	P_{CO2}* (Pa)	k$_g$' (1.05)	k$_g$' (3.0)
0.35	-	-	-	0.1	45.23	45.22
0.40	0.0	50.39	50.39	6.5	38.36	38.35
0.45	1.8	28.99	28.98	55.1	34.87	34.79
0.50	39.0	24.35	24.30	198.2	30.72	30.44
0.55	189.6	19.76	19.53	528.4	25.73	25.06
0.60	635.2	15.16	14.55	1289.6	19.94	18.65
0.65	1792.1	10.95	9.79	3206.0	13.60	11.60
0.70	4476.3	7.31	5.79	8330.2	7.65	5.55
0.75	10376.4	4.38	3.00	21195.4	3.56	2.18
0.80	23462.1	2.27	1.37	49690.0	1.53	0.86
0.85	53914.7	0.99	0.55	108538.6	0.67	0.37

Table D.24. Partial Pressure and Rate Predictions in K$^+$/PZ at 80°C

Loading	3.6 m K$^+$/0.6 m PZ			3.6 m K$^+$/1.8 m PZ		
	P_{CO2}* (Pa)	k$_g$' (1.05)	k$_g$' (3.0)	P_{CO2}* (Pa)	k$_g$' (1.05)	k$_g$' (3.0)
0.35	-	-	-	0.5	63.54	63.54
0.4	0.0	67.84	67.84	24.9	52.15	52.06
0.45	6.9	39.60	39.56	174.0	45.69	45.21
0.5	109.4	32.47	32.19	589.2	38.15	36.73
0.55	465.8	25.72	24.78	1561.0	29.21	26.35
0.6	1421.0	18.72	16.72	3928.4	19.18	15.17
0.65	3797.0	12.05	9.30	10374.3	9.73	6.36
0.7	9379.0	6.69	4.33	28904.6	3.71	2.09
0.75	22358.4	3.21	1.84	77670.4	1.30	0.71
0.8	54560.2	1.33	0.72	187432.0	0.52	0.30

Table D.25. Partial Pressure and Rate Predictions in K$^+$/PZ at 100°C

Loading	3.6 m K$^+$/0.6 m PZ			3.6 m K$^+$/1.8 m PZ		
	P_{CO2}* (Pa)	k_g' (1.05)	k_g' (3.0)	P_{CO2}* (Pa)	k_g' (1.05)	k_g' (3.0)
0.3	-	-	-	0.1	148.89	148.89
0.35	-	-	-	2.1	90.76	90.71
0.4	0.3	92.46	92.45	59.2	70.45	69.98
0.45	18.2	55.27	55.09	357.9	57.33	55.42
0.5	216.2	42.57	41.53	1154.3	43.18	38.83
0.55	852.0	31.47	28.77	3047.6	28.15	22.05
0.6	2492.9	20.65	16.58	8117.5	14.06	9.06
0.65	6541.5	11.58	7.84	25564.5	4.59	2.58
0.7	16229.7	5.62	3.34	91047.7	1.24	0.71
0.75	39863.2	2.43	1.35	278997.0	0.44	0.27
0.8	105711.4	0.88	0.48	-	-	-

Table D.26. Partial Pressure and Rate Predictions in K$^+$/PZ at 120°C

Loading	3.6 m K$^+$/0.6 m PZ			3.6 m K$^+$/1.8 m PZ		
	P_{CO2}* (Pa)	k_g' (1.05)	k_g' (3.0)	P_{CO2}* (Pa)	k_g' (1.05)	k_g' (3.0)
0.3	-	-	-	0.5	196.86	196.83
0.35	0.3	191.21	191.18	6.1	128.99	128.71
0.4	1.6	125.86	125.76	99.6	93.68	91.90
0.45	37.4	77.47	76.62	528.7	69.03	63.91
0.5	328.5	54.31	51.32	1624.9	46.36	38.10
0.55	1226.2	36.21	30.83	4233.0	26.08	18.00
0.6	3559.5	21.06	15.49	11748.6	10.36	5.87
0.65	9466.7	10.63	6.87	47211.2	2.05	1.10
0.7	23991.1	4.86	2.88	268332.4	0.38	0.25
0.75	60590.4	2.00	1.11	-	-	-
0.8	170747.9	0.64	0.34	-	-	-

Table D.27. Partial Pressure and Rate Predictions in K$^+$/PZ at 40°C

Loading	5.0 m K$^+$/2.5 m PZ			6.2 m K$^+$/1.2 m PZ		
	P_{CO2}* (Pa)	k_g' (1.05)	k_g' (3.0)	P_{CO2}* (Pa)	k_g' (1.05)	k_g' (3.0)
0.40	0.6	25.59	25.59	-	-	-
0.45	8.2	23.60	23.60	0.2	22.40	22.40
0.50	35.3	21.11	21.09	6.4	18.74	18.73
0.55	102.2	18.01	17.97	41.0	14.68	14.66
0.60	271.7	14.38	14.27	189.5	10.84	10.78
0.65	781.6	10.54	10.30	684.8	8.00	7.83
0.70	2399.9	7.13	6.66	1951.3	5.94	5.62
0.75	6720.6	4.48	3.80	4815.3	4.28	3.81
0.80	16271.5	2.56	1.89	11102.2	2.84	2.30
0.85	35804.7	1.30	0.84	25104.3	1.60	1.13
0.90	78454.8	0.56	0.34	58668.6	0.70	0.43

Table D.28. Partial Pressure and Rate Predictions in K⁺/PZ at 60°C

Loading	5.0 m K⁺/2.5 m PZ			6.2 m K⁺/1.2 m PZ		
	P_{CO2}* (Pa)	k_g' (1.05)	k_g' (3.0)	P_{CO2}* (Pa)	k_g' (1.05)	k_g' (3.0)
0.35	0.0	41.97	41.97	-	-	-
0.40	5.0	35.03	35.02	0.0	50.68	50.68
0.45	49.3	31.93	31.88	2.0	30.48	30.48
0.50	185.4	28.25	28.09	34.5	25.55	25.52
0.55	508.8	23.78	23.38	165.0	20.32	20.20
0.60	1292.1	18.51	17.66	604.1	15.14	14.78
0.65	3446.6	12.61	11.13	1949.3	10.72	9.90
0.70	9918.1	6.96	5.20	5466.8	7.11	5.86
0.75	27457.8	3.11	1.92	13985.8	4.19	2.96
0.80	66936.3	1.30	0.72	34877.6	2.05	1.24
0.85	-	-	-	87578.4	0.79	0.43

Table D.29. Partial Pressure and Rate Predictions in K⁺/PZ at 80°C

Loading	5.0 m K⁺/2.5 m PZ			6.2 m K⁺/1.2 m PZ		
	P_{CO2}* (Pa)	k_g' (1.05)	k_g' (3.0)	P_{CO2}* (Pa)	k_g' (1.05)	k_g' (3.0)
0.35	0.3	59.20	59.20	-	-	-
0.4	21.4	48.50	48.46	0.0	68.23	68.23
0.45	164.7	43.10	42.82	9.1	42.13	42.11
0.5	569.9	36.65	35.76	109.8	35.02	34.85
0.55	1533.3	28.74	26.76	449.3	27.56	26.97
0.6	4005.3	19.38	16.16	1457.9	19.77	18.35
0.65	11553.8	9.77	6.66	4401.8	12.50	10.12
0.7	36619.6	3.41	1.93	12298.9	6.68	4.41
0.75	108653.8	1.09	0.59	32972.2	2.96	1.68
0.8	-	-	-	92751.4	1.05	0.56

Table D.30. Partial Pressure and Rate Predictions in K⁺/PZ at 100°C

Loading	5.0 m K⁺/2.5 m PZ			6.2 m K⁺/1.2 m PZ		
	P_{CO2}* (Pa)	k_g' (1.05)	k_g' (3.0)	P_{CO2}* (Pa)	k_g' (1.05)	k_g' (3.0)
0.3	0.1	139.24	139.24	-	-	-
0.35	1.5	83.52	83.49	-	-	-
0.4	54.7	66.03	65.78	0.2	90.14	90.14
0.45	353.0	55.63	54.45	25.0	57.70	57.58
0.5	1143.8	43.72	40.65	234.6	46.63	45.95
0.55	3019.2	30.02	24.95	878.2	35.25	33.30
0.6	8227.0	15.67	10.67	2706.1	23.19	19.59
0.65	28838.0	4.76	2.71	8028.3	12.40	8.58
0.7	123911.3	1.08	0.61	22734.4	5.43	3.17
0.75	-	-	-	63695.1	2.06	1.12

Table D.31. Partial Pressure and Rate Predictions in K$^+$/PZ at 120°C

Loading	5.0 m K$^+$/2.5 m PZ			6.2 m K$^+$/1.2 m PZ		
	P_{CO2}* (Pa)	k$_g$' (1.05)	k$_g$' (3.0)	P_{CO2}* (Pa)	k$_g$' (1.05)	k$_g$' (3.0)
0.3	0.3	174.87	174.86	-	-	-
0.35	4.6	114.93	114.82	0.1	177.19	177.19
0.4	96.1	87.24	86.30	1.2	114.89	114.86
0.45	534.5	68.30	64.96	48.6	77.18	76.73
0.5	1631.2	48.95	42.41	366.4	59.49	57.54
0.55	4196.1	29.54	21.78	1299.4	42.00	37.55
0.6	11710.0	12.38	7.32	3995.6	24.43	18.68
0.65	52608.9	2.15	1.15	12228.8	11.21	7.23
0.7	-	-	-	35884.6	4.48	2.61
0.75	-	-	-	104411.6	1.59	0.88

D.3. Concentration Profiles

The following tables show the concentration profile predicted for various solvents with a factor of 10 driving force ($P_{CO2,i} = 10.0 \times P_{CO2}$*). The liquid film coefficient was constant at 1.0×10^{-4} m/s.

Table D.32. Concentration Profile in 1.8 m PZ, 60°C

r	CO_2	PZ	PZH^+	$PZCOO^-$	H^+PZCOO^-	$PZ(COO^-)_2$	HCO_3^-	CO_3^{2-}	OH^-
0.0E+00	1.46E-03	1.54E-01	6.48E-01	1.77E-01	3.31E-01	1.58E-01	1.27E-01	1.34E-02	4.88E-05
1.0E-04	1.44E-03	1.54E-01	6.48E-01	1.77E-01	3.31E-01	1.58E-01	1.27E-01	1.34E-02	4.88E-05
2.0E-04	1.43E-03	1.54E-01	6.48E-01	1.77E-01	3.31E-01	1.58E-01	1.27E-01	1.34E-02	4.88E-05
3.0E-04	1.41E-03	1.54E-01	6.48E-01	1.77E-01	3.31E-01	1.58E-01	1.27E-01	1.34E-02	4.88E-05
4.0E-04	1.40E-03	1.54E-01	6.48E-01	1.77E-01	3.31E-01	1.58E-01	1.27E-01	1.34E-02	4.88E-05
5.0E-04	1.38E-03	1.54E-01	6.48E-01	1.77E-01	3.31E-01	1.58E-01	1.27E-01	1.34E-02	4.88E-05
6.0E-04	1.37E-03	1.54E-01	6.48E-01	1.77E-01	3.31E-01	1.58E-01	1.27E-01	1.34E-02	4.88E-05
7.0E-04	1.36E-03	1.54E-01	6.48E-01	1.77E-01	3.31E-01	1.58E-01	1.27E-01	1.34E-02	4.88E-05
8.0E-04	1.34E-03	1.54E-01	6.48E-01	1.77E-01	3.31E-01	1.58E-01	1.27E-01	1.34E-02	4.88E-05
9.0E-04	1.33E-03	1.54E-01	6.48E-01	1.77E-01	3.31E-01	1.58E-01	1.27E-01	1.34E-02	4.88E-05
1.0E-03	1.32E-03	1.54E-01	6.48E-01	1.77E-01	3.31E-01	1.58E-01	1.27E-01	1.34E-02	4.88E-05
2.0E-03	1.20E-03	1.54E-01	6.48E-01	1.77E-01	3.31E-01	1.58E-01	1.27E-01	1.34E-02	4.88E-05
3.0E-03	1.10E-03	1.54E-01	6.48E-01	1.77E-01	3.31E-01	1.58E-01	1.27E-01	1.34E-02	4.88E-05
4.0E-03	1.01E-03	1.54E-01	6.48E-01	1.77E-01	3.31E-01	1.58E-01	1.27E-01	1.34E-02	4.88E-05
5.0E-03	9.42E-04	1.54E-01	6.48E-01	1.77E-01	3.31E-01	1.58E-01	1.27E-01	1.34E-02	4.88E-05
6.0E-03	8.81E-04	1.54E-01	6.48E-01	1.78E-01	3.31E-01	1.58E-01	1.27E-01	1.34E-02	4.89E-05
7.0E-03	8.30E-04	1.54E-01	6.48E-01	1.78E-01	3.31E-01	1.58E-01	1.27E-01	1.35E-02	4.89E-05
8.0E-03	7.86E-04	1.55E-01	6.48E-01	1.78E-01	3.31E-01	1.58E-01	1.27E-01	1.35E-02	4.90E-05
9.0E-03	7.49E-04	1.55E-01	6.48E-01	1.78E-01	3.31E-01	1.58E-01	1.27E-01	1.35E-02	4.90E-05
1.0E-02	7.19E-04	1.55E-01	6.48E-01	1.78E-01	3.31E-01	1.58E-01	1.27E-01	1.35E-02	4.91E-05
2.0E-02	5.61E-04	1.56E-01	6.48E-01	1.79E-01	3.29E-01	1.57E-01	1.27E-01	1.36E-02	4.96E-05
3.0E-02	5.19E-04	1.58E-01	6.47E-01	1.80E-01	3.28E-01	1.56E-01	1.27E-01	1.38E-02	5.01E-05
4.0E-02	5.02E-04	1.60E-01	6.47E-01	1.82E-01	3.26E-01	1.55E-01	1.27E-01	1.39E-02	5.07E-05
5.0E-02	4.90E-04	1.62E-01	6.47E-01	1.83E-01	3.25E-01	1.55E-01	1.27E-01	1.40E-02	5.13E-05
6.0E-02	4.81E-04	1.63E-01	6.47E-01	1.84E-01	3.23E-01	1.54E-01	1.27E-01	1.42E-02	5.19E-05
7.0E-02	4.71E-04	1.65E-01	6.46E-01	1.85E-01	3.22E-01	1.53E-01	1.26E-01	1.43E-02	5.25E-05
8.0E-02	4.63E-04	1.67E-01	6.46E-01	1.86E-01	3.20E-01	1.52E-01	1.26E-01	1.45E-02	5.30E-05
9.0E-02	4.54E-04	1.69E-01	6.46E-01	1.87E-01	3.18E-01	1.52E-01	1.26E-01	1.46E-02	5.36E-05
1.0E-01	4.46E-04	1.71E-01	6.46E-01	1.88E-01	3.17E-01	1.51E-01	1.26E-01	1.47E-02	5.42E-05
2.0E-01	3.76E-04	1.89E-01	6.45E-01	1.97E-01	3.00E-01	1.46E-01	1.25E-01	1.61E-02	6.00E-05
3.0E-01	3.23E-04	2.07E-01	6.45E-01	2.04E-01	2.83E-01	1.41E-01	1.23E-01	1.75E-02	6.57E-05
4.0E-01	2.80E-04	2.24E-01	6.44E-01	2.10E-01	2.68E-01	1.37E-01	1.22E-01	1.88E-02	7.15E-05
5.0E-01	2.47E-04	2.41E-01	6.42E-01	2.15E-01	2.54E-01	1.33E-01	1.21E-01	2.01E-02	7.72E-05
6.0E-01	2.19E-04	2.58E-01	6.39E-01	2.19E-01	2.41E-01	1.29E-01	1.19E-01	2.13E-02	8.28E-05
7.0E-01	1.96E-04	2.74E-01	6.36E-01	2.23E-01	2.30E-01	1.25E-01	1.18E-01	2.25E-02	8.83E-05
8.0E-01	1.77E-04	2.90E-01	6.33E-01	2.25E-01	2.19E-01	1.22E-01	1.17E-01	2.37E-02	9.39E-05
9.0E-01	1.60E-04	3.05E-01	6.29E-01	2.28E-01	2.09E-01	1.18E-01	1.16E-01	2.48E-02	9.95E-05
1.0E+00	1.46E-04	3.20E-01	6.25E-01	2.30E-01	1.99E-01	1.14E-01	1.14E-01	2.60E-02	1.05E-04

Table D.33. Concentration Profile in 3.6 m K$^+$/0.6 m PZ, 60°C

r	CO_2	PZ	PZH^+	$PZCOO^-$	H^+PZCOO^-	$PZ(COO^-)_2$	HCO_3^-	CO_3^{2-}	OH^-
0.0E+00	4.14E-04	2.31E-02	7.63E-03	1.45E-01	2.96E-02	3.47E-01	7.85E-01	8.49E-01	2.70E-04
1.0E-04	4.05E-04	2.31E-02	7.63E-03	1.45E-01	2.96E-02	3.47E-01	7.85E-01	8.49E-01	2.70E-04
2.0E-04	3.96E-04	2.31E-02	7.63E-03	1.45E-01	2.96E-02	3.47E-01	7.85E-01	8.49E-01	2.70E-04
3.0E-04	3.88E-04	2.31E-02	7.63E-03	1.45E-01	2.96E-02	3.47E-01	7.85E-01	8.49E-01	2.70E-04
4.0E-04	3.79E-04	2.31E-02	7.63E-03	1.45E-01	2.96E-02	3.47E-01	7.85E-01	8.49E-01	2.70E-04
5.0E-04	3.71E-04	2.31E-02	7.63E-03	1.45E-01	2.96E-02	3.47E-01	7.85E-01	8.49E-01	2.70E-04
6.0E-04	3.63E-04	2.31E-02	7.63E-03	1.45E-01	2.96E-02	3.47E-01	7.85E-01	8.49E-01	2.70E-04
7.0E-04	3.56E-04	2.31E-02	7.63E-03	1.45E-01	2.96E-02	3.47E-01	7.85E-01	8.49E-01	2.70E-04
8.0E-04	3.48E-04	2.31E-02	7.63E-03	1.45E-01	2.96E-02	3.47E-01	7.85E-01	8.49E-01	2.71E-04
9.0E-04	3.41E-04	2.31E-02	7.63E-03	1.45E-01	2.96E-02	3.47E-01	7.85E-01	8.49E-01	2.71E-04
1.0E-03	3.34E-04	2.31E-02	7.63E-03	1.45E-01	2.96E-02	3.47E-01	7.85E-01	8.49E-01	2.71E-04
2.0E-03	2.74E-04	2.31E-02	7.63E-03	1.45E-01	2.96E-02	3.47E-01	7.85E-01	8.49E-01	2.71E-04
3.0E-03	2.29E-04	2.31E-02	7.63E-03	1.45E-01	2.97E-02	3.47E-01	7.85E-01	8.49E-01	2.71E-04
4.0E-03	1.94E-04	2.31E-02	7.63E-03	1.45E-01	2.97E-02	3.47E-01	7.85E-01	8.49E-01	2.71E-04
5.0E-03	1.69E-04	2.31E-02	7.64E-03	1.45E-01	2.97E-02	3.47E-01	7.85E-01	8.49E-01	2.71E-04
6.0E-03	1.49E-04	2.32E-02	7.64E-03	1.45E-01	2.97E-02	3.47E-01	7.85E-01	8.49E-01	2.71E-04
7.0E-03	1.35E-04	2.32E-02	7.65E-03	1.45E-01	2.97E-02	3.47E-01	7.84E-01	8.49E-01	2.71E-04
8.0E-03	1.24E-04	2.32E-02	7.65E-03	1.45E-01	2.97E-02	3.47E-01	7.84E-01	8.50E-01	2.71E-04
9.0E-03	1.17E-04	2.32E-02	7.65E-03	1.45E-01	2.97E-02	3.47E-01	7.84E-01	8.50E-01	2.71E-04
1.0E-02	1.11E-04	2.32E-02	7.66E-03	1.45E-01	2.97E-02	3.47E-01	7.84E-01	8.50E-01	2.71E-04
2.0E-02	8.91E-05	2.34E-02	7.71E-03	1.46E-01	2.97E-02	3.46E-01	7.83E-01	8.51E-01	2.72E-04
3.0E-02	8.61E-05	2.37E-02	7.75E-03	1.46E-01	2.98E-02	3.45E-01	7.82E-01	8.52E-01	2.73E-04
4.0E-02	8.51E-05	2.39E-02	7.80E-03	1.47E-01	2.98E-02	3.44E-01	7.81E-01	8.53E-01	2.73E-04
5.0E-02	8.43E-05	2.41E-02	7.85E-03	1.48E-01	2.98E-02	3.43E-01	7.79E-01	8.54E-01	2.74E-04
6.0E-02	8.35E-05	2.43E-02	7.90E-03	1.48E-01	2.99E-02	3.42E-01	7.78E-01	8.56E-01	2.75E-04
7.0E-02	8.28E-05	2.46E-02	7.96E-03	1.49E-01	2.99E-02	3.41E-01	7.77E-01	8.57E-01	2.76E-04
8.0E-02	8.20E-05	2.48E-02	8.01E-03	1.49E-01	2.99E-02	3.41E-01	7.76E-01	8.58E-01	2.77E-04
9.0E-02	8.13E-05	2.50E-02	8.06E-03	1.50E-01	3.00E-02	3.40E-01	7.75E-01	8.59E-01	2.77E-04
1.0E-01	8.05E-05	2.53E-02	8.11E-03	1.51E-01	3.00E-02	3.39E-01	7.74E-01	8.60E-01	2.78E-04
2.0E-01	7.36E-05	2.77E-02	8.65E-03	1.56E-01	3.03E-02	3.31E-01	7.62E-01	8.72E-01	2.86E-04
3.0E-01	6.76E-05	3.03E-02	9.19E-03	1.61E-01	3.04E-02	3.23E-01	7.51E-01	8.83E-01	2.94E-04
4.0E-01	6.24E-05	3.28E-02	9.70E-03	1.66E-01	3.05E-02	3.15E-01	7.40E-01	8.94E-01	3.02E-04
5.0E-01	5.78E-05	3.54E-02	1.02E-02	1.71E-01	3.05E-02	3.08E-01	7.29E-01	9.05E-01	3.10E-04
6.0E-01	5.37E-05	3.80E-02	1.07E-02	1.75E-01	3.05E-02	3.01E-01	7.19E-01	9.15E-01	3.18E-04
7.0E-01	5.02E-05	4.05E-02	1.11E-02	1.79E-01	3.04E-02	2.94E-01	7.09E-01	9.25E-01	3.26E-04
8.0E-01	4.70E-05	4.31E-02	1.15E-02	1.83E-01	3.03E-02	2.87E-01	6.99E-01	9.35E-01	3.34E-04
9.0E-01	4.41E-05	4.57E-02	1.19E-02	1.86E-01	3.02E-02	2.81E-01	6.90E-01	9.44E-01	3.42E-04
1.0E+00	4.14E-05	4.83E-02	1.23E-02	1.89E-01	3.00E-02	2.75E-01	6.80E-01	9.53E-01	3.51E-04

Table D.34. Concentration Profile in 5.0 m K$^+$/2.5 m PZ, 60°C

r	CO$_2$	PZ	PZH$^+$	PZCOO$^-$	H$^+$PZCOO$^-$	PZ(COO$^-$)$_2$	HCO$_3^-$	CO$_3^{2-}$	OH$^-$
0.0E+00	3.08E-04	2.60E-01	6.96E-02	6.71E-01	1.43E-01	7.71E-01	6.63E-01	5.18E-01	1.66E-04
1.0E-04	2.93E-04	2.60E-01	6.96E-02	6.71E-01	1.43E-01	7.71E-01	6.63E-01	5.18E-01	1.66E-04
2.0E-04	2.78E-04	2.60E-01	6.96E-02	6.71E-01	1.43E-01	7.71E-01	6.63E-01	5.18E-01	1.66E-04
3.0E-04	2.65E-04	2.60E-01	6.96E-02	6.71E-01	1.43E-01	7.71E-01	6.63E-01	5.18E-01	1.66E-04
4.0E-04	2.53E-04	2.60E-01	6.96E-02	6.71E-01	1.43E-01	7.71E-01	6.63E-01	5.18E-01	1.66E-04
5.0E-04	2.41E-04	2.60E-01	6.96E-02	6.71E-01	1.43E-01	7.71E-01	6.63E-01	5.18E-01	1.66E-04
6.0E-04	2.30E-04	2.60E-01	6.96E-02	6.71E-01	1.43E-01	7.71E-01	6.63E-01	5.18E-01	1.66E-04
7.0E-04	2.19E-04	2.60E-01	6.96E-02	6.71E-01	1.43E-01	7.71E-01	6.63E-01	5.18E-01	1.66E-04
8.0E-04	2.10E-04	2.60E-01	6.96E-02	6.71E-01	1.43E-01	7.71E-01	6.63E-01	5.18E-01	1.66E-04
9.0E-04	2.00E-04	2.60E-01	6.96E-02	6.71E-01	1.43E-01	7.71E-01	6.63E-01	5.18E-01	1.66E-04
1.0E-03	1.92E-04	2.60E-01	6.96E-02	6.71E-01	1.43E-01	7.71E-01	6.63E-01	5.18E-01	1.66E-04
2.0E-03	1.30E-04	2.60E-01	6.96E-02	6.71E-01	1.43E-01	7.71E-01	6.63E-01	5.19E-01	1.66E-04
3.0E-03	9.58E-05	2.60E-01	6.96E-02	6.71E-01	1.43E-01	7.71E-01	6.63E-01	5.19E-01	1.66E-04
4.0E-03	7.75E-05	2.60E-01	6.96E-02	6.71E-01	1.42E-01	7.71E-01	6.63E-01	5.19E-01	1.66E-04
5.0E-03	6.75E-05	2.60E-01	6.96E-02	6.72E-01	1.42E-01	7.71E-01	6.63E-01	5.19E-01	1.66E-04
6.0E-03	6.22E-05	2.60E-01	6.96E-02	6.72E-01	1.42E-01	7.71E-01	6.63E-01	5.19E-01	1.66E-04
7.0E-03	5.93E-05	2.60E-01	6.96E-02	6.72E-01	1.42E-01	7.71E-01	6.62E-01	5.19E-01	1.66E-04
8.0E-03	5.77E-05	2.60E-01	6.96E-02	6.72E-01	1.42E-01	7.71E-01	6.62E-01	5.19E-01	1.66E-04
9.0E-03	5.69E-05	2.60E-01	6.96E-02	6.72E-01	1.42E-01	7.70E-01	6.62E-01	5.19E-01	1.66E-04
1.0E-02	5.66E-05	2.60E-01	6.96E-02	6.72E-01	1.42E-01	7.70E-01	6.62E-01	5.19E-01	1.66E-04
2.0E-02	5.53E-05	2.61E-01	6.95E-02	6.73E-01	1.42E-01	7.69E-01	6.61E-01	5.21E-01	1.67E-04
3.0E-02	5.50E-05	2.62E-01	6.94E-02	6.74E-01	1.42E-01	7.68E-01	6.60E-01	5.22E-01	1.68E-04
4.0E-02	5.46E-05	2.63E-01	6.94E-02	6.75E-01	1.41E-01	7.67E-01	6.59E-01	5.23E-01	1.68E-04
5.0E-02	5.42E-05	2.64E-01	6.93E-02	6.76E-01	1.41E-01	7.66E-01	6.57E-01	5.24E-01	1.69E-04
6.0E-02	5.39E-05	2.64E-01	6.92E-02	6.77E-01	1.40E-01	7.65E-01	6.56E-01	5.25E-01	1.70E-04
7.0E-02	5.35E-05	2.65E-01	6.91E-02	6.78E-01	1.40E-01	7.64E-01	6.55E-01	5.26E-01	1.70E-04
8.0E-02	5.32E-05	2.66E-01	6.91E-02	6.79E-01	1.40E-01	7.63E-01	6.54E-01	5.28E-01	1.71E-04
9.0E-02	5.29E-05	2.67E-01	6.90E-02	6.79E-01	1.39E-01	7.62E-01	6.53E-01	5.29E-01	1.72E-04
1.0E-01	5.25E-05	2.68E-01	6.90E-02	6.80E-01	1.39E-01	7.61E-01	6.51E-01	5.30E-01	1.72E-04
2.0E-01	4.93E-05	2.76E-01	6.84E-02	6.88E-01	1.35E-01	7.50E-01	6.40E-01	5.42E-01	1.79E-04
3.0E-01	4.63E-05	2.85E-01	6.78E-02	6.96E-01	1.31E-01	7.41E-01	6.28E-01	5.53E-01	1.87E-04
4.0E-01	4.35E-05	2.94E-01	6.72E-02	7.02E-01	1.27E-01	7.31E-01	6.16E-01	5.65E-01	1.94E-04
5.0E-01	4.10E-05	3.02E-01	6.65E-02	7.08E-01	1.23E-01	7.22E-01	6.05E-01	5.77E-01	2.02E-04
6.0E-01	3.86E-05	3.11E-01	6.58E-02	7.14E-01	1.20E-01	7.13E-01	5.93E-01	5.88E-01	2.10E-04
7.0E-01	3.65E-05	3.19E-01	6.50E-02	7.19E-01	1.16E-01	7.04E-01	5.82E-01	5.99E-01	2.18E-04
8.0E-01	3.44E-05	3.28E-01	6.42E-02	7.24E-01	1.12E-01	6.96E-01	5.71E-01	6.11E-01	2.27E-04
9.0E-01	3.26E-05	3.36E-01	6.33E-02	7.29E-01	1.09E-01	6.87E-01	5.60E-01	6.22E-01	2.35E-04
1.0E+00	3.08E-05	3.44E-01	6.24E-02	7.33E-01	1.06E-01	6.79E-01	5.48E-01	6.33E-01	2.45E-04

281

Bibliography

Design Institute for Physical Properties (DIPPR). (2004). New York, American Institute of Chemical Engineers.

Energy Information Administration, (2002). *Annual Energy Review 2002*.

IEA Greenhouse Gas R&D Programme, (1995). *Carbon Dioxide Utilisation*.

IEA Greenhouse Gas R&D Programme, (2001). *Putting Carbon Back into the Ground*.

IEA Greenhouse Gas R&D Programme, (2002). *Ocean Storage of CO_2*.

Kirk-Othmer Encyclopedia of Chemical Technology. (2004). Wiley.

Method of Separating CO_2 and H_2S from Gas Mixtures. (1959). **U.S. Patent 2,886,405**.

U.S. EPA, (2004). *Inventory of U.S. Greenhouse Gas Emissions and Sinks: 1990-2002*. Washington, D.C.

Ackermann, T. (1958). The Self-Dissociation of Water from Measurements of Molar Heats of Dissolved Electrolytes. *Zeitschrift fuer Elektrochemie und Angewandte Physikalische Chemie* **62**: 411-419.

Albery, W. J., A. R. Greenwook and R. F. Kibble (1967). Diffusion Coefficients of Carboxylic Acids. *Trans. Faraday Soc.* **63**(2): 360-368.

Al-Ghawas, H. A., D. P. Hagewiesche, G. Ruiz-Ibanez and O. C. Sandall (1989). Physicochemical Properties Important for Carbon Dioxide Absorption in Aqueous Methyldiethanolamine. *J. Chem. Eng. Data* **34**(4): 385-391.

Al-Juaied, M. (2004). Carbon Dioxide Removal from Natural Gas by Membranes in the Presence of Heavy Hydrocarbons and by Aqueous Diglycolamine®/Morpholine. Ph.D. Dissertation. The University of Texas at Austin.

Alper, E. (1990a). Kinetics of Reactions of Carbon Dioxide with Diglycolamine and Morpholine. *Chem. Eng. J. (Amsterdam, Netherlands)* **44**(2): 107-111.

Alper, E. (1990b). Reaction Mechanism and Kinetics of Aqueous Solutions of 2-Amino-2-Methyl-1-Propanol and Carbon Dioxide. *Ind. Eng. Chem. Res.* **29**(8): 1725-1728.

Amdur, I., J. W. Irvine, E. A. Mason and J. Ross (1952). Diffusion Coefficients of the Systems CO_2-CO_2 and CO_2-N_2O. *J. Chem. Phys.* **20**: 436-443.

Apelblat, A. (1992). The Vapor Pressures of Water over Saturated Aqueous Solutions of Barium Chloride, Magnesium Nitrate, Calcium Nitrate, Potassium Carbonate, and Zinc Sulfate, at Temperatures from 283 K to 313 K. *J. Chem. Thermodyn.* **24**(6): 619-626.

Aroua, M. K. and R. M. Salleh (2004). Solubility of CO_2 in Aqueous Piperazine and Its Modeling Using the Kent-Eisenberg Approach. *Chem. Eng. Tech.* **27**(1): 65-70.

Aseyev, G. G. (1999). <u>Electrolytes: Equilibria in Solutions and Phase Equilibria. Calculation of Multicomponent Systems and Experimental Data on the Activities of Water, Vapor Pressures, and Osmotic Coefficients</u>. New York, Begell House.

Austgen, D. M. (1989). A Model of Vapor-Liquid Equilibria for Acid Gas-Alkanolamine-Water Systems. Ph.D. Dissertation. The University of Texas at Austin.

Barradas, R. G., M. C. Giordano and W. H. Sheffield (1971). Electrochemical Oxidation of Piperidine at Mercury and Platinum. *Electrochim. Acta* **16**: 1235-1249.

Bates, S. J. and W. P. Baxter (1929). <u>International Critical Tables of Numerical Data, Physics, Chemistry and Technology</u>. New York, McGraw-Hill.

Bell, R. P. and A. F. Trotman-Dickenson (1949). Acid-Base Catalysis in Non-Aqueous Solvents. Part XII. The Amine-Catalysed Decomposition of Nitramide in Anisole Solution. *J. Chem. Soc., Abs.*: 1288-1297.

Benson, H. E., J. H. Field and R. M. Jimeson (1954). Carbon Dioxide Absorption Employing Hot Potassium Carbonate Solutions. *Chem. Eng. Prog.* **50**: 356-364.

Benson, H. E., J. H. Field and W. P. Haynes (1956). Improved Process for Carbon Dioxide Absorption Uses Hot Carbonate Solutions. *Chem. Eng. Prog.* **52**: 433-438.

Benson, S. W. (1960). <u>The Foundations of Chemical Kinetics</u>. New York, McGraw-Hill.

Bird, R. B., W. E. Stewart and E. N. Lightfoot (1960). <u>Transport Phenomena</u>. New York, Wiley.

Bishnoi, S. (2000). Carbon Dioxide Absorption and Solution Equilibrium in Piperazine Activated Methyldiethanolamine. Ph.D. Dissertation. The University of Texas at Austin.

Bishnoi, S. and G. T. Rochelle (2000). Absorption of Carbon Dioxide into Aqueous Piperazine: Reaction Kinetics, Mass Transfer and Solubility. *Chem. Eng. Sci.* **55**(22): 5531-5543.

Bishnoi, S. and G. T. Rochelle (2002a). Absorption of Carbon Dioxide in Aqueous Piperazine/Methyldiethanolamine. *AIChE J.* **48**(12): 2788-2799.

Bishnoi, S. and G. T. Rochelle (2002b). Thermodynamics of Piperazine/ Methyldiethanolamine/ Water/Carbon Dioxide. *Ind. Eng. Chem. Res.* **41**(3): 604-612.

Blauwhoff, P. M. M., G.F. Versteeg and W. P. M. V. Swaaij (1984). A Study on the Reaction between CO_2 and Alkanolamines in Aqueous Solutions. *Chem. Eng. Sci.* **39**(2): 207-225.

Bocard, J. P. and B. J. Mayland (1962). New Charts for Hot Carbonate Process. *Hydrocarbon Processing and Petroleum Refiner* **41**(4): 128-132.

Bosch, H., G. F. Versteeg and W. P. M. Van Swaaij (1989). Gas-Liquid Mass Transfer with Parallel Reversible Reactions-Ii. Absortpion of CO_2 into Amine-Promoted Carbonate Solutions. *Chem. Eng. Sci.* **44**(11): 2735-2743.

Bosch, H., G. F. Versteeg and W. P. M. Van Swaaij (1990). Kinetics of the Reaction of Carbon Dioxide with the Sterically Hindered Amine 2-Amino-2-Methylpropanol at 298 K. *Chem. Eng. Sci.* **45**(5): 1167-1173.

Bronsted, J. N. and J. Teeter, C. E. (1924). On Kinetic Salt Effect. *J. Phys. Chem.* **28**: 579-587.

Bronsted, J. N. and C. V. King (1925). Secondary Kinetic Salt Effect in the Case of Hydroxyl-Ion Catalysis. *J. Am. Chem. Soc.* **47**: 2523-2531.

Bronsted, J. N. and E. A. Guggenheim (1927). Contribution to the Theory of Acid and Basic Catalysis. The Mutarotation of Glucose. *J. Am. Chem. Soc.* **49**: 2554-2584.

Bronsted, J. N. (1928). Acid and Basic Catalysis. *Chem. Rev.* **5**(3): 231-338.

Browning, G. J. and R. H. Weiland (1994). Physical Solubility of Carbon Dioxide in Aqueous Alkanolamines Via Nitrous Oxide Analogy. *J. Chem. Eng. Data* **39**: 817-822.

Cabani, S., G. Conti, D. Giannessi and L. Lepori (1975). Thermodynamic Study of Aqueous Dilute Solutions of Organic Compounds. 3. Morpholines and Piperazines. *J. Chem. Soc., Faraday Trans. 1* **71**(5): 1154-1160.

Cabani, S., G. Conti, P. Gianni and E. Matteoli (1976). Heat Capacity Changes in the Protonation of Amines in Aqueous Solution. *Gazz. Chim. Ital.* **106**(3-6): 541-547.

Campbell, A. N. and S. Y. Lam (1973). The Densities, Viscosities, and Diffusion Coefficients of Solutions of Mono-, Di-, and Triethylamine in Water. *Can. J. Chem.* **51**(24): 4005-4008.

Caplow, M. (1968). Kinetics of Carbamate Formation and Breakdown. *J. Am. Chem. Soc.* **90**(24): 6795-6803.

Caracotsios, M. (1986). Model Parametric Sensitivity Analysis and Nonlinear Parameter Estimation. Theory and Applications. Ph.D. Dissertation. The University of Wisconsin.

Chen, C. C., H. I. Britt, J. F. Boston and L. B. Evans (1982). Local Composition Model for Excess Gibbs Energy of Electrolyte Systems. Part I: Single Solvent, Single Completely Dissociated Electrolyte Systems. *AIChE J.* **28**(4): 588-596.

Chen, C. C. and L. B. Evans (1986). A Local Composition Model for the Excess Gibbs Energy of Aqueous Electrolyte Systems. *AIChE J.* **32**(3): 444-454.

Chen, C.-C., H. I. Britt, J. F. Boston and L. B. Evans (1979). Extension and Application of the Pitzer Equation for Vapor-Liquid Equilibrium of Aqueous Electrolyte Systems with Molecular Solutes. *AIChE J.* **25**(5): 820-831.

Chen, C.-C. and P. M. Mathias (2002). Applied Thermodynamics for Process Modeling. *AIChE J.* **48**(2): 194-199.

Clarke, J. K. A. (1964). Kinetics of Absorption of Carbon Dioxide in Monoethanolamine Solutions at Short Contact Times. *Ind. Eng. Chem. Fund.* **3**(3): 239-245.

Cook, H. L. and B. M. Lowe (1976). Viscosity B-Coefficients for Pinacol and Piperazine in Aqueous Solution at 25 and 35°C. *Electrochim. Acta* **21**: 153-154.

Critchfield, J. E. (1988). CO_2 Absorption/Desorption in Methyldiethanolamine Solutions Promoted with Monoethanolamine and Diethanolamine: Mass Transfer and Reaction Kinetics. Ph.D. Dissertation. The University of Texas at Austin.

Crooks, J. E. and J. P. Donnellan (1989). Kinetics and Mechanism of the Reaction between Carbon Dioxide and Amines in Aqueous Solution. *J. Chem. Soc., Perkin Trans. 2*(4): 331-333.

Crooks, J. E. and J. P. Donnellan (1990). Kinetics of the Reaction between Carbon Dioxide and Tertiary Amines. *J. Org. Chem.* **55**(4): 1372-1374.

Cullinane, J. T. (2002). Carbon Dioxide Absorption in Aqueous Mixtures of Potassium Carbonate and Piperazine. M.S. Thesis. The University of Texas at Austin.

Cullinane, J. T. and G. T. Rochelle (2004). Thermodynamics of Aqueous Potassium Carbonate, Piperazine, and CO_2 Mixtures. *Fluid Phase Equilib.* **227**(2): 197-213.

Cuta, F. and F. Strafelda (1954). The Second Dissociation Constant of Carbonic Acid between 60 and 90°. *Chemicke Listy pro Vedu a Prumysl* **48**: 1308-1313.

da Silva, E. F. and H. F. Svendsen (2004). Ab Initio Study of the Reaction of Carbamate Formation from CO_2 and Alkanolamines. *Ind. Eng. Chem. Res.* **43**(13): 3413-3418.

Danckwerts, P. V. (1951). Significance of Liquid-Film Coefficients in Gas Absorption. *Ind. Eng. Chem.* **43**: 1460-1467.

Danckwerts, P. V. and M. M. Sharma (1966). Absorption of Carbon Dioxide into Solutions of Alkalies and Amines. Hydrogen Sulfide and Carbonyl Sulfide. *Chemical Engineer (1904-20)* **No. 202**: CE244-CE280.

Danckwerts, P. V. (1979). The Reaction of Carbon Dioxide with Ethanolamines. *Chem. Eng. Sci.* **34**(4): 443-446.

Dang, H. (2001). CO_2 Absorption Rate and Solubility in Monoethanolamine/ Piperazine/Water. M.S. Thesis. The University of Texas at Austin.

Donaldson, T. L. and Y. N. Nguyen (1980). Carbon Dioxide Reaction Kinetics and Transport in Aqueous Amine Membranes. *Ind. Eng. Chem. Fund.* **19**(3): 260-266.

Edwards, T. J., G. Maurer, J. Newman and J. M. Prausnitz (1978). Vapor-Liquid Equilibria in Multicomponent Aqueous Solution of Volatile Weak Electrolytes. *AIChE J.* **24**(6): 966-976.

Ellis, A. (1959). The Effect of Pressure on the First Dissociation Constant of "Carbonic Acid". *J. Chem. Soc.*: 3689-3699.

Enea, O. and G. Berthon (1973). Heats of Dissolution and Protonation of Piperazine and Its Derivatives in Different Water-Ethanol Mixtures. *Electrochim. Acta* **18**(8): 579-582.

Ermatchkov, V., A. Perez-Salado Kamps and G. Maurer (2003). Chemical Equilibrium Constants for the Formation of Carbamates in (Carbon Dioxide + Piperazine + Water) from ^{1}H-NMR-Spectroscopy. *J. Chem. Thermodyn.* **35**(8): 1277-1289.

French, C. C. (1928). The Effect of Neutral Salts on Certain Catalytic Decompositions. *J. Phys. Chem.* **32**: 401-414.

Glasscock, D. and G. T. Rochelle (1989). Numerical Simulation of Theories for Gas Absorption with Chemical Reaction. *AIChE J.* **35**(8): 1271-1281.

Glasscock, D. (1990). Modeling and Experimental Study of Carbon Dioxide Absorption into Aqueous Alkanolamines. The University of Texas at Austin.

Gmehling, J., P. Rasmussen and A. Fredenslund (1982). Vapor-Liquid Equilibriums by UNIFAC Group Contribution. Revision and Extension. 2. *Ind. Eng. Chem. Process Des. Dev.* **21**(1): 118-127.

Goncalves, F. A. and J. Kestin (1981). The Viscosity of Na_2CO_3 and K_2CO_3 Aqueous Solutions in the Range 20-60°C. *Int. J. Thermophys.* **2**(4): 315-322.

Grube, G. and G. Schmid (1926). The Law of Neutral Salt Action in Concentrated Solutions. I. The Neutral Salt Action in the Acid Hydrolysis of Cyanamide. *Z. Phys. Chem.* **119**: 19-45.

Harned, H. and R. Davis (1943). The Ionization Constant of Carbonic Acid in Water and the Solubility of Carbon Dioxide in Water and Aqueous Salt Solutions from 0 to 50°C. *J. Am. Chem. Soc.* **65**: 2030-2037.

Harned, H. S. and R. A. Robinson (1940). Temperature Variation of the Ionization Constants of Weak Electrolytes. *Trans. Faraday Soc.* **36**: 973-978.

Harned, H. S. and S. R. Scholes (1941). The Ionization Constant of HCO_3^- from 0 to 50°C. *J. Am. Chem. Soc.* **63**: 1706-1709.

Harned, H. S. and B. B. Owen (1958). <u>The Physical Chemistry of Electrolytic Solutions</u>. New York, Reinhold Publishing.

Helgeson, H. C. and D. H. Kirkham (1974). Theoretical Prediction of the Thermodynamic Behavior of Aqueous Electrolytes at High Pressures and Temperatures. I. Thermodynamic/Electrostatic Properties of the Solvent. *Am. J. Sci.* **274**(10): 1089-1198.

Hetzer, H. B., R. A. Robinson and R. G. Bates (1968). Dissociation Constants of Piperazinium Ion and Related Thermodynamic Quantities from 0 to 50°. *J. Phys. Chem.* **72**(6): 2081-2086.

Higbie, R. (1935). The Rate of Absorption of a Pure Gas into a Still Liquid During Short Periods of Exposure. *Trans. Am. Inst. Chem. Engrs.* **31**: 365-389.

Hikita, H. and S. Asai (1963). Gas Absorption with (M,N)Th Order Irreversible Chemical Reactions. *Kagaku Kogaku* **27**(11): 823-830.

Hikita, H., S. Asai, H. Ishikawa and M. Honda (1977). The Kinetics of Reactions of Carbon Dioxide with Monoethanolamine, Diethanolamine and Triethanolamine by a Rapid Mixing Method. *Chem. Eng. J.* **13**: 7-12.

Hikita, H., H. Ishikawa, T. Murakami and T. Ishii (1981). Densities, Viscosities and Amine Diffusivities of Aqueous MIPA, DIPA, DGA and EDA Solutions. *J. Chem. Eng. Jap.* **14**(5): 411-413.

Hitchcock, L. B. and J. S. Mcilhenny (1935). Viscosity and Density of Pure Alkaline Solutions and Their Mixtures. *Ind. Eng. Chem.* **27**(4): 461-466.

Hobler, T. (1966). <u>Mass Transfer and Absorbers</u>. Oxford, Pergamon Press.

Jensen, A., M. B. Jensen and C. Faurholt (1952). Carbamates. VIII. The Carbamates of Benzylamine, Piperidine, and Alanine. *Acta Chem. Scand.* **6**: 1073-1085.

Jensen, A. and R. Christensen (1955). Carbamates. XI. The Carbamate of Ethylenediamine. *Acta Chem. Scand.* **9**: 486-492.

Jensen, M. B., E. Jorgensen and C. Fourholt (1954). Reactions between Carbon Dioxide and Amino Alcohols. I. Monoethanolamine and Diethanolamine. *Acta Chem. Scand.* **8**(7): 1137-1140.

Joosten, G. E. H. and P. V. Danckwerts (1972). Solubility and Diffusivity of Nitrous Oxide in Equimolar Potassium Carbonate-Potassium Bicarbonate Solutions at 25° and 1 Atm. *J. Chem. Eng. Data* **17**(4): 452-454.

Jorgensen, E. (1956). Reactions between Carbon Dioxide and Amino Alcohols. III. Diethanolamine. *Acta Chem. Scand.* **10**: 747-55.

Kamps, A. P.-S., J. Xia and G. Maurer (2003). Solubility of CO_2 in (H_2O + Piperazine) and in (H_2O + MDEA + Piperazine). *AIChE J.* **49**(10): 2662-2670.

King, C. J. (1966). Turbulent Liquid-Phase Mass Transfer at a Free Gas-Liquid Interface. *Ind. Eng. Chem. Fund.* **5**(1): 1-8.

Kloosterman, E. G., S. M. De Vries, H. Kalsbeek and B. Drinkenburg (1987). Influence of Ionic Strength on the Absorption of Carbon Dioxide in

Carbonate/Bicarbonate Buffer Solutions. *Ind. Eng. Chem. Res.* **26**(11): 2216-2222.

Kohl, A. L. and F. C. Riesenfeld (1985). <u>Gas Purification</u>. Houston, Gulf Publishing.

Kumar, P. S., J. A. Hogendoorn, G. F. Versteeg and P. H. M. Feron (2003). Kinetics of the Reaction of CO_2 with Aqueous Potassium Salt of Taurine and Glycine. *AIChE J.* **49**(1): 203-213.

Laddha, S. S. and P. V. Danckwerts (1981). Reaction of Carbon Dioxide with Ethanolamines. Kinetics from Gas-Absorption. *Chem. Eng. Sci.* **36**(3): 479-482.

Laddha, S. S. and P. V. Danckwerts (1982). The Absorption of Carbon Dioxide by Amine-Potash Solutions. *Chem. Eng. Sci.* **37**(5): 665-667.

Le Bas, G. (1915). <u>The Molecular Volumes of Liquid Chemical Compounds</u>. London, Longman Green.

Lee, M.-J., Y.-K. Chang, H.-M. Lin and C.-H. Chen (1997). Solid-Liquid Equilibria for 4-Methoxyphenol with Catechol, Ethylenediamine, or Piperazine. *J. Chem. Eng. Data* **42**(2): 349-352.

Lewis, W. K. and W. G. Whitman (1924). Principles of Gas Absorption. *Ind. Eng. Chem.* **16**: 1215-1220.

Lide, D. R., Ed. (2000). <u>CRC Handbook of Chemistry and Physics</u>. London, CRC Press.

Linke, W. F. and A. Seidell (1966). <u>Solubilities of Inorganic and Metal Organic Compounds Vol. II. 4th Ed.</u>

Littel, R. J., M. Bos and G. J. Knoop (1990a). Dissociation Constants of Some Alkanolamines at 293, 303, 318, and 333 K. *J. Chem. Eng. Data* **35**(3): 276-277.

Littel, R. J., W. P. M. Van Swaaij and G. F. Versteeg (1990b). Kinetics of Carbon Dioxide with Tertiary Amines in Aqueous Solution. *AIChE J.* **36**(11): 1633-1640.

Littel, R. J. (1991). Selective Carbonyl Sulfide Removal in Acid Gas Treating Processes. Ph.D. Dissertation. Twente University.

Littel, R. J., G. F. Versteeg and W. P. M. Van Swaaij (1992a). Kinetics of Carbon Dioxide with Primary and Secondary Amines in Aqueous Solutions. I. Zwitterion Deprotonation Kinetics for Dea and Dipa in Aqueous Blends of Alkanolamines. *Chem. Eng. Sci.* **47**(8): 2027-2035.

Littel, R. J., G. F. Versteeg and W. P. M. Van Swaaij (1992b). Solubility and Diffusivity Data for the Absorption of COS, CO_2, and N_2O in Amine Solutions. *J. Chem. Eng. Data* **37**: 49-55.

Littel, R. J., G. F. Versteeg and W. P. M. Van Swaaij (1992c). Kinetics of CO_2 with Primary and Secondary Amines in Aqueous Solutions--II. Influence of Temperature on Zwitterion Formation and Deprotonation Rates. *Chem. Eng. Sci.* **47**(8): 2037-2045.

Liu, J., K. Sepehrnoori and G. A. Pope (1995). A High-Resolution Finite-Difference Scheme for Nonuniform Grids. *Appl. Math. Modeling* **19**: 163-172.

Livingston, R. (1930). An Introduction to Chemical Catalysis in Homogeneous Systems. *J. Chem. Educ.* **7**(12): 2887-2903.

Mahajani, V. V. and P. V. Danckwerts (1982). Carbamate-Bicarbonate Equilibrium for Several Amines at 100°C in 30% Potash. *Chem. Eng. Sci.* **37**(6): 943-944.

Mahajani, V. V. and P. V. Danckwerts (1983). The Stripping of Carbon Dioxide from Amine-Promoted Potash Solutions at 100°C. *Chem. Eng. Sci.* **38**(2): 321-327.

Mahajani, V. V. and J. B. Joshi (1988). Kinetics of Reaction between Carbon Dioxide and Alkanolamines. *Gas Sep. Purif.* **2**.

Mock, B., L. B. Evans and C. C. Chen (1986). Thermodynamic Representation of Phase Equilibria of Mixed-Solvent Electrolyte Systems. *AIChE J.* **32**(10): 1655-1664.

Moniuk, W. and R. Pohorecki (1991). Viscosity and Density of Sodium and Potassium Alkaline Solutions. *Hungarian J. Ind. Chem. Veszprem* **19**: 175-178.

Mshewa, M. M. (1995). Carbon Dioxide Desorption/Absorption with Aqueous Mixtures of Methyldiethanolamine and Diethanolamine at 40 to 120°C. Ph.D. Dissertation. The University of Texas at Austin.

Nijsing, R. A. T. O., R. H. Hendriksz and H. Kramers (1959). Absorption of Carbon Dioxide in Jets and Falling Films of Electrolyte Solutions, with and without Chemical Reaction. *Chem. Eng. Sci.* **10**: 88-104.

Olson, A. R. and T. R. Simonson (1949). Rates of Ionic Reactions in Aqueous Solutions. *J. Chem. Phys.* **17**(12): 1167-1173.

Oscarson, J. L., G. Wu, P. W. Faux, R. M. Izatt and J. J. Christensen (1989a). Thermodynamics of Protonation of Alkanolamines in Aqueous Solution to 325 Degc. *Thermochim. Acta* **154**(1): 119-127.

Oscarson, J. L., R. H. Van Dam, J. J. Christensen and R. M. Izatt (1989b). Enthalpies of Absorption of Carbon Dioxide in Aqueous Diethanolamine Solutions. *Thermochim. Acta* **146**: 107-114.

Pacheco, M. A. (1998). Mass Transfer, Kinetics and Rate-Based Modeling of Reactive Absorption. Ph.D. Dissertation. The University of Texas at Austin.

Pagano, J. M., D. E. Goldberg and W. C. Fernelius (1961). A Thermodynamic Study of Homopiperazine, Piperazine, and N-(2-Aminoethyl)Piperazine and Their Complexes with Copper(II) Ion. *J. Phys. Chem.* **65**: 1062-1064.

Paoletti, P., M. Ciampolini and A. Vacca (1963). Thermochemical Studies. VII. Heats and Entropies of Stepwise Neutralization of Piperazine and Triethylenetetramine. *J. Phys. Chem.* **67**: 1065-1067.

Penny, D. E. and T. J. Ritter (1983). Kinetic Study of the Reaction between Carbon Dioxide and Primary Amines. *J. Chem. Soc., Faraday Trans. 1* **79**(9): 2103-2109.

Perrin, D. D., B. Dempsey and E. P. Serjeant (1981). pK_a Prediction for Organic Acids and Bases**:** 6-9, 36-37.

Pigford, R. L. (1941). Counter-Diffusion in a Wetted-Wall Column. Ph.D. Dissertation. University of Illinois.

Pinsent, B. R. W., L. Pearson and F. J. W. Roughton (1956). Kinetics of Combination of Carbon Dioxide with Hydroxide Ions. *Trans. Faraday Soc.* **52**: 1512-1520.

Pohorecki, R. and W. Moniuk (1988). Kinetics of Reaction between Carbon Dioxide and Hydroxyl Ions in Aqueous Electrolyte Solutions. *Chem. Eng. Sci.* **43**(7): 1677-1684.

Pohorecki, R., D. T. Xoan and W. Moniuk (1988). Study of Carbon Dioxide Absorption in Aqueous Solution of Potassium Carbonate Containing Ethylaminoethanol. II. Kinetic Relations for 2-(Ethylamino)Ethanol. *Chemiczna i Procesowa* **9**(4): 667-680.

Posey, M. L. (1996). Thermodynamic Model for Acid Gas Loaded Aqueous Alkanolamine Solutions. Ph.D. Dissertation. The University of Texas at Austin.

Prasher, B. D. and A. L. Fricke (1974). Mass Transfer at a Free Gas-Liquid Interface in Turbulent Thin Films. *Ind. Eng. Chem. Process Des. Dev.* **13**(4): 336-340.

Puchkov, L. V. and V. V. Kurochkina (1970). Saturated Vapor Pressure over Aqueous Solutions of Potassium Carbonate. *Zhur. Priklad. Khim.* **43**(1): 181-183.

Rao, A. B. and E. S. Rubin (2002). A Technical, Economic, and Environmental Assessment of Amine-Based CO_2 Capture Technology for Power Plant Greenhouse Gas Control. *Environ. Sci. Technol.* **36**(20): 4467-4475.

Redlich, O. and J. N. S. Kwong (1948). On the Thermodynamics of Solutions. V. An Equation of State. Fugacities of Gaseous Solutions. *Chem. Rev.* **44**: 233-244.

Renon, H. and J. M. Prausnitz (1968). Local Compositions in Thermodynamic Excess Functions for Liquid Mixtures. *AIChE J.* **14**(1): 135-144.

Rinker, E. B., S. S. Ashour and O. C. Sandall (1995). Kinetics and Modeling of Carbon Dioxide Absorption into Aqueous Solutions of N-Methyldiethanolamine. *Chem. Eng. Sci.* **50**(5): 755-768.

Rochelle, G. T., S. Bishnoi, S. Chi, H. Dang and J. Santos, U.S. Department of Energy, (2001). *Research Needs for CO_2 Capture from Flue Gas by Aqueous Absorption/Stripping*. Pittsburg. DE-AF26-99FT01029.

Roy, R. N., J. J. Gibbons, R. Williams, L. Godwin, G. Baker, J. M. Simonson and K. S. Pitzer (1984). The Thermodynamics of Aqueous Carbonate Solutions. II. Mixtures of Potassium Carbonate, Bicarbonate, and Chloride. *J. Chem. Thermodyn.* **16**(4): 303-315.

Rubin, E. S., A. B. Rao and C. Chen (2004). Comparative Assessments of Fossil Fuel Power Plants with CO_2 Capture and Storage. 7th International conference on Greenhouse Gas Control Technologies, Vancouver, Canada.

Ryzhenko, B. N. (1963). Dissociation Constants for Carbonic Acid at Elevated Temperatures. *Doklady Akademii Nauk SSSR* **149**: 639-641.

Sada, E., H. Kumazawa and M. A. Butt (1976a). Gas Absorption with Consecutive Chemical Reaction: Absorption of Carbon Dioxide into Aqueous Amine Solutions. *Can. J. Chem. Eng.* **54**(5): 421-424.

Sada, E., H. Kumazawa and M. A. Butt (1976b). Chemical Absorption Kinetics over a Wide Range of Contact Time: Absorption of Carbon Dioxide into Aqueous Solutions of Monoethanolamine. *AIChE J.* **22**(1): 196-198.

Sada, E., H. Kumazawa and M. A. Butt (1978). Solubility and Diffusivity of Gases in Aqueous Solutions of Amines. *J. Chem. Eng. Data* **23**(2): 161-163.

Sarbar, M., A. K. Covington, R. L. Nuttall and R. N. Goldberg (1982). Activity and Osmotic Coefficients of Aqueous Potassium Carbonate. *J. Chem. Thermodyn.* **14**(7): 695-702.

Sartori, G. and D. W. Savage (1983). Sterically Hindered Amines for Carbon Dioxide Removal from Gases. *Ind. Eng. Chem. Fund.* **22**(2): 239-249.

Savage, D. W., G. Sartori and G. Astarita (1984). Amines as Rate Promoters for Carbon Dioxide Hydrolysis. *Faraday Discuss. Chem. Soc.*(77): 17-31.

Schramke, J. A., S. F. Murphy, W. J. Doucette and W. D. Hintze (1999). Prediction of Aqueous Diffusion Coefficients for Organic Compounds at 25°C. *Chemosphere* **38**(10): 2381-2406.

Schwarzenbach, D. (1968). Structure of Piperazine Hexahydrate. *J. Chem. Phys.* **48**(9): 4134-4140.

Schwarzenbach, V. G., B. Maissen and H. Ackermann (1952). Metallkomplexe Mit Polyaminen VII: Diamine Und Silber(I). *Helv. Chim. Acta* **35**(289): 2333-2336.

Seo, D. J. and W. H. Hong (2000). Effect of Piperazine on the Kinetics of Carbon Dioxide with Aqueous Solutions of 2-Amino-2-Methyl-1-Propanol. *Ind. Eng. Chem. Res.* **39**(6): 2062-2067.

Sharma, M. M. (1965). Kinetics of Reactions of Carbonyl Sulphide and Carbon Dioxide with Amines and Catalysis by Bronsted Bases of the Hydrolysis of COS. *Trans. Faraday Soc.* **61**: 681-687.

Shrier, A. L. and P. V. Danckwerts (1969). Carbon Dioxide Absorption into Amine Promoted Potash Solutions. *Ind. Eng. Chem. Fund.* **8**(3): 415-423.

Simonson, J. M., R. N. Roy and J. J. Gibbons (1987). Thermodynamics of Aqueous Mixed Potassium Carbonate, Bicarbonate, and Chloride Solutions to 368 K. *J. Chem. Eng. Data* **32**(1): 41-45.

Smith, J. M., H. C. Van Ness and M. M. Abbott (1996). <u>Introduction to Chemical Engineering Thermodynamics</u>. New York, McGraw-Hill.

Smith, W. R. and R. W. Missen (1988). Strategies for Solving the Chemical Equilibrium Problem and an Efficient Microcomputer-Based Algorithm. *Can. J. Chem. Eng.* **66**(4): 591-598.

Snijder, E. D., M. J. M. Te Riele, G. F. Versteeg and W. P. M. Van Swaaij (1993). Diffusion Coefficients of Several Aqueous Alkanolamine Solutions. *J. Chem. Eng. Data* **38**(3): 475-480.

Soave, G. (1972). Equilibrium Constants from a Modified Redlich-Kwong Equation of State. *Chem. Eng. Sci.* **27**(6): 1197-1203.

Steele, W. V., R. D. Chirico, S. E. Knipmeyer, A. Nguyen and N. K. Smith (1997). Thermodynamic Properties and Ideal-Gas Enthalpies of Formation for Dicyclohexyl Sulfide, Diethylenetriamine, Di-N-Octyl Sulfide, Dimethyl Carbonate, Piperazine, Hexachloroprop-1-Ene, Tetrakis(Dimethylamino) Ethylene, N,N'-Bis-(2-Hydroxyethyl)Ethylenediamine, and 1,2,4-Triazolo[1,5-a]Pyrimidine. *J. Chem. Eng. Data* **42**(6): 1037-1052.

Tamimi, A., E. B. Rinker and O. C. Sandall (1994a). Diffusivity of Nitrous Oxide in Aqueous Solutions of N-Methyldiethanolamine and Diethanolamine from 293 to 368 K. *J. Chem. Eng. Data* **39**(2): 396-398.

Tamimi, A., E. B. Rinker and O. C. Sandall (1994b). Diffusion Coefficients for Hydrogen Sulfide, Carbon Dioxide, and Nitrous Oxide in Water over the Temperature Range 293-368 K. *J. Chem. Eng. Data* **39**(2): 330-332.

Toman, J. J. and G. T. Rochelle (1989). Carbon Dioxide Absorption Rates and Physical Solubility in 50% Aqueous Methyldiethanolamine Partially Neutralized with Sulfuric Acid. *Unpublished*.

Tosh, J. S., J. H. Field, H. E. Benson and W. P. Haynes (1959). Equilibrium Study of the System Potassium Carbonate, Potassium Bicarbonate, Carbon Dioxide, and Water. *U.S. Bur. Mines, Rept. Invest.* **No. 5484**: 23 pp.

Trotman-Dickenson, A. F. (1949). The Basic Strength of Amines. *J. Chem. Soc., Abs.*: 1293-1297.

Tseng, P. C., W. S. Ho and D. W. Savage (1988). Carbon Dioxide Absorption into Promoted Carbonate Solutions. *AIChE J.* **34**(6): 922-931.

Van Der Wielen, L. A. M., J. H. Zomerdijk and K. C. A. M. Luyben (1997). Diffusivities of Organic Electrolytes in Water. *Chem. Eng. J.* **66**: 111-121.

Vazquez, P. G., F. Chenlo, R. Moreira and P. Pardo (1994). Viscosity of the Following Na_2CO_3, $NaHCO_3$, K_2CO_3, $KHCO_3$, Na_2CO_3-$NaHCO_3$, and K_2CO_3-$KHCO_3$ Solutions Important in Absorption Processes. *Afinidad Li* **May-June**: 211-216.

Verevkin, S. P. (1998). Thermochemistry of Amines: Strain in Six-Membered Rings from Experimental Standard Molar Enthalpies of Formation of Morpholines and Piperazines. *J. Chem. Thermodyn.* **30**(9): 1069-1079.

Versteeg, G. F. (1987). Mass Transfer and Chemical Reaction Kinetics in Acid Gas Treating Processes. Ph.D. Dissertation. Twente University.

Versteeg, G. F. and W. P. M. Van Swaaij (1988a). On the Kinetics between Carbon Dioxide and Alkanolamines Both in Aqueous and Non-Aqueous Solutions - II. Tertiary Amines. *Chem. Eng. Sci.* **43**(3): 587-591.

Versteeg, G. F. and W. P. M. Van Swaaij (1988b). Solubility and Diffusivity of Acid Gases (CO_2, N_2O) in Aqueous Alkanolamine Solutions. *J. Chem. Eng. Data* **33**(1): 29-34.

Versteeg, G. F. and M. H. Oyevaar (1989). The Reaction between Carbon Dioxide and Diethanolamine at 298 K. *Chem. Eng. Sci.* **44**(5): 1264-1268.

Versteeg, G. F., L. A. J. Van Duck and W. P. M. Van Swaaij (1996). On the Kinetics between CO_2 and Alkanolamines Both in Aqueous and Nonaqueous Solutions. An Overview. *Chem. Eng. Commun.* **144**: 113-158.

Vivian, J. E. and D. W. Peaceman (1956). Liquid-Side Resistance in Gas Absorption. *AIChE J.* **2**: 437-443.

Weiland, R. H., J. C. Dingman, D. B. Cronin and G. J. Browning (1998). Density and Viscosity of Some Partially Carbonated Aqueous Alkanolamine Solutions and Their Blends. *J. Chem. Eng. Data* **43**(3): 378-382.

Weisenberger, S. and A. Schumpe (1996). Estimation of Gas Solubilities in Salt Solutions at Temperatures from 273 K to 363 K. *AIChE J.* **42**(1): 298-300.

Wilke, C. R. and P. Chang (1955). Correlation of Diffusion Coefficients in Dilute Solutions. *AIChE J.* **1**: 264-270.

Wilson, G. M. (1964). Vapor-Liquid Equilibrium. XI. A New Expression for the Excess Free Energy of Mixing. *J. Am. Chem. Soc.* **86**(2): 127-130.

Wilson, H. L. and W. V. Wilding (1994). Vapor-Liquid and Liquid-Liquid Equilibrium Measurements on Twenty-Two Binary Mixtures. Experimental Results for DIPPR 1990-91 Projects on Phase Equilibria and Pure Component Properties. J. R. Cunningham and D. K. Jones**:** 63-115.

Xu, S., Y.-W. Wang, F. D. Otto and A. E. Mather (1993). Kinetics of the Reaction of Carbon Dioxide with Aqueous 2-Piperidineethanol Solutions. *AIChE J.* **39**(10): 1721-1725.

Yaws, C. L. (1994). Handbook of Vapor Pressure. Houston, Gulf Publishing.

Yih, S. M. and K. P. Shen (1988). Kinetics of Carbon Dioxide Reaction with Sterically Hindered 2-Amino-2-Methyl-1-Propanol Aqueous Solutions. *Ind. Eng. Chem. Res.* **27**(12): 2237-2241.

Vita

John Timothy Cullinane was born on September 17, 1976 in Jackson, Mississippi to Murdock John Cullinane, Jr. and Gwendolyn Anthony Cullinane. After graduating from Clinton High School in Clinton, Mississippi in 1995, he enrolled at Mississippi State University. As an undergraduate, he participated in the cooperative education program for three semesters as an employee of The Dow Chemical Company in Plaquemine, Louisiana and Freeport, Texas. He graduated summa cum laude with a Bachelor of Science in chemical engineering in December of 1999. His graduate studies at The University of Texas at Austin commenced in August 2000. In the interim, he served as teaching assistant at Mississippi State University and an engineering intern at the Engineering Research and Development Center in Vicksburg, Mississippi. In May of 2002, he received a Master of Science from The University of Texas at Austin. He has accepted a full-time employment offer with ExxonMobil Upstream Research Company in Houston, Texas.

Permanent Address: 104 Concord Drive

Clinton, Mississippi 39056

This dissertation was typed by the author.